E
O
S

ELECTRO-OPTICAL SYSTEMS, INC.
A Subsidiary of Xerox Corporation
300 N. Halstead Street, Pasadena, California

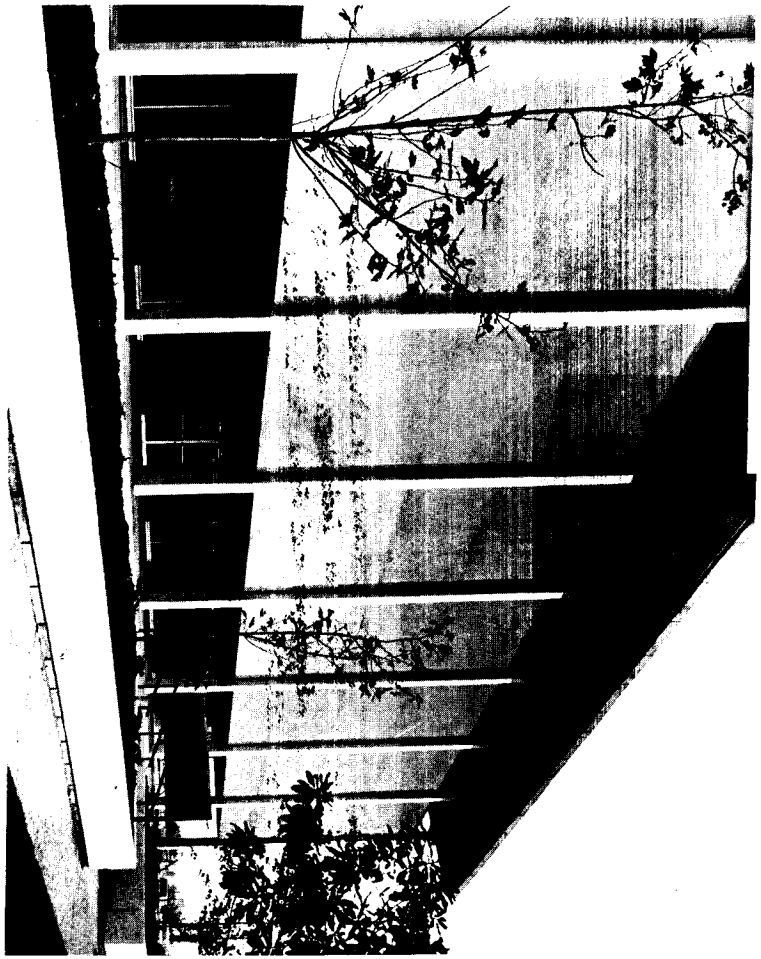

Final Report

ANALYSIS OF ANCILLARY EQUIPMENT FOR SOLAR-THERMIONIC SYSTEM

Prepared for
Jet Propulsion Laboratory
4800 Oak Grove Drive
Pasadena, California
Attention: R. Boring

Contract 950699 - Task III

EOS Report 4326-Final 10 March 1965

Volume II: Technical Background
Section 7 through 11 - Appendix I and II

Prepared by Staff
Space Power Systems

Approved by

W. R. Menetrey, Manager
Space Power Systems

Approved by

J. Neustein, Associate Manager
Program Management and Systems Engineering

This work was performed for the Jet Propulsion Laboratory, California Institute of Technology, sponsored by the National Aeronautics and Space Administration under Contract NAS7-100.

ELECTRO-OPTICAL SYSTEMS, INC. — PASADENA, CALIFORNIA

7. INSTRUMENTATION

An examination was made of the types of instrumentation required for operation of the solar-thermionic system and the types of sensors which would be applicable.

Figure 7-1 illustrates those instruments which are needed for control of the system and which are useful for monitoring performance and/or variation of operational conditions by ground command.

Techniques for measurement are available for all vital functions with the exception of emitter temperatures. Long term stability of thermocouples or resistance elements at emitter temperatures is poor. Passive methods are possible to indicate when temperature levels are passed; these include bimetallic elements, melting solids, etc. None of these methods is sufficiently accurate for control purposes. However, it should be possible to extrapolate emitter temperatures from current and voltage measurements of the converter.

Sensing of high current is easily accomplished by a small saturated core circuit. The coil is wound around the dc lead and the current level is sensed by modulation of the coil. Such current sensors will weigh a few ounces and can operate in a relatively high temperature environment. However, long term stability tests are required.

To date, cesium reservoir and radiator temperatures on converters have been measured using thermocouples. It is also possible to use resistance elements; these devices have not yet been used with converters. The primary advantages of a resistance element are linearity and lack of extensive backup circuitry.

A tradeoff will have to be made between the amount of instrumentation desirable for monitoring. The weight and cabling problems associated with a large number of instruments are further considerations.

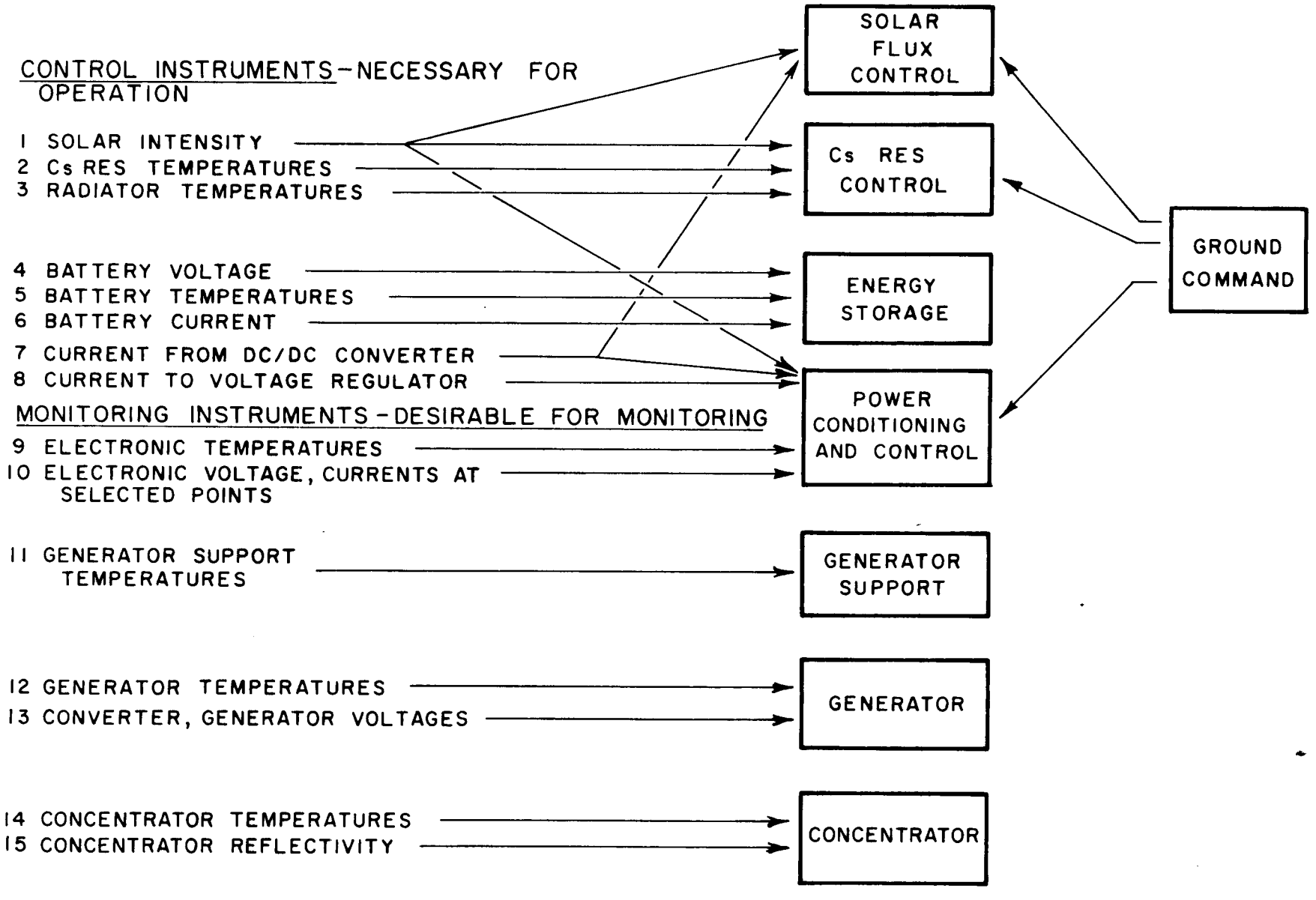

FIG. 7-1 INSTRUMENTATION REQUIREMENTS

The instrumentation for monitoring will be determined from a reasonable compromise between available telemetry system capacity and the minimum number of data points desired to evaluate the thermionic generator, concentrator, support system, and other component performance. In some instances it may be desirable to record redundant outputs from the same source to assure a minimum of at least 1 data point from certain critical measurements. In general, most of the data of interest is of a low response rate and it may be adequate to scan each output at a low repetition rate thereby simplifying the data storage and handling system for the vehicle.

7.1 Instrumentation for Various Components

This section discusses general aspects of the uses and need for instrumentation on several system components.

7.1.1 Generator Instrumentation

The instrumentation for the generator generally falls into two categories, temperature measurements and voltage measurements. The former comes directly from the output of various elements and the latter from directly tapping off with probes in appropriate parts of the circuit.

A typical survey of the instrumentation requirements for the generator is summarized in Table 7-I. All interesting temperatures on each of the four converters and several temperatures on the generator assembly are indicated.

Each converter emitter utilizes a tungsten (5 percent rhenium) - tungsten (26 percent rhenium) thermocouple. The long-term stability of the W-Re thermocouple is such that 5 to 30 hours of life can be anticipated. The primary limit on life is diffusion at high temperature. W-Re thermocouples have been used in the laboratory because of relatively high voltage output and linearity at high temperature. The thermocouple material becomes rapidly embrittled, however.

All other temperatures are measured with platinum resistance elements. With the ±5 percent measurements, it may be possible

TABLE 7-I

TYPICAL FLIGHT INSTRUMENTATION FOR 4-DIODE GENERATOR

Measurement	Type of Sensor	Number	Range	Accuracy Limits Desired
Emitter Temp.	T.C.[1]	4	1100-1800°C	±1%
Cesium Res. Temp.*	RE[2]	4	-100-500 °C	±1%
Collector Base Temp.	RE[2]	4	-100-800 °C	±5%
Radiator Temp.	RE[2]	4	-100-700 °C	±5%
Seal Temp.	RE[2]	4	-100-600 °C	±5%
Generator Block Temp.	RE[2]	3	-100-800 °C	±5%
Front Cone Face Temp.	RE[2]	2	-100-800 °C	±5%
Cesium Heater Voltage	Tap leads	4	0-2 volts	±5%
Cesium Heater Current	Shunt Load	4	0-5 amps	±5%
Converter Voltage	Tap leads	4	0-1.2 volt	±1%
Generator Voltage	Tap leads	1	0-4 volt	±1%
Generator Current	Saturated Coil	1	0-70 amp	±1%
		39		

Note: T.C.[1] Tungsten (5% rhenium) - Tungsten (26% rhenium) Thermocouples

RE[2] Resistance Elements

* Required Temperature Measurement

to use chromel-alumel thermocouples with reference junctions with all outputs falling in the range of 0 to 30 millivolts. A total of about 39 data points are shown, with a modest increase possible if certain critical parameters are recorded redundantly.

It might be desirable, for diagnostic purposes, to determine the I-V curve of the generator or individual converter. It is anticipated that a reliable, versatile load simulator can be provided using high power semiconductor diodes to sweep the I-V characteristics of the generator. Several diodes mounted in thermal heat sinks with adequate radiating surface area and operating in parallel should be suitable for this function. Control power to operate the gate network of the diodes can be furnished from a sequence programmer upon ground or vehicle command. This approach appears to offer a relatively simple, reliable load system that can cover the range from about 10 to 100 percent of rated conditions without any load carrying switches, relays, or other electromechanical parts. Voltage probes would be provided across the terminals of each individual converter and the generator as a whole. A simple technique for making individual voltage measurements is to start from the No. 1 converter (whose collector is connected to ground) and sweep each successive emitter voltage probe up to and including the total generator. Individual converter voltages can be determined by taking the difference between readings. Although some accuracy may be lost by this method, the number of interconnections is greatly reduced and telemetry capacity is conserved.

7.1.2 Concentrator Instrumentation

It would be desirable to verify that the accuracy and reflectance of the concentrator is maintained in space. If the thermionic system output does not deteriorate with time, it can be inferred that the mirror performance has not degraded. If, however, system power output falls off, diagnostic information on mirror performance can pin down the cause of failure.

The torus-supported shell structure is conceptually simple. Its static and dynamic response to mechanical and thermal inputs, however, is difficult to analyze particularly when the generator support arms are included. Four types of concentrator instrumentation can be considered:

1. Temperature sensors to determine equilibrium temperatures and thermal gradients
2. Strain gages to detect bending of shell, torus, or support arms
3. Reflectance device to minitor mirror surface reflectance
4. Angular error detector to monitor mirror distortion.

A summary of typical instrumentation is given in Table 7-II.

7.1.2.1 Strain and Thermal Instrumentation

Deformation of the shell and torus can be ascertained by mounting strain gages in critical locations. The greatest effect is expected to occur near the rim of the mirror shell. Strains can be correlated with thermal gradients by mounting temperature sensors at various points on the shell and torus and by noting the temperatures throughout the orbital cycles. Strain gages and temperature sensors would also be placed on the generator support arms to gain some indication of the absorber aperture misalignment and misfocus resulting from thermal deformation of the support arms. Figure 7-2 shows typical locations of the strain gages and temperature sensors on the shell, torus, and arms.

Each indicated strain gage is actually a set of two orthogonal pairs to allow measurement of both tensile and compressive strain in two directions. Temperature sensors would be placed immediately adjacent. The strain gages and temperature sensors are located to provide at least the following information:

1. Thermal gradient from center to rim of mirror
2. Thermal gradient around torus and between torus and shell
3. Thermal gradient between shadowed (by arms) area and sunlit area on shell

TABLE 7-II

CONCENTRATOR INSTRUMENTATION

Measurement	Sensor	Type	Sampling Rate	Range (mv)	Accuracy (percent)
Temperature of concentrator shell and torus	Temperature sensors	Silicon semiconductor	1/sec	0-5 volts	1%
Bending strain of concentrator shell and torus	Strain gauges	Silicon semiconductor	1/sec	0-2 volts	2%
Mirror surface angular error	Lateral photocell	Silicon semiconductor	1/sec	0-20 mv	1%
Mirror surface reflectance	Photoconductive detector	Lead sulfide	Slow	0-20 mv	0.5%
Housekeeping temperature	Temperature sensor	Silicon semiconductor	1/sec	0-5 volts	5%

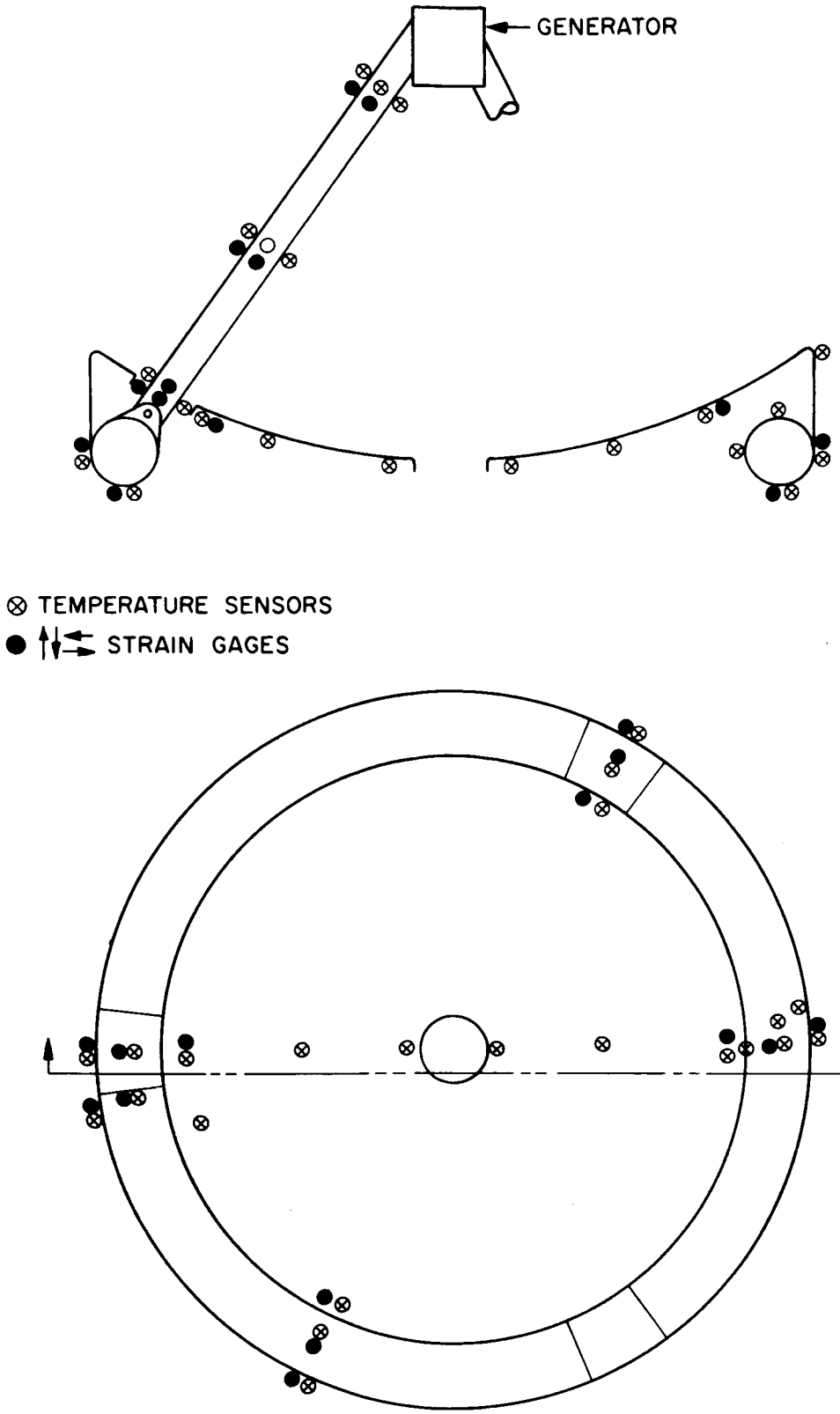

FIG. 7-2 TYPICAL LOCATION OF STRAIN GAGES AND TEMPERATURE SENSORS

4. Circumferential thermal gradients on shell and torus
5. Thermal gradients along support arms
6. Deformation of shell near rim
7. Deformation of torus at end near brackets
8. Deformation of torus between brackets
9. Deformation of support arms

Both the strain gages and the temperature sensors would probably be of the silicon semiconductor type for maximum sensitivity and minimum weight. Weight (or thermal mass) is particularly important on the shell because of the possibility of local distortion.

7.1.2.2 Reflectance and Angular Error Instrumentation

These measurements can be considered, although some further study will be required to establish definite feasibility. Reflectance measurements made directly on the concentrator would provide diagnostic information in case of a power loss from the main system.

The same is true for angular deformation. Both reflectance and angular deformation at selected locations on the mirror surface can be measured by the devices shown typically in Fig. 7-3. These involve small collimating light projectors that send beams of light to the mirror surface. The beams are reflected to sensors which detect either intensity or motion of the beams resulting from angular deformation of the surface. The reflectance detector could be a lead sulfide cell or silicon cell. The X-Y detector could be a lateral photocell (Radiation Tracking Transducer). The instruments would be placed so as not to interfere with the main experiment. Of course, many other optical arrangements are possible and would be evaluated before choosing a final configuration.

The direct structural and thermal measurements on the concentrator and support arms involve only temperature sensors and strain gages which are available and well understood. If the direct reflectance and angular deformation measurements are

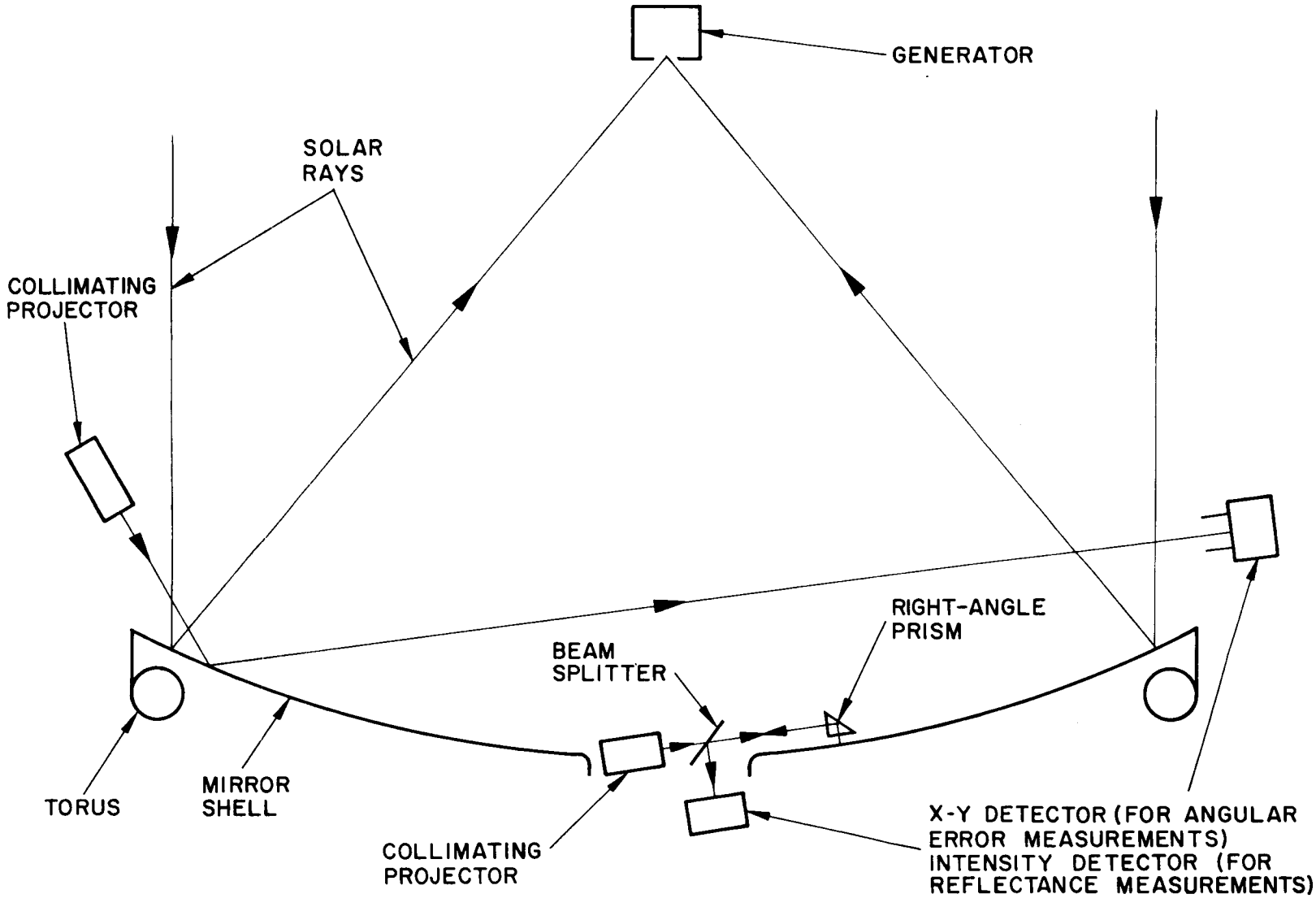

FIG. 7-3 TWO TYPICAL OPTICAL ARRANGEMENTS FOR MEASUREMENT OF MIRROR REFLECTANCE AND ANGULAR DISTORTION

made, some development will be needed on the instrument. However, since they involve no new optical instrumentation techniques, they are not foreseen to present severe development problems.

7.2 Temperature Sensors

Three types of temperature sensors were considered for use in system measurements in the range of 0 to 800°C. These are:

1. Wire type resistance sensors
2. Thermocouples
3. Thermistors

The thermistor is a semiconductor having a high negative temperature coefficient of resistance. If a thermistor is used in a Wheatstone bridge, the bridge will be balanced at only one temperature. At other temperatures there will be a bridge output which will be a measure of the deviation of the temperature. For the generator application, thermistors cannot be considered due to the fact that aging at high temperatures is greatly accelerated and the reliability above 250°C is open to question. No accuracy or instrumentation weight advantages over resistance elements are apparent at the present time.

Thermocouples are available for use and have been used in the laboratory. Thermocouples have the following advantages:

1. Small size
2. Linearity over a wide range (generally under one percent accuracy)

The disadvantages of a thermocouples are:

1. The need for a reference junction. Thermocouples do not measure the temperature at a junction but rather the difference in temperature between the measuring junction and a reference junction. Either the reference junction must be held at a constant temperature or some form of compensation must be used to distinguish between changes in the measuring temperature and those in the ambient temperature. Examination of reference junctions suitable for use with

chromel-alumel thermocouples indicates that a weight of approximately 0.8 lbs would be required for five thermocouples.

2. Low level output. The output voltage of the most sensitive thermocouple is about 16 millivolts at 300°C. A high gain amplifier is required for use with the thermocouple to prevent drift and noise effects from affecting calibration.
3. Long term stability and accuracy. Each thermocouple used in a system must be calibrated. Precalibration will mean a 1 to 2°C error in the measured temperature (up to 4°C). The total cumulative error including the thermocouple and cold junction, compensation can easily be as high as ±5°C. Furthermore, long term stability in a space environment at temperature is debatable.
4. Lead wire. Where long runs of thermocouple leads are required, special care must be taken to use special compensating lead wire to keep circuit resistance low and avoid unwanted thermal junctions.
5. Non-fail-safe. If the thermocouple becomes disconnected for any reason the controller turns full on unless special circuits are provided to prevent it.

A wire type resistance sensor seems most suitable for reliable temperature measurements. However, to date, these types of sensors have not been integrated with system components. Integration should be fairly easy to accomplish; however, estimated costs for development of a platinum resistance sensor for operation at 300 to 400°C for converter application are estimated to be $300 per unit for 10 units ($100/unit for 100 units). Nickel, nickel-iron and platinum wires all have fairly high positive temperature coefficients of resistance. In a wire sensor, a length of wire having the desired resistance is wound into any convenient physical form and is electrically connected as one arm of a Wheatstone bridge. The output of the bridge is a measure of resistance variation in the sensor and hence of the temperature.

The advantages of wire type resistance sensors are:

1. Higher sensitivity, about 100 times the output per degree C of thermocouples.
2. Superior long term stability; special units have stabilities within $0.001^{\circ}C$ per year.
3. Area sensing; a wire sensor can be spread over several square inches of surface and tends to average out differences in temperature over a surface. Wire type sensors are useful therefore whenever it is desirable to control or measure temperature over a surface rather than simply at a particular point.
4. Linearity; wire sensors are almost linear, a typical platinum sensor will have a nonlinearity of less than 0.3 percent over a temperature range of $200^{\circ}C$, e.g., 200 to $400^{\circ}C$.
5. Interchangeability; wire sensors are furnished with tolerances of from 1 to 0.1 percent or better and can be interchanged without calibration.
6. Fail-safe; wire sensors have a positive temperature coefficient, if a sensor opens up, therefore, a controller will turn off thus protecting other circuitry.

Analysis of the three temperature sensors above indicates that the wire type resistance sensors are probably best and efforts should be made to reduce the cost of these sensors for integration into the system. Platinum sensors are recommended by the manufacturer as being most applicable to applications above $200^{\circ}C$ on the basis of long-term stability.

Although emitter temperature measurement is not considered to be essential to system operation, it would be extremely interesting to obtain such measurements from a diagnostic viewpoint. The present state of art allows long-term measurement by means of an optical pyrometer only. Short-term measurements have been made by using special thermocouples but because of the extremely high temperatures,

diffusion of the metals occurs and the thermocouple shortly becomes useless. A list of possible methods to measure emitter temperature is shown in Table 7-III.

TABLE 7-III

POSSIBLE METHODS OF MEASURING EMITTER TEMPERATURE

1. Electron probes - utilizes the emission of the outer surface of the emitter which occurs due to high temperatures - the probe more likely will measure the average cavity temperature.
2. Radiometer (pyrometer) in conjunction with a black body hole.
3. Photovoltaic or photoconductive cells - similar to item 2. - a suitable optical system must be devised and the cells must be cooled.
4. Thermocouple - thermoelectric
5. Resistance vs. temperature
   a. of emitter itself
   b. of an attached metallic gage
   c. of an attached insulating material
6. Thermal expansion of emitter and a strain gage
7. Melting point of materials
8. Indirect methods
   a. Radiator temperature
   b. Seal temperature
   c. I-V characteristics
9. Radioactivity - possible change of particle emission as a function of temperature
10. Monochromator or other techniques for spectrum analysis of the hot cavity
11. Methods 2, 3, or 10 only used in comparison with a calibrated black body hole
12. Pyrometer sighted into the generator cavity

Each of the emitter temperature measurement methods cited above needs laboratory demonstration to verify its validity. Preliminary results obtained at Aerojet-General indicated that it was possible to obtain an average cavity temperature measurement by locating a pyrometer at the center of the concentrator and sighting into the cavity after adequate calibration.

7.3 Current Measurements

It is essential that currents from the dc/dc converter and into the load be measured for system control. Depending on power level and other factors, the measured current might be fairly high in a region where measurement by use of series resistors introduces excessive losses. This section is concerned primarily with this type of current measurement.

High currents can be measured by one of the following methods:

1. Voltage drop across a series resistor
2. Voltage drop across conductor leads
3. Magnetic modulator
4. Indirect - e.g., measure ac current in dc/dc converter input.

Items 1 and 2 above would require an amplifier to provide a large enough output voltage to be usable. To be practical, less than one percent of the power should be consumed by the series resistance. This would mean that the voltage drop across the series would have to be less than about 7 millivolts per thermionic diode. If an output voltage of 5 volts is required, an amplifier gain of nearly 1000 would be necessary. Item 2 would not be too practical because of the temperature coefficient of resistance of the conductor leads. The current measurement would, therefore, be highly dependent on an uncalibrated resistance.

The third method appears to be the most practical. In that the voltage drop would be insignificant and the power consumed by the circuitry would be low. Figure 7-4 shows one form of this method. If the total current through the lead is too great, the lead can be

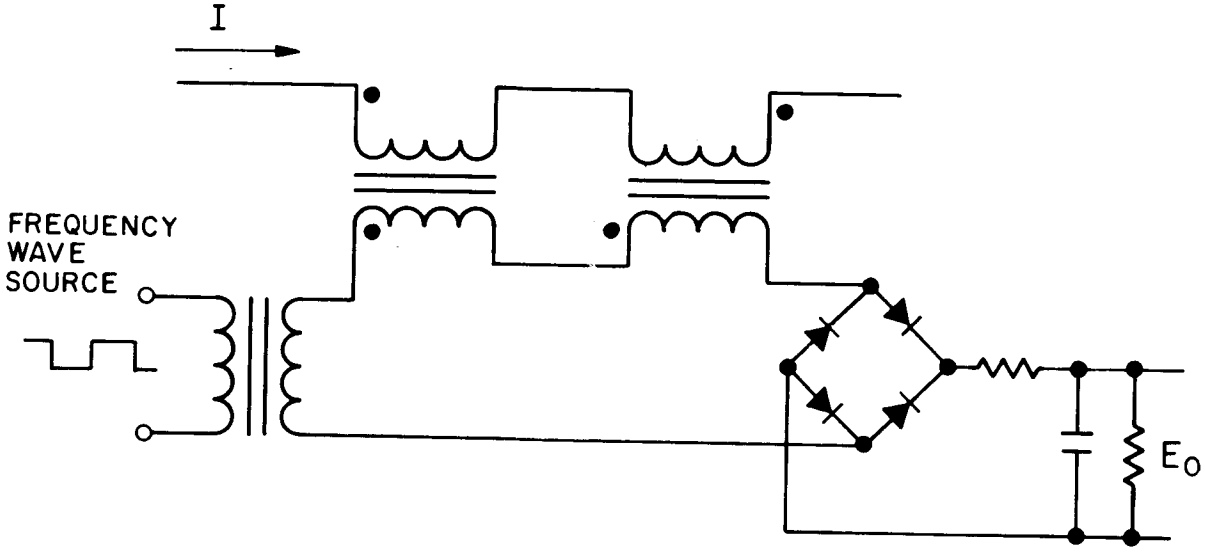

CURRENT MONITOR

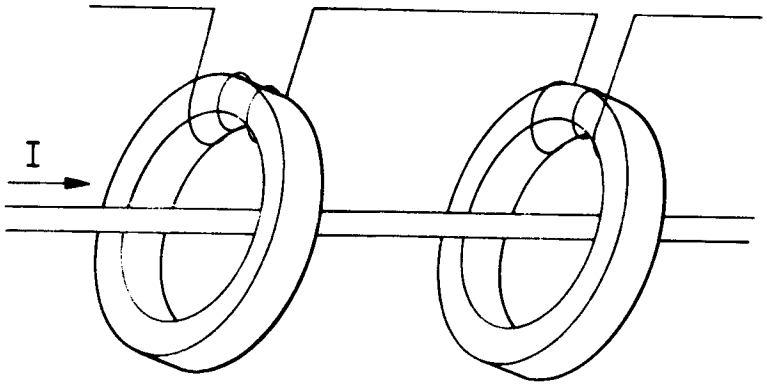

FIG. 7-4 CURRENT MEASURING DEVICE

split and only a portion of the total current routed through the cores. The output voltage can be made to any desirable value within reason.

The technique shown in Fig. 7-4 is a magnetic amplifier bridge circuit used as a transducer. The device depends for its operation on the switching characteristics of a rectangular hysteresis-loop core material and the imposition of an ac excitation to "draw out" the information in the dc bus. An explanation of the circuit is contained in "Measurement of Large Direct Currents" by P. Covert, page 106, Electro-Technology, October 1964.

7.4 Voltage Measurements

Voltage measurements can be made directly (if ground loops are not a problem) or by some indirect form. Figure 7-5 shows a series string of 4 thermionic diodes with direct measurements being made. By subtracting the results of one measurement from another, individual diode measurements can be obtained.

If ground loops become a problem, a magnetic modulator can be used similar to that used for the current measurements. A large number of turns are wound on the "primary" of the cores so that only a very small current is required. A resistor is placed in series to "swamp out" the copper resistance which is temperature sensitive. The device (shown in Fig. 7-6) has the advantage that any reasonable output voltage can be obtained and that the output is isolated from the input. Therefore, individual thermionic diode voltages can be measured with ease.

Outside of the generator voltages, other system voltages can be handled by "normal" means. One technique for measurement of a large number of voltages involves an analog/digital converter in conjunction with a solid-state commutator. For a single voltage, a solid-state VFO (variable frequency output) device is used along with suitable detectors.

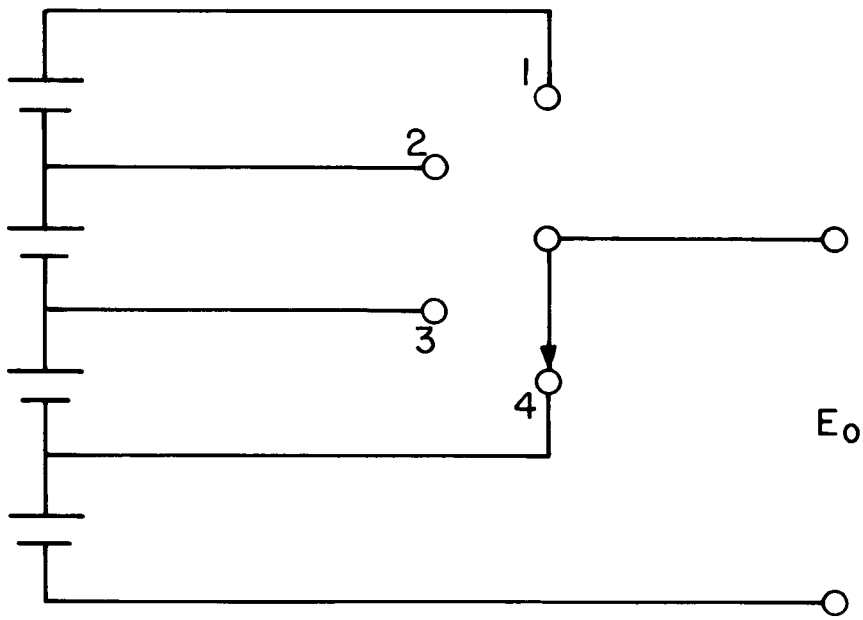

FIG. 7-5 DIRECT MEASUREMENT OF THERMIONIC GENERATOR VOLTAGES

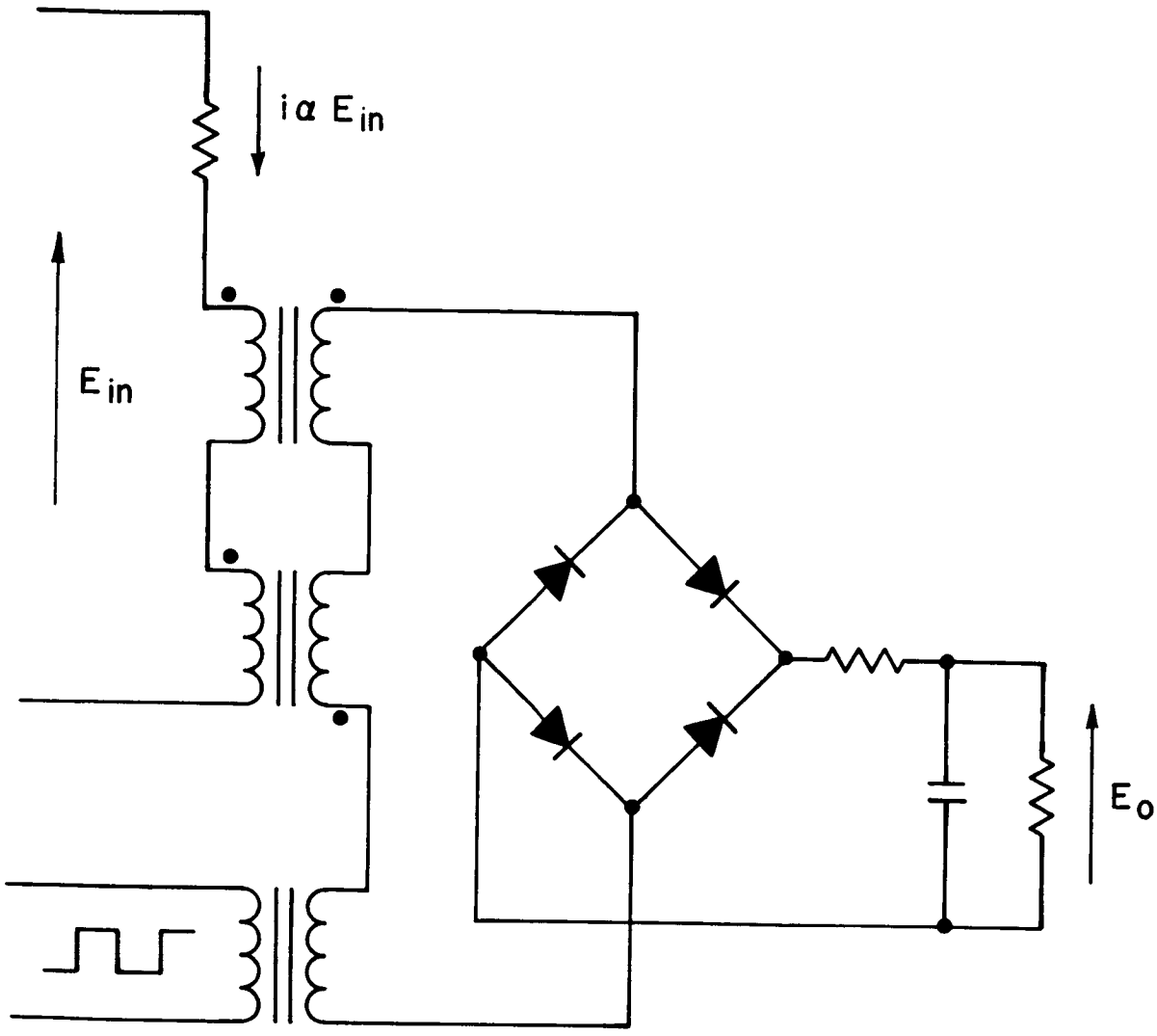

FIG. 7-6 VOLTAGE MEASURING DEVICE

8. SOLAR FLUX CONTROL

Solar flux controls would be used for missions which present non-equilibrium conditions to the solar-thermionic system such as orbital darkness, continually increasing or decreasing solar flux, etc. For equilibrium conditions, solar flux control is not required.

For orbital application, solar flux control could be used for the following:

1. Closing off of the cavity entrance during darkness to prevent radiation losses and to maintain higher generator temperatures.
2. Regulation of solar input during startup to minimize temperature rise rates.
3. Regulation of solar input to account for degradation of the concentrator.

None of the above functions is mandatory from a system viewpoint; i.e., the system will function without solar flux control. Furthermore, the value of solar flux control for the above reasons is doubtful. During darkness, the heat loss from the cavity is a small portion of the heat loss from the rest of the generator. For startup, laboratory experience indicates that high performance converters will require a maximum of solar input at startup in order to insure opening of the diode. If severe degradation of a concentrator is expected, the usefulness of the entire solar-thermionic system is in question. On this basis, the use of solar flux control for orbital applications is not recommended. This conclusion might be changed with the introduction of thermal energy storage, or with further data on startup of converters.

For missions which take the vehicle away from earth, solar flux control would be used to regulate the input of the solar flux to the generator. If constant power output is a requirement, then an "active" solar flux control is necessary.

However, if some variation in power output can be tolerated, it appears possible to use an entirely "passive" system on an interplanetary mission without exceeding generator temperature limits. If further experimental data verifies this conclusion, the need for an active solar flux control is negated.

Compensation for large solar intensity variations with variable loads or adjustments of cesium reservoir temperature is not possible without considerable overheating of the emitter or seals during one part of the mission. An examination of converter design to date indicates that seal and emitter temperatures would become extremely high and the reliability of the device would be in question.

The use of load control as a means of compensation for variations in solar flux should not be discarded, however, but should be considered in a separate converter development program with this specific goal in mind.

An examination was made of solar flux control mechanisms, actuators, electronics, etc. The recommended mechanism is a clam shell configuration. The most predictable actuator in the high temperature environment is a bimetallic element. Control of the element would be by a heater. An index mechanism could be used so that movement would always be one-way.

If no degradation of concentrator or components occurred, the solar flux control could be actuated on a preprogrammed basis. However, the preferred mode of control is by ground command based on monitoring of system operation. Automatic controls are feasible but are relatively more complex.

The principal objective of a solar flux control subsystem for interplanetary journeys is to maintain preprogrammed energy input to the cavity. On a trip from Earth to Venus, it is conceivable that a system could be designed to operate at a low cavity temperature near Earth and increased cavity temperature at Venus. Thus, the power output at Earth would be low and the output at Venus would be high. On a journey from Earth to Mars, the reverse situation would occur.

It is possible to devise a "passive" system, without active solar flux control, which would maintain relatively constant power into the cavity during the journey. However, as explored in Subsection 8.2, the price for constant flux input is an inefficient system and larger mirror diameters. "Passive" control is feasible if power variation is allowed and generator temperatures are allowed to vary.

The basic techniques for solar flux control are:

1. Passive control
2. Misorientation
3. Variable cavity aperture
4. Shutter controls

Shutter controls could be used to obscure the concentrator; however, the same degree of obscuration can be obtained with much less weight and more sensitivity by obscuring the reflected radiation input to the cavity; obscuration of the concentrator is not considered here.

8.1 Passive Control

Passive control implies that the physical constants of the system are designed such that the variation in solar flux input to the cavity is tolerable in terms of variation in cavity temperatures.

The use of passive control is illustrated in Figs. 8-1 and 8-2. In Fig. 8-1, the mirror efficiency is shown as a function of the ratio of cavity entrance diameter to mirror diameter. A perfect concentrator with a rim angle of 60 degrees is assumed. As expected, due to a change in the size of the sun's image, the mirror efficiency will reach a maximum at a smaller entrance diameter at Mars and a larger entrance diameter at Venus.

The second curve of Fig. 8-1 illustrates the change in mirror efficiency which occurs with a given cavity entrance diameter and change in distance from the sun. For large entrance diameters, the change is slight. For small entrance diameters, the change can be dramatic. Figure 8-2 illustrates the effectiveness of passive solar flux control in terms of the relative power input to the cavity with

ASSUMPTIONS

(1) $\theta_R = 60°$

(2) REFLECTIVITY = 1.0

(3) PERFECT CONCENTRATOR

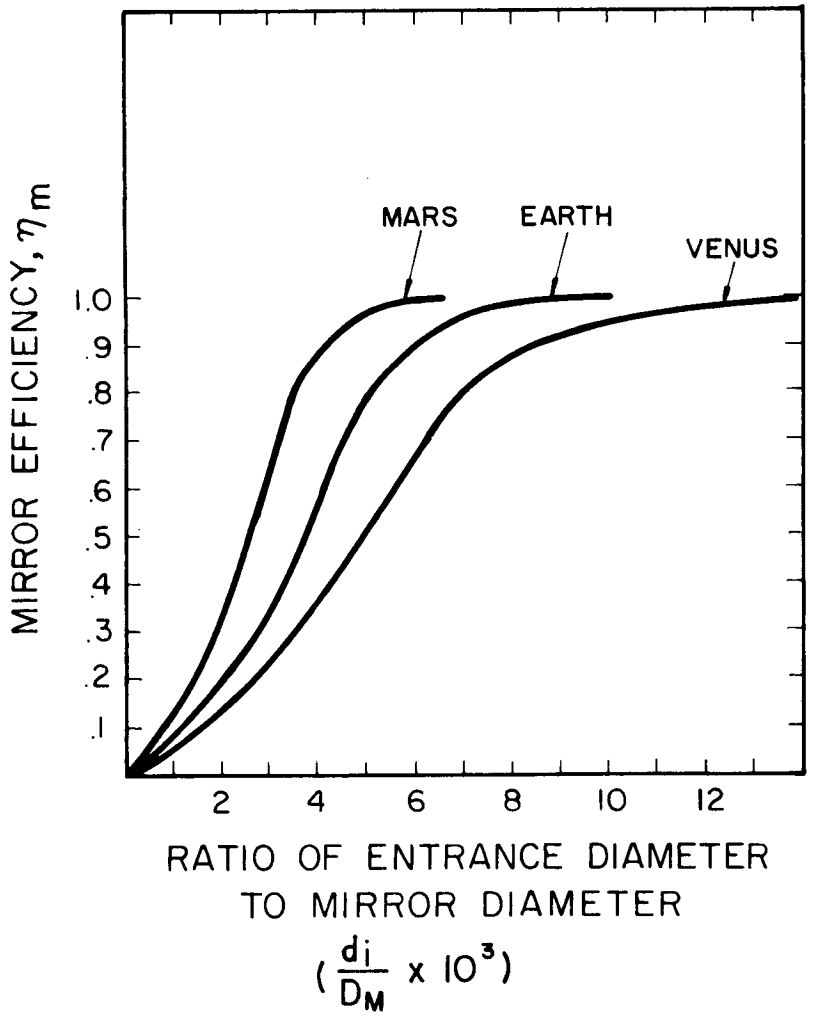

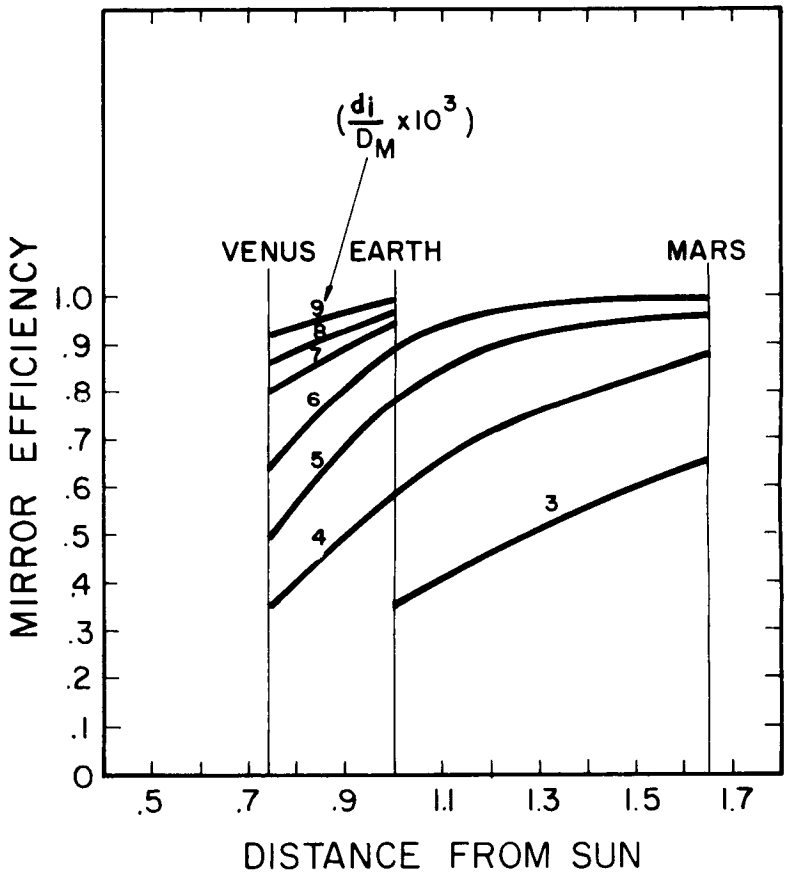

FIG. 3-1 MIRROR EFFICIENCY LIMITS

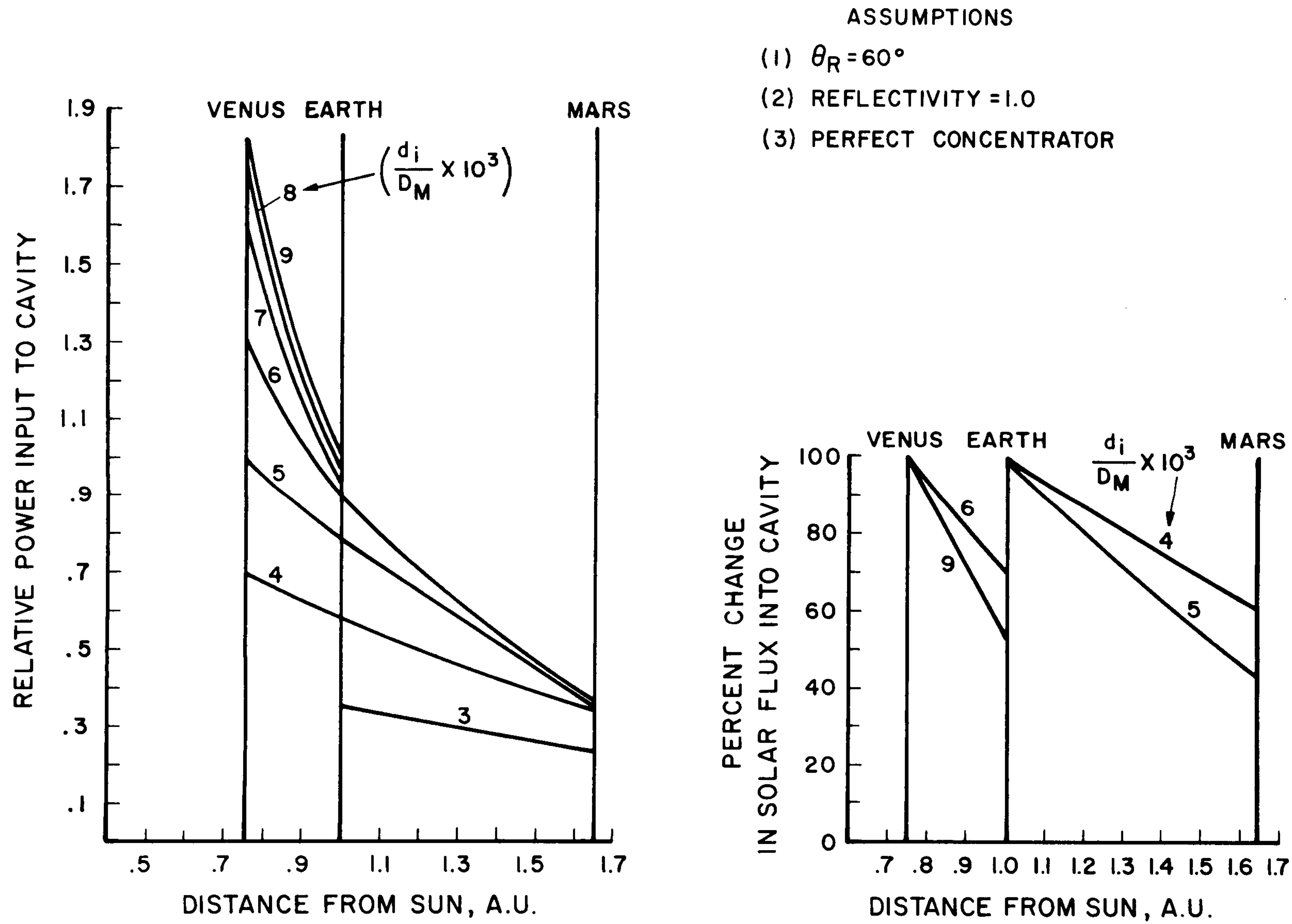

FIG. [illegible]-2 EFFECTIVENESS OF PASSIVE SOLAR FLUX CONTROL

a given entrance diameter at varying distances from the sun. Also shown is the percent change in solar flux into the cavity. As shown, it is possible to have small variations on an Earth to Venus mission if small entrance diameters are used. However, the efficiency of the concentrator-absorber will be low and a larger mirror will be required to produce a given power. The curves of Fig. 8-2 do not account for reflection and reradiation losses from the cavity; however, these losses will not significantly effect the ratio of absorbed energy.

On the Earth-Mars mission, a 40 percent change in power from earth to Mars can be obtained with an entrance diameter which allows relatively high concentrator-absorber efficiency at Mars.

The effects of variations in flux input to the cavity are illustrated in Fig. 8-3, which shows two sets of experimental data and the projected curve for a 15 percent efficient generator. As shown, an increase in flux input to the cavity from 1000 to 1500 watts results in power output increases ranging from 60 to 100 percent, with a cavity temperature change probably in the neighborhood of 1500 to 1700^{o}C. Referring to Fig. 8-2, it appears possible to choose an entrance diameter that allows solar flux input variations from 40 to 60 percent at an overall loss in system efficiency of 5 to 10 percent. Assuming the system is designed for 1700^{o}C operation at maximum input, the power output would be approximately 1/3 less at minimum input conditions. Thus, a 1000 watt system at Earth would produce 650 watts at Mars or 1500 watts at Venus.

The results of Figs. 8-1 and 8-2 assume the use of a perfect concentrator. The mirror efficiency curves shown in Fig. 8-1 will be grouped closer together using concentrators with finite surface errors; i.e., the mirror efficiency at Mars and Venus will be more like that at Earth; however the conclusions regarding the use of passive control are not significantly effected. For mirrors with large surface errors (e.g., >20 minutes) the energy into the cavity will vary simply as the inverse square of the distance from the sun. Variation in rim angle also does not effect the conclusions significantly in the 45^{o} to 60^{o} range; somewhat greater control can be obtained with the 60^{o} rim angle.

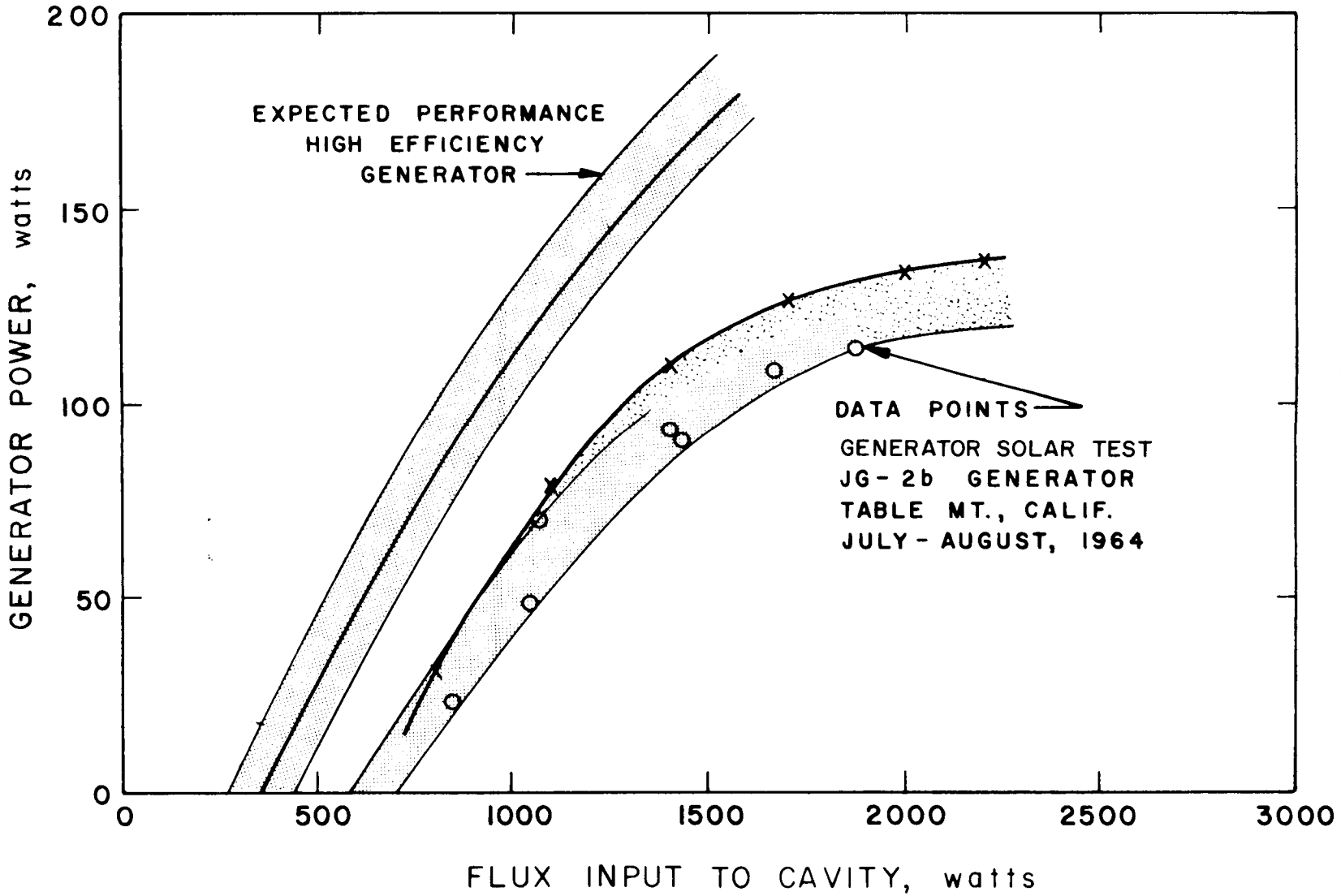

FIG. 8-3 TYPICAL GENERATOR OUTPUT VS POWER INPUT

In conclusion, the price for passive flux control would be a small decrease in system efficiency. The gain would be the elimination of a somewhat complex control system. Further investigation into the use of passive flux control is warranted with particular emphasis on the effects of temperature variations on converter reliability.

8.2 Control and Misorientation

It is possible to consider the use of deliberate misorientation as a mechanism of controlling the solar flux input to the cavity. The use of misorientation control has many problems. These include:

1. As shown in Figs. 8-2 and 8-1, mirror efficiency changes on the order of 50 percent are required for journeys to Venus and Mars. To lose as much as 50 percent of the energy, misorientations on the order of 1.5 to 2^{o} are required. This would place a major portion of the focal zone of the concentrator onto some structural element of the generator and probably cause severe overheating.
2. The primary effect of misorientation is to create an uneven thermal distribution within the cavity. Uniform temperature distribution is the primary criteria which establishes the need for maintaining orientations to ± ten minutes of arc. To maintain constant power output through misorientation, several converters will be cooler while others may be warmer. The uncertainty of what temperatures may be reached introduces undesirable life problems.
3. Misorientation implies the use of an attitude control system exercising positive control. Deliberate misorientation will influence attitude control design by requiring more gas, changing the center of radiation pressure on the vehicle, and introducing additional complexity.

   In the event of failure of one or more converters, the misorientation angle would have to be changed. This change introduces additional complexity in the attitude control system.

Also, while the power output from the generator remains constant within ±5 min. of arc centered about zero misorientation the "deadband" shrinks to perhaps ±1 min. of arc if deliberate misorientation is introduced.

For these reasons, the use of misorientation as a means for solar flux control is not recommended.

8.3 Solar Thermionic Generator Cavity Shutters and Controls

8.3.1 Basic Requirements

Since a thermionic generator must be designed to produce full power at the lowest level of input, a device such as a shutter or metering unit can be considered to block off the energy reflected by the collector into the cavity when the collector is in the high flux density section of its orbit for two reasons: (1) to prevent overheating and degradation of the material which generates the electrical power and (2) to keep the energy level being fed to the associated load constant without extra equipment.

The operating conditions which the shutter and its controls must meet are listed as follows:

1. The shutter, links, and controls must be able to withstand the rigors of takeoff, orbital flight, landing on a planet, subsequent takeoff, flight, reentry into the earth's atmosphere, and final landing on the earth's surface. In particular, the shutter must be able to withstand temperatures as high as 600°C for long periods of time without metallurgical and mechanical deterioration.
2. The shutter probably must be locked in its closed position for takeoff, so that the forces due to acceleration and vibration cannot damage the shutter, its actuators and controls, and the cavity cannot "see", and possibly be damaged by, the radiant solar flux.
3. At the proper time during orbit, the shutter must be released. The release latch must not interfere with the operation of the shutter.

4. At startup, the shutter must be at the full open position to speed the process of power generation.
5. As soon as the generator reaches full power, the shutter must begin to control the input flux. The shutter may begin to cut back the cavity aperture before full power has been reached to prevent overshoot. This type of control will be subsequently treated in detail.
6. The shutter will allow the correct amount of flux to enter the cavity regardless of the energy concentration or change of energy level due to satellite position in orbit, that is, distance from the sun.
7. The shutter must be able to compensate for collector degradation during orbital flight.
8. If the satellite vehicle suddenly were to lose its attitude and the sun's image no longer were concentrated on the generator cavity for short periods of time, the shutter must react correctly. It must remain open, or open wider than the setting held before loss of image. And on the sudden acquisition of the sun's image due to jet trimming for attitude control, the shutter must react quickly and close down fast enough to prevent damage to the thermionic generator, if such action is necessary.
9. Should the earth's shadow obscure the sun during orbit for long periods of time, the shutter must open wide to speed the startup of power generation as soon as the sun's image is reacquired by the solar collector.
10. The shutter, its linkages, and its control devices must have high reliability; at least as reliable as any other components of the satellite.
11. If they fail at all, the shutter and associated controls must fail "safe" during all stages of the life cycle of the power generation equipment. For example, should any single part of

the shutter fail to operate, it must necessarily fail in the minimum open position to prevent possible overheating and degradation of the thermionic surfaces.

12. Thermal lag of the shutter and the controls must be short for optimum control.
13. The energy drain due to the shutter controls should be held to a minimum, so that almost all the radiant flux may be used for power generation. This topic will be more fully discussed below where possible auxiliary thermal devices are postulated and the benefits derived therefrom are listed.
14. The shutter, links, and controllers must be producible from "state-of-the-art" technology if possible, to obviate lengthy development programs.

8.3.2 Types of Shutters

As indicated above, a device is needed to meter the quantity of flux entering the thermionic generator cavity. The device can take the form of a movable shutter or could conceivably be something more exotic which does not require motion in operation. For example, photochromic glass or thermometric films could block the correct amount of radiant energy for every operating condition. Only the opaque, mechanically movable shutter does not interpose a constant energy drain on the flux entering the cavity. All transparent materials which would be the substrate for photochromic or thermometric shutters filter energy in varying amounts. Only movable mechanical shutters will be discussed.

There are three basic types of mechanical shutters applicable to this type of operation. They are (1) the flap, (2) the clam shell, and (3) the iris diaphragm.

8.3.2.1 The Flap Shutter

The flap-type shutter consists of a number of sheet metal plates which hinge about their individual pivots. They would be actuated by links and levers attached to the controller

(Figure 8-4). By geometry, the minimum number of sheet metal segments in the group could be two.

The hinge for each segment must be fairly close to the cavity aperture. Since the segments will intercept some of the concentrated flux, because of the high rate of conduction, the hinges must be able to withstand fairly high temperatures. Also the pivot for the operating link which would connect the segment to the controller would be subjected to high temperatures.

The amount of obscuration by the shutter depends on shutter angle, size, etc. Fig. 8-5 shows the percent of flux from a concentrator as a function of cone angle. As shown, interception of reflected rays from the concentrator rim is more effective than near the center. Fig. 8-6 shows a typical case of obscuration as a function of flap angle.

8.3.2.2 The Clam Shell Shutter

The clam shell shutter differs from the flap shutter in that each sheet metal segment is fastened directly to an arm which has a remote hinge (Fig. 8-7) The clam shell requires only two segments to be effective. In this construction, no sensitive parts, such as pivots, would be in high temperature zones. However, this mechanical arrangement is more subject to the affects of vibration due to the long pivot arms.

8.3.2.3 The Iris Diaphragm Shutter

The iris diaphragm shutter consists of a set of overlapping sheet metal segments, each of which has its own pivot (Fig. 8-8). Each leaf or segment has a pin which rides in a slot in a common rotary, adjustable ring. The controller attaches to the ring to regulate the circular aperture.

The iris diaphragm has two weaknesses for this application. They are (1) the leaf pivots would be subjected to high temperatures and (2) the leaf pins would also be quite hot and

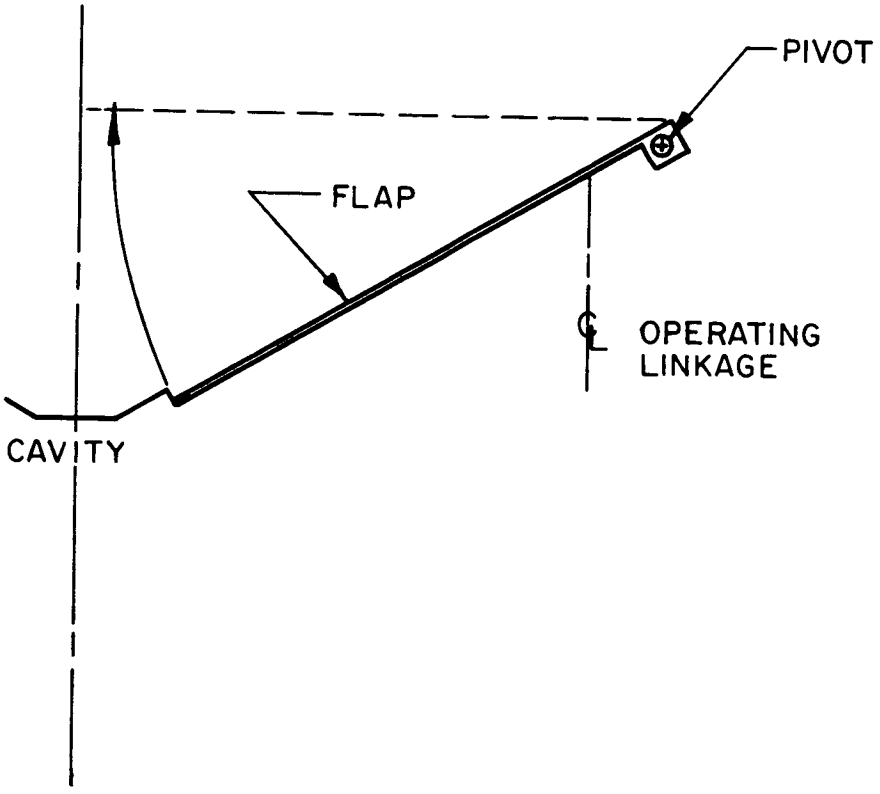

FIG. 8-4 SCHEMATIC OF A FLAP TYPE SHUTTER SHOWN IN MAXIMUM APERTURE POSITION

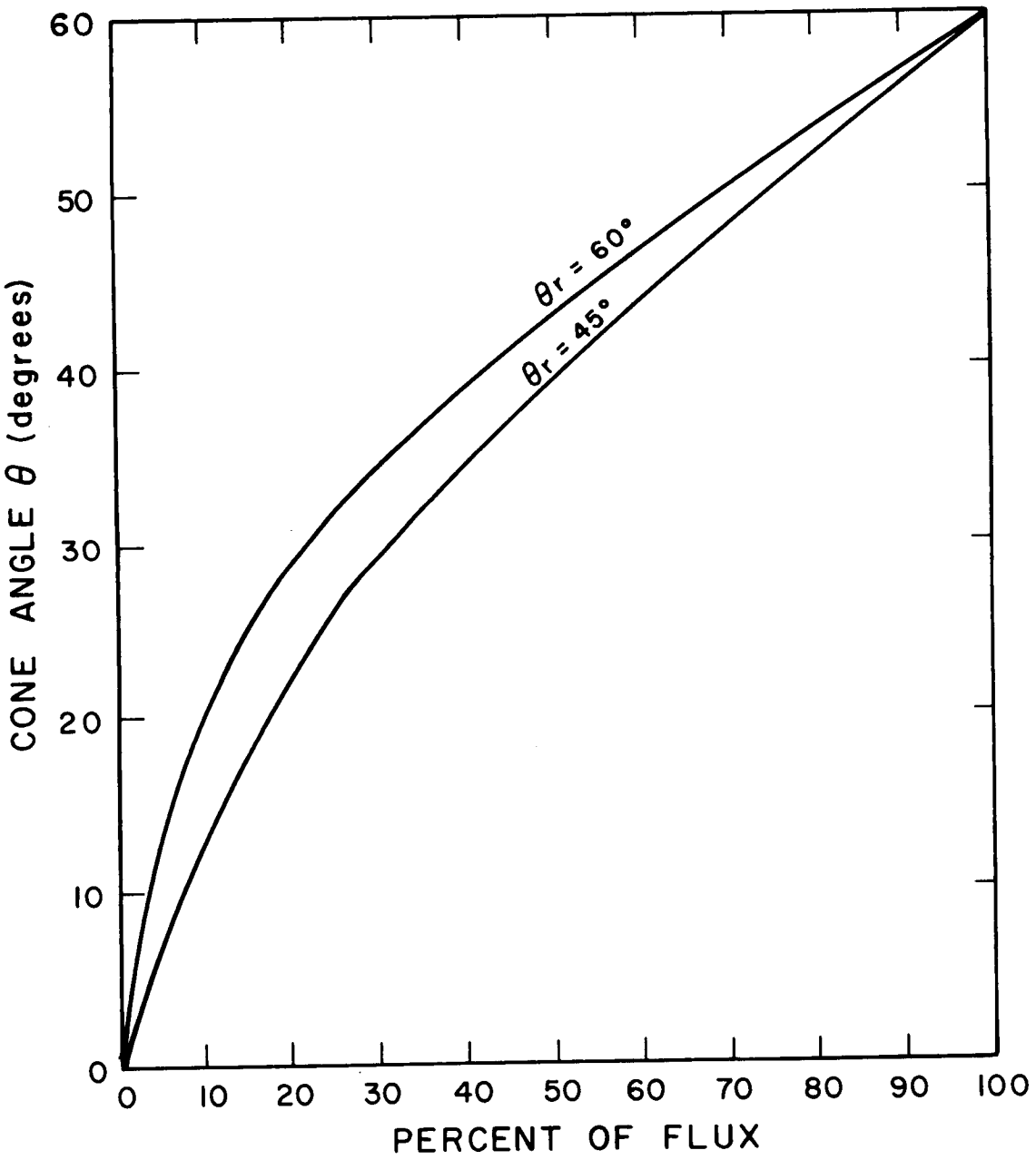

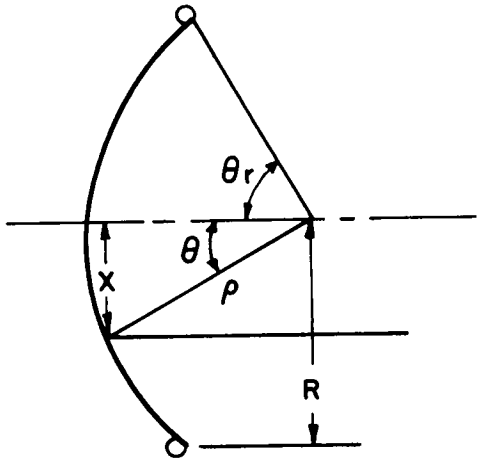

$$\text{PERCENT} = \frac{X^2}{R^2}$$

$$X = \rho \sin\theta$$

$$\rho = \frac{2f}{1+\cos\theta}$$

$$\frac{2R}{f} = \frac{4\sin\theta r}{1+\cos\theta r}$$

$$f = \frac{2R(1+\cos\theta r)}{4\sin\theta r}$$

$$\rho = \frac{R(1+\cos\theta r)}{\sin\theta r(1+\cos\theta)}$$

$$\text{PERCENT} = \frac{\sin^2\theta \quad (1+\cos\theta r)^2}{\sin^2\theta r \quad (1+\cos\theta)^2}$$

FIG. 8- PERCENT OF FLUX REFLECTED FROM PYREX VS CONE ANGLE

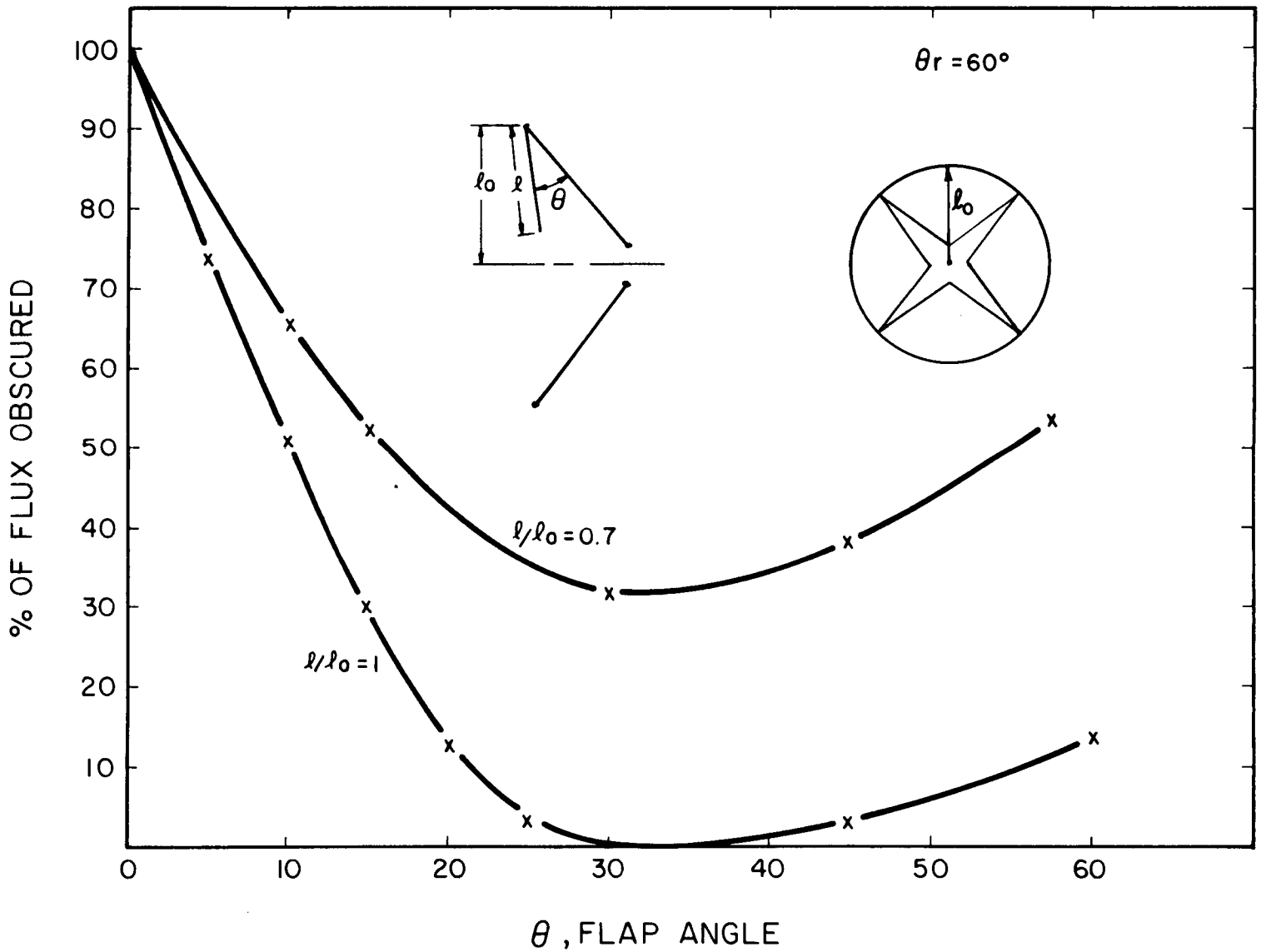

FIG. 3-6 TYPICAL CASE OF PERCENT OF FLUX OBSURED BY SHUTTER FLAP

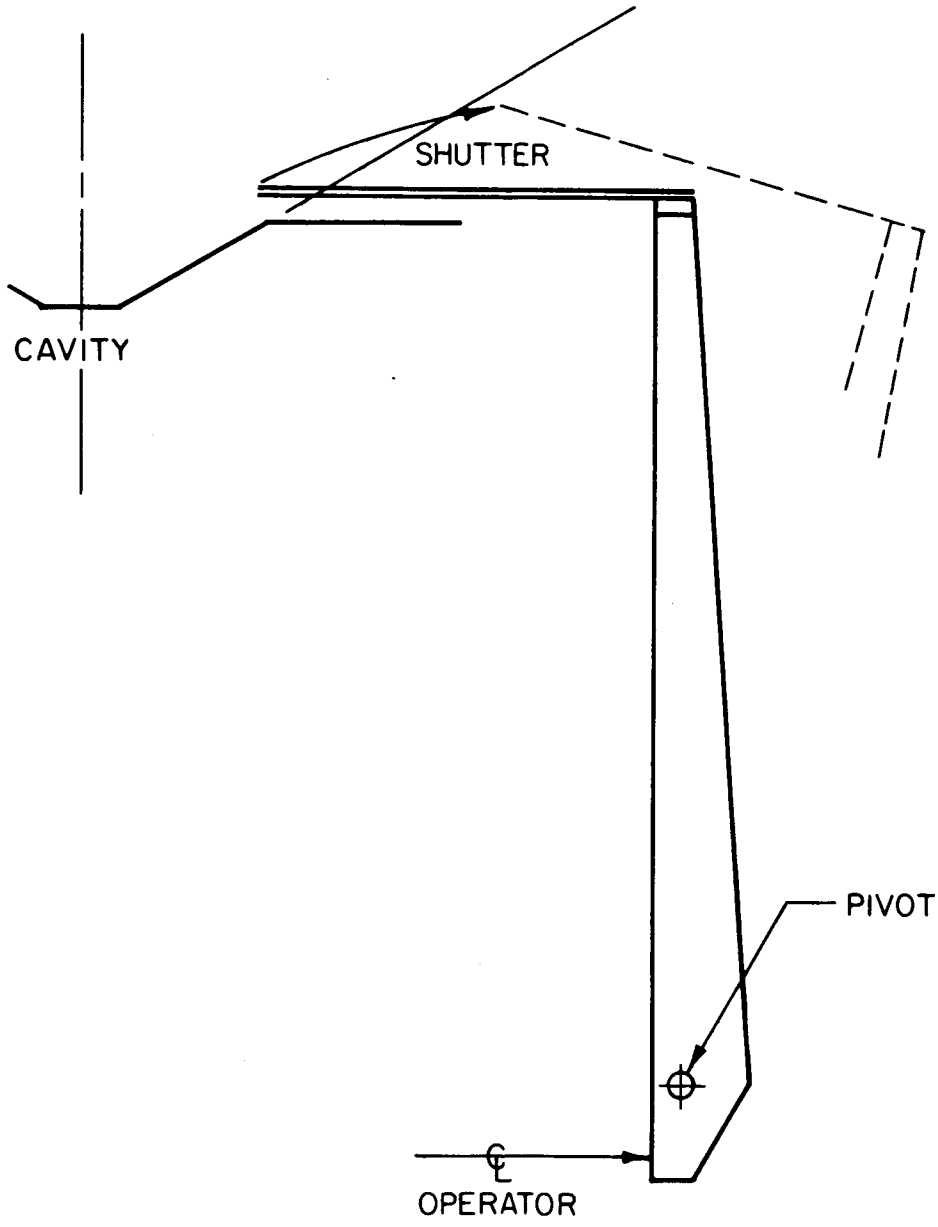

FIG. -, SCHEMATIC OF CLAMSHELL TYPE SHUTTER SHOWN IN CLOSED POSITION

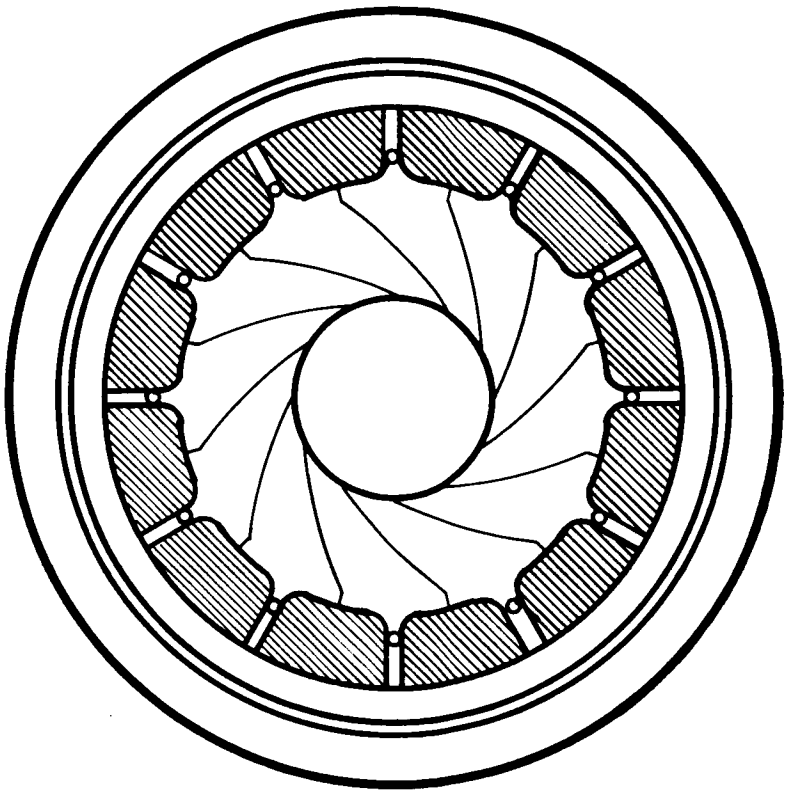

FIG. 8-5 PICTORIAL REPRESENTATION OF AN IRIS DIAPHRAGM SHUTTER WITH SLIDING BLADES FIXED TO A STATIONARY RING. APERTURE ADJUSTMENT IS BY MOVEMENT OF A ROTATING RING WHICH IS SLOTTED AND FORCES THE PINS FIXED TO EACH BLADE TO MOVE AND CHANGE ITS POSITION.

have to slide along the setting ring grooves in a high vacuum--a condition very conducive to friction welding.

8.3.2.4 Flux Distribution in the Cavity

Since the sun's radiant energy will vary for a trip to Mars from a high of about 130 watts-ft^{-2} to a low of about 44 watt-ft^{-2}, the shutter might have to intercept approximately 65 percent of the energy available near the Earth. Of course, the cavity aperture would be wide open at Mars. This means that all three types of shutters discussed above cause poor flux distribution in the thermionic generator cavity, particularly at the maximum flux condition. This is when the aperture is at a minimum and the resultant image in the cavity is small and highly intense - a situation conducive to high temperature gradients. The flap shutter forms an odd-shaped opening at minimum aperture; the shape slows transforms during transition from minimum to maximum to become a true circle. The clam shell aperture shape changes in quite a different manner. At minimum opening the aperture would be circular, and as the opening increased, the aperture would no longer be circular; but as it neared the full open position, the aperture would begin to approximate a circle, and in the wide open position, the aperture would be circular again. The iris diaphragm shutter aperture would be approximately circular in all positions.

8.3.3 Shutter Operators

While it is possible to conceive of various types of operators to actuate the thermionic generator cavity, the feasibility of use of most operators is low due to limitations of the energy sources. These energy sources are limited to heat and electrical power. For the application under consideration, heat is available either from the flux reflected by the solar collector or an auxiliary reflective device; or electrical energy can be obtained from the thermionic generator or an auxiliary device. Stored energy in the form of high pressure gas or batteries does not appear feasible for long term space journeys.

8.3.3.1 Operators Energized by Heat

There are three basic types of operators which can be energized by heat. They are the bimetallic, bourdon tube, and bellows operators. Each type will be discussed, including its advantages and weaknesses applicable in the design under consideration.

Bimetallic Operator

Two thin prismatic bars of identical geometric shape and length but made of different material will expand linearly at different rates as their temperature is increased. If the bars are bonded together, the affect of temperature increase will cause the bars to attempt to increase in length, each bar at its own rate. But the bond between the bars will restrain the bar of higher expansive rate from expanding to its free length, and at the same time will strain the bar with the lower expansion rate and cause it to elongate. The total increase in length will be shorter than for the higher expansion metal, but longer than that of the lower expanding metal. The strain will cause the composite bar to curve, so that the more expansive metal will be under compression, the lesser expansive metal will have tensile stresses. The bar will bend in circular arc, because the stresses will be uniform along its entire length. These stresses may be represented by a couple at each end of the bar. The motion caused by the bending is the action that makes this behavior a useful operator by means of proper linkage to the shutter.

For uniformly heated, freely deflecting prismatic bars of equal thickness and of equal elastic moduli fonded together, the stress at the bond can be shown to be

$$S = \frac{E}{2}(\alpha_2 - \alpha_1)(T_2 - T_1) = \frac{EF}{3}(T_2 - T_1) \quad \text{(Ref. 8-1)}$$

where S = stress in psi; E = modulus of elasticity, psi; α_1 and α_2 = coefficients of expansion of each metal, inches/inch/F; $T_2 - T_1$ = temperature change affecting the bimetallic operator, ^{o}F; and F = flexivity, a measure of the deflection rate of the bimetal. Figure 8-9

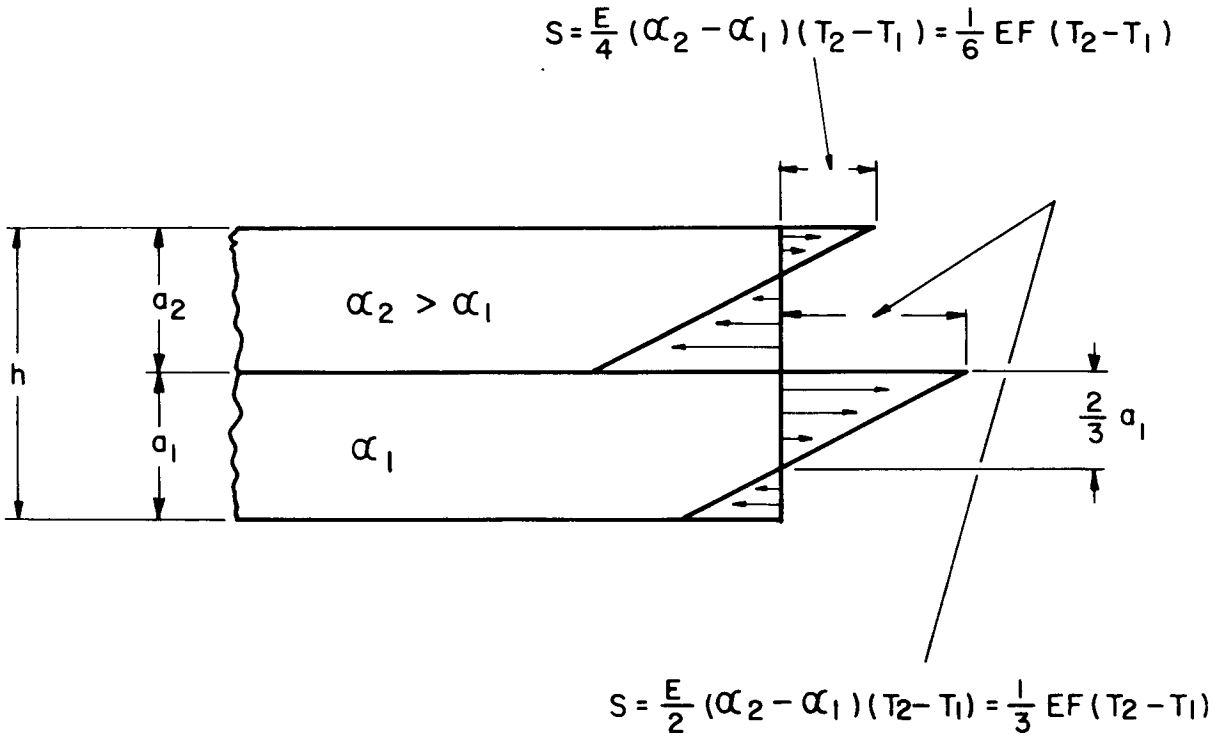

S = STRESS IN PSI, E = MODULUS OF ELASTICITY, α_2 AND α_1 = COEFFICIENTS OF EXPANSION, T_2 AND T_1 = TEMPERATURE CHANGE, AND F = FLEXIBILITY

FIG. 8-9 STRESS DISTRIBUTION IN UNIFORMLY HEATED FREELY DEFECTING BEAM

shows the stress distribution in the composite bar. The high expansion metal will be in compression at the bond, and its extreme fiber will be in tension; the low-expansion alloy will be in tension at the bond, and its extreme fiber will be in compression. As noted in Figure 8-9, the stresses at the extreme fibers are one-half the stresses at the bond line, and the neutral stress axis of each part of the composite bar is two-thirds of the distance from the bond line to the extreme fiber.

S. Timoshenko (Ref. 8-[illegible]) developed the following equation to determine the deflection of bimetallics:

$$\frac{1}{R} = \frac{6(\alpha_2 - \alpha_1)(T_2 - T_1)(1 + m)^2}{h\left[3(1 + m)^2 + (1 + mn)\left(m^2 + \frac{1}{mn}\right)\right]}, \quad m = \frac{t_1}{t_2} \text{ and } n = \frac{E_1}{E_2}$$

In this formula, R = radius of curvature, inches; α_2 and α_1 = coefficient of thermal expansion, inches/inch/^{o}F; T_2-T_1 = temperature difference in operation, ^{o}F; h = total thickness of bimetallic bar, inches; E_2 and E_1 = modulus of elasticity, psi, of each alloy in the bimetallic bar; and t_1, and t_2 = thickness of each metallic layer, inches.

On inspection of the formula, it is noted that the deflection is measured by the radius of curvature, R; as the deflection increases, R becomes smaller. The deflection then varies directly, as the differences in coefficients of expansion between the two metals, the temperature difference, and the thickness of the bimetal. However, since the coefficients of expansion do not remain constant for almost all materials, the affect of these coefficients will be discussed more fully below.

To determine the affect of the moduli of elasticity of the two alloys, E_1, and E_2, or the ratio of the two, n, unitize the equation for curvature--that is, set all the factors in the equation equal to one, except R and n. This yields the following expression:

$$\frac{1}{R} = \frac{24n}{n^2 + 14n + 1}$$

To obtain maximum curvature, the equation is differentiated and set = 0. R is the dependent variable; n is the independent variable. This yields the interesting fact that n = 1 for maximum curvature, and under this condition, $\frac{1}{R} = 1.5$. If the equation is changed so that it reads in % of maximum curvature, it is written

$$\% K_{max} = \frac{1600n}{n^2 + 14n + 1}$$

A plot of this equation is shown in Figure 8-10. Because the curve has a long, relatively flat section at its peak, even such rather large ratios of elastic moduli of 2 to 1 will yield about 95% of the maximum possible curvature or deflection. Even this can be compensated for by increasing the thickness of the lower modulus material by the ratio of $\sqrt{\frac{E_2}{E_1}}$.

To investigate the affects of component thickness on deflection, the equation is again unitized, except for $\frac{1}{R}$ and m. Then,

$$\frac{1}{R} = \frac{6m}{(1 + m)^2}$$

After differentiating as above, m = 1, and $\frac{1}{R} = 1.5$. The equation for % of maximum curvature is

$$\% K_{max} = \frac{400m}{(1 + m)^2}$$

A plot of the equation is shown in Figure 8-11. It was assumed here that the elastic moduli were equal. Any deviation from a 1:1 thickness ratio will reduce the allowable deflection drastically. Even

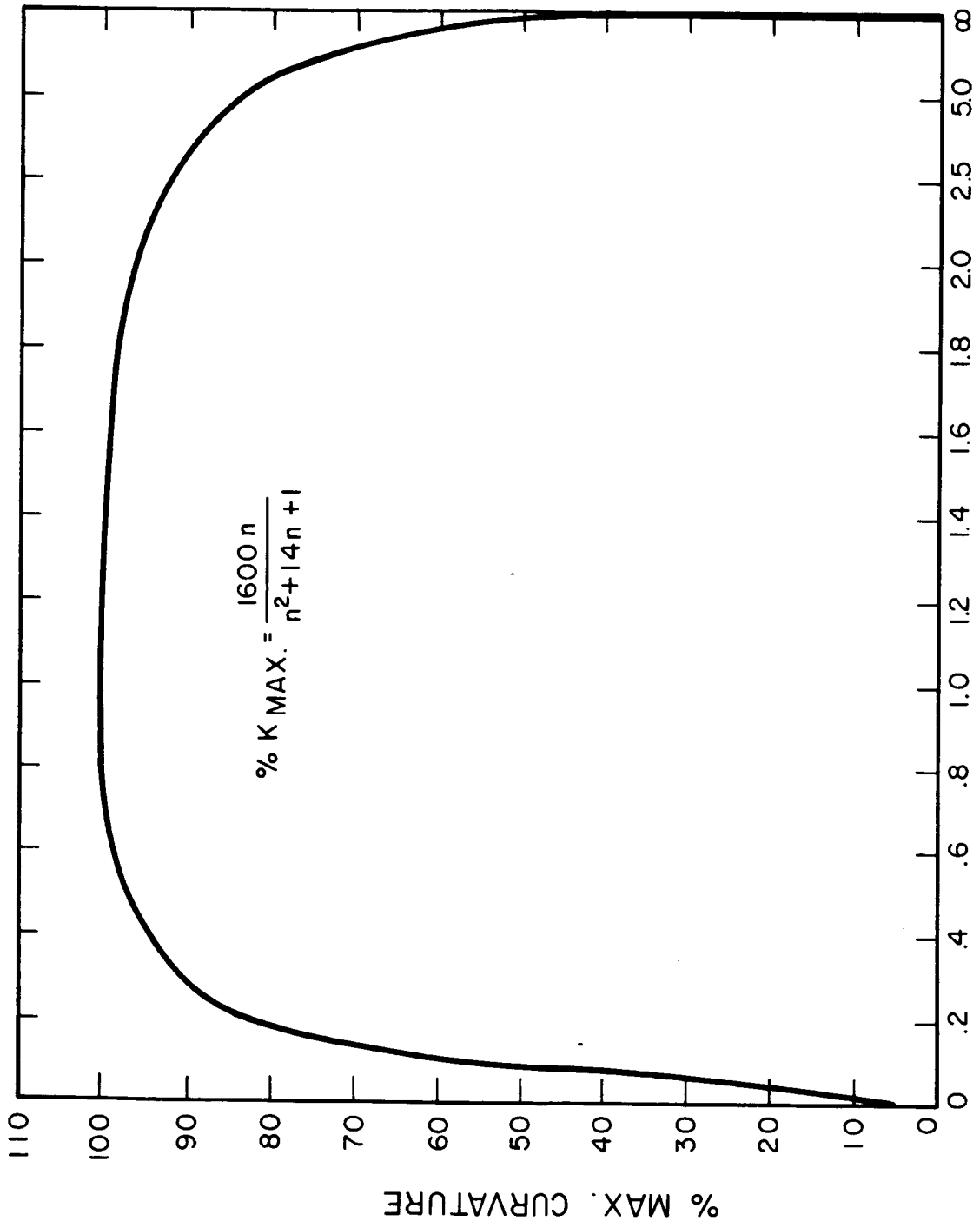

FIG. 8-10 PLOT OF MAXIMUM CURVATURE VS RATIO OF ELASTIC MODULI FOR EQUAL THICKNESS

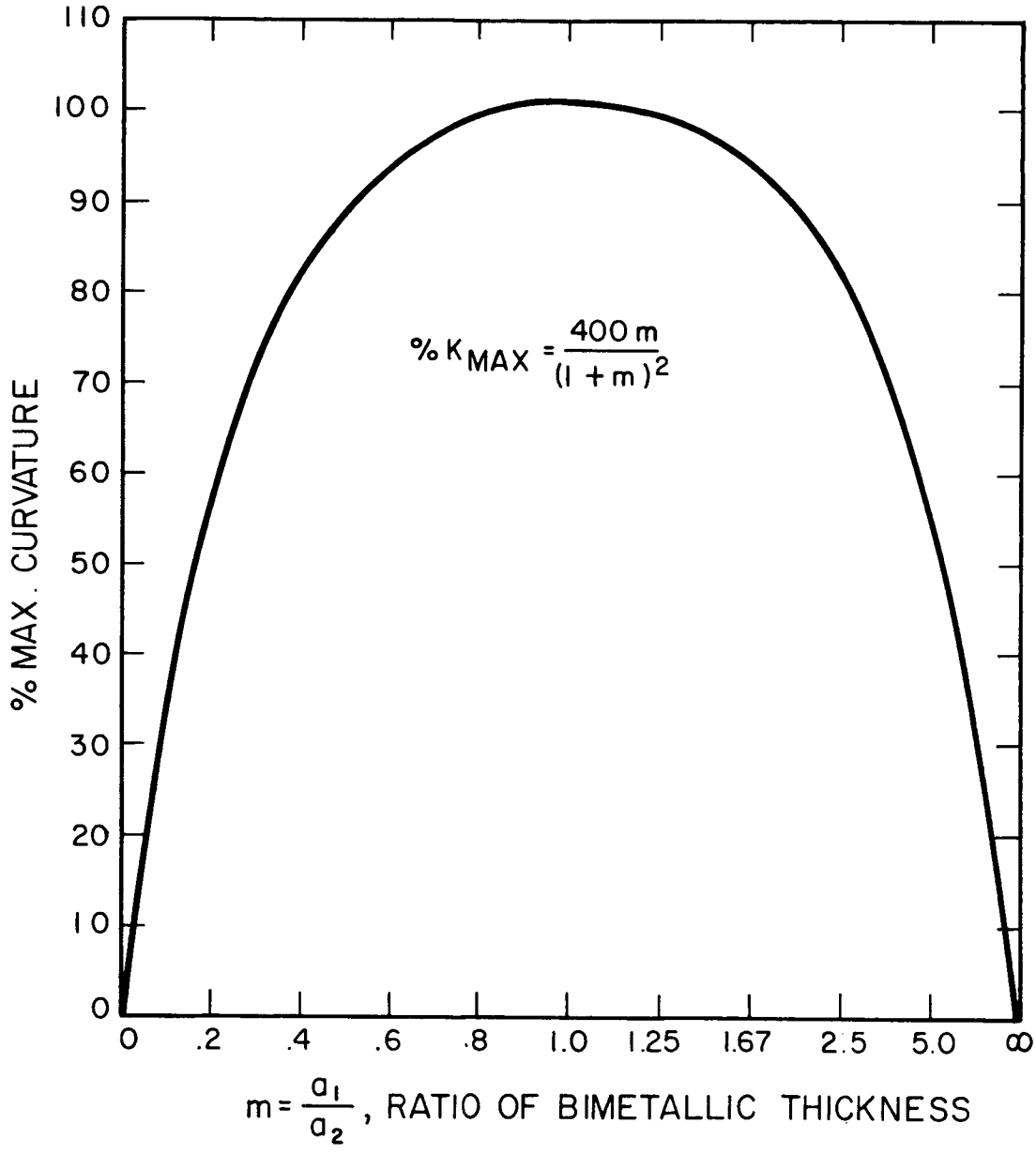

FIG. 8-11 PLOT OF MAXIMUM CURVATURE OF BIMETALLIC ELEMENT VS THE RATIO OF THE TWO THICKNESSES FOR THE CASE WHERE THE MODULI OF ELASTICITY ARE EQUAL

though it is possible to compensate for mismatch of moduli of elasticity by increasing material thickness, it is usually better to keep the 1:1 thickness ratio than to modify it. The net deflection is usually greater.

The coefficients of thermal expansion for most bimetallic operators are nearly linear up to 200°C. Usually, the manufacturer of these materials will provide curves or charts which contain the values over the permissible useful range of temperatures. In computing the deflections for specific applications, an average coefficient is used; it is not often necessary to integrate the affects of temperature for a more accurate value.

In applications of bimetallic operators, the deflection of the unit must produce a force. Some of the heat absorbed produces the deflection and some of it produces a force. If F, the flexivity of the material is considered a measure of the rate of deflection, then it can be shown that

$$B \propto \frac{F\Delta T_B L^2}{h} \qquad \text{(Ref. 8-1)}$$

and

$$P \propto \frac{EF\Delta T_p wh^2}{L},$$

where B = deflection, inches
F = flexivity
L = length, inches
h = thickness, inches
ΔT_B = temperature change to produce deflection, F
ΔT_p = temperature change to produce the operator force, F
P = force, lbs
E = modulus of elasticity, psi
w = width, inches

Note that the thinner the operator, the greater the deflection, and the greater the length, the greater the deflection.

The product of the two above equations is

$$BP \alpha EF^2 \Delta T_B \Delta T_P whL$$

but $whL = V$ = volume

$$BP \alpha EF^2 \Delta T_B \Delta T_P V$$

For equal values of force and deflection, B and P, and for the same temperature range,

$$V \alpha \frac{1}{EF^2}$$

The volume of active material is inversely proportional to the $E F^2$ value of the materials. It is also inversely proportional to the manner in which the temperatures are allocated between deflection and force, that is,

$$V \alpha \frac{1}{\Delta T_B \Delta T_P} .$$

Since ΔT_B and ΔT_P are the component parts of the temperature difference which cause the bimetallic to deflect and to exert a force,

$$\Delta T_B = \frac{x}{1-x} \Delta T_P$$

where x = percentage of ΔT_B of total temperature range. Then,

$$V \alpha \frac{1-x}{x(\Delta T_P)^2} , \text{ and also, } V \frac{x}{(1-x)(\Delta T_P)^2}$$

Per unit temperature change, $V \alpha \frac{1-x}{x}$ and $\frac{x}{1-x}$.

Figure 8-12 is a plot of this equation, and indicates clearly that for maximum utilization of material--minimum volume for maximum deflection --the temperature difference for deflection should be maintained equal to the temperature difference for force.

The affect of operator width on performance is empirical and quite small. The corrections for width are obtainable from material manufacturers' catalogs and specifications.

Flexivities for various bimetallics are obtained by a standard ASTM test and the values are also available in suppliers' manuals.

Bimetallic operators are made in three main types -- coils, strips, and formed parts. The coils are further subdivided into spirals, helices, and double helices. The spiral and helix are usually used where rotary motion is desired; the double helix where linear motion is wanted. However, there is some longitudinal motion with a helix coil and some rotary with a double helix. Straight line motion is obtainable from a simple beam, cantilever beam, C-shape and multiple C-shape formed by welding reversed bimetallic lengths. This list by no means exhausts the different possible combinations.

Bimetallic operators have the following advantages:

1. Low mass and relatively small heat absorption for operation.
2. Short thermal lag.
3. High reliability, if operated within the design limits.

Bimetallic operators have serious limitations, too. They are:

1. Upper limit of operating temperature is approximately 575^{o}C.
2. Operator force and stroke is fairly low.
3. Linkage is required to connect operator to item being operated on or moved.

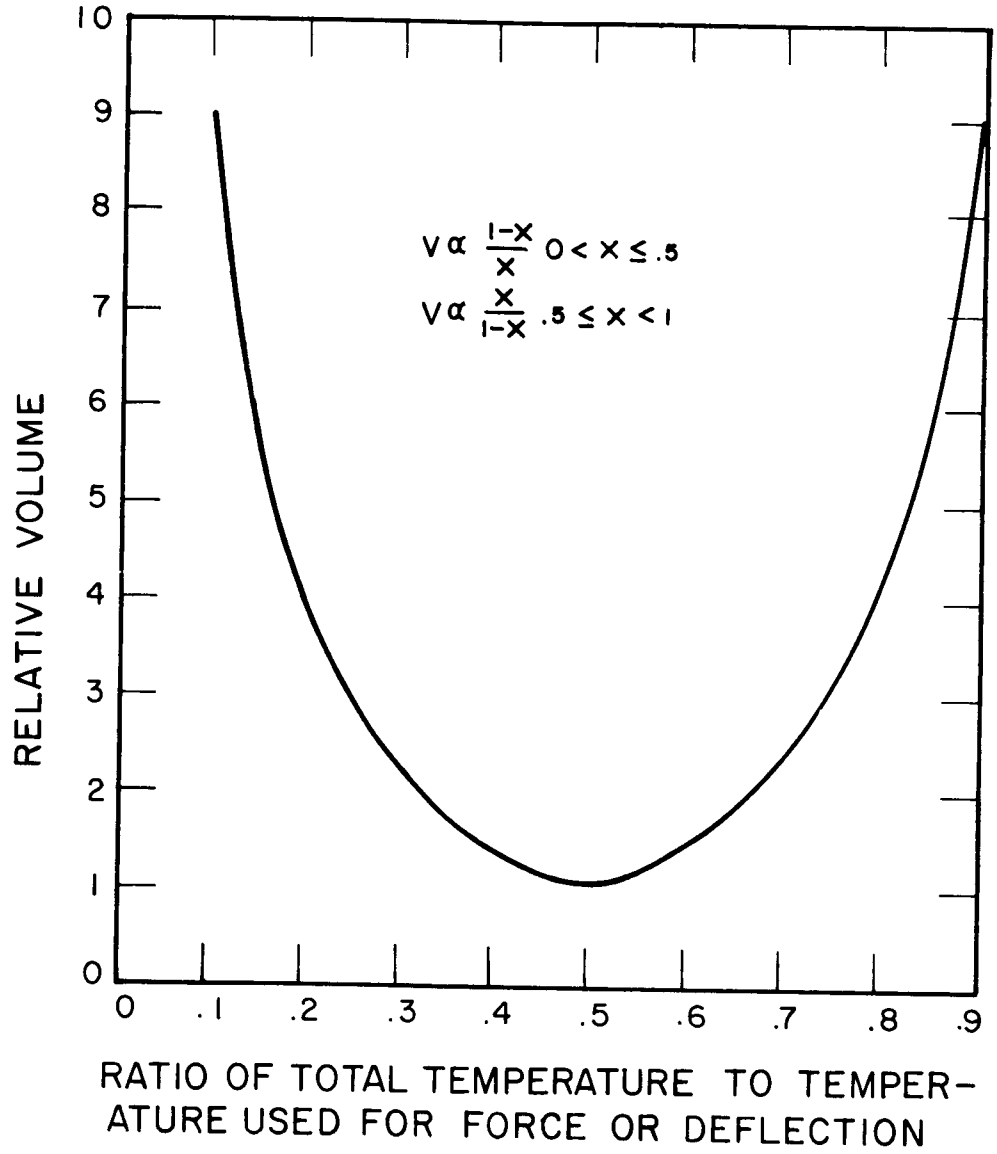

FIG. [illegible] BIMETALLIC RELATIVE VOLUME REQUIREMENTS FOR DIVISION OF TOTAL TEMPERATURE CHANGE REQUIREMENTS BETWEEN FORCE AND DEFLECTION

Bourdon Tube Operator

In principle, a liquid or gas-filled bent tube of noncircular cross section and sealed at one end will, when subjected to a temperature change, and hence an internal pressure change, distort from its original shape. The internal increase in pressure tries to make the tube become more circular. This results in a motion of one end of the tube, if the other end is fixed. The motion of the free end is called "tip travel". When the tube is formed into a C, a helix, or a spiral, it becomes a bourdon tube operator.

Because exact analyses of the behavior of a bourdon tube under pressure and temperature is extremely complicated, bourdon tube design has been based on empirical equations. A typical equation for a flat cross section is

$$\Delta a = 0.05 \frac{aP}{E} \left(\frac{R}{t}\right)^{\frac{1}{5}} \left(\frac{A}{B}\right)^{\frac{1}{3}} \left(\frac{A}{t}\right)^{3} \quad \text{(Ref. 8-3)}$$

where Δa = angular deflection of tip, deg

a = total angle subtended by the bourdon tube, deg

P = differential pressure between inside and outside of the tube, psi

E = modulus of elasticity of the tube material

A, B = cross-sectional dimensions of the tube, inches.

t = thickness of tube material, inches

R = radius of curvature of the tubing, inches--a constant for helical and C-type units, a variable for spiral units

Both P and E in the above equation are temperature dependent. E, the modulus of elasticity, decreases for most materials with an increase in temperature, except such specialized materials as Ni-Span C [8-3]. This latter material has a constant modulus over only a temperature range of $-50^{\circ}F$ to $+150^{\circ}F$, then decreases as other metallics do. The average value of the modulus through the operating temperature range is used to compute the angular deflection.

The pressure P varies with temperature for a gas-filled bourdon tube system. In fact,

$$P = \frac{w\ r\ T}{V_o}$$

where w = weight of gas in the fill, lb.

r = gas constant of the fill, ft.-lb/lb-^{o}R (nitrogen = 55.2)

T = temperature, ^{o}R

V_o = original volume, cu. ft.

Then,

$$\Delta a = 0.05\ a\ \frac{w\ R\ T}{V_o E} \left(\frac{R}{t}\right)^{\frac{1}{5}} \left(\frac{A}{B}\right)^{\frac{1}{3}} \left(\frac{A}{t}\right)^{3}$$

A liquid filled system develops pressure changes in the bourdon tube by the differences in volumetric coefficients of thermal expansion. If 3 times the linear coefficient of thermal expansion is less than the volumetric coefficient of thermal expansion of the liquid, then the liquid will be compressed as follows:

$V_c = V_o\ (\alpha_L - 3\ \alpha_M)\ \Delta^{T}$, where

V_c = volume lost by compressibility of liquid, cu. inches

V_o = original volume of liquid, cu. inches

α_L = volumetric coefficient of thermal expansion of liquid, cu. inches/cu. inch/^{o}F

α_M = linear coefficient of thermal expansion of metal container, inches/inch/^{o}F

ΔT = temperature increase, ^{o}F

$P = K\ V_c = K\ V_o\ (\alpha_L - 3\ \alpha_M)\ \Delta T$, where K is the bulk modulus of the liquid fill. Then for the liquid-filled bourdon tube,

$$\Delta a = 0.05a\ \frac{K\ V_o\ (\alpha_L - 3\ \alpha_M)\ \Delta T}{E} \left(\frac{R}{t}\right)^{\frac{1}{5}} \left(\frac{A}{B}\right)^{\frac{1}{3}} \left(\frac{A}{t}\right)^{3}$$

The torque-gradient constant for a bourdon tube is defined as the force the tip of the tube applies as it deflects one

degree. Thus, if the torque-gradient constant is known, it is possible to determine what mechanisms can be operated with the desired sensitivity and accuracy. The torque-gradient is then determined by

$G = C \frac{P}{\Delta a}$ (Ref. 8-3), where G = torque-gradient in lb-inches/deg of deflection, C = torque gradient constant (determined by test), P = pressure in the bourdon tube, psi, and Δa = angular deflection, degrees.

Another type of rating is often used for measuring the output of a bourdon element. It is called "power rating", and is formulated from the following equation:

$W = FM$

where F = force required at the tip, parallel to the direction of motion, to restrain the element when it is acting at the pressure level of interest; M = motion of the element, unrestrained when the pressure is applied; and W = power rating or work factor element.

The bourdon tube operator has the following advantages to recommend its use as a temperature sensing device and controller:

1. Direct connection without intermediate linkage is possible.
2. Linearity is high and hysteresis low.
3. Sensitivity is good.
4. Life is long and unit is very reliable, if not operated beyond design parameters.

On the other hand, the bourdon tube has some undesirable characteristics as listed below:

1. Large thermal lag due to gas or liquid fill in bulb which would be in the high temperature zone.
2. Maximum operating temperatures below 500°C.
3. Operator force and stroke is fairly low.

Bellows and Diaphragm Operators

A bellows element is a one-piece expansible and collapsible unit, with its flexibility mainly in an axial direction.

It is obtainable as a formed thin seamless metallic tube which is deeply folded or corrugated, or it can be obtained as a series of stampings or spinnings welded together to make a corrugated bellows structure.

Bellows are available from many sources. Manufacturers' catalogs list the characteristics of the various designs they produce in a wide range of materials. They also list the maximum stroke and pressure each unit can sustain. For high reliability, bellows should be operated at pressures and strokes well below their assigned maximums. The bellows should be used under such conditions that the stress in the metal does not exceed 25 percent of the yield strength at low temperatures; at temperatures high enough to affect the modulus of elasticity of the material of construction appreciably, it is best to use the creep strength of the metal at that temperature as the stress limit.

For the general case of a spring-opposed bellows, the equation of the deflection is

$$P = \frac{d(K_b + K_s)}{A_e} \quad \text{(Ref. 8-4)}$$

where d = deflection of the bellows, inches

P = applied pressure, psi

A_e = effective area of the bellows, sq. inches,
$= \frac{\pi}{16}$ (Outside Dia. - Inside Dia.)^2

K_b = spring rate of bellows, lb./inch

K_s = spring rate of restraining spring, lb./inch

If the bellows has to actuate a mechanism that resists with a force, F lb., over a distance, S, inches, then

$$P = \frac{F + S\,(K_b + K_s)}{A_e}$$

As indicated in the preceding section on bourdon tube elements, in gas filled bellows systems, the pressure,

$$P = \frac{w\ r\ T}{V_o}$$

then, $$A_e = \frac{V_o [F + S (K_b + K_s)]}{w r T}$$

For a liquid filled system,

$$P = K V_o (\alpha_L - e \alpha_M) \Delta T$$

and $$A_e = \frac{F + S (K_b + K_s)}{K V_o (\alpha_L - 3 \alpha_M) \Delta T}$$, where K is the bulk modulus of the liquid fill.

A metallic diaphragm capsule consists of two diaphragm shells soldered, brazed, or welded together. One or more capsules rigidly connected together make a diaphragm element. The diaphragm measures pressure change by deflection. And a pressure change in the application of operators under consideration would be caused by temperature change of gas or fluid contained within the system.

The pressure-deflection relationship is given empirically in the equation,

$$d = K N (P - P_o) t^{-1.5} D^4 \quad \text{(Ref. 8-5)}$$

where

d = deflection of center of the diaphragm, inches

K = capsule constant which takes into consideration the modulus of elasticity of the metal and the shape of shell and its corrugations

P = applied pressure, psi

P_o = initial pressure, psi

D = active shell diaphragm diameter, inches

t = metal thickness of diaphragm, inches

As indicated in the discussion of bellows and bourdon tubes, P, the pressure can be obtained for a gas-fill unit from

$$P = \frac{w r T}{V_o}$$

and for a liquid filled system from

$$P = K V_o (\alpha_L - 3 \alpha_M) \Delta T$$

The deflection varies as the active diameter to the fourth power, which means that for the same pressure range, doubling the diameter increases the deflection by a factor of 16. K is affected by high temperatures, because it varies inversely with the modulus of elasticity. K can also be changed by corrugation design to yield as much as a threefold increase.

Both the bellows and diaphragm operators have the same virtues and weaknesses, the differences are so slight that they need not be enumerated. The bellows and diaphragms have the following advantages:

1. The deflection forces can be moderately large and the deflection distances great enough to eliminate the need for linkages, if so desired.
2. The operator itself need not be in the high temperature zone; only the bulb which contains the gas or fluid-fill being heated needs to be in the "hot spot."
3. The reliability of the system is high, if operated within the design limitations.
4. Linearity, hysteresis, and sensitivity are good, if the system is correctly designed and fabricated.

The weaknesses of bellows and diaphragm operators generally are as follows:

1. Thermal lag is high.
2. State-of-the-art technology limits the system to operation below 500°C.

8.3.3.2 Operators Energized by Electric Power

Two types of operators energized by electric power are the linear motor (solenoid) and the rotary motor. Each type require electric energy for motivation, This energy would have to come from the prime energy source, in this case the thermionic generator, or from some secondary source, such as an auxiliary generator or storage batteries. This latter source of power could be a provisional source, much like an automobile storage battery, which is used only for startup

and kept charged by engine or main power source so that the stored energy will be available as needed to start a new cycle.

If the auxiliary electric power source for the operator is an auxiliary small generator, the time lag before some energy would be available to the operator would be smaller than waiting for the main generator to begin producing energy. This assumes that the auxiliary generator would be also subjected to concentrated solar energy.

No matter what the energy source, the shutter position for the period when no solar energy is being reflected by the concentrator should be "safe." This means that the shutter should be masking the generator cavity as though it were in the position of maximum flux. Thus, on acquiring the sun's image in the worst case - near the earth - the cavity would not run the danger of being degraded by excessive flux absorption before the controls had a chance to react; or if by failure of one or more parts to operate properly, the entire system would degenerate to uselessness.

Linear Motor Operator

Linear or solenoid operators provide only two-position operation. Although they can be made to operate a mechanical stepping device which would provide more than two positions of the shutter, the complications of such a device, especially for space vehicle application, are an unnecessary burden, if other simpler systems are available.

A two-position shutter as operated by a solenoid would provide the simplest type of temperature control, known as "on-off" control. In the open position, the aperture presented to the solar collector would be the maximum necessary to generate the required power under the minimum solar energy conditions, in the closed position, the aperture would be only about 1/3 as large as the open position - just large enough to admit a percentage of the concentrated energy near the earth continuously without overheating the generator.

The advantages of a linear operator are as follows:

1. It is a simple, very reliable device.
2. Large forces and long strokes are possible.
3. Since it does not use heat as energy source, it need not not be subjected to high temperature.
4. The operator would be designed with an opposing spring, and hence would be fail safe.

The weaknesses of a solenoid operator are as follows:

1. Because it uses electric power, it requires a converter which turns heat into energy.
2. The solenoid plunger would slide in linear bearings, a severe problem in interplanetary space.
3. Only on-off type shutter control is possible with this operator.

Rotary Motor Operator

Rotary electric motor operators usually consist of electric motors, a gear reduction unit and output shafts to each of which is fastened a lever arm. The driving motor size depends on the actuation requirements. The motors can be unidirectional or reversing, and may incorporate mechanical brakes to prevent overrunning.

There are four general types of rotary motor operators: two-position types, multiposition types, reversing floating types, and proportioning types. The basis for their selection depends on the sensing element and the type of control system with which they are used.

Two-position rotary motor operators may be either unidirectional or a reversing type. Like the linear operators, they travel toward and stop only at either extremes of travel. This action is accomplished by holding and limit contacts which are part of the motor circuit.

Multiposition rotary electric motor operators are of the reversing type and are similar to the two-position type, except that they are provided with one or more additional sets of contacts, so that they may have intermediate adjustable positions between the two extremes. Multiposition operators require multicontact control systems.

Floating-control type rotary electric operators are reversing motors which usually have limit switches at each extreme of travel. The gear reduction is very high so that the actuator travels slowly. The control instrument has a single-pole double-throw switching action with a dead neutral of adjustable width. The operation would be as follows if it were used to operate the shutters of a thermionic generator: If the cavity were becoming too hot, the control unit would pass current to motor windings which would cause the armature to rotate in such a direction as to move the shutters very slowly to a position of smaller aperture. Since the motion is very slow, thermal changes could pace with shutter position. As soon as the cavity would cool to the correct temperature, the control unit would cease to feed current to the motor. On the other hand, if the cavity were too cool, the control unit would pass current to the reverse set of windings, and the armature would rotate in the reverse direction until change was no longer called for by the control unit. Limit switches would prevent overtravel at each extreme end of stroke.

Proportioning-control rotary operators have reversible electric motors and limit switches to prevent overtravel. They also have a slidewire control resistor. The slidewire contact position is related to the operator position and moves from one end of the slidewire to the other as the actuator moves from one extreme of travel to the other. The associated control instrument has a slidewire resistor similar to the one within the operator. By means of a balancing relay, any displacement to either side of the slidewire set point causes current to flow in the motor windings so that the armature will turn to correct the inbalance.

More complex versions of the proportioning-control operators add a reset action for closer control. Others, even more complex, can be used, but their very complexity mitigates against their use.

Since the four basic rotary electric motor operators are directly associated with the particular type of control unit, an examination of their virtues and weaknesses will be limited in this section to a generic critique. Rotary electric motor operators have the following advantages:

1. They are electrically powered and hence do not have to operate in zones of high temperature.
2. Their output in torque is limited only by the available energy; their length of stroke is also high.

Electric motor operators have the following weaknesses when used in space-vehicle power generation systems:

1. They require a source of electric energy other than heat.
2. They are complex mechanisms which require rotary bearings, gears, seals, lubricants, electrical contacts, etc.
3. They are not inherently fail-safe devices. Some external means, mechanical or electrical, must be used to assure the fail-safe condition.

8.3.4 Shutter Systems

A shutter system is an integrated device which includes the shutter, the linkages, the control device, the operator, and the various associated items of hardware, such as bearings, springs, and fasteners.

8.3.4.1 Control System

Not all types of control systems can provide satisfactory performance of a dynamically functioning device which has to meet variable conditions. The open-loop control system represents the simplest type of control system. It is not a satisfactory type for a thermionic generator which requires the control of an aperture by

shutter movement. The aperture could be programmed timewise on, say, a trip to Mars to move the shutters to open up the aperture. However, because there is no feedback of information to the controller, unforeseen events or circumstances or errors of design could allow the wrong magnitude flux to enter the cavity. In order to maintain accurate control of the flux entering the cavity, the actual output or condition of the system must be monitored and compared with the desired output, which becomes the input signal. An actuating signal, mechanical or electrical, proportional to the difference between the output and the input must then be sent through the system to correct the error.

A system with a feedback path as described above is a closed-loop system. It must be noted that the output displacement cannot respond instantaneously. The system has all the characteristics of an electrical feedback system with time logs, oscillation, phase difference, etc.

Although a closed-loop system can offer more accuracy in control than open-loop system, it can also be unstable. In most feedback control systems, if the gain - the ratio of the increase of the output over the input signal - is too high, the system may tend to overshoot and overcorrect the error, and its output may oscillate unduly. An unstable system is useless. Also, when the final output of a feedback control system does not equal exactly the referenced input owing to friction or errors inherent in the feedback system, the system may have a steady state error. Feedback control systems must be designed as a compromise between stability and accuracy.

8.3.4.2 Types of Controls

Closed-loop control systems have two important features of control: (1) the feedback and control signal and (2) the response of the controller to the signal or its mode. The feedback system may be classified in a number of ways, some of which are as follows: (1) continuous-data feedback control, (2) relay-type feedback control, and (3) sampled-data feedback control.

Continuous-Data Feedback Control. In continuous-data feedback, the signal is a continuous function of time. The continuous data may be modulated, in which case it has an a-c carrier signal, or, if unmodulated, the feedback control is called a d-c system. In the latter system the feedback signal is steady state or of low frequency.

Relay-Type Feedback Control. In a relay-type feedback control system, the full power for correction is applied as soon as the error signal is large enough. The feedback control signal is an on-off type, and makes the entire control system nonlinear.

Sampled-Data Feedback Control. In a sampled-data feedback type system, the control signal is sampled at intermittent intervals. The signals are in the form of a pulse train. A radar tracking system is an example of a sampled-data system, because information on the azimuth and altitude is in the form of pulsed-data from the scanning operation.

8.3.4.3 Modes of Control

There are at least six common modes of control. Each of them is applicable to processes to be controlled with varying degrees of closeness of control. Each mode of control will cause the process to perform in such a manner that the output will follow any rate change at a certain speed and will have a certain inherent amount of lag or dead time. Each mode of control is inherently best suited for certain process changes, which may be small and slow, small and fast, large and slow, large and fast, or any other possible permutation.

The six common modes of control are two-position, floating, proportional, proportional plus reset, proportional plus rate, and proportional plus reset plus rate.

Two-Position Mode. On-off or two-position mode of control is the simplest. In two-position control, the final control element is quickly moved to one of two positions (high or low,

or open or closed) when the controlled variable deviates a predetermined amount from the set point of the controller.

In general, two-position control functions satisfactorily between the desired control limits of a given process if the service requirements are a slow reaction rate and minimum lag or dead time, and if the operator adjusts the position of the controlling device so that it permits an input slightly above (on position) or slightly below (off position) the normal operation.

Although two-position control will accommodate load changes to some extent, such changes must not occur rapidly. As the load changes, it is possible for the controlled variable to deviate markedly before it is reestablished by cycling. Cycling time at the new load will vary, too, and its average value will be higher or lower, depending on the direction of load change.

Floating Mode. In the floating mode, the final control element is moved gradually at a constant rate toward either the open or the closed position as may be required to control the variable and keep it within the neutral zone. The final control element moves at a much slower rate than the final control element of a two-position controller.

In floating control, there are no fixed positions for the final control element. The element can assume any positions between the extremes. When the controlled variable is outside the neutral zone of the controller, the final control element travels toward the corrective position until the controlled variable is again in the neutral zone, or until the controller reaches its extreme position.

Floating controls are usually found in electrically operated systems. They tend to produce cycling of the controlled system. If the operator were to move too fast, two-position control would result; if the operator were to move too slowly, the control system would be unable to keep pace with changes. Thus, the rate of operator motion with the most rapid anticipated changes that can occur

within the system. The greatest advantage of floating control is the smoothness with which gradual changes are met.

Proportional Control. There are two types of proportional control: (1) proportional-position action which is generally called just "proportional control," and (2) average-position action, generally called "time-proportioning control."

In proportional control, the final control element assumes a definite position for each value of the controlled variable. For each change of the controlled variable, the operator changes its position by an amount which is proportional to the change of the variable.

The time-proportioning control mode, which can be provided by an electrically-operated controller, is an off time and on time rather than a position of the final control element. The on-off time, are proportioned to the value of the controlled variable. For each value of the controlled variable there is a definite on-off cycle. The length of the on plus off cycles is constant through the entire range of the controller; only the ratio of on-to-off time varies within each cycle.

For flexibility in application of electrically-operated controllers, a calibrated adjustment called the "proportional band" is usually provided in both types of proportional controllers. The proportional band is that range of the final control element in proportional-position control, or to the percentage of an on-to-off time in time-proportioning control. The band is usually expressed as a percentage of the full-scale range of the controller.

The size of the proportional band will influence the size of correction which the controller will dictate for a deviation from the set point. The formula for percent of motion for the operator, $S = \frac{\Delta T}{P} \times 100$, where ΔT is deviation from set point in degrees, and P = the length of the proportional band in percent of total instrument range. Thus, for a change of one degree, the operator motion in percent

of total motion from one extreme position of the operator to the other extreme is inversely proportional to the proportional band.

Proportional Plus Reset Mode. The set point of a controller is at some intermediate value of the controlled variable within the proportional band, usually at or near the middle. With load changes or changes of operating conditions, it is helpful to change the range of the operator. This can be accomplished by an automatic reset action incorporated in the electrically operated controller.

In proportional control, there is only one position of the final control element for each value of the the controlled variable with the proportional band. If the new position of the operator is not sufficient to compensate for the conditions, then the automatic reset shifts the proportional band upward or downward as may be required to meet the new conditions.

Proportional Plus Rate Mode. If the process to be controlled has a large dead time or a high transfer lag, even the proportional plus reset mode of control is unsatisfactory. The proportional band must be set exceptionally wide and the reset rate unusually slow to avoid excessive cycling. These cause wide deviations and long time periods for return of controlled variable to the set point. The addition of rate action to proportional control may solve the problem.

Rate action initiates a large corrective action for a deviation. Then, after the controller has made the large initial change, it reduces the first change to the corrective change of a proportional band response to determine the position of the final control element or operator. The extra change tends to counteract the unfavorable effect of process lag. It is a temporary overcorrection proportional to the deviation from the set point.

Proportional Plus Reset Plus Rate Action Mode. The proportional plus reset plus rate action mode of control adds one more control factor to the proportional plus rate action mode discussed above. It adds the reset factor. The proportional plus reset plus rate

action mode produces operator response in proportion to (1) the deviation of the controlled variable (proportional action), (2) the size and time length of the deviation (reset), and (3) the rate of change of the controlled variable (rate action).

8.3.4.4 Operator and Type of Control

Heat-Energized Operator and Type of Control. A heat-energized operator, be it a bimetallic strip, bourdon tube, or a bellows unit, is a closed-loop combination device. It senses change of temperature and at the same time is the operator and controller. It has its own built-in continuous feedback and also is a proportional control device. For every deviation from the set point, the controller has one, and only one, position. The operator can act either directly or through a linkage. In fact, the heat-energized operator is a complete control system in itself. It can be made to monitor more than one variable by the use of combinations of two or more heat-energized operators attached by common linkages to the controlled element, which in the case under discussion is a shutter.

Electrically-Energized Operator and Type of Control. Both electrically-energized types of operators, the linear and rotary motor, require a sensing device to feed back a signal to the controller that the temperature is deviating either above or below the set point. This sensor performs its role in the manner of a relay-type data feedback system.

If a linear electrically-powered operator is the actuating device, only an on-off electrically operated controller can be used. Actually, the controller would be in the form of a relay. The error signal from the temperature sensing device (probably a thermocouple) would travel through the coil of a sensitive relay which would feed electric power from the thermionic generator or auxiliary power source to the linear operator coil. The operator armature would move to its extreme position to change the shutter to the wide open position. As soon as the

error signal from the thermocouple sensor was cancelled out by the temperature increase, the relay contact would disengage and the shutters would return to the minimum aperture position.

The rotary electrically-powered operator, on the other hand, could be fitted with any of the 6 modes of control devices as noted in Sec. 4.3. The aperture created by the shutter could be controlled as closely and as precisely as desired by use of progressively complex modes of control. Of course, the controlling device and the operator would require electrical energy either from the thermionic generator or an auxiliary device.

8.3.4.5 Mechanical Components of Shutter System

All mechanical components of the shutter system must meet the test of reliability. If they are to be reliable, the components must not degrade under the operating condition of high temperature in a high vacuum and the nonoperating conditions of space vehicle environment during storage, terrestrial shipment vehicle takeoff and ascent, and, finally, deployment in orbit.

Bearings. To eliminate the problems of lubrication and the sliding of one surface over another in space, only flexure type pivots should be used. See Fig. 8-13 for a pictorial representation of their construction.

The pivots have no friction because the moving parts are connected by flexing springs. This eliminates lubrication and seal problems. Performance is stable and highly reliable over a wide temperature range. Angular rotation is almost directly proportional to the applied torque. The pivots have a long service life if used within recommended loads and angular rotation.

Materials of Construction. Materials of construction pose many problems. For example, the material to be used for the shutter must be refractory enough to withstand the concentration of solar energy it intercepts, particularly during periods of maximum solar intensity, as may be encountered near the earth. During the period it is

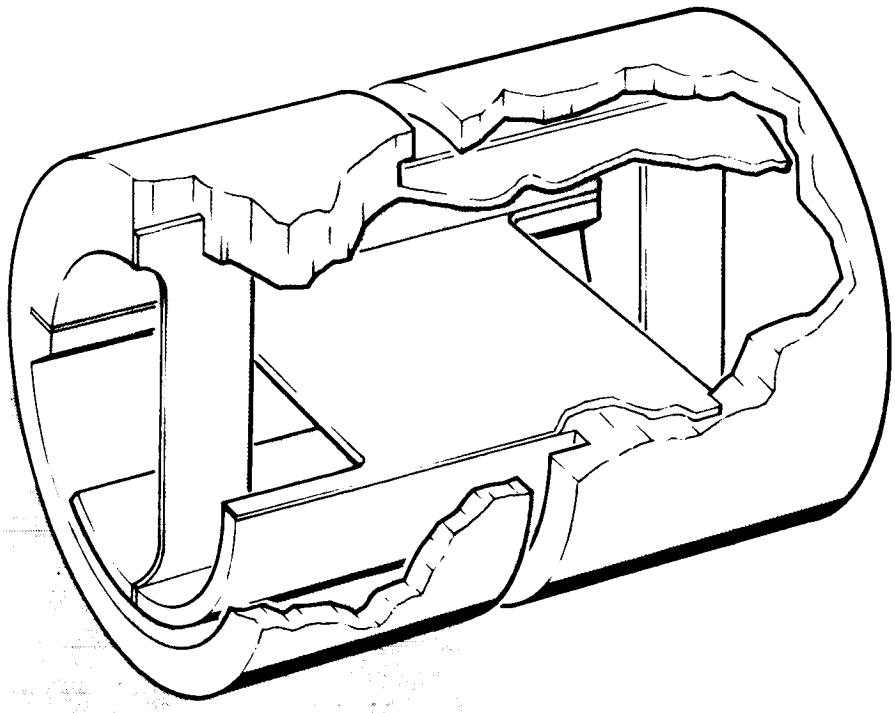

FIG. 8-13 PICTORIAL REPRESENTATION OF A BENDIX FREE-FLEX® PIVOT. (NOTE THAT MOVING PARTS ARE INTERCONNECTED ONLY BY FLEXING SPRINGS)

being so heated near its extremities, the shutter must not deform geometrically or degrade metallurgically despite the fact that it is in high vacuum environment. Since the shutter must have a low mass, it must be made of thin gage material. It would also be better if the shutter were to have a very low coefficient of absorptivity; that is, reflect to space most of the intercepted unneeded energy. Thus, the shutter and its attachments could operate at somewhat lower temperatures. Yet the shutter must be strong enough to withstand the rigors of takeoff with its attendant twin sources of stress due to vibrations and acceleration.

To choose a shutter material, it is important to know what temperature will be encountered by the shutter. To simplify the task certain assumptions must be made. First, the shutter tip is heated only by the radiant flux from the mirror because it is assumed that the temperature of the tip is approximately the same as the cavity temperature. Second, the plane of the shutter is always parallel to the collector focal plane - a condition that is most nearly met by the clam-shell-type shutter. Third, the worst case is when the shutter must intercept 2/3 of the solar flux available just above the Earth's atmosphere, namely 430 Btu (hr) (sq. ft). Fourth, the shutter "sees" only the mirror whose temperature is so small that it may be neglected in computation.

Then in the steady state condition for the worst case,

$$\alpha\ 2/3\ QA_m = \sigma F_e F_a A_s (T_s^4 - T_m^4)$$

where

α = absorptivity of shutter

Q = energy input from the sun = 130 w/ft^2

A_m = projected area of the mirror, sq. ft.

σ = Boltzmann's constant

F_a = configuration factor =

$$1/2 \quad 1-\left[\frac{1-\left(\frac{D_m}{f}\right)^2}{\sqrt{1+\left(\frac{D_m}{f}\right)^2}}\right] = 0.615 \text{ for a 5' mirror}$$

D_m = mirror diameter in feet and f = focal length in feet

F_e = emissivity factor = $E_1 E_2$ where E_1 = emissivity of the mirror and E_2 = emissivity of the shutter

Assume each = (0.5), then $F_e = 0.5 \times 0.5 = 0.25$

$F_e = 0.9 \times 0.9 = 0.81$

A_s = area of shutter to intercept the energy, determined by geometry to be approximately 0.02 sq. ft. for a 5' mirror

T_s = temperature of the shutter

T_m = temperature of the mirror

Under the assumptions above, in the worst case, the shutter temperature is 2750°C.

Due to the construction of the shutter, the part of the shutter which does not intercept the solar flux aimed at the thermionic generator cavity acts as a radiator. The shutter conducts the heat away from the hot area according to

$$Q = k_m \frac{A_2 - A_1}{2.3 \log_{10} \frac{A_2}{A_1}} \cdot \frac{\Delta T}{x_2 - x_1}$$

where

Q = steady rate of heat flow

k_m = mean coefficient of thermal conduction over the ΔT temperature range, Btu/(hr) (°F)

A_2 = area through which heat flows at right angles at outer perimeter of shutter, sq. ft.

A_1 = area through which heat flows at right angles at edge of hot zone, sq. ft.

$\Delta T = T_2 - T_1$ = temperature difference of hot zone to tip, ^{o}F.

X_1, X_2 = distance of hot zone boundary and shutter tip from center of the shutter cavity, ft.

Radiation from the radiation surface is

$$Q = \sigma F_e F_a A_s (T_s - \frac{\Delta T}{2})^4$$

If some probable values are substituted into this equation, such as $k_m = 92.5$ for tungsten, $F_e = 0.45$, $F_a = 1$, etc., then $\Delta T \approx 900^{o}C$. The temperature on the shutter will range from $2750^{o}C$ to $1800^{o}C$ for this case. These numbers are only ballpark but illustrate the problems.

Such high temperatures developed within the shutter can be reduced by relatively small percentages by adjusting values for emissivity, the so-called "view factor," F_a, changing the area of shutter which intercepts the flux, and other parameters. It is possible to live with such high temperatures in space, if the proper base material is selected for the shutter, such as tungsten or tantalum which has high conductivity and a high melting point.

Materials for fasteners, linkages, and bearings will have to withstand temperatures perhaps as high as $500^{o}C$. These temperatures will not place a severe burden on material selection. However, care must be exercised in design to allow for compensation for high temperature gradients which may exist.

Materials for use for heat-energized operators - bimetallic strip, bourdon tube, and bellows - do not exist at present for operation above $500^{o}C$. If it is necessary to monitor temperatures beyond this range, an indirect method must be employed, such as fastening the monitor to a conductive refractory material (tantalum) in such a way that the monitor temperature will not go beyond $500^{o}C$.

Materials for electrically-energized operators are an even more complex problem than material requirements for the heat-energized operators. First there is the problem of the temperature sensor.

The sensor can be a thermocouple but long-life operation above 600°C is not probable. Second, the electric operators, linear or rotary motors, have a top operating temperature of 350-400°F. They would require shielding and good radiators to keep their ambient temperature below the maximum allowable level. The operators also have sliding bearings, gear, and seals which all have their attendant problems for operation in space. Third, the controlling devices for the operators must have materials suitable for space operation or they must be completely sealed and have sufficient radiator capability to operate without overheating. Their position on the generator package is immaterial, hence it is possible to locate them in the most convenient cool zone.

There are three important factors which affect the choice of mode of control. They are (1) stability of the control loop, (2) sensitivity of the system, and (3) the reliability of the system under all operating conditions.

Stability of the Control Loop. A feedback control loop is stable when a disturbance causes a change in the system to bring the variable to a steady, noncyclic value.

Automatic control calls for measurement of the error from the set point, comparison with the standard, corrective action to reduce the error signal to zero, and the reaction to the corrective action. This chain of energy exchanges goes through the control system and the process continuously. The process and the control system usually retard and delay these energy exchanges. Control-loop stability can be described in terms of these items of retardation in time and energy loss or gain around the loop.

Since corrections to process input must oppose changes in process output to restore the desired value of output, it means that the correction to input must be negative compared to the change in process output. Therefore, the feedback signal must be as negative as possible (-180°) with respect to the change in process output. This is known as negative feedback.

Both process and control-system resistance to response are negative phase shift in nature and add to the 180° phase shift inherent in the control system. In fact, it is possible for the out-of-phase additions could add so much lag to the 180° phase shift that the controller correction could be in phase in process output and increase it instead of opposing it.

In the energy exchanges around the loop, energy is added consumed, or gained and lost. If the added energy just equals the energy used, the gain is one. If more is added than used, the gain is more than one. Phase shift and gain define and measure stability. A control loop will be stable if the gain around the loop is less than one when the total phase shift is 360° during the corrective cycling action.

Three modes of control and combinations of the three affect stability. The basic three modes are proportional position, reset, and rate. The proportional-position mode affects stability by making it possible to adjust the gain or proportional band; the reset mode affects stability by causing a negative phase shift; and the rate mode increases stability by producing a positive phase shift, but at the same time may contribute to instability by increasing the gain excessively.

To judge how stable or how well the control system is operating, the most common criterion used is the minimum-area summation under recovery curve (Fig. 8-14). When the area under this curve is minimum, the average of the deviations has the smallest amplitude for the shortest time. It has been established that the area is minimum when the amplitude ratio between successive peaks in the cycle is 0.25, or each succeeding wave is 1/4 as big as the preceding one. This minimum area will have a phase shift of 330° when the gain is one. The match between this best case and the actual performance of the control system is the measure of performance.

Sensitivity of the System. Sensitivity is the ratio of output response to an input change whose size is specified by

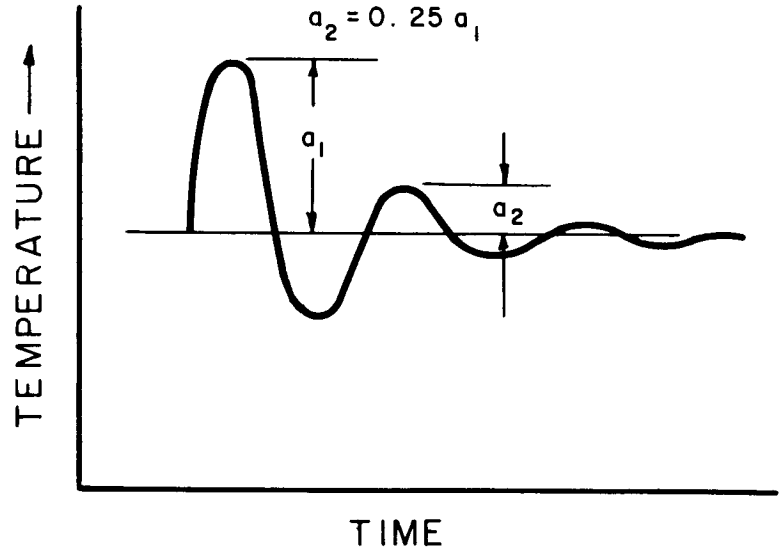

FIG. 8-1 MINIMUM-AREA CRITERION OF CONTROL SYSTEM PERFORMANCE

the requirements of the overall process. For an automatic closed-loop controller, the resolution sensitivity is the minimum change in the measured and controlled variable which produces an effective response. It can be expressed as a fraction (or percent) of the full-scale value of the variable; or it can be expressed in actual values of the variable, such as $5^{\circ}F$. In the latter form it is known as the threshold sensitivity. The range of values through which the input variable to the control system can vary without response is known as the dead band.

It is obvious that the minimum sensitivity which will meet the requirements of the process to be controlled is the desirable choice. Also, the control systems with lower sensitivities are simpler than systems with high sensitivities, because sensitivity is related to gain, and it has been shown above that the finer the gain control, the more complex is the mode of control.

In the case of the thermionic generator, it is then necessary to know how closely the electrical output must be maintained to determine the maximum allowable temperature deviation within the cavity. If this were not the controlling factor (the electrical regulation requirements may be quite low), then the maximum temperature thermionic diodes could sustain without degradation would be the controlling factor. After the mean temperature and its maximum allowable deviations have been fixed upon, the simplest control system should be selected to maintain the cavity temperature within the set limits.

It is easier to determine what the sensitivity of the control system will be in advance of the finished design, if it is possible to compare it with existing standard units available from many sources. Electrically-energized control systems, in particular, are most easily compared with what is readily procurable. Heat-energized systems are not so handily compared. They can only be judged by past performance in installations resembling the application under consideration.

Reliability of the Mode of Control. The reliability of the mode of control is related to the ability of the control to function for long periods of time without failure. Here, failure can mean catastrophic failure to function completely, or it can mean partial failure, such as an increase of hysteresis (the difference between the increasing input correction and the decreasing output correction), or degradation of the self-regulation parameter so that the deviation of the controlled variable (temperature) might be greater than allowed. Catastrophic failure is, of course, to be avoided. And it is usually easier to overcome by careful design. It is the partial failure which is so hard to anticipate and avoid, except by the usual techniques of careful design and long term simulated tests under worst condition parameters.

Intuitively, the simplest mode of control should be the most reliable, for it has the simplest input and output. If the temperature within the cavity differs from the set mean, the controller signals a constant correction. This means that the shutter would either be positioned to a condition of maximum or minimum aperture. It is easy to see that the on-off mode of control is very likely to cause much oscillation about the set point and much temperature variation.

The next step in complexity is the proportional-band mode of control. The main feature of this mode is that the corrective signal is proportional to the deviation so that a small deviation calls for a small corrective action; a larger deviation, a larger corrective action. Basically, this describes the action of heat-energized system, for as the temperature deviates, the combination sensor-controller-operator reacts proportionally to position the shutter to control the variable. The proportional position is only modified by the inherent hysteresis and sensitivity of the system. Electrically-energized operators and controllers are also available for this mode of control, as has already been indicated.

As it has been already shown, more complex modes of control for closer control are possible. These only exist as electrically-energized controllers which require electrically-energized operators. Unless closer control is required than is possible to achieve with the proportional mode of control, it is not necessary to discuss the reliability of these more complex modes. Although it is impossible to predict in advance what the maximum range of the deviation of temperature from the set point will be for any system plus or minus 10 percent, if acceptable, is not all unlikely for this mode.

8.3.4.7 Control System Selection

It has been indicated that if an approximately plus or minus 10 percent temperature variation can be tolerated, the proportional mode is the type to use. What remains yet to be done is to indicate the order of preference for heat-energized or electrically-energized systems. After this comes the choice of operator. Then comes the implementing of the choice to optimize the design.

It is possible to argue that both systems can be designed and built equally well within present state-of-the-art knowledge, for much is known about the behavior of many materials in space. If this is so, then the reliability factor is the final arbiter of rank. Reliability is difficult to determine, because so many factors are involved. However, since overall reliability is the product of the reliability of the parts, the heat-energized system seems to be more reliable simply because it has fewer components. In the heat system the sensor, controller, and operator are the same unit; in the electrical system they are distinctly separate. Intuitively, it is felt that, even with very high reliability of each of the separate components of the electrically-energized system, a higher reliability will exist for the heat-energized unit. For this reason, it is felt that the heat system should be first choice.

Heat-energized sensor-controller-operators have been described and discussed above, but were not ranked in order of

reliability and feasibility. As has already been indicated, the bimetallic strip, the bourdon tube, and the bellows suffer from the same limitations - namely, they cannot usually tolerate more than 500°C. Both the bourdon tube and the bellows units require a liquid or gas-filled bulb connecting to the bourdon tube or bellows. These two devices have more thermal lag than a bimetallic strip, hence could cause larger deviations, more cycling, and take more time to reach a steady state. Therefore, the bimetallic device is considered to be the first choice.

Assuming that a bimetallic control device is the unit which will be used to control the shutters of the thermionic generator, it is now necessary to devise a design to fulfill all the requirements in detail so that the device will have the greatest reliability. To explain further, assume that the sensor-controller-operator (the bimetallic element) were placed in the cavity, and that this is the only controlling action. Then, it is possible, given any disturbance to the process such as loss of lock on the sun and eventual relock, that the cavity may overheat due to the large gain in the system. A system is needed which will adjust the gain or proportional band in fine increments, a vernier adjustment.

If the primary bimetallic device were placed in such a position that it would "see" the sun at the same time that the paraboloidal mirror sees it, it would react just as effectively as if it were in the path of the reflected energy. Such a position could be in front of a sunshade for the thermionic generator (see Fig. 8-15). The solar flux would be concentrated by a small cylindrical mirror which would not only concentrate enough energy to furnish sufficient power for the bimetallic element to operate reliably, but it would also furnish this energy in the form of a narrow rectangular image to heat the element uniformly over its length.

The vernier automatic adjustment would consist of another bimetallic element fastened at one end to a refractory strip

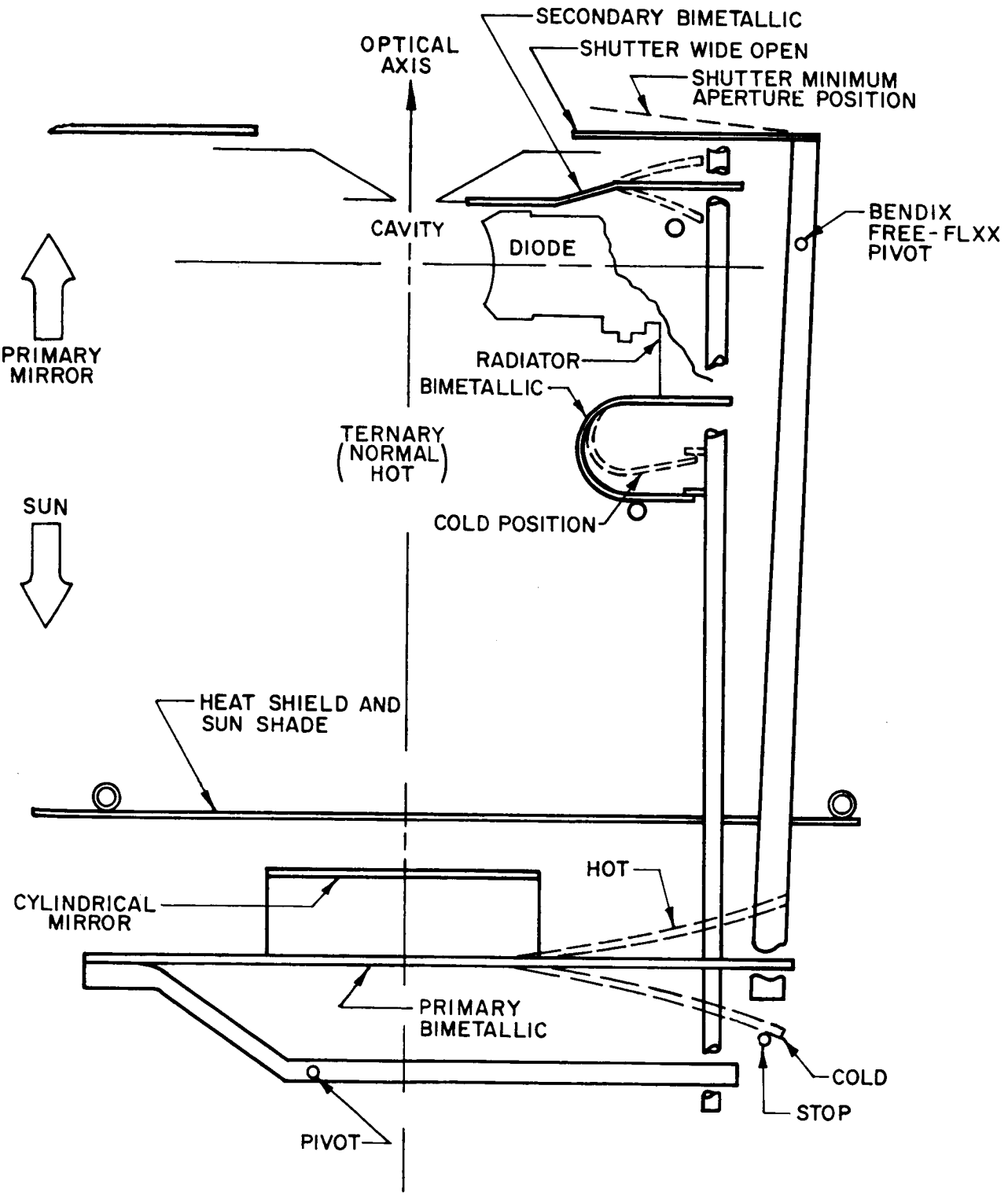

FIG. 3-13 BIMETALLIC TEMPERATURE CONTROL SYSTEM SCHEMATIC

of metal such as tantalum. The strip would project into the cavity and act as a conductor for the secondary bimetallic strip, so that the cavity temperature would be sensed at a lower scale than the cavity proper. This has to be, because, as has been already pointed out, bimetallic elements do not operate well above 500°C. By means of a lever arrangement as shown in Fig. 8-15, the cavity temperature would automatically modify the primary setting of the shutter position.

On initial startup of the generator or if a major reduction in the amount of flux the cavity should occur, the shutter would open as wide as possible. Upon acquisition of the sun's image of the primary collector, the reaction to the temperature change would be rapid. The shutters could begin to close down to limit the flux before the thermionic diodes reached their proper operating temperature. The system would oscillate until a steady state was reached. To eliminate this problem, a ternary bimetallic element would be added to the control system to override the secondary vernier adjustment. The ternary element would be attached to the diode radiator, and would, by its designed relationship with its effect on the vernier setting of the control, keep the shutter in the open longer, or until the diode was at the proper temperature.

Figure 8-15 shows the bimetallic flux-cavity temperature control system in schematic form. It is obvious that fulfillment of all system requirements has introduced complexity into the solar flux control which is undesirable.

REFERENCES

Section 8

8-1 R. M. Sears, "Fundamentals of Thermostat Metals," Materials Research and Standards, Dec 1963, pp. 981-6

8-2 S. Timoshenko, "Analysis of Bimetal Thermostats," J. Am. Opt. Soc., Vol. 2, No. 3, Sep 1925, p. 233

8-3 L. E. Smith, "Mechanical Pressure Elements," Process Instruments and Controls Handbook, D. M. Considine, Editor, pp. 3-22, McGraw-Hill (1957)

8-4 Ibid, pp. 3-14

8-5 Ibid, pp. 3-9

9. CESIUM RESERVOIR CONTROL

This section discusses the need for cesium reservoir control, the effects of passive control, and a recommended technique for active control of each individual cesium reservoir on the generator.

9.1 Need for Control - Effect on Performance

Figure 9-1 illustrates the expected variation and output current of a converter as a function of cesium reservoir temperature. The curves are extrapolated from available experimental data. Extrapolation was based on theoretical curves of diode performance versus cesium reservoir temperature derived over the past several years.

Calculations were based on the use of a 2 cm^2 diode as a typical size. The design point for the diode was 0.7 volt; for example, in Fig. 9-1 the diode will produce 30 watts at 0.7 volt at peaked cesium reservoir temperature. Based on the excited mode, operation at 0.5 volt will produce higher power outputs while operation at 1 volt will produce lower power outputs at the optimum cesium reservoir temperatures. It is believed that Fig. 9-1 represents a reasonable expectation of operation of converters in a generator with emitters at 1,700°C.

It is seen that a region of approximately ±10°C exists, at 0.7 volt operation, within which the variation of output current is small. Thus, a dead band of ±10°C appears reasonable for cesium reservoir control although ±5°C might "tune up" the converter a small amount. Advantages of higher voltage operation are shown; power output is not as sensitive to cesium reservoir temperature variation.

In general, lower emitter temperature (e.g., 1,500°C) operation also results in less sensitivity to a reservoir temperature and higher emitter temperature will result in increased sensitivity.

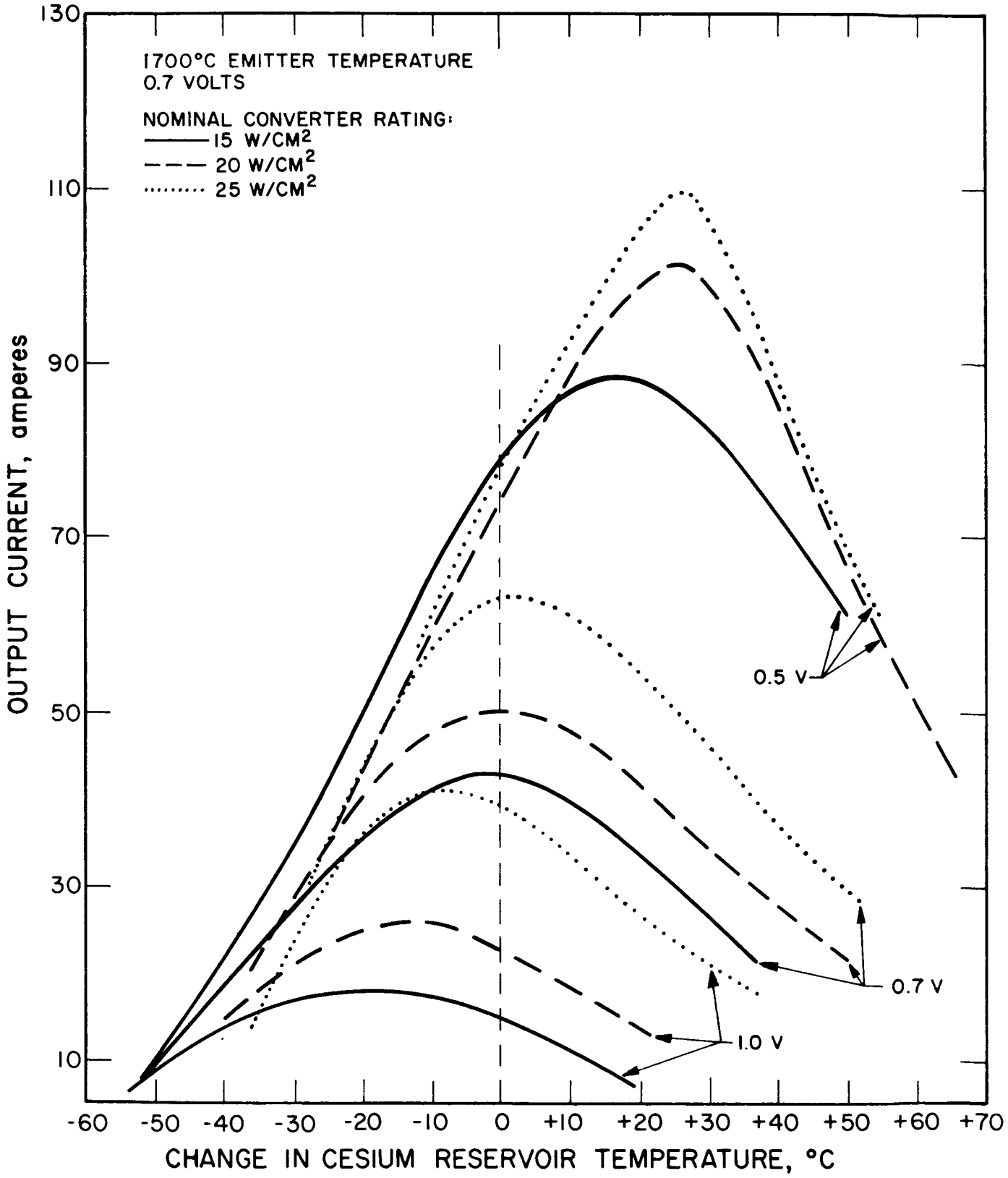

FIG. 9-1 TYPICAL CONVERTER OUTPUT CHANGE WITH CESIUM RESERVOIR TEMPERATURE CHANGE

Experimental data are not available in these regions. Figure 9-1 indicates temperature differential and not absolute temperature. For the converter of 15 watts/cm^2, it is expected that the optimum cesium reservoir at 0.7 volt will be about 380 to 400°C. For a 25 watts/cm^2 converter, it is expected that optimum cesium reservoir temperatures will be lower, about 340°C, although this has not been confirmed.

9.2 Startup and Passive Cesium Control

The passive control of cesium temperature can be approached in many ways. The reservoir receives heat from conduction down the reservoir tube and radiation from the converter radiator. The simplest concept in establishing cesium temperatures is to size the conduction path from the converter assembly to the cesium reservoir to transfer sufficient heat to just equal the heat radiated by the reservoir at the design temperature.

Passive control can be easily achieved if the converter is in equilibrium and the environment is static. This is not at all the case with an orbital application of thermionic conversion where the background radiation, concentrator radiation, converter operation, collector radiator temperatures, etc., are all varying as the system cycles through sun and shade conditions. More sophisticated controls are therefore necessary to maintain proper temperature in the cesium reservoir. Applicable techniques for passive control are:

1. Equalizing of conduction to the reservoir with radiation from the reservoir (for steady-state conditions only)
2. A conduction path modulator control using a temperature sensing or bimetallic switching circuit
3. Placement of the reservoir in a position where it will intercept a portion of the concentrator energy

The collector cycle must be maintained above the desired cesium temperature or elevated at that temperature very rapidly.

Figure 9-2 illustrates typical cesium reservoir temperature responses under various conditions. With no auxiliary heat input, a typical experimental curve is shown which illustrates the length of time required for a cesium reservoir to assume operating temperatures. As shown, up to 20 minutes might be required to achieve optimum temperatures without auxiliary heating using designs which are currently being contemplated for converters. For the experimental curve, the collector temperature was also rising at the same time as the cesium reservoir temperature; in general, the collector temperature will rise at a much faster rate.

Calculations were performed to determine the response of the cesium reservoir heater to auxiliary heaters during a period of time at startup sufficient to achieve operating temperature. It was assumed that the radiator already had achieved 400°C temperature; 5 mil copper tubing was also assumed. Startup with auxiliary heaters would occur after a collector temperature had been achieved which was above the minimum cesium reservoir temperature desired.

As shown, a 10-watt heater would require up to 4 minutes in this particular example to achieve reservoir operating temperatures. Thus, after coming out of the earth's shadow (which had lasted a sufficient length of time so that the reservoir had cooled to 100°C), at least 4 minutes would be required for complete startup. However, since the collector/radiator must come up to temperature also, a time on the order of 10 minutes is more likely.

Figure 9-3 illustrates a typical startup sequence. Startup is as follows:

1. After emergence from darkness, cesium reservoir and radiator have each reached an equilibrium temperature of about 100°C.
2. The radiator and reservoir begin to heat due to conduction from the generator cavity.
3. At 400°C radiator temperature, the cesium reservoir heater is turned on.

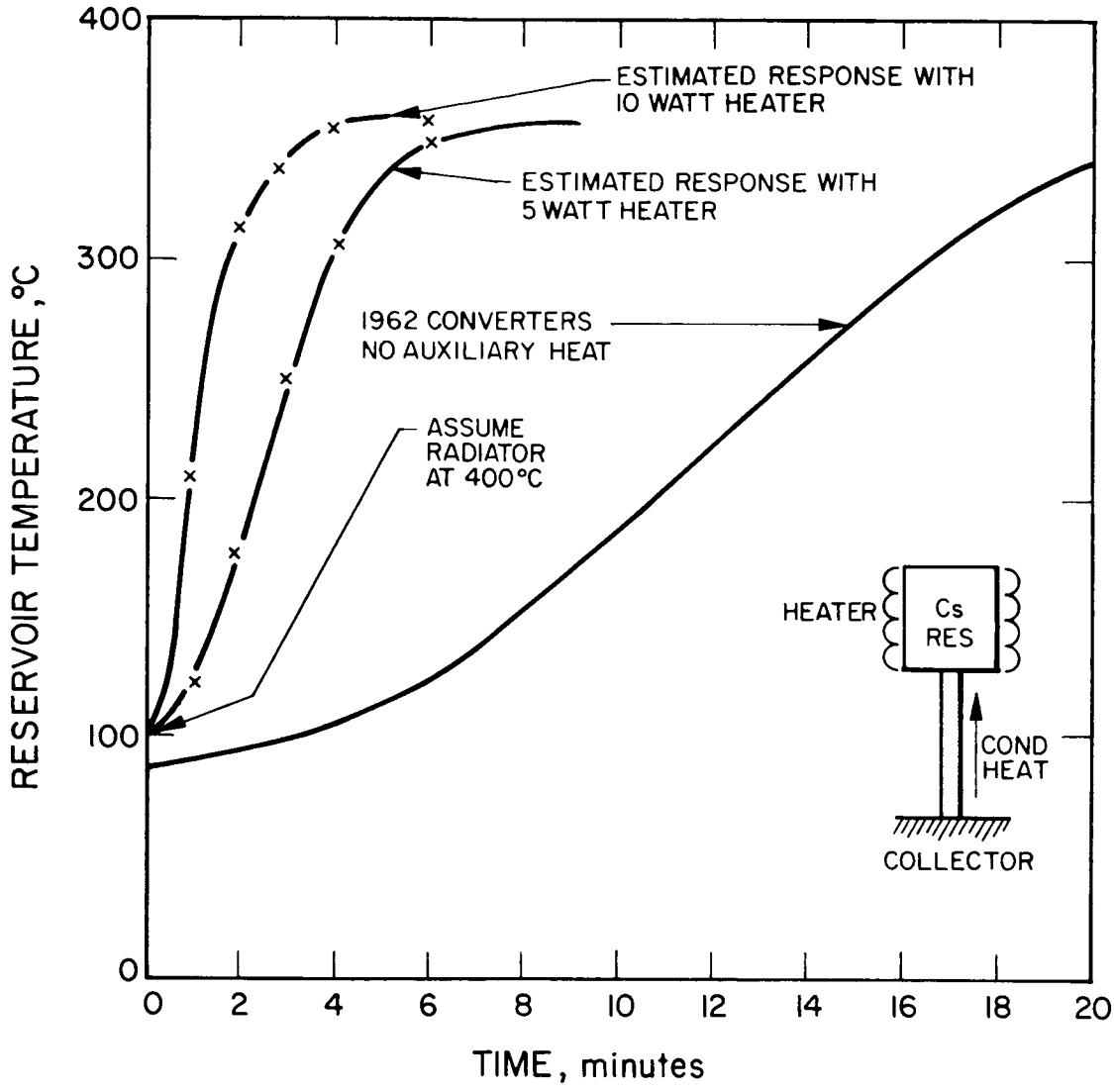

FIG. 9-2 TYPICAL Cs RESERVOIR TEMPERATURE RESPONSE

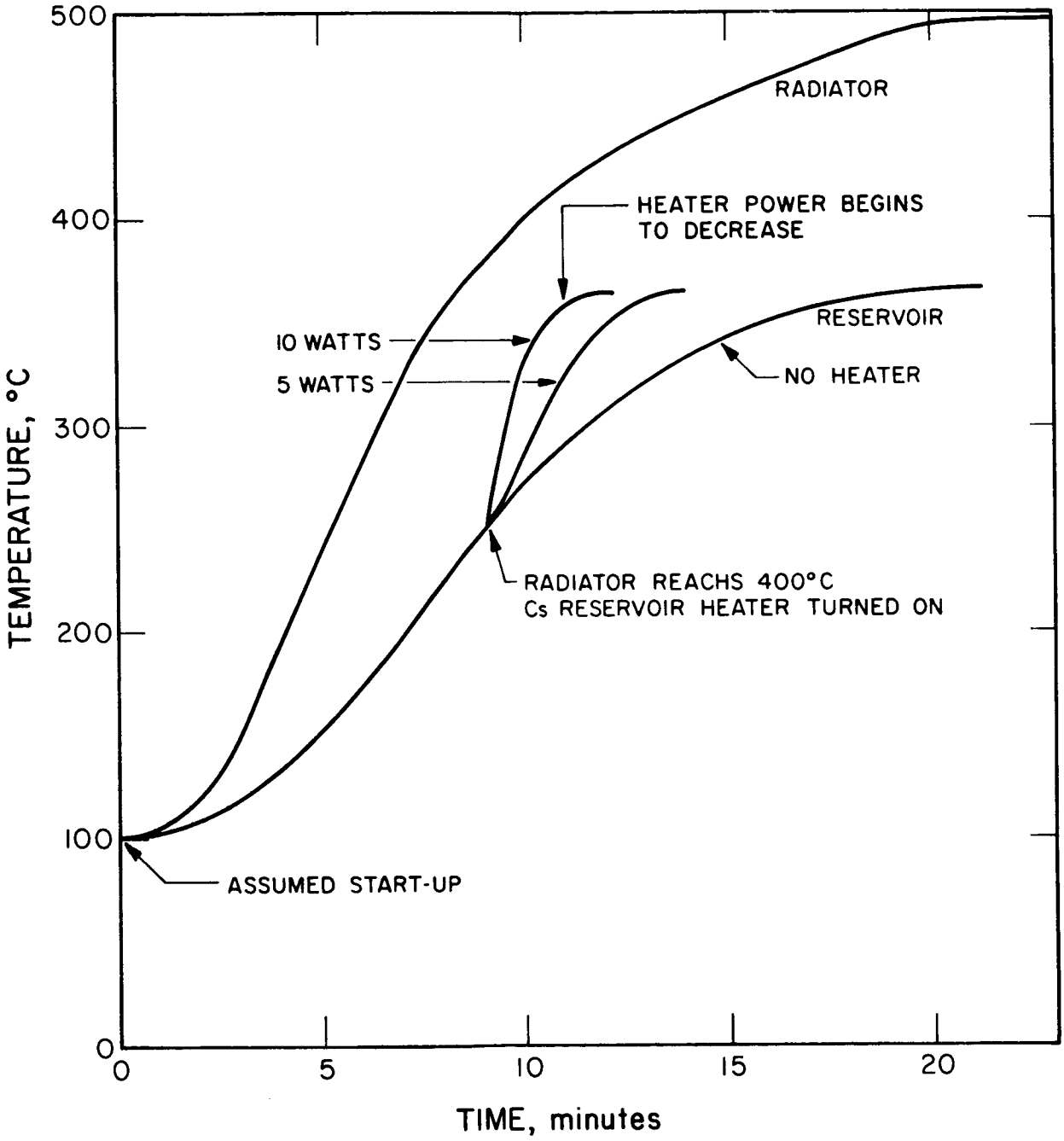

FIG. 9-3 TYPICAL STARTUP SEQUENCE

4. Depending on heater power, the cesium reservoir quickly reaches equilibrium temperature.

As illustrated in Fig. 9-3 the watt/hours required for startup can vary but approximately 1 watt/hour can be anticipated.

In conclusion, the following comments with regard to passive cesium reservoir control are applicable:

1. In an equilibrium condition, with no darkness, passive cesium reservoir control can be used and has been demonstrated in the laboratory.
2. In nonequilibrium control situation, the use of passive cesium reservoir control will result in nonoperative periods while the converters are warming up for periods as long as 20 minutes and perhaps longer. Three mechanisms are suggested for investigation to solve this problem.
   a. Active heaters
   b. Passive bimetallic or other conduction path modulator controls
   c. Use of concentrated energy to heat the reservoir - this may be difficult for "side" converters

Items b and c have not been investigated extensively and introduce complexity into converter design; however, a tradeoff occurs against the weight and reliability of the electronics.

9.3 Heater Characteristics

A most important feature of the cesium reservoir heater is the amount of power required on a steady-state basis to maintain a given cesium reservoir temperature. If active control is used, the converter should be designed so that normally, without heater power, the cesium reservoir temperature is about 10°C lower than optimum.

If variable conditions are encountered where emitter temperatures (and reservoir temperature) become higher than design point conditions, cesium reservoir temperatures without heaters should be lower; the tradeoff is the need for continuous heater power.

Figure 9-4 illustrates the heater power input requirements as a function of the required ΔT of the cesium reservoir based on cesium reservoir heaters which have been used to date in the laboratory. As shown, about 1 watt is sufficient for increasing the temperature approximately $10^{o}C$. For a 5-watt converter, therefore, 2 percent of the output would be consumed in cesium reservoir temperature control.

9.4 Active Temperature Control

Using present design approaches, it is assumed that each cesium reservoir, if actively controlled, would be controlled independently within an individual heater and individual circuits. This section compares the sensors which can be used and arrives at a recommended cesium reservoir control circuit.

9.4.1 Temperature Sensors

Three types of temperature sensors were considered for use in cesium reservoir temperature control systems. These are:

1. Wire type resistance sensors
2. Thermocouples
3. Thermistors

The thermistor is a semiconductor having a high negative temperature coefficient of resistance. If a thermistor is used in a Wheatstone bridge, the bridge will be balanced at only one temperature. At other temperatures there will be a bridge output which will be a measure of the deviation of the temperature. For the cesium reservoir application, thermistors cannot be considered due to the fact that aging at high temperatures is greatly accelerated and the reliability above $250^{o}C$ is open to question.

Thermocouples are available for use with cesium reservoir control and have been used in the laboratory.

$\Delta T_{cesium} = T_{cesium} - \text{DESIGN CESIUM TEMPERATURE, °C}$

$T_{cesium} \approx 350°C$

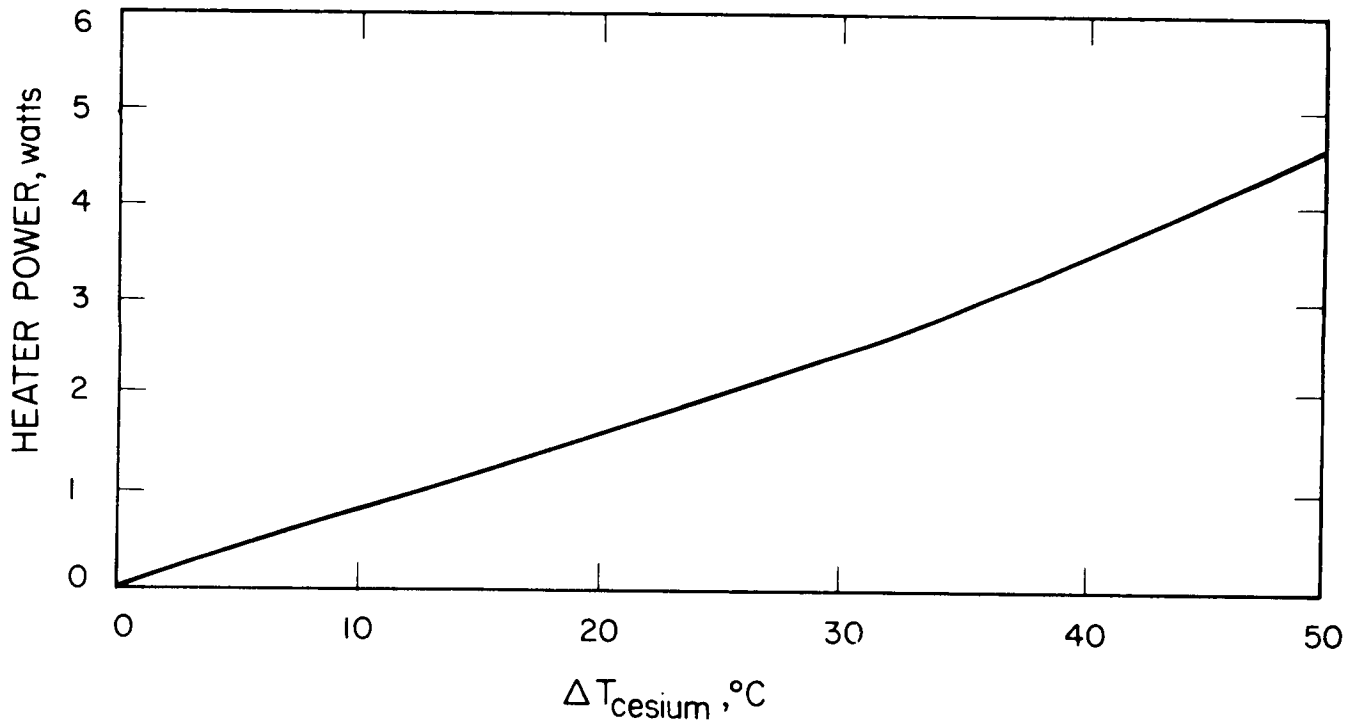

FIG. 9-1 STEADY-STATE HEATER POWER INPUT REQUIREMENT VS INCREASE IN CESIUM RESERVOIR TEMPERATURE ABOVE DESIGN VALUE

Thermocouples have the following advantages:

1. Small size
2. Linearity over a wide range, generally under 1 percent accuracy

The disadvantages of a thermocouple are:

1. The need for a reference junction. Thermocouples do not measure the temperature at a junction but rather the difference in temperature between the measuring junction and a reference junction. Either the reference junction must be held at a constant temperature or some form of compensation must be used to distinguish between changes in the measuring temperature and those in the ambient temperature. Examination of reference junctions suitable for use with chromel-alumel thermocouples indicates that a weight of approximately 1 pound would be required for 5 thermocouples.
2. Low level output. The output voltage of the most sensitive thermocouple is about 16 millivolts at 300°C. A high gain amplifier is required for use with the thermocouple to prevent drift and noise effects from affecting calibration.
3. Long-term stability and accuracy. Each thermocouple used in a system must be calibrated. Precalibration will mean an error in the measured temperature (up to 4°C). The total cumulative error, including the thermocouple and cold junction compensation can easily be as high as ±5°C. Furthermore, long term stability in a space environment at temperature is debatable.
4. Lead wire. Where long runs of thermocouple leads are required, special care must be taken to use special compensating lead wire to keep circuit resistance low and avoid unwanted thermal junctions.
5. Nonfail safe. If the thermocouple becomes disconnected for any reason, the controller turns full on unless special circuits are provided to prevent it.

A wire type resistance sensor seems most suitable for reliable temperature measurements of cesium reservoirs. However, to date, this type of sensor has not been integrated with converters in the laboratory. Integration should be fairly easy to accomplish; however, estimated costs for development of a platinum resistance sensor for operation of thermocouples on the cesium reservoir are estimated to be $300 per unit for 10 units ($100 per unit for 100 units). Nickel, nickel-iron, and platinum wires all have fairly high positive temperature coefficients of resistance. In a wire sensor, a length of wire having the desired resistance is wound into any convenient physical form and is electrically connected as one arm of a Wheatstone bridge. The output of the bridge is a measure of resistance variation in the sensor and, hence, of the temperature.

The advantages of wire type resistance sensors are:

1. High sensitivity. About 100 times the output per degree C of thermocouples.
2. Superior long-term stability. Special units have stabilities within 0.001^{o}C per year.
3. Area sensing. A wire sensor can be spread over several square inches of surface and tends to average out differences in temperature over a surface. Wire type sensors are useful, therefore, whenever it is desirable to control or measure temperature over a surface rather than simply at a particular point.
4. Linearity. Wire sensors are almost linear, a typical platinum sensor will have a nonlinearity of less than 0.3 percent over a temperature range of 200^{o}C up to temperatures of 800^{o}C.
5. Interchangeability. Wire sensors are furnished with tolerances of from 1 to 0.1 percent or better and can be interchanged without calibration.

6. Fail-safe. Wire sensors have a positive temperature coefficient, if a sensor opens up, therefore, a controller will turn off thus protecting other circuitry.

Analysis of the three temperature sensors above indicates that the wire type resistance sensors are probably best and efforts should be made to reduce the cost of these sensors for integration into converters. Platinum sensors are recommended by the manufacturer as being most applicable to the cesium reservoir application due to relatively high voltage output and better long-term stability.

9.4.2 Block Diagram and Principles of Operation

Figure 9-5 illustrates a general block diagram for a cesium reservoir control unit.

The platinum resistance thermometer senses the temperature of the reservoir by a change in resistance. The signal conditioner converts this change in resistance into a voltage suitable for use by the comparator.

The comparator samples the temperature of the cesium reservoir and comparies it to the commanded temperature. If the temperature is low, then the error signal will turn on the heater and raise the reservoir temperature. The cesium reservoir temperature is controlled by turning the heater on and off.

Several types of circuits were examined for use. If dc power is available, the circuit shown in Fig. 9-6 is applicable.

In the case where ac power is available, mag-amp and tunnel diode circuits were examined. Unless a high frequency of ac power is available (5 to 10 kc), mag-amp circuits are significantly heavier than the tunnel diode circuit illustrated in Fig. 9-7.

Figure 9-6 shows a circuit using dc power. This comparator consists of a summing circuit, a sawtooth generator, and a Schmitt trigger. The switching circuit consists of a pulse generator, gates, switching amplifier, and a matching transformer.

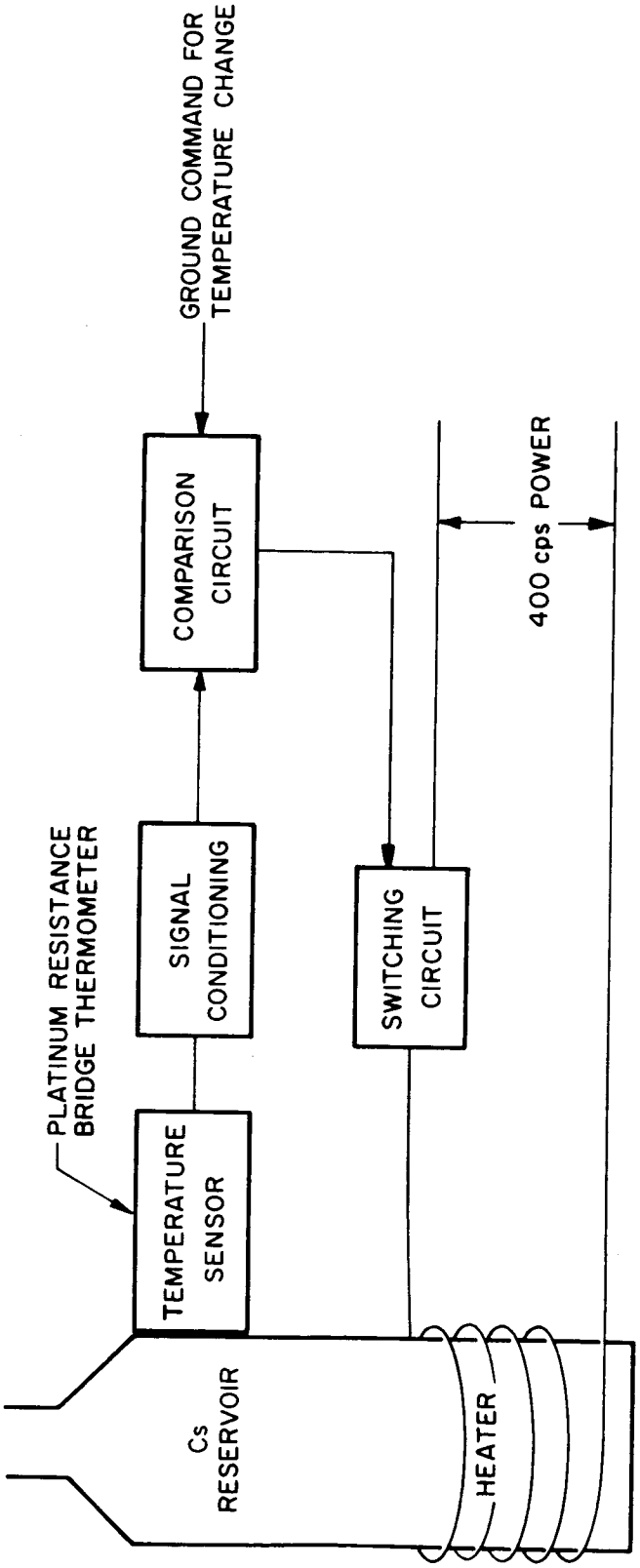

FIG. 9-5 BLOCK DIAGRAM OF Cs RESERVOIR CONTROL

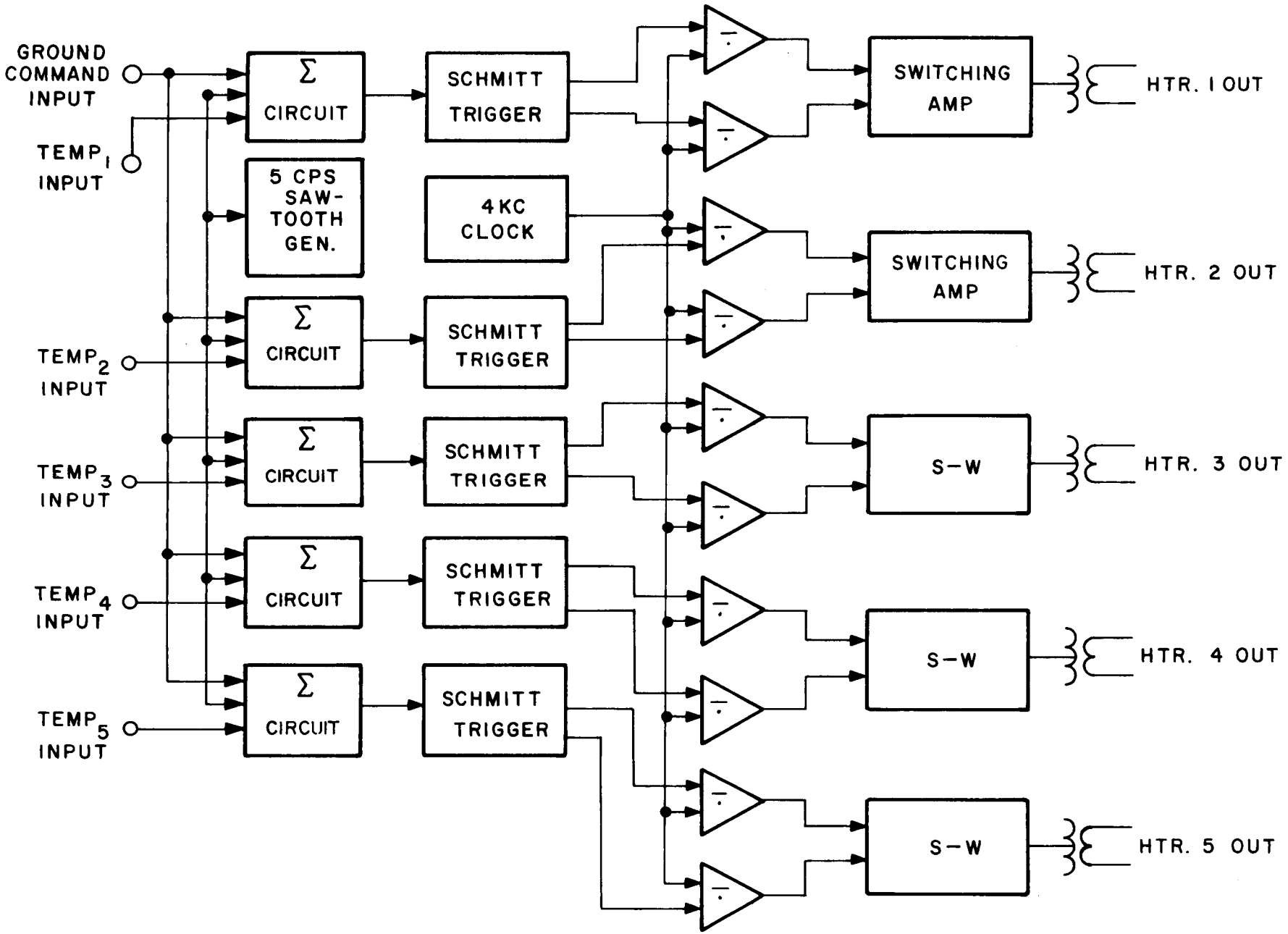

FIG. 9-6 DETAILED BLOCK DIAGRAM OF Cs RESERVOIR CONTROL USING DC POWER INPUT

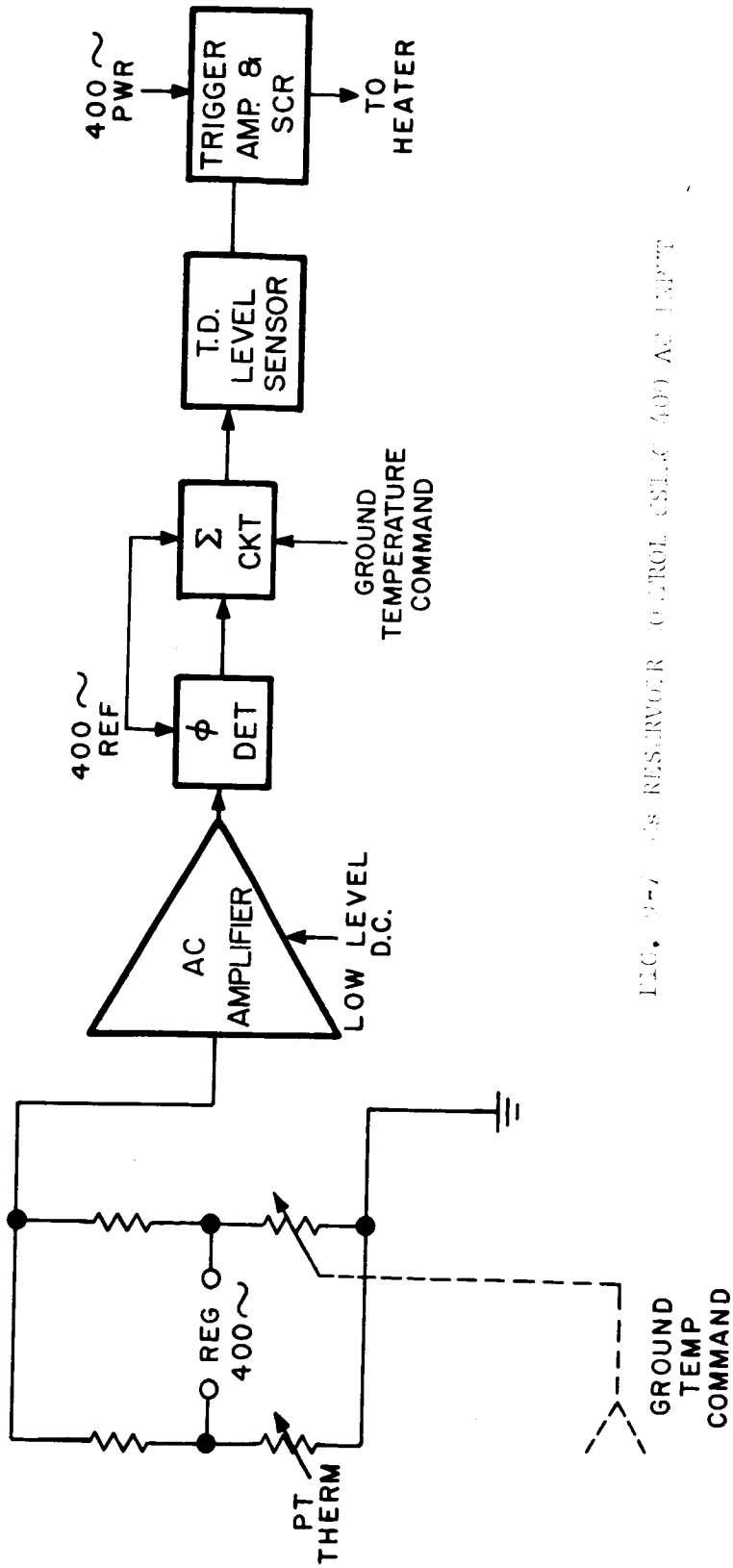

FIG. [illegible] RESERVOIR CONTROL USING 400 A.C. INPUT

615627

The comparator adds together the temperature analog voltage and the ground command voltage with a 5 cps sawtooth wave. These combined voltages are sensed by the Schmitt trigger. If the temperature of the reservoir is low, the combined voltages will drop below the threshold of the Schmitt trigger. The Schmitt will then change state permitting the pulsewidth modulator (switch) to apply heater power to the reservoir. The amount of heater power required is proportional to the temperature of the reservoir. This proportional control is obtained by means of the sawtooth wave which is used to sample the temperatures. The pulsewidth modulator consists of two AND gates with sufficient power output to drive the output switching amplifier. When the comparator senses a low temperature, the output signal permits the pulses from the pulse generator to be applied to the switching amplifier. The output of the switching amplifier is fed to a matching transformer before being applied to the heater. A transformer is used because the heater requires low voltage and relatively high current.

Figure 9-7 illustrates a circuit which uses ac power input. The platinum resistive element is shown as part of a Wheatstone bridge arrangement. The ac amplifier has a gain of about 50 and utilizes two-stage feedback. The phase detector utilizes 4 diodes and is a standard type of circuit. The summation circuit is a resistive sum network and contains an integrator for generating a 400-cps triangular wave. The tunnel diode level sensor is a simple circuit using 2 resistors and 1 tunnel diode. The trigger amplifier uses a single transistor to generate a gate signal for a silicon controlled rectifier which turns the heater on and off.

The use of the tunnel diode circuit in Fig. 9-7 is recommended to minimize weight. The use of the null procedure on the bridge eases the power supply regulation requirements. Temperature compensation of the resistance element is simple since the variation is linear over a fairly wide range. Possible problems will arise due

to thermal gradient EMF's being generated in the leads from the sensor and stray capacitance affecting the bridge null.

Figure 9-8 illustrates the waveforms in different parts of the tunnel diode cesium reservoir control circuit.

9.4.3 Weight and Power Requirements

The estimated power requirement for either of the circuits discussed is less than 1/4 watt steady state. For a generator with 5 diodes, approximately 1 watt would be required.

Weight estimates have been made for the cesium reservoir control units using welded cordwood module techniques, standard in the industry. Estimates were made by assuming the weight and volume for each circuit component and adding about 30 percent for packaging. Weight estimates do not include leads for the temperature sensing element.

Weight and volume are shown in Table 9-I. Weight and volume for the circuit using dc power is higher than the tunnel diode using ac power. Tables are based on the use of a 5-diode generator with heater currents up to 5 watts per heater.

An extrapolation of weight to other systems besides a 5-diode generator is approximately linear; although components will be selected wherever possible which would lead to a low-weight system.

9.4.4 Heater Design

Heater design has used tungsten, tantalum, and other types of wire in varying diameters. Tantalum is recommended due to its ability to remain ductile and its availability in clad-form. Forty-mil diameter wire (with 60-mil sheath) is currently used in laboratory diodes. One watt of heater power is available at low heater voltages.

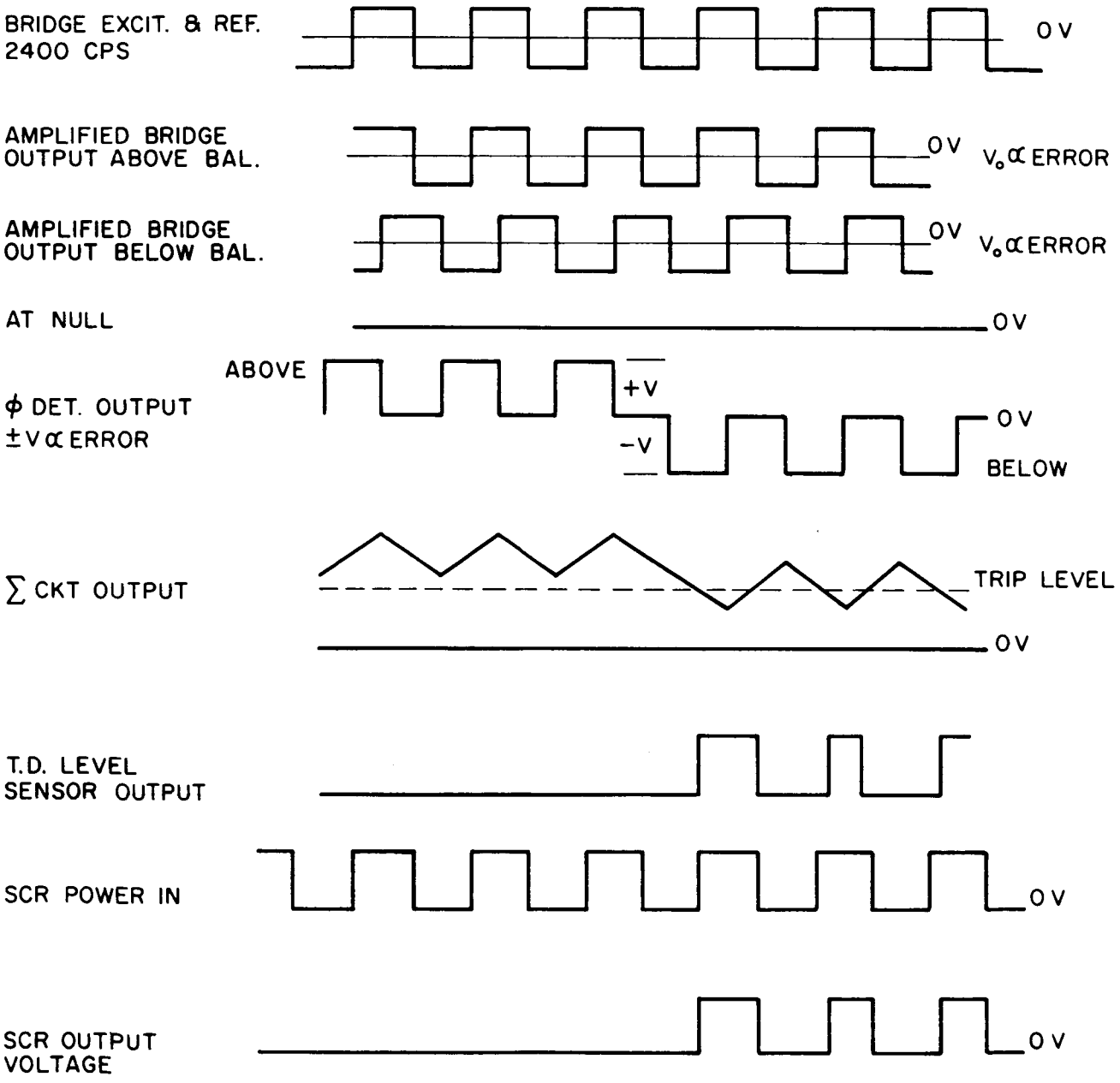

FIG. 9-8 WAVE FORMS IN TUNNEL DIVIDE Cs RESERVOIR CONTROL CIRCUIT

TABLE 9-I

WEIGHT AND VOLUME OF CESIUM RESERVOIR CONTROL CIRCUITS - 5 DIODE CONVERTER

1. DC Circuit

Item	Quantity	Wt (oz)	Vol (in^3)
Schmitt Trigger	5	3.2	0.28
Σ ckt.	5	1.0	0.06
High Power Gates	10	3.2	0.28
Switching Amp.	5	3.2	0.56
Transformer	5	6.3	6.3
4kc Clock	1	1.2	0.12
5 cps Sawtooth	1	1.2	0.12
		19.3	7.72 in^3
100% packaging, wiring		19.3	2.3 (30%)
		38.6 oz	10 in^3

2. AC Circuit (Tunnel Diode)

Bridge	5	0.053	0.25
AC Amp.	5	0.053	0.25
Power Transformer	5	6.0	0.4
Δ Det and Σ ckt.	5	0.053	0.25
TD Level Sensor	5	0.053	0.25
Trigger Amp. and SCR	5	0.106	0.5
		6.318	1.9 in^3
100% wiring, etc.		6.318	0.57
		12.6 oz	2.47 in^3

10. POWER CONDITIONING AND CONTROL

This section deals with the techniques to be used for electrical conversion and control of the power output of thermionic generators. Solar flux control, cesium reservoir control, and other types of control requirements for the solar-thermionic system are discussed elsewhere.

The input to the power conditioning and control subsystem is the generator(s) power output. The output of the subsystem is considered, for study purposes, to be regulated direct current.

The basic functions of the power conditioning and control system are:

1) Provide proper loading to the generator
2) Provide energy storage for peak power demands
3) Provide an output which meets power voltage and regulation requirements
4) Provide, where possible, compensation or adjustment for partial failure of the generator

Investigation of the conditioning and control problem has resulted in a recommended subsystem conceptually illustrated in Fig. 10-1. The components shown, properly designed, will best perform the basic functions of conditioning and control as discussed in this section.

Two features of the recommended conditioning and control systems are:

1) The generator output will be controlled to maintain a constant current output. As discussed later, constant current control provides a more efficient and reliable method of thermionic generator control in contrast to voltage control which is commonly practiced on photovoltaic systems.

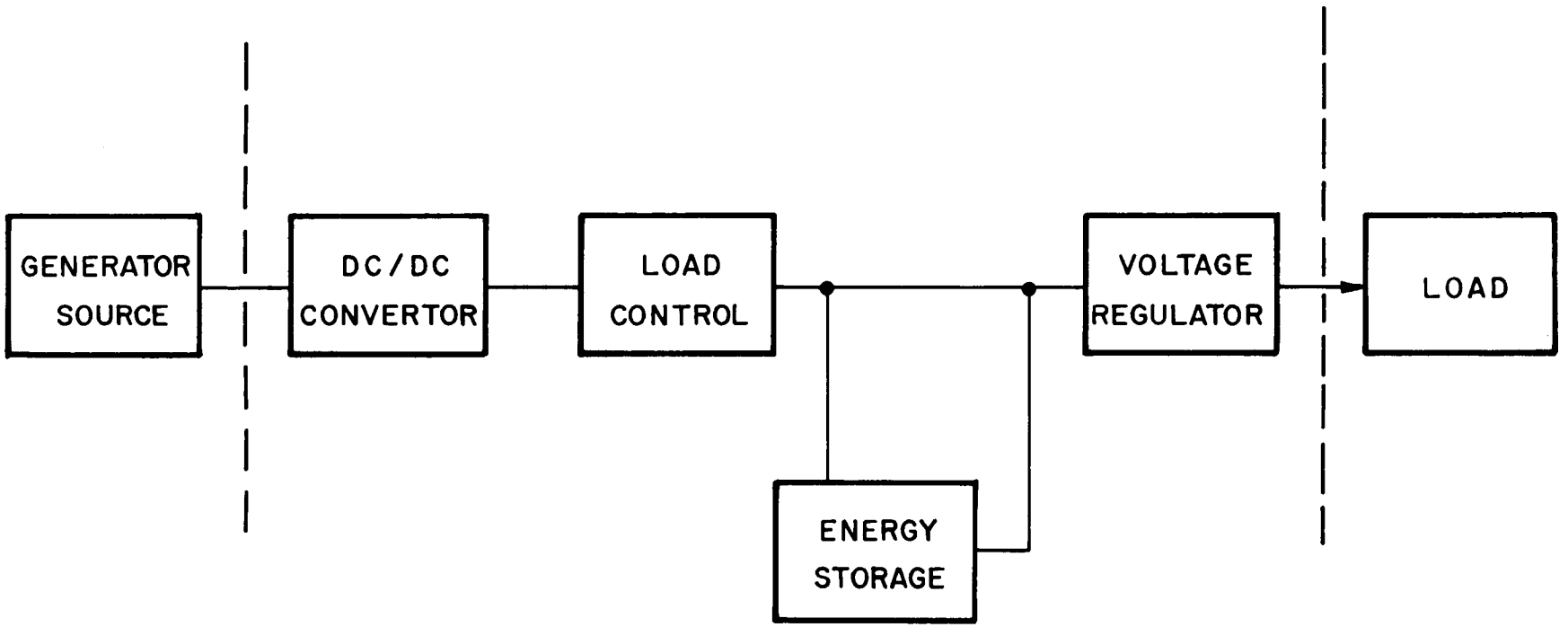

FIG. 10-1 BASIC BLOCK DIAGRAM OF SOLAR-THERMIONIC POWER CONDITIONING AND CONTROL SUBSYSTEM

It is mandatory that the generator output be controlled to assure reliable operation. This is illustrated in a typical curve in Fig. 10-2, which shows that the seal and collector will tend to increase temperature if the operating point moves towards low voltage, high current operation. On the other hand, the emitter temperature increases significantly when high voltage, low current operation occurs.

2) The power switch unit, commonly used in photovoltaic systems, is eliminated.

The following paragraphs discuss the design features of each component, their integration into a system, and the matching of the power conditioning and control subsystem with the generator source.

10.1 Series Versus Parallel Connection of Diodes/Generators

The thermionic diodes used in a generator or multiple generators can theoretically be electrically connected in series, parallel, or various series and parallel combinations. The series/parallel selection will depend on the following basic tradeoff:

Series/Parallel Tradeoffs

Series	Parallel
a) Higher Voltage	a) Better compensation for diode open failure
b) Less power loss due to diode matching	
c) Better compensation for diode short failure	

These items are discussed below:

10.1.1 Electrical Matching

Figure 10-3 illustrates a typical mismatch between diodes. At the present time, limited prototype production has resulted in diodes with I-V curves closely matched in slope, but displaced from each other by a small ΔV.

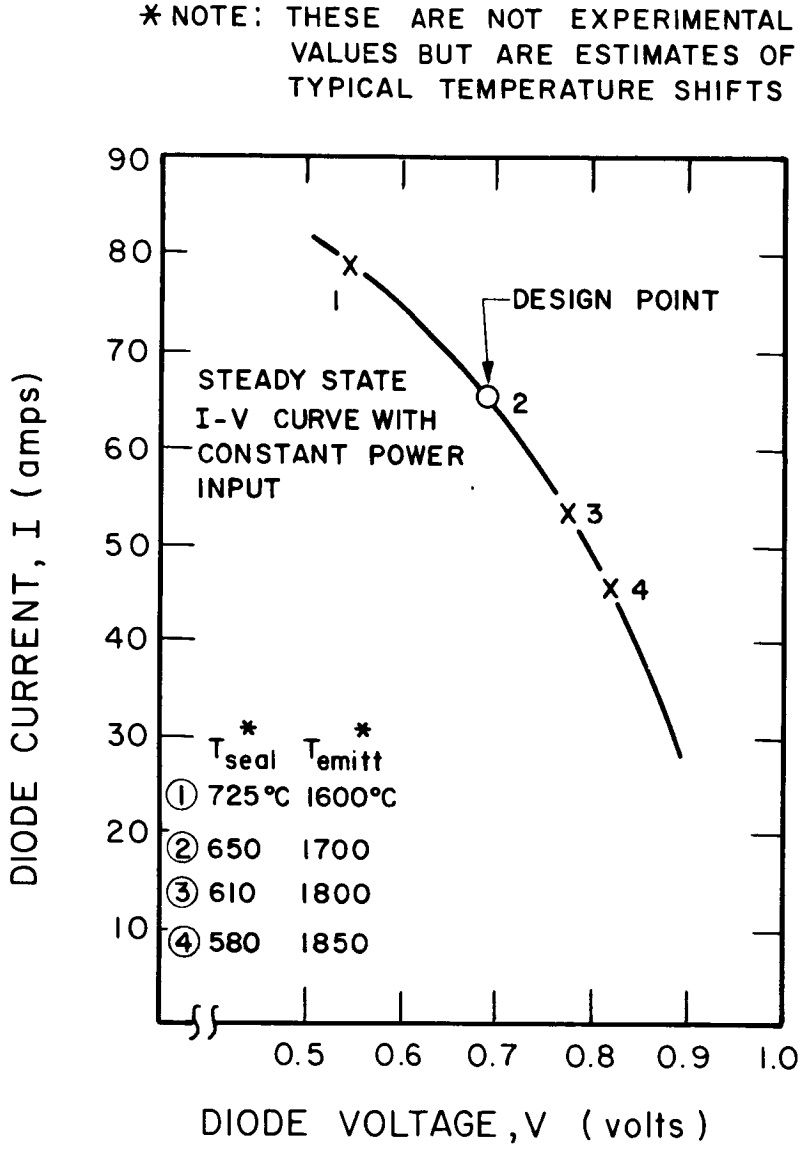

FIG. 10-2 TYPICAL EFFECT OF LOAD VARIATION ON DIODE TEMPERATURES

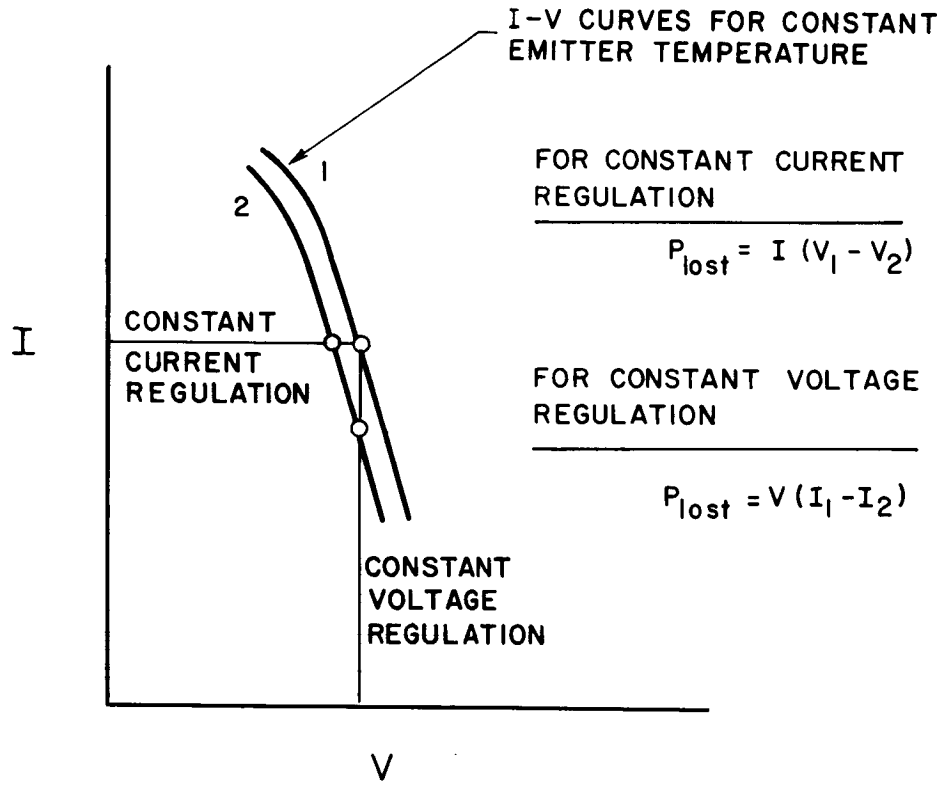

FIG. 1 - TYPICAL MISMATCH BETWEEN DIODES

For series connection, each diode provides the same current and the power from diode (2) is less than the power from diode (1) by an amount proportional to $I\Delta V$.

For a parallel connection, each diode provides the same voltage and the power from diode (2) is less than the power from diode (1) by an amount proportional to $V\Delta I$.

Due to the steep slope of the I-V curves, the parallel connection will result in less power than the series connection when the diodes are operated at voltages in the range of 0.5 to 0.9 volts.

As an illustration of the advantages in matching when diodes are series connected, two diode curves were assumed with typical mismatched characteristics.

Typical steady-state I-V curves for two diodes are shown in Fig. 10-4. These are steady-state curves rather than dynamic curves in that, for matching purposes, the dynamic I-V curve is not useful. The curves presented in Fig. 10-4 assume a constant generator solar power input and constant reservoir temperatures for each of the two diodes. Figures 10-5 and 10-6 show the power output of each diode as a function of output voltage and output current, respectively. If the two diodes were to be connected in series, they would both operate at the same current at any given point. If, on the other hand, they were connected in parallel, they would both operate at the same voltage at any given point. Figure 10-7 shows the power output difference of the two diodes as a function of the common voltage for a parallel connection. It will be noted that at lower voltages the output powers are relatively close while at higher voltages the output powers depart quite rapidly.

Figure 10-8 is a similar presentation of the difference in power output of the two diodes but it is plotted as a function of current and therefore represents a series connection. Again, at lower currents the power difference is fairly small and

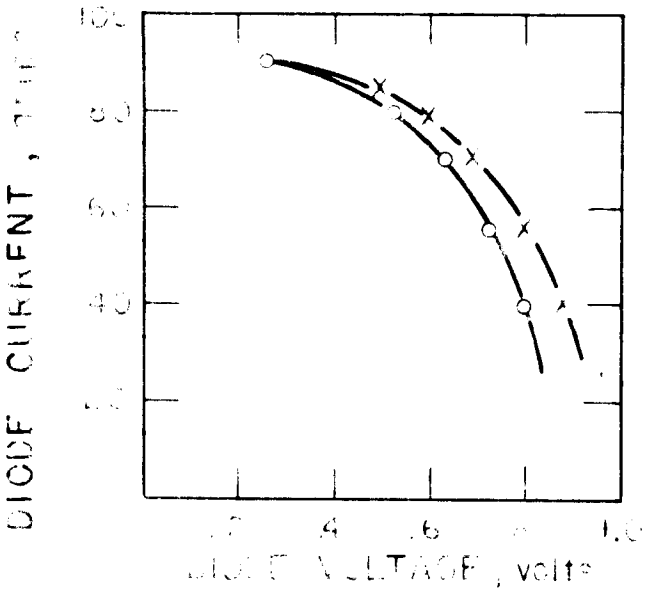

FIG. 10-4 STEADY STATE I-V CURVES FOR TWO TYPICAL THERMIONIC DIODES

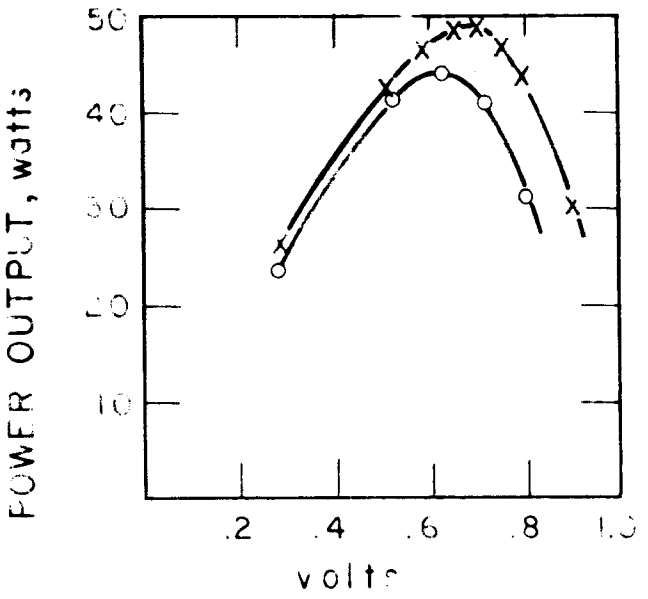

FIG. 10-5 TYPICAL OUTPUT POWER VS TERMINAL VOLTAGE

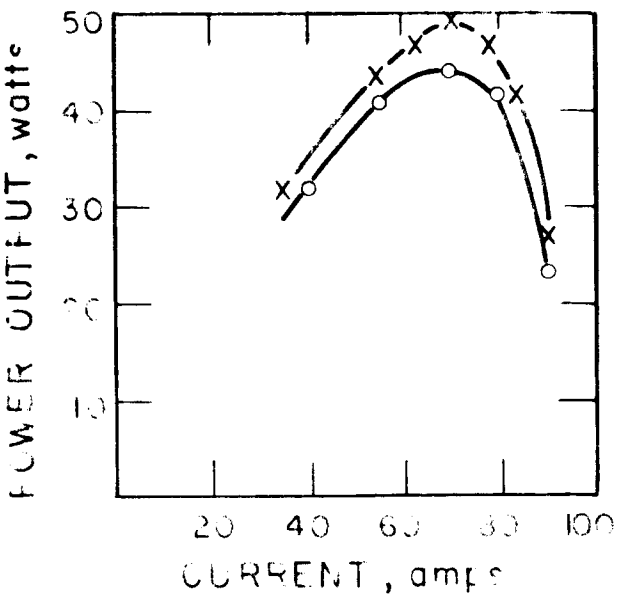

FIG. 10-6 TYPICAL OUTPUT POWER VS DIODE CURRENT

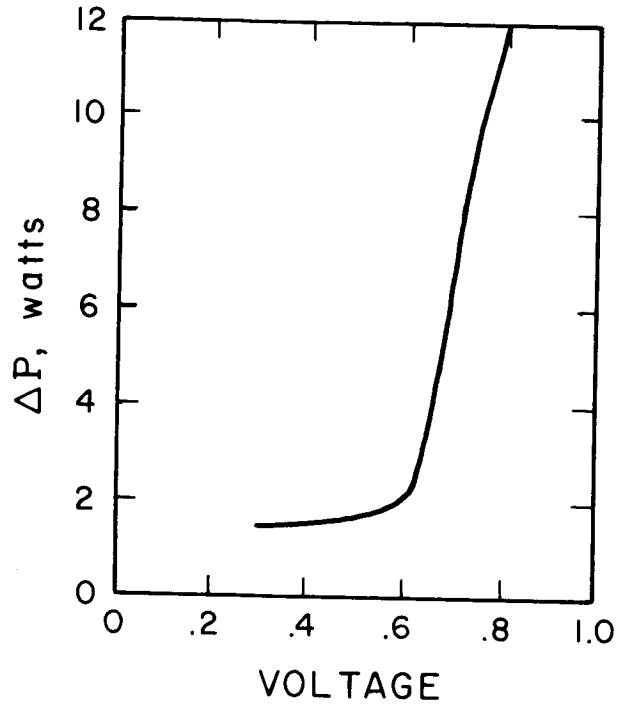

FIG. 10-7 TYPICAL POWER DIFFERENCE VS VOLTAGE FOR PARALLEL DIODES

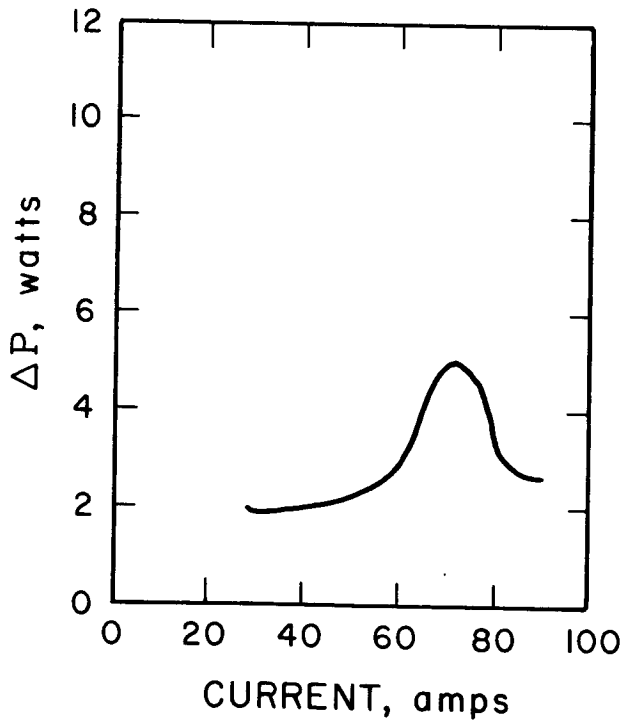

FIG. 10-8 TYPICAL DIFFERENCE VS CURRENT FOR DIODES IN SERIES

nearly equivalent to the parallel connection case but as the current increases, the power difference reaches a peak value and then diminishes as the current increases.

The comparison between Fig. 10-7 and Fig. 10-8 indicates the potential advantage of series connections.

The same reasoning can be applied to cases where a greater number of diodes are used in each generator. In all cases examined, it was found that the diodes should be connected in series and not in parallel. If a large system is used, where more than one generator is employed, it will also be found that the generator outputs should in one form or another be connected in series rather than in parallel. Series connection infers a common current or at least power addition that is current controlled rather than voltage controlled. Configurations shown in later paragraphs of this section will indicate methods of power summation between diodes and generators as well as protection for open circuit conditions of individual diodes or generators.

10.1.2 Reliability/Redundancy Considerations

Failure mode data is not available for thermionic diodes operating in a system. Individual diode data gathered in the laboratory is incomplete, and is not applicable to system operation. Mechanisms of failure are identified elsewhere, but can be categorized as:

1) Gradual degradation of performance
2) An open condition
3) A shorted condition
4) A condition where gradual degradation or catastrophe can lead to an open, then shorted, condition (or vice versa).

The last case, where both open and shorted conditions can occur in some sort of cyclic fashion, is not well explored but appears possible. For example, seal failure can cause

an open condition, followed by overheating of the emitter, followed by shorting of the emitter and collector.

Present data indicates that an open condition is the most likely mode of failure, but this conclusion is tentative and must be confirmed with experimental data.

Since the diodes are to be connected at least partially in series, a single diode open failure may completely abort the mission. Therefore, means must be found to bypass a failed diode if operation is to continue.

Assuming 50 watts of output power per diode, a 300 watt system (at the generator output) would employ 6 diodes. This number is nominally consistent with the use of a 5 foot diameter mirror at or near earth space. A larger power system would probably consist of an appropriate number of lower power modules. For example, a 900 watt system might consist of 3 mirrors, 3 generators with 6 diodes per generator.

10.1.2.1 Single Module - 6 Diode System

In order to provide a means to bypass a thermionic diode that has failed, leads must be brought from each diode or group of diodes to the control system. This will, of course, provide an additional burden to the system in the form of weight and thermal losses. (There will not be additional IR drop losses since the additional leads will not carry current unless a failure of a diode occurs.)

There are two reasonably practical methods to bypass a failed diode. The first is to short out the failed diode with a high current switch, such as a relay. One of the problems associated with the use of a shorting relay is the question of how to determine if a thermionic diode has failed. If a diode short circuits, there will be no need to short it further. However, if it open circuits, it must be bypassed. If it open circuits, a reverse voltage will be developed across the diode

which is caused by the other active diodes remaining in the circuit. Therefore, a reverse voltage sensor can be added to each diode to detect the condition and then cause the shorting switch to activate. However, if a switch is used for each diode when it activates, it will reduce the reverse voltage to zero which in turn will open the switch; therefore, the relay must incorporate a self-lock feature. This system can be used in groups of two or more diodes. Figure 10-9 shows such a configuration where one switch is used for each two diodes. Referring to the figure, if diode No. 1 fails, a reverse voltage will appear across its terminals which will activate relay RL1. The switch will bypass both diodes No. 1 and No. 2. Diode No. 2 will still operate and supply the required reverse voltage across diode No. 1 so that the switch will remain activated. However, diode No 2 should fail rather quickly due to overheating and the reverse voltage will disappear and the switch will open. The switch must, therefore, have a self-locking feature. The use of switches with the need for a locking feature is not recommended.

The second method to provide a bypass around a failed thermionic diode is shown in Fig. 10-10. In this system, six low input voltage DC/DC converters are used; one for each diode. If we assume an output voltage of 30 volts (total) for individual diode voltages of 0.6 volts, each DC/DC converter must provide a step-up of 6.33 to 1 with individual output voltages of 5 volts. Diodes CR1 through CR6 are connected across each DC/DC converter in the reverse direction so that under normal operation, they conduct no current. Now, if we assume thermionic diode No. 1 fails due to opening, the output voltage of DC/DC converter No. 1 will drop to zero and then reverse (due to the output current flow). Diode CR1 will then conduct providing the necessary current path for the remaining active segments of the system.

The system shown in Fig. 10-10 is the extreme case of providing "redundancy" or the ability to bypass failed thermionic diodes. Quite a heavy penalty in weight and

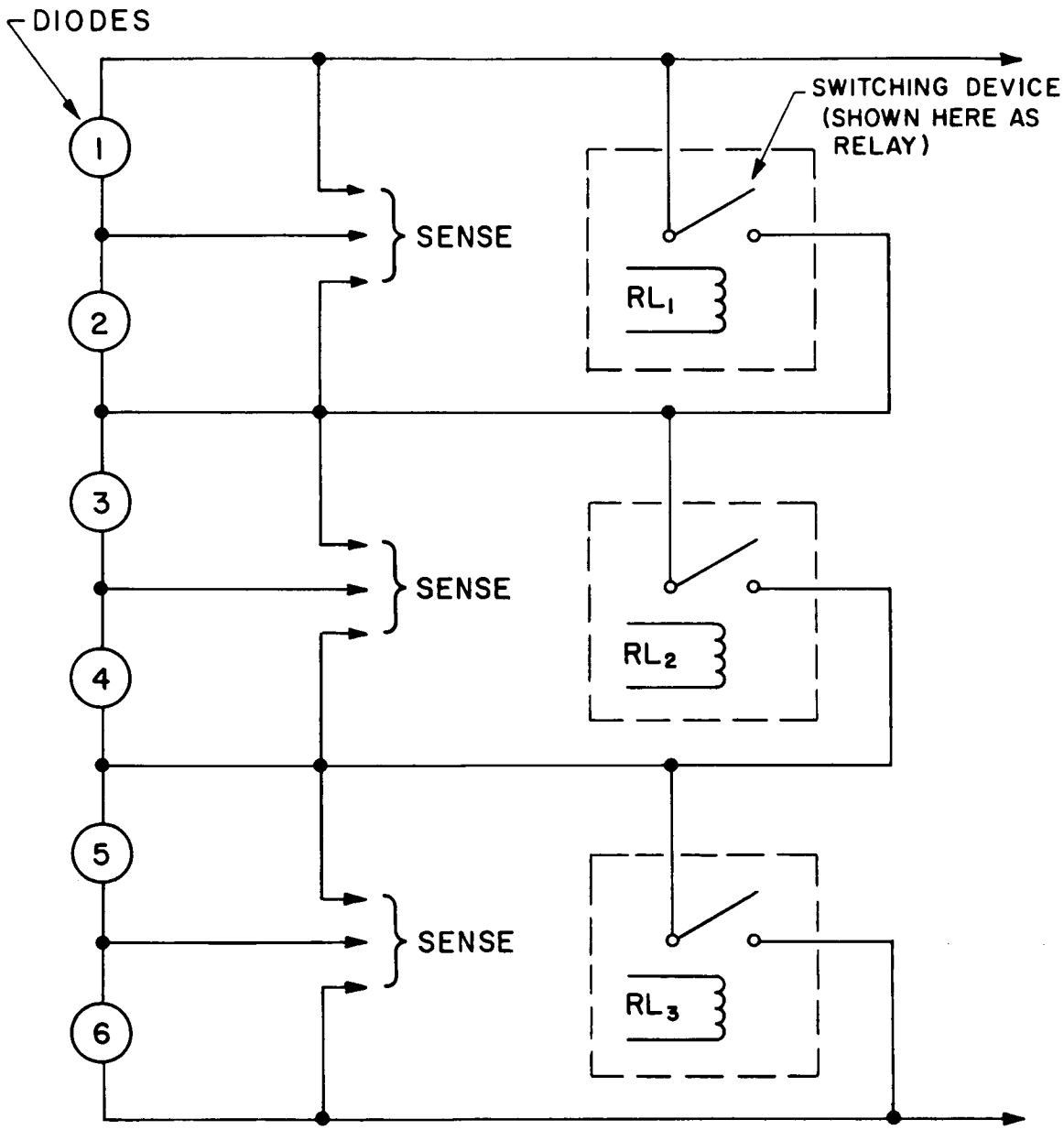

FIG. 10-9 EXAMPLE OF SWITCHING DEVICE USED TO BYPASS FAILED THERMIONIC DIODES

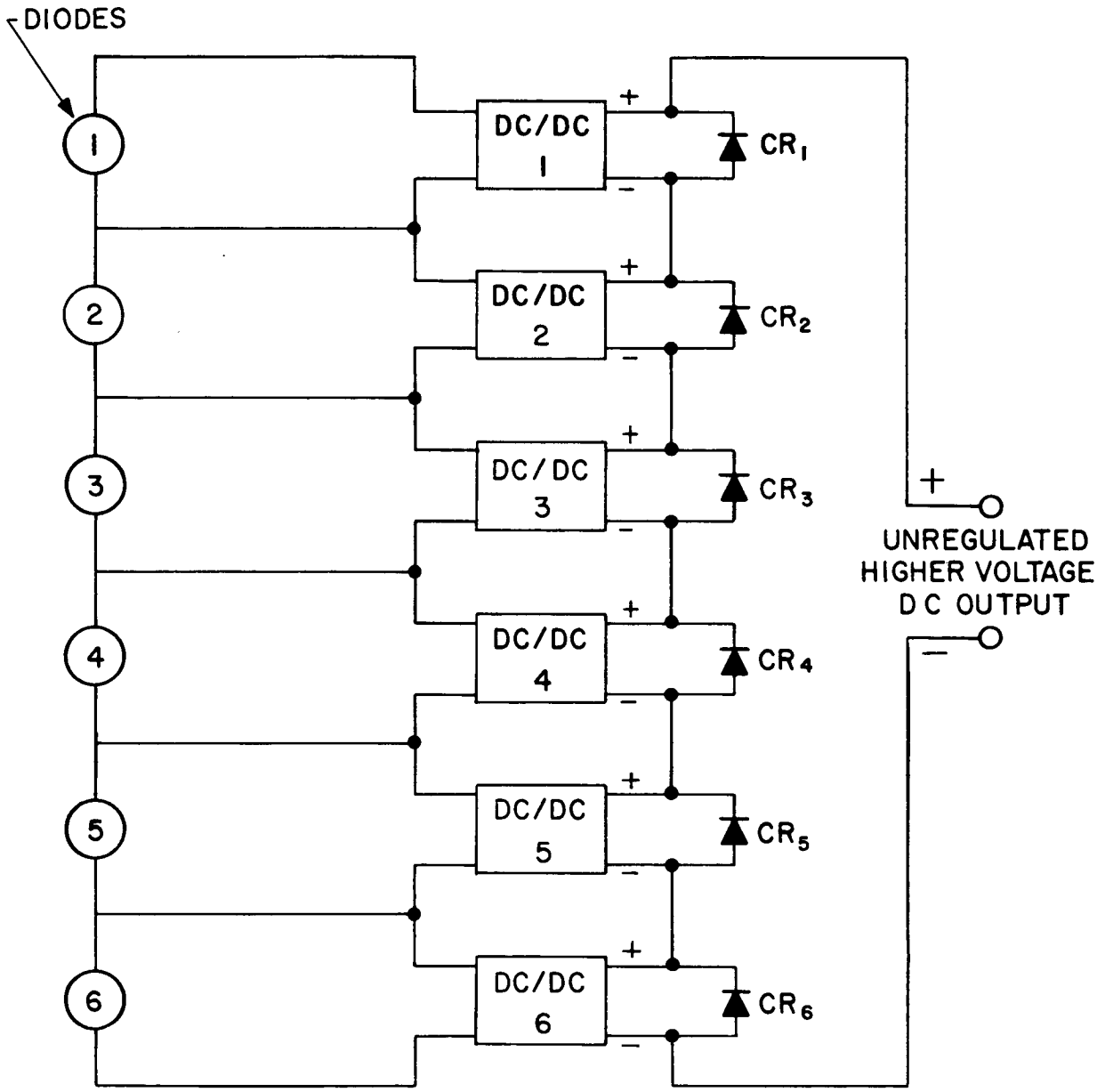

FIG. 10-10 EXAMPLE OF MULTIPLE DC/DC CONVERTERS USED TO BYPASS FAILED DIODES

complexity is paid in this case. A tradeoff must occur to determine how many diodes at one time must be bypassed.

10.1.2.2 Multiple Generator System

Similar reasoning can be applied to a higher power system where more than one generator is employed. In one extreme, all diodes of the system can be series connected with appropriate bypass capabilities included, or each generator can be considered as an individual entity and provisions be made to bypass a complete generator should a failure occur in it. The determination of the extent of bypassing will depend heavily on the total power of the system and the number of diodes or generators required.

A careful reliability study and analysis will have to be made before final recommendations can be made as to the extent and method of failure protection. However, at this time, the second method shown for bypassing (using DC/DC converters with diodes rather than switches) is the preferred method in that it is automatic and more foolproof.

10.2 Subsystem Operation

Two basic methods exist for control of the generator ouput; current or voltage regulation. Voltage regulation schemes can be devised which are similar in many respects to the conditioning and control subsystems used in photovoltaic systems.

For reasons discussed below, current control was found to be more favorable for efficient and lightweight control subsystems.

10.2.1 Voltage Controlled Subsystems

10.2.1.1 Examples of Solar Panel Voltage Control

It is felt worthwhile to discuss techniques for voltage control used on solar panels as these techniques can be used for comparison with thermionic generator control subsystems.

Many of the space power systems of the past have had some sort of voltage limiting device to prevent the solar array voltage from exceeding a certain value. The solar panel output voltage depends heavily on the load and the voltage is also quite temperature dependent. Certain types of system voltage regulators (such as the booster regulator used on Ranger) operate only over a relatively narrow input voltage range, and above a certain voltage, regulation is lost. In these systems, input voltage limiting is necessary. Many systems use power zener diodes for the voltage limiting (shunt regulation) function.

The shunt regulator must dissipate a considerable amount of power under certain loading conditions. A typical I-V curve of a solar panel regulated by a zener diode is shown in Fig. 10-11. The voltage limiting occurs at about V'. Under no load (system) conditions, the current through the shunt regulator is equal to I'. At a load current of I' or higher, no current is shown. The greatest power occurs at no load with its value depending on the shunt regulation voltage.

A second method to regulate the total array output voltage is to connect an active shunt regulator across only a portion of the solar array as shown in Fig. 10-12. The control voltage for the active regulator is obtained from the total output voltage. However, the regulator shunts current only in the lower portion of the array. The I-V curve shows the resulting voltage of each portion of the array as a function of load current. Also shown is the current through each portion of the system as a function of the load current. It will be noted that the current through the

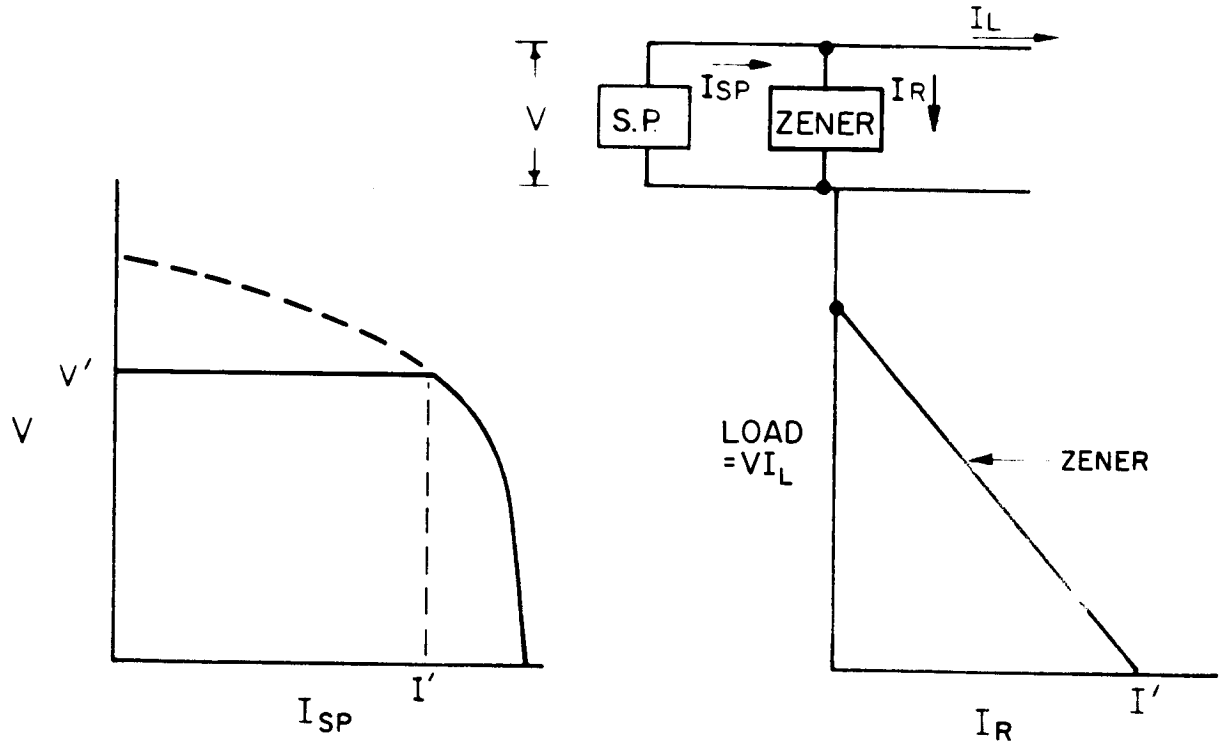

FIG. 10-11 ZENER DIODE SHUNT REGULATED SOLAR PANEL

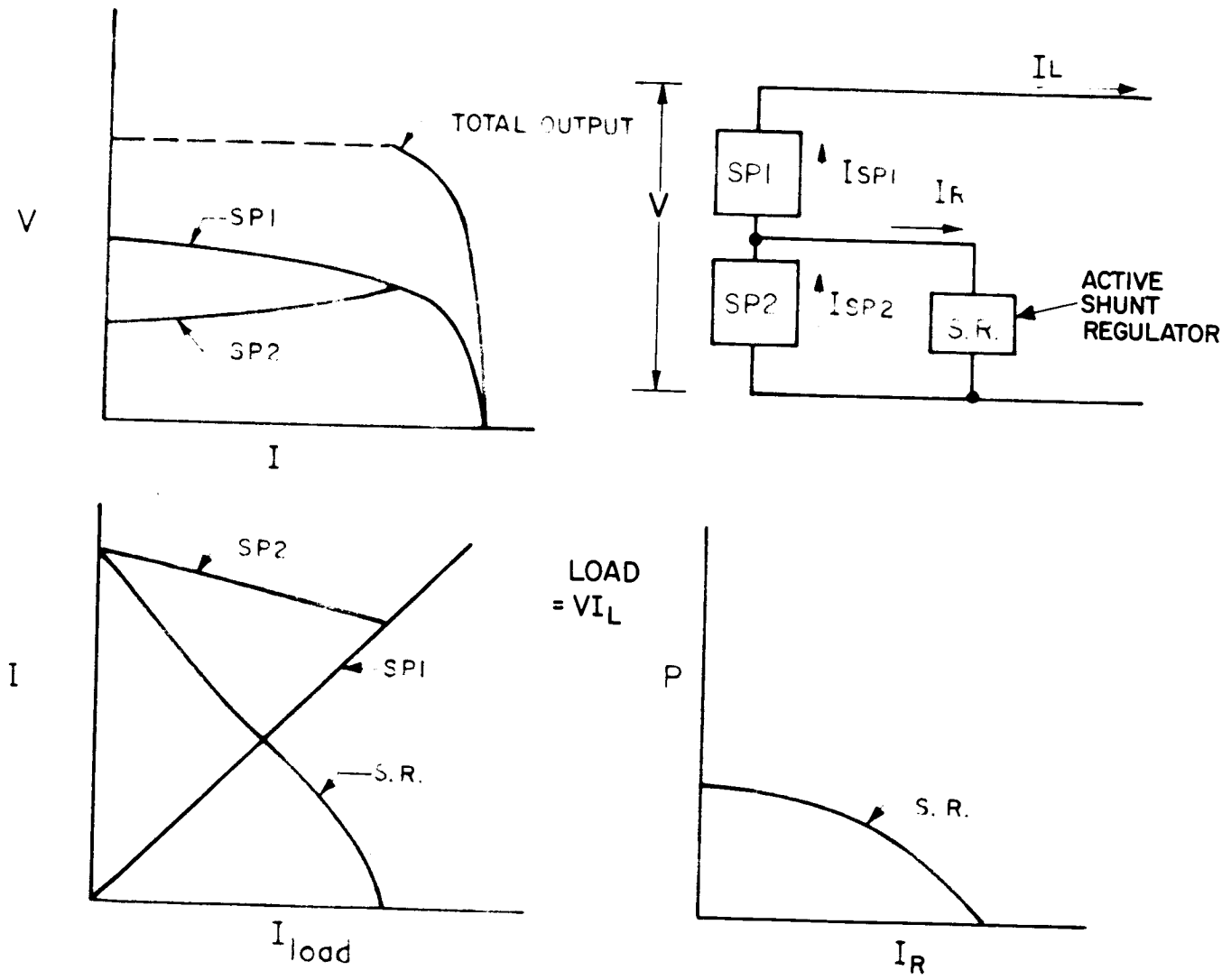

FIG. 10-12 MODIFIED SHUNT REGULATED SOLAR PANEL

upper portion of the array (SP_1) equals the load current. The power dissipated in the active shunt regulator is considerably less than the first case since the voltage (at high currents) across the regulator is somewhat less than one-half that for the first case. The shunt regulator can be connected to the array at a point other than the "center" of the array so that the optimum point can be selected for a particular mission. The obvious advantage of this system is the reduced amount of power that must be dissipated from the shunt regulator.

A third method to be considered for a shunt regulator is to switch resistive loads onto the array depending on the load current (or array voltage). A fairly large number of resistors would be used to provide a "step-wise" loading on the array. The primary advantage of this system is that the power would be dissipated in resistors rather than semiconductors. The resistors can operate reliably at higher temperatures than the semiconductors and therefore, the radiator (to dissipate the heat) would be considerably smaller and lighter.

10.2.1.2 Load Matching and Stability Considerations in a Voltage Control of Thermionic Generator Output

To obtain the maximum utilization of power output, the load must be properly matched to the thermionic source. Otherwise, instabilities and loss of regulation can result, and maximum power cannot be extracted.

Type of Load

The first item to be determined during the system design is the type of load that will be connected to the thermionic generator. For example, the load may be a purely resistive load such that as the input voltage is increased, the input current proportionately increases; or the load may be a constant current load that would result by using a series regulator with loss characteristics in the system. In such a case, as the input voltage increases, the input current decreases.

Figure 10-13 is a current versus voltage plot showing a typical generator I-V curve and the input characteristics of the three types of loads mentioned (constant resistance, constant current, and constant power). Point A of Fig. 10-13 is the intersection of the constant resistance load line with the I-V curve. This intersection point determines the operating point for the particular load line shown. Point B shows the intersection of a constant current load. It will be noted that both the constant resistance and constant current load have only one operating point for a given load and I-V curve. However, it will also be noted that a constant power load intersects the I-V curve at two points labeled C and D. It can be shown that Point D is a stable operating point and point C is unstable if the load appears predominately capacitive whereas the converse is true if the load is connected to the source through an inductor. The first case represents the common use of a high efficiency converter/regulator such as is found in the Ranger or Mariner power subsystems. The second case will apply with loads which predominantly use magnetic components.

A simplified explanation of the stable versus unstable operating points for the two load types is presented in the following two paragraphs. (It should be understood that the load need not actually be a constant power load but that it has a sloping characteristic similar to a constant power device).

Shunt Capacity

Figure 10-14 shows the steady state I-V characteristics of the source and the load (similar to a constant power load). Assume that a capacitor of significant value is connected across the system such as would be the case when using a converter or inverter. Operation can normally occur only at points C and D where the two curves intersect. However, assume for a moment that the system voltage is "forced" to V_1 and then released. At V_1 the current required by the load is less than that available from the power source. This "excess" current can only go into the capacitor and therefore, will cause the

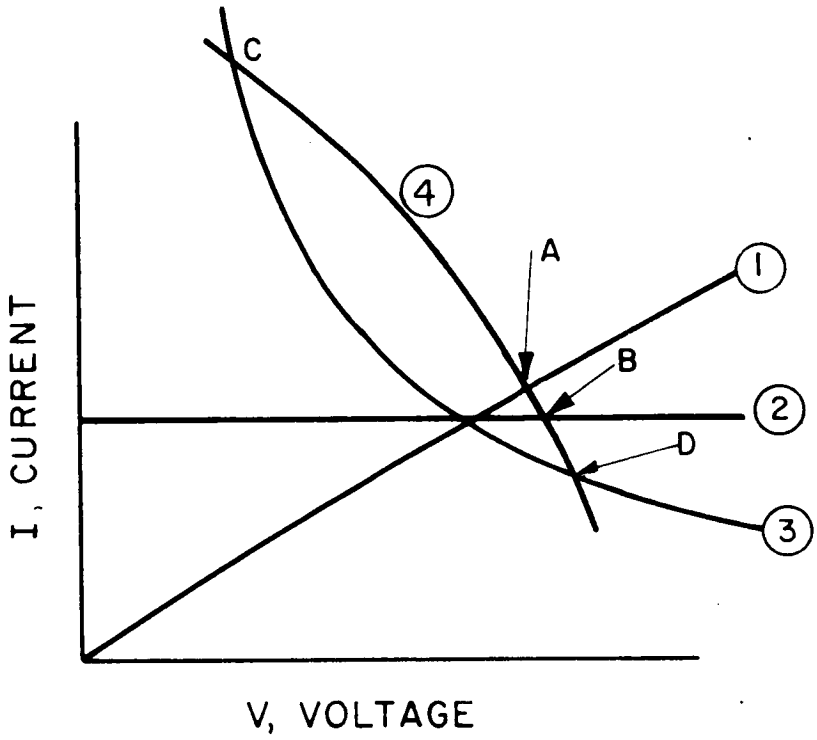

1. = CONSTANT RESISTANCE LOAD
2. = CONSTANT CURRENT LOAD
3. = CONSTANT POWER LOAD
4. = GENERATOR I-V CURVE

FIG. 10-15 GENERATOR I-V CURVE WITH THREE TYPES OF LOADS

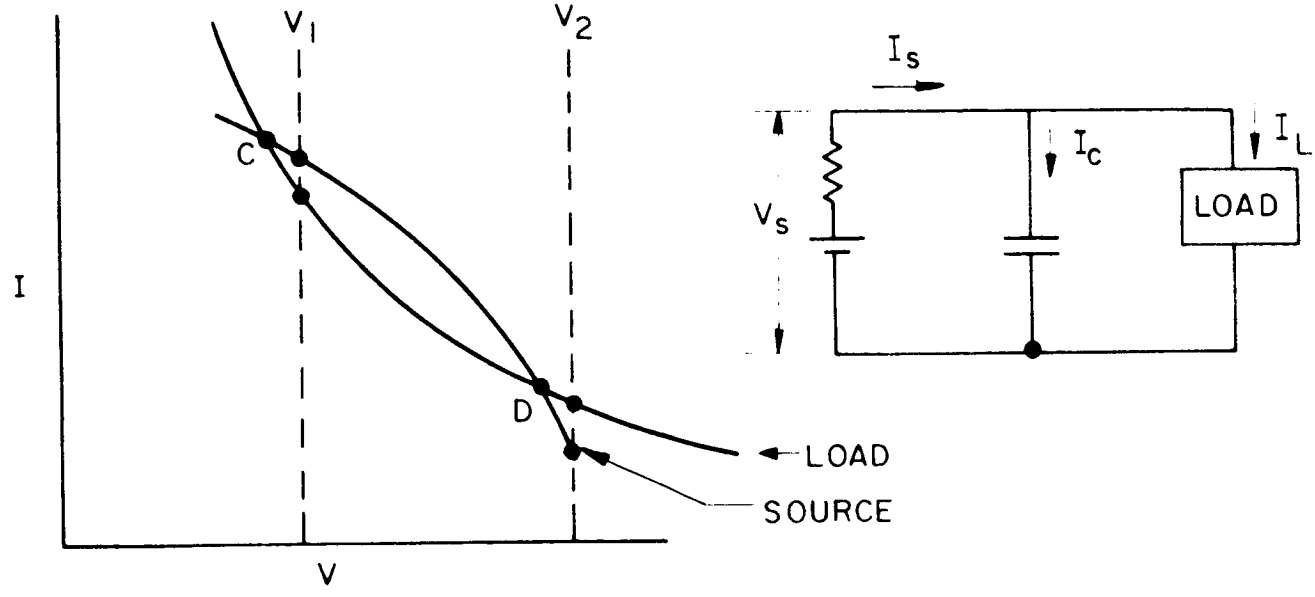

FIG. 10-14 CIRCUIT WITH SHUNT CAPACITANCE

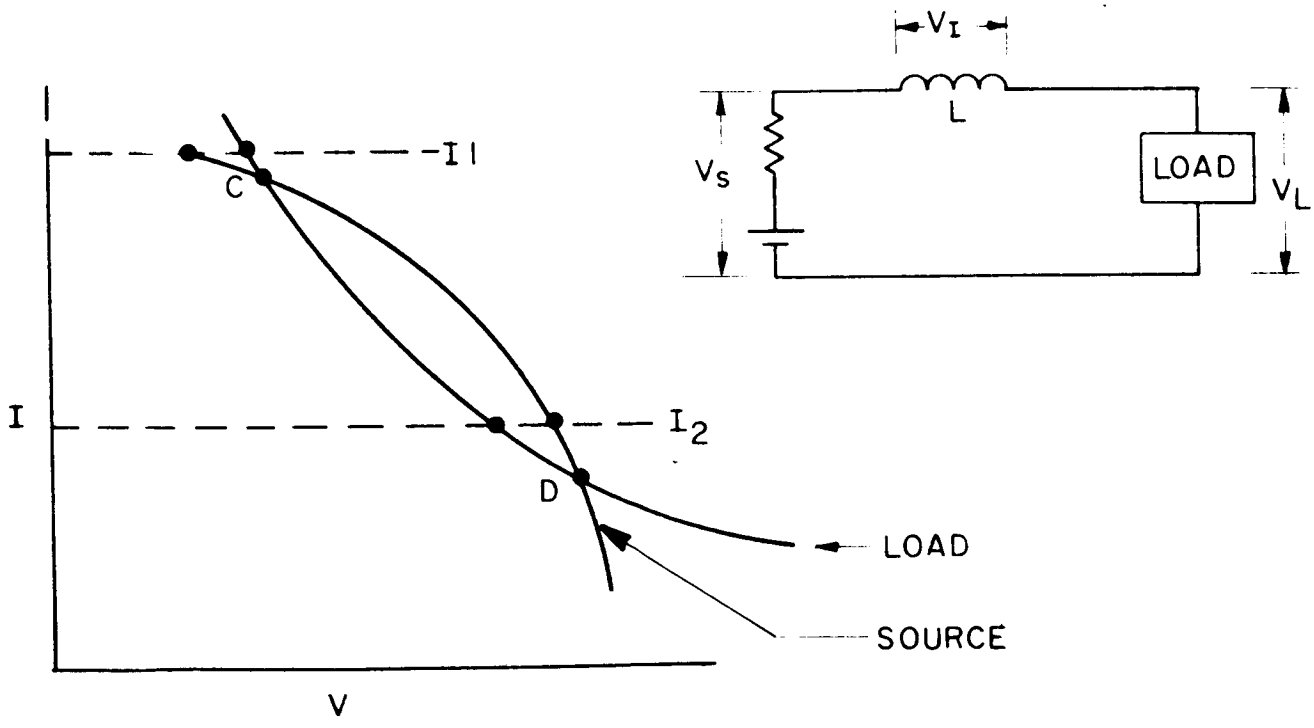

FIG. 10-15 CIRCUIT WITH SERIES INDUCTANCE

total system voltage to increase further until point D is reached. At point D, no excess current remains, the capacitor will no longer be charged upward and the voltage will remain stable at the new point. Now, assume the voltage is forced to V_2 and then released. The load requires a greater capacitor which then discharges down to point D and remains there.

Figure 10-15 indicates the same steady state source and load characteristics as before but indicates a circuit that includes inductance. Since all elements are in series, the current at all times is equal in each element. Assume that the current is momentarily forced to I_2 and then released. At point I_2, the load voltage is less than the source voltage with the difference appearing across the inductor. The inductor voltage will diminish and in doing so, will increase the system current, forcing the operation towards point C. Now assume the system current is forced to I_1 and then released. In this case, the load voltage is greater than the source voltage with the inductor's voltage reversed with respect to the first case. The diminishing inductor voltage in this case will decrease the system current, restoring operation back to point C.

Regulated Constant Power Load (DC to DC Converter Type)

In a system that must provide regulation to its loads, and which must operate at high efficiency due to power input limitations, a constant power load will invariably be the result. The fact that there is more than one operating point with this type of load can lead to difficulty in the system's operation, as previously described.

Figure 10-16 shows again the I-V characteristics of a thermionic generator together with the input characteristics of a typical high efficiency power converter. At very low input voltages to the converter, the regulation portion is unable to function properly and therefore, the output voltage increases as the input voltage increases. During this portion of the operation, the input current must increase. This continues to happen until point O is reached, at which time the

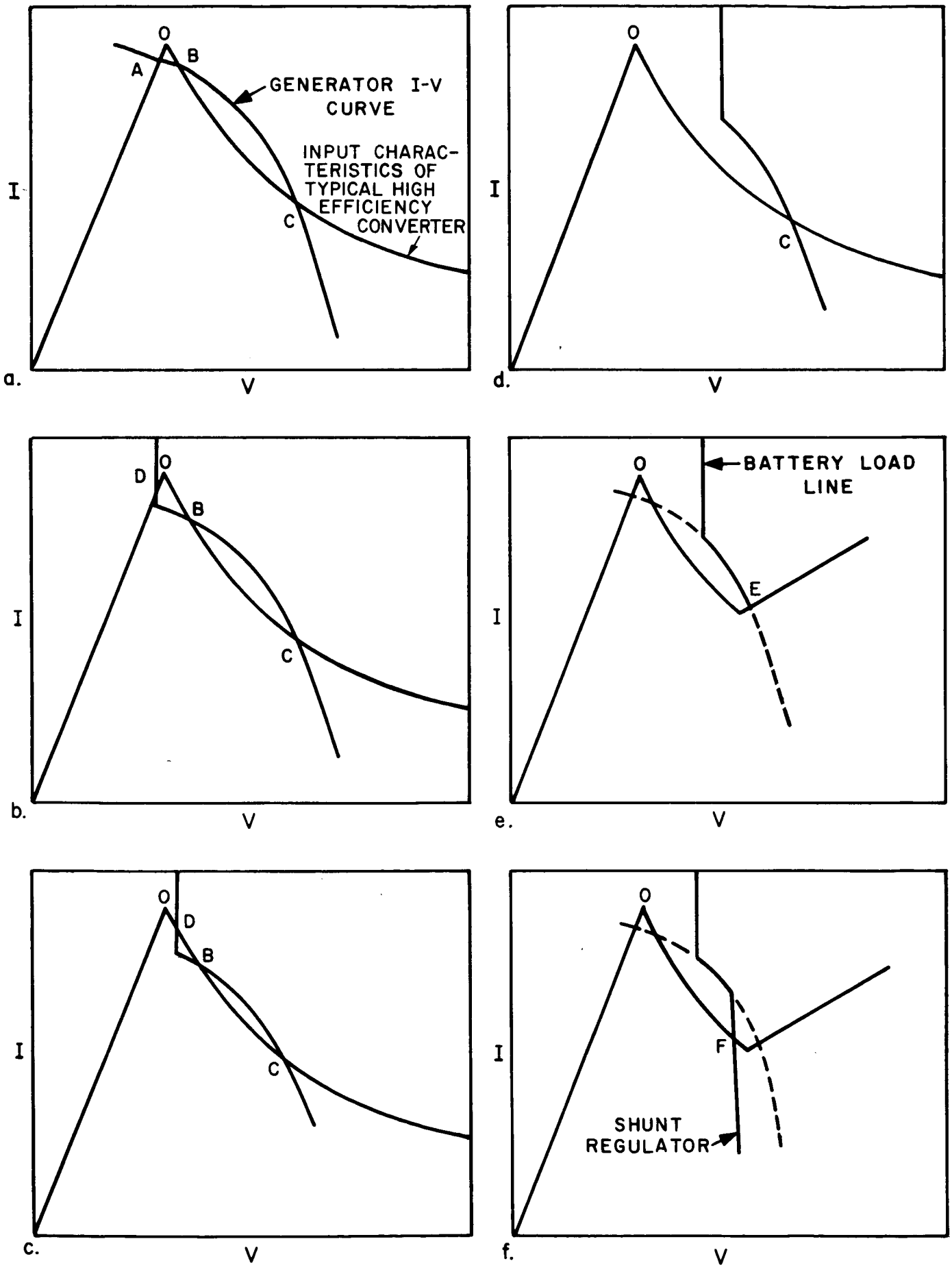

FIG. 10-16 I-V CHARACTERISTICS OF VOLTAGE CONTROLLED SYSTEMS

converter goes into regulation. From that point the input power is held constant and the input current decreases as the voltage increases. It will be noted that there are three points crossing the I-V curve of the generator. Points A and C are stable operating points whereas point B is unstable and will not occur in practice. Operation at point A is undesirable in that the power converter is not in regulation at this point. Therefore, the system must contain some provision to prevent operation at that point.

Addition of a Battery

Many solar-powered systems also contain a storage battery used either during dark portions of a mission, or to supply peak loads when they occur beyond the capabilities of the solar array. Power can automatically be added to the system from the batteries by connecting a series "logic" diode to both the generator and the battery. In this case, when the generator is loaded to a voltage that is equal to or less than the battery voltage, the battery will supply power to the system. Figure 10-16 (b) shows an I-V curve characteristic which includes the addition of a battery. It will be noted that at low input voltages, the battery provides power to the system such that as the load current increases, the system voltage will be maintained at the battery voltage. It will be noted here that there are now the three operating points D, B and C. Again, point B is unstable, but point D is still an undesirable operating point since the power converter is not in regulation. Figure 10-16 (c) shows a curve where a higher voltage battery is used. Point D is a stable operating point and is within the regulating range of the power converter. But, again, point D is an undesirable operating point because power for the load is obtained both from the generator and the battery. Again, means must be provided in the system to force operation over to point C, to relieve the battery of the unnecessary load.

Figure 10-16(d) shows a condition where battery of even higher voltage is employed. It will be noted here that only point C is stable and it is the only operating point for the specific condition shown. In other words, in this system the battery is used only for peak load demands and to insure that operation is always at a stable and regulated point.

Addition of a Shunt Regulator

Figure 10-16(e) shows a characteristic similar to Fig. 10-16(a) except that the power converter regulates only over a certain input voltage range. In this case, as the input voltage is increased to a particular point, the converter goes out of regulation, its output voltage increases as the input voltage increases, and therefore its input current increases. This is indicated by the rising characteristic at the high voltage end of the curve.

As shown, there is one possible operating point, E. Point E is stable but undesirable since the power converter is out of regulation. This can be remedied by including a shunt regulator in the solar array such that as the array voltage increases to a certain point, the shunt regulator will add to the system load to maintain the voltage at the desired regulating point. This is indicated in 10-16(f). In this case, operating point F is a stable operating point and within the regulation capabilities of the power converter.

As an example, Fig. 10-17 shows curves of an actual booster regulator used on the JPL Ranger spacecraft. Two different operating loads are shown along with I-V characteristics of the system with a battery at approximately 20 volts and a shunt regulator at approximately 31.5 volts. It will be noted that during the higher power operation, the system can operate in a battery sharing mode (point B) or the solar panel mode only (point D). During the lower power operation, the system operation is at one point only (point F).

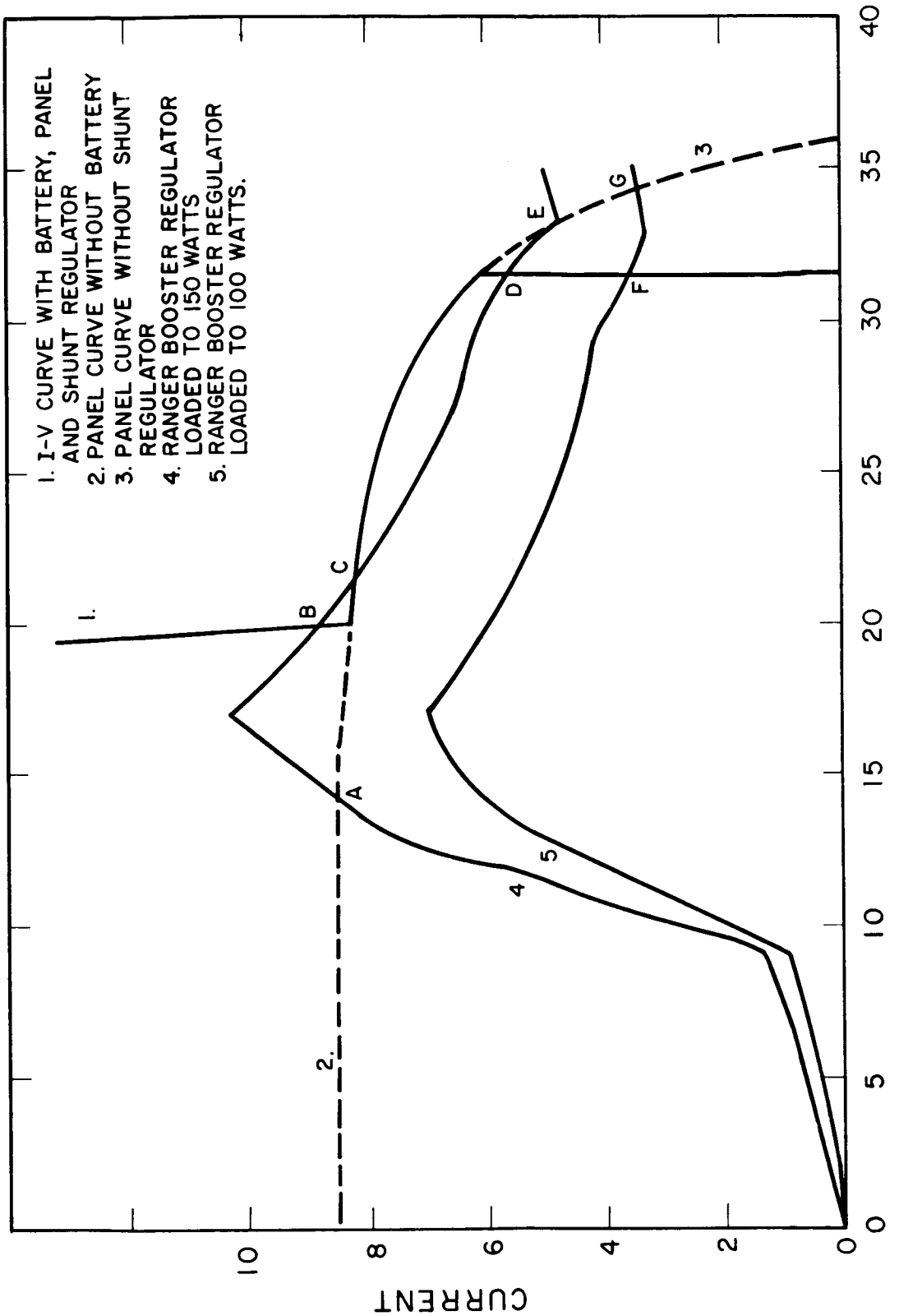

FIG. 10-17 RANGER BOOSTER REGULATOR OPERATION WITH SOLAR PANELS

10.2.2 Systems Which Utilize a PS&L Unit

It is possible to design a power conditioning and control subsystem which uses a power switch and logic unit in a manner similar to a photovoltaic power system.

An investigation was made of this type of subsystem as described in the following paragraphs. The design of the subsystem will depend considerably on the output voltage and current levels.

The design approaches considered are illustrated in Figs. 10-18, 10-19 and 10-20. Three basic approaches are possible, depending on input voltage and regulated output voltage.

Table 10-I gives a representative picture of the voltage and power levels that were covered in the study.

TABLE 10-I

CASES CONSIDERED IN PS&L SUBSYSTEMS

Case Number	Ein / Pwr	Design Approaches 1	2	3
I	1.4v - 100w	✓	✓	
II	2.8v - 200w	✓	✓	
III	5.6v - 400w	✓	✓	
IV	14v - 1kw	✓	✓	✓
V	14v - 4kw	✓	✓	✓

Approach No. 1

This design approach is perhaps the simplest of all the approaches selected. A block diagram of this scheme is shown in Fig. 10-18. This scheme can be utilized for input voltage levels ranging from 1.4 volts up to and including 14 volts. Because of its simplicity, this circuit can yield high circuit efficiencies. This is mainly due to the fact that the input power is switched only once throughout the entire circuit. This occurs in the DC-DC converter shown as the last block in the diagram.

FOR GENERATOR OUTPUT
VOLTAGES OF 1.4 TO 14 V.

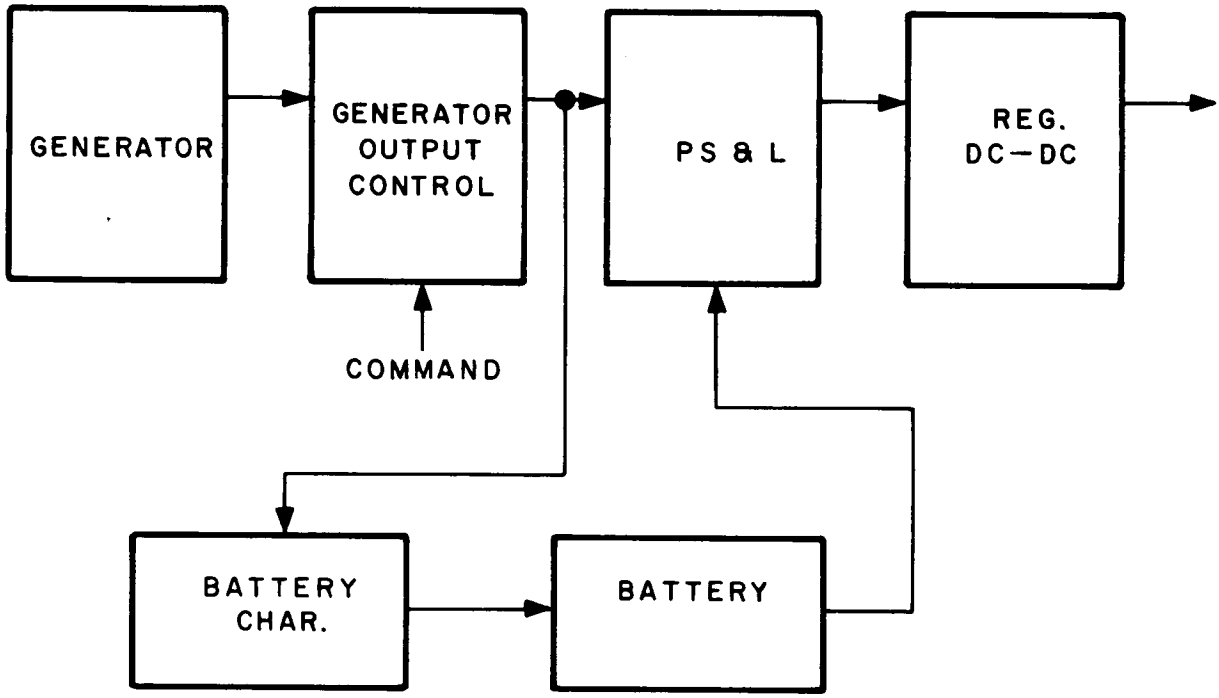

FIG. 16-18 BLOCK DIAGRAM-APPROACH #1 USING A PS AND L UNIT

FOR GENERATOR OUTPUT
VOLTAGE 1.4 TO 14 V.

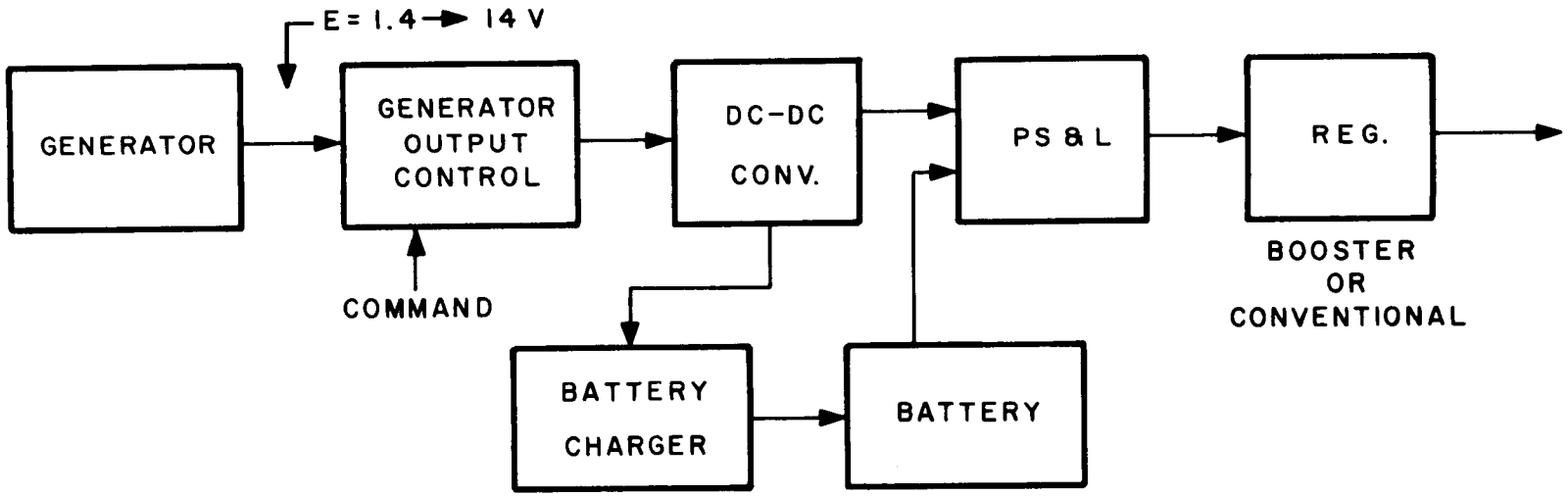

FIG. 10-19 BLOCK DIAGRAM-APPROACH #2 USING A PS AND L UNIT

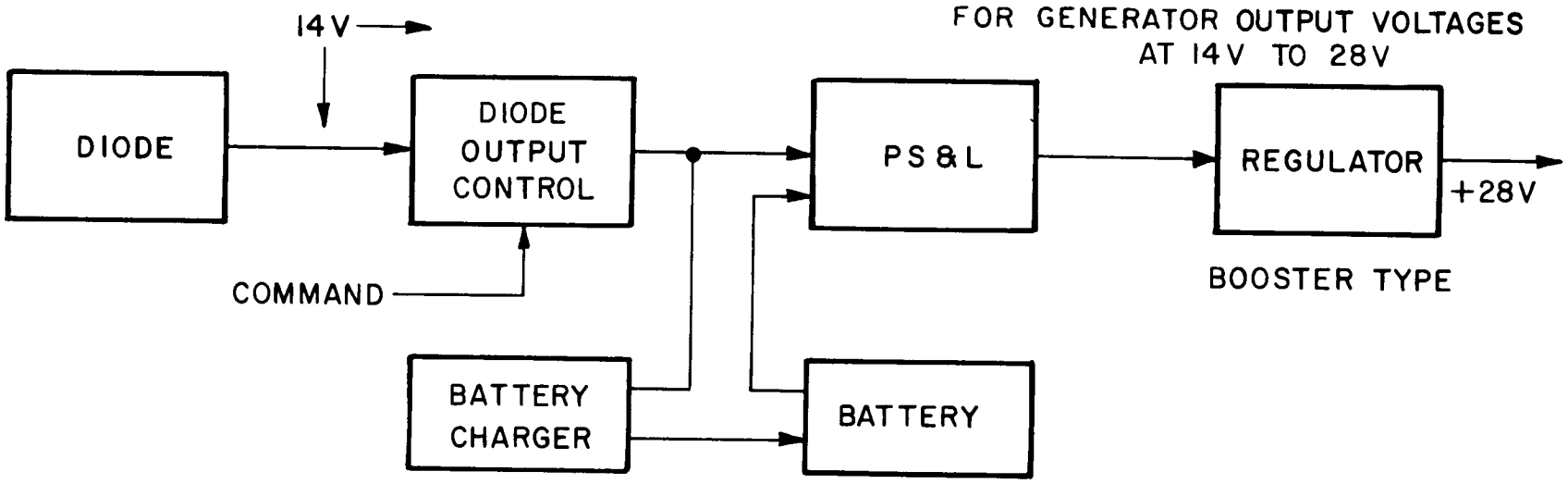

FIG. 10-20 BLOCK DIAGRAM-APPROACH NO. 3 USING A, PS, AND L UNIT

A thermionic generator system is shown as the power source. The diode output control circuit serves to maintain the thermionic generator load current constant at a predetermined value. It also enables changing the output current and power levels of the thermionic generator by external command. The power and switching logic unit channels power from the diode output control circuit or the battery system to the DC-DC converter. The switching will be accomplished automatically at a predetermined value of output voltage from the main power source. A system battery will be required to insure system operation whenever the thermionic diode is not receiving solar energy. The battery charger unit shown will serve to keep the system battery charged.

Approach No. 2

This approach is to be considered for input voltage ranges from 1.4 volts to 14 volts, with power levels ranging from 100 watts to 4000 watts. The output voltage will be either 28 volts dc or 56 volts dc. A block diagram of this scheme is shown in Fig. 10-19. With this scheme a thermionic diode generator system will serve as the primary source of power. The diode output control circuit will be used to control the output operating power point of the thermionic diode system. It will also serve to change the operating point through an external command. The DC to DC converter shown in the circuit will serve to step up the low voltages to higher dc levels. The type of converter circuit indicated here is an unregulated DC to DC converter. Because of the power levels, a driven converter was selected. The power switching and logic unit shown in the diagram will receive power from either one of two sources. Primary power will be channeled from the DC to DC converter or from the system battery. Switching of the main power source from the DC to DC converter to the battery or vice versa will be done automatically as determined by a preset system voltage level. System power channeled through the power switching and logic unit will be coupled directly to the system voltage regulator

shown in the diagram. The voltage regulator will be either a booster type of regulator or a conventional type. A comparison of detailed performance characteristics will be required before a selection is made.

Approach No. 3

This approach can be considered only for system input voltages varying from 14 vdc to 28 vdc. For a regulated output voltage of 28 vdc, it appears possible to eliminate a DC/DC converter. This feature is extremely desirable and is shown in Fig. 10-20.

Power Switching and Logic Design

The PS&L unit will channel power from the generator output control or the battery. Figure 10-21 shows three different schemes of switching:

1. Diodes
2. Transistors
3. Relays

Diode Output Control Circuit

The diode output control circuit can best be described as a variable parasitic load for the system. The diode output control circuit recommended for approach 1 is shown in Fig. 10-21. In this scheme the system current is used as the control current for a mag-amp. The output from the magnetic amplifier is then used to fire a number of Schmitt trigger circuits, which in turn serve to control the series switches indicated as Q1 through QN. The series switches are used only as saturated switches and will not dissipate much power. Resistors R_1 through R_N will comprise the variable resistor. The actual number of resistors and transistors used will depend on the amount of resolution that will be required in the system. In order to change the level of thermionic diode output current, the gain of the magnetic amplifier can be changed, or the firing level of the various Schmitt triggers can be altered; whichever provides better control will be utilized.

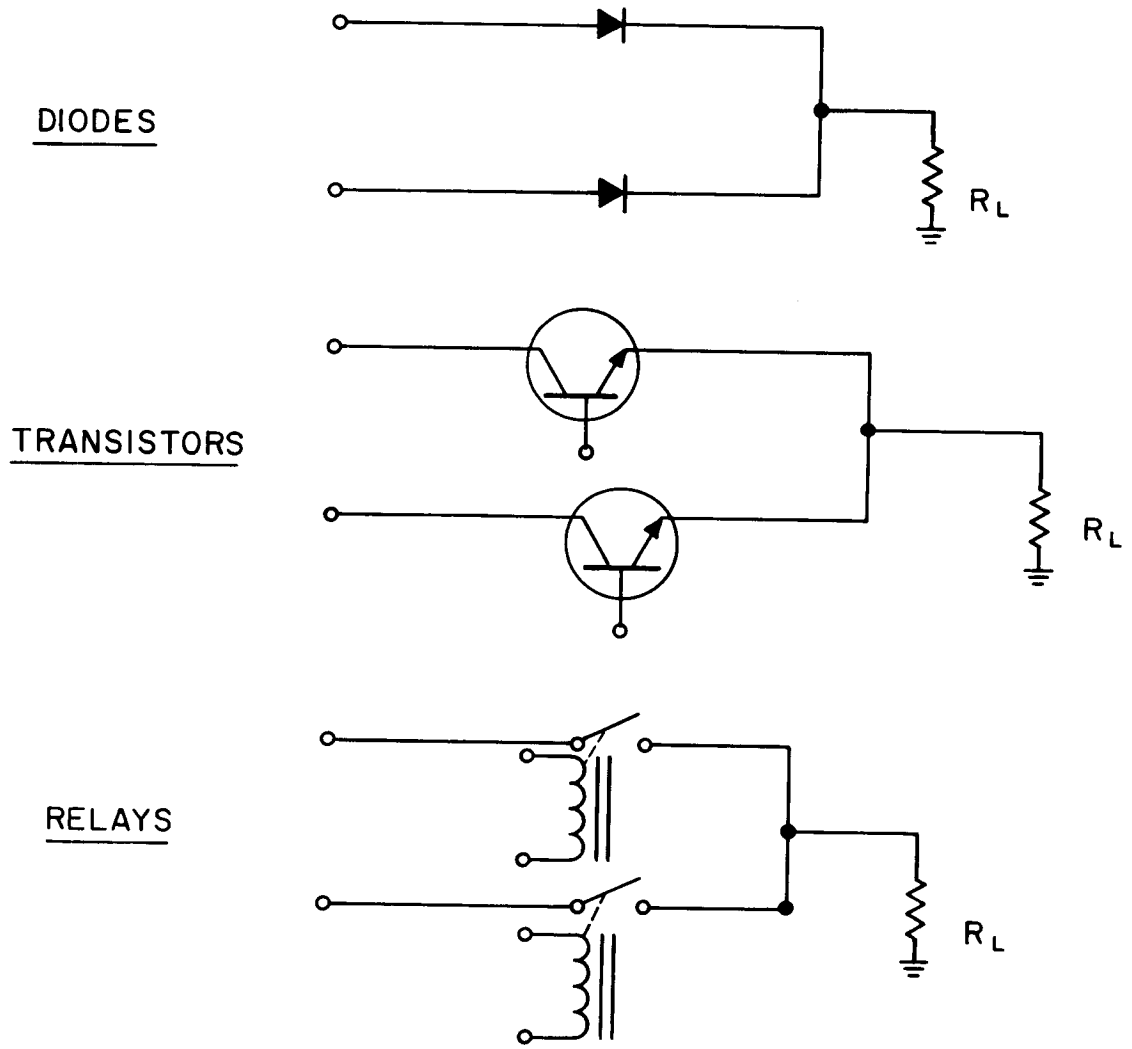

FIG. 10-21 POWER SWITCHING AND LOGIC CIRCUITS

Power Switching and Logic Circuit

The power switching and logic circuit shown in Fig. 10-21 will serve to channel power from the diode output control unit or the system battery to the DC-DC converter. Figure 10-21 shows three different schemes of switching the system power by diodes, by transistors, and by relays. The diode scheme was used successfully on the Ranger Spacecraft power system. The line voltage was 31.5vdc. Unfortunately, at low voltage levels (such as 1.4 volts) diodes appear unattractive. For example, with a 1.4 volt input at a power level of 100 watts, the current will be 70 amps. Power lost in the diode alone would be in the neighborhood of 70 - 75 watts or approximately 75 percent of the input power.

The transistor approach appears attractive for the low input voltage range from the standpoint that they dissipate very little power in the saturated condition. For example, for a system current of approximately 50 amps, a series transistor switch would drop approximately 50 millivolts (2.5w) as compared to approximately 1 volt (50w) for a silicon diode. As the input voltage increases, these low voltage transistors can no longer be employed as it is possible to exceed the collector-to-emitter breakdown voltage of 10 volts. At the higher input voltage and the current levels, we can then consider other types of germanium transistors which typically have a saturation voltage of 0.45 volts at 50 amperes. The use of silicon transistors can also be considered. Silicon transistors are currently available with 10 milliohms saturation resistance for a collector current of 150 amps (1.5v). The use of vacuum relays for power switching in the power and switching logic unit should also be considered. Relays capable of switching several 100 amps even up to thousands of amps are currently available.

10.2.3 Recommended System Description

A system has been devised which eliminates the PS&L unit and utilizes constant current control of the generator.

In a simplified form the system will consist of a generator, a load control device, a battery, a battery charger and a regulator. System connections for single generator systems and multiple systems are shown in the following paragraphs.

A simplified block diagram of a single generator system is shown in Fig. 10-22. To simplify the explanation of the system's operation, it will be assumed that the generator output voltage and current can be readily handled by the various components of the system. A system consists of the generator, the parasitic load which in itself consists of a shunt load and a battery charger, a battery for energy storage, a battery converter and a voltage regulator. From earlier discussions it was determined that the generator's load should be constant and that it should be a constant current load. Since the system load is assumed to be a variable, the parasitic load must vary in accordance with the system load to maintain the generator current at a constant value.

During times when the load current is less than the constant generator output current, the parasitic load must make up the difference. The parasitic load is the sum of the shunt load and the battery charger load. The battery charger input current will therefore be limited by the parasitic load requirement. Additionally it will be controlled by the charge condition of the battery. The excess parasitic load current required to maintain a constant generator load will be absorbed by the shunt load. The control for the shunt load will therefore be the difference between the generator output current (a constant value) minus the charger current and the load current. The basic current equations for this operation are shown below.

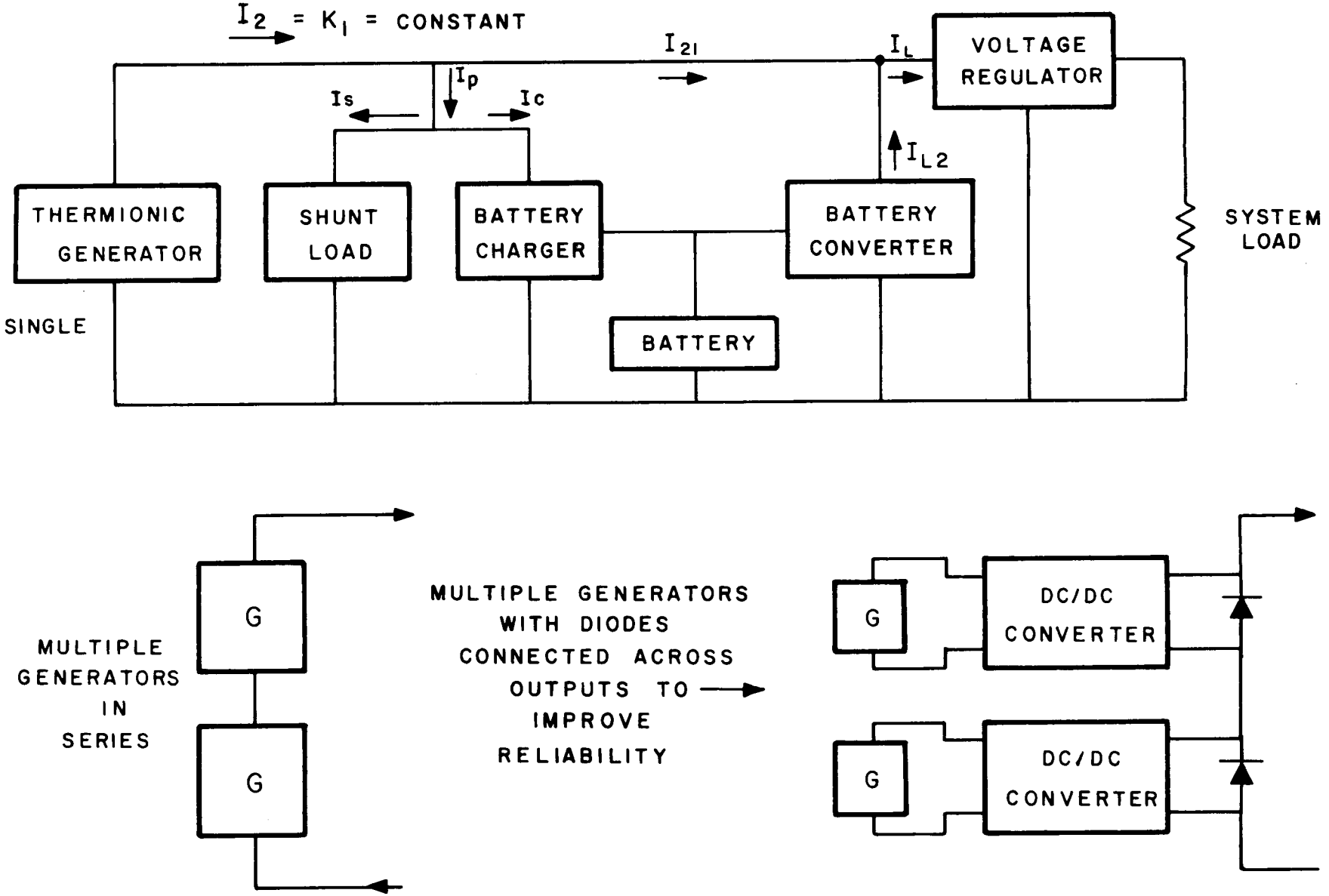

FIG. 10-22 SIMPLIFIED BLOCK DIAGRAM OF A RECOMMENDED POWER CONTROL AND CONDITIONING SUBSYSTEM

1. $I_g = K_i =$ Constant current load on the generator under all operational conditions
2. $I_L < K_i$ (Generator output capabilities greater than the load current demand)
3. $I_{L2} = 0$ (no power supplied from battery)
4. $I_{Li} = I_L$
5. $I_p = I_g - I_L$ (parasitic load current requirement)
6. $I_p = I_s + I_c$ (I_c is a function of state of charge of the battery)
7. $I_s = I_g - (I_c + I_2) =$ control for shunt load

The second operating condition exists when the load current is greater than the generator output current. In this case the extra current requirement will be provided by the battery. The battery charger is disabled as is the shunt load to reduce the parasitic load current to zero. A DC to DC converter (connected between the battery and the input to the voltage regulator) is activated. This DC to DC converter is controlled with respect to current and specifically with respect to the difference between the load current and the generator current (a constant value). The equations for this operation are shown below.

1. $I_L > I_g$ (Generator output capability is less than load demand and therefore battery must supply power difference)
2. $I_L = I_{Li} + I_{L2}$ (Load current equals sum of battery current plus generator current)
3. $I_p = 0$ (no parasitic load)
4. $I_g = I_{Li}$
5. $I_{L2} = I_L - I_{Li} = I_L - K_i =$ control for battery converter

It will be noted that this system requires a DC to DC converter between the battery and the system voltage regulator.

In solar cell systems this has generally not been required. The primary reason for this is that in a solar cell system the choice of whether to connect or not connect the battery to the system has been proportional to voltage rather than current. Since the voltage level cannot be used as a control in the thermionic generator system and current must be used as the control, the DC to DC converter is required.

The basic concept for a multiple generator system is the same as a single generator system except means for summing the outputs of the generator must be employed. Figure 10-22 shows one method of summing the outputs of the two generators of a two generator system by simply connecting the two in series. The remainder of the system operates exactly as described for the single generator system. Another variation is shown where a DC to DC converter is connected between each generator and the load. The outputs of the load of the two DC to DC converters are connected in series. Again, beyond this point the operation of the system is as described before. However, in this system it is possible to connect a diode across the output of each converter in its reversed direction so that should one generator fail, power from the second generator will still be fed to the load Of course the system voltage will be reduced by a factor of two as will the total power capabilities. The electronic equipment that follows the DC to DC converters will have to be able to operate under these reduced voltage conditions. Figure 10-23 shows a system that is similar to the above system except that rather than connecting the two (or more) generators in series, they are connected in parallel. Each individual output is controlled with respect to current. In this case a DC to DC converter is connected at the output of each generator with the DC to DC converter controlled with respect to generator output current. The output to the remaining portion of the system is the sum of the two currents from each of the two generators shown. In this system the failure of one generator will again reduce

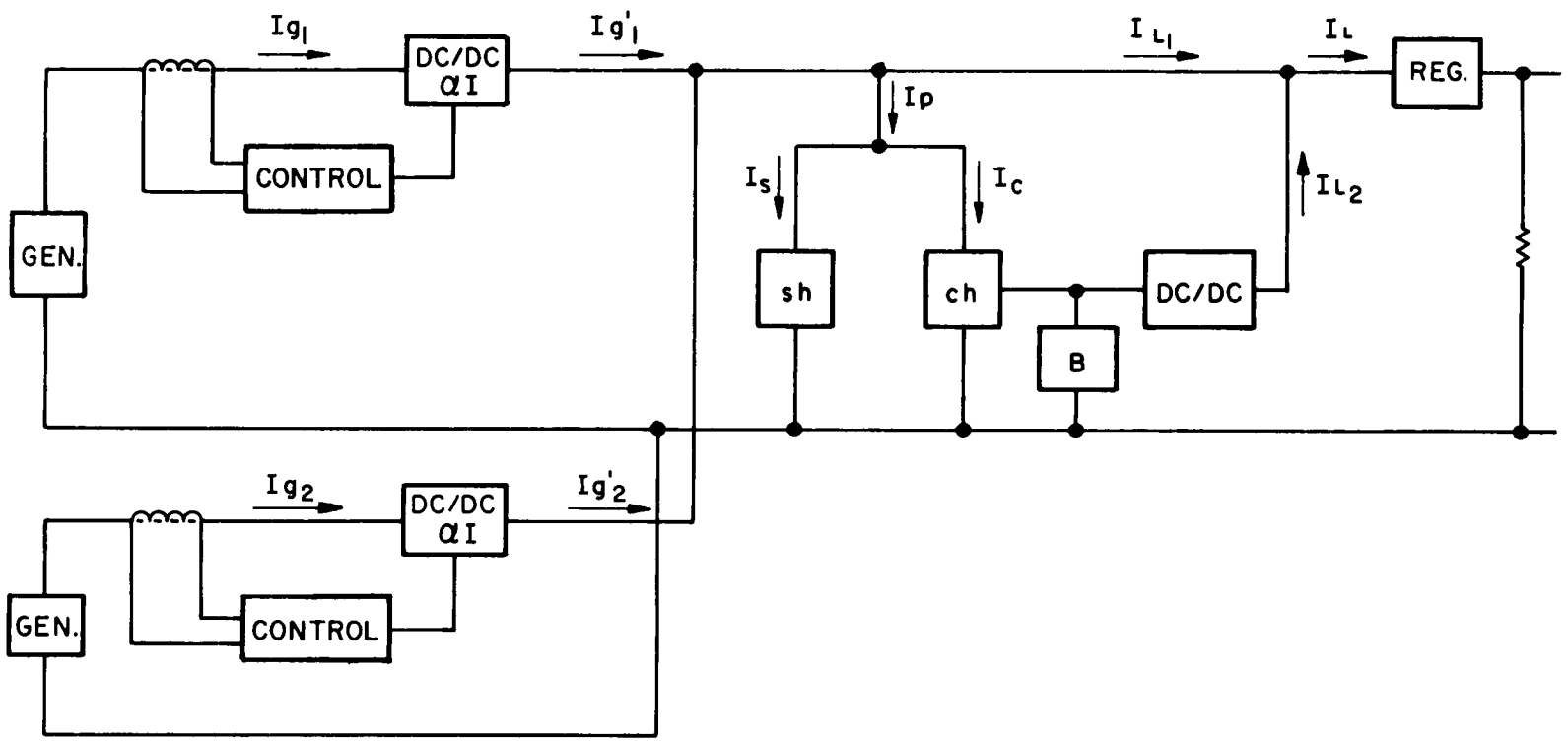

FIG. 10-2 SIMPLIFIED BLOCK DIAGRAM OF RECOMMENDED SUBSYSTEM WITH GENERATORS IN PARALLEL

the system power by a factor of two (of course if a greater number of generators are employed, the power reduction will be less).

10.2.4 Low Input Voltage DC/DC Converter

A basic block diagram of the low voltage DC/DC Converter is shown in Fig. 10-24. This block diagram applies to most DC/DC converters. Three basic circuits for low input voltage DC/DC converters are shown in Figs. 10-25, 10-26, and 10-27, respectively. There are many variations possible.

The converter shown in Fig. 10-25 is basically a standard unregulated type of saturating transformer device like that found in many power converters used commercially. The primary difference in this case is that the input voltage is considerably lower than in most other applications. Because of the low voltage and high current, the power transistors must have a very low saturation voltage. With present day technology, germanium power transistors must be used to obtain the high efficiency desired. Further, the power transformer design is more critical than normal because of the high current requirement and the relatively high voltage step-up ratio. Because of the few turns required on the primary, special design techniques must be used to provide good coupling between the primary and the secondary windings.

The output circuit of the converter is standard and is uncoupled (dc wise) from the input so that the output can be added to outputs from other converters if required.

The circuit shown in Fig. 10-26 is similar except that a low power driver transformer is used which provides the saturating device for the circuit. The advantage of this connection is that the peak currents obtained in the collectors of the power transistors are reduced somewhat. However, the disadvantage is that the power transformer will weigh approximately 30 percent more than in the first circuit because it must have a larger core with more wire. Again, the output circuit of the converter is isolated so that it can be added to other converter outputs.

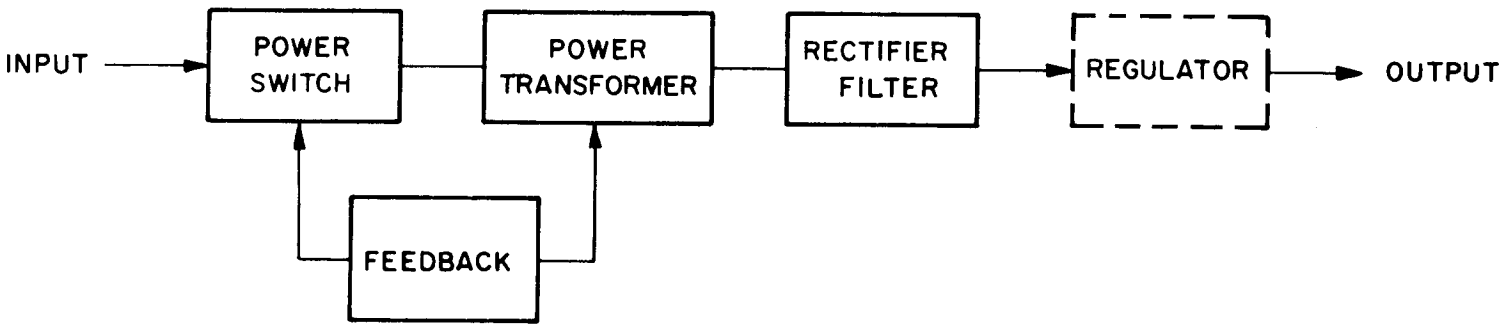

FIG. 10-24 BASIC BLOCK DIAGRAM OF DC/DC CONVERTER

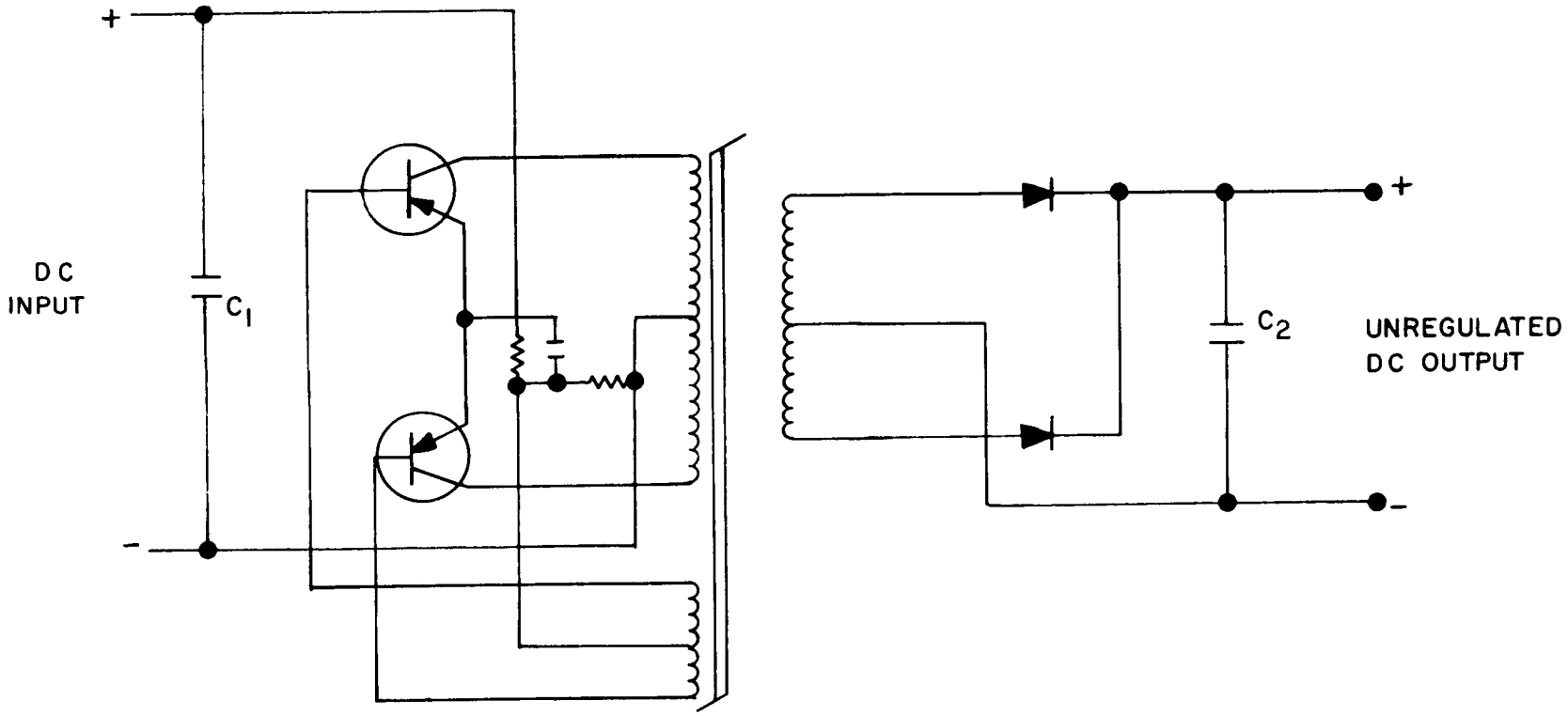

FIG. 10-25 LOW INPUT VOLTAGE DC/DC CONVERTER WITH SATURATING POWER TRANSFORMER

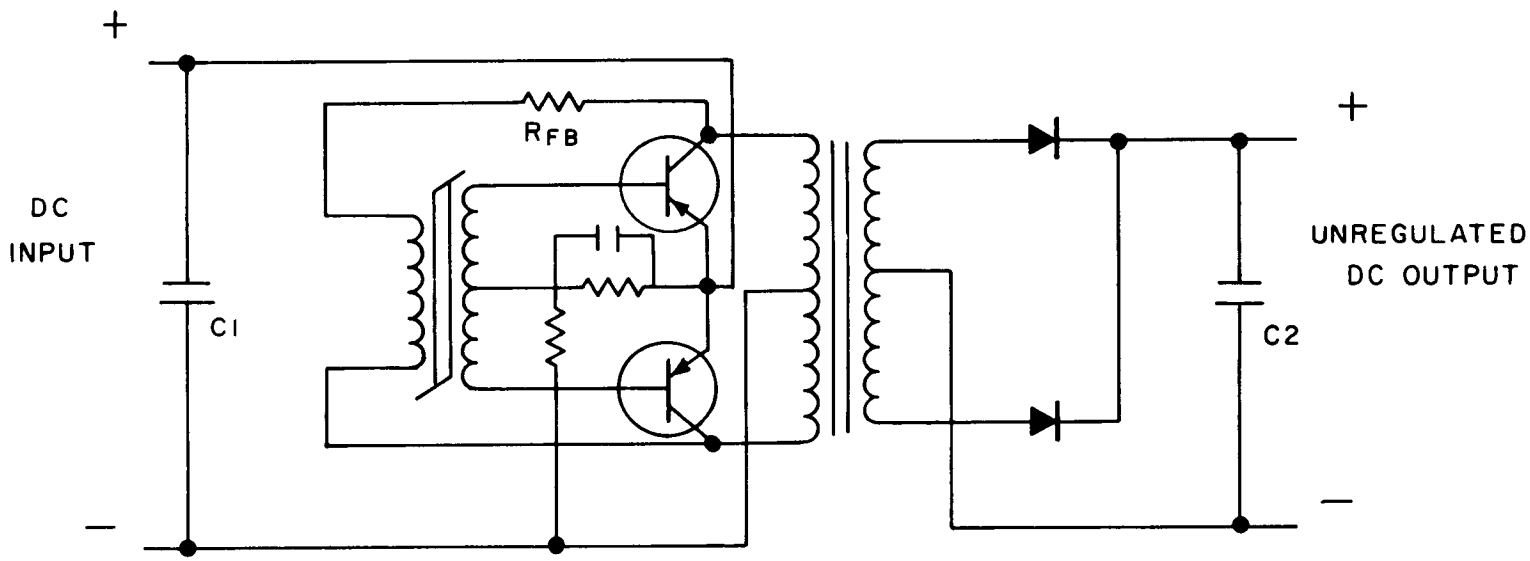

FIG. 10-26 LOW INPUT VOLTAGE DC/DC CONVERTER WITH SATURATING DRIVER TRANSFORMER

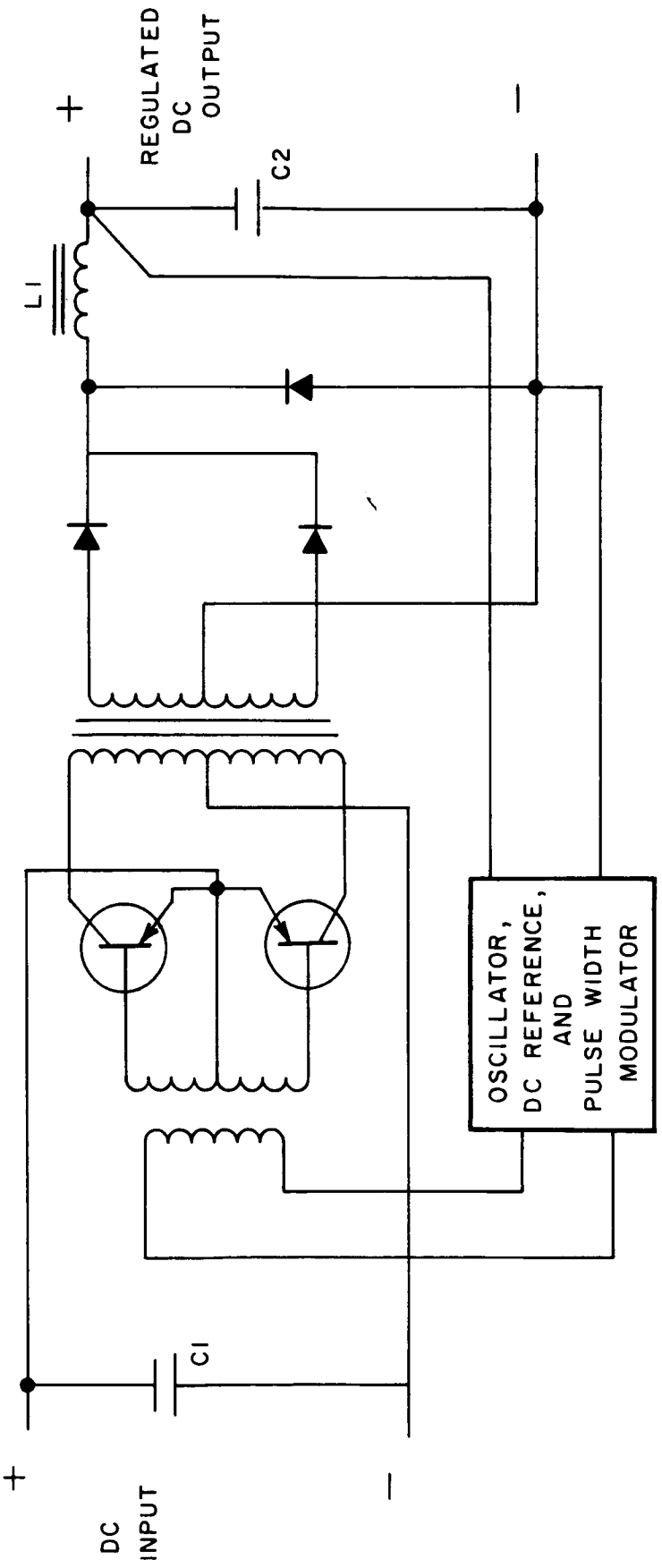

FIG. 10-27 LOW INPUT VOLTAGE DC/DC CONVERTER WITH PULSE WIDTH MODULATION

The third circuit, Fig. 10-27, is similar to the second except that it is a driven device so that it can be pulse-width modulated and can, therefore, incorporate voltage regulation. In the connection shown, the output voltage is compared to a reference voltage and the difference used to provide the pulse-width modulation. By measuring and then referencing the input current, the device can be made to regulate with respect to input current and therefore, be able to control the current loading on the thermionic diode.

Because of the pulse-width modulation, the converter must have an averaging output L/C filter in addition to the non-saturating power transformer and therefore its weight will be greater than either of the other two DC/DC converters shown in Figs. 10-25 and 10-26. The input capacitor C1 must be able to store a large amount of energy so as to limit the input current ripple imposed on the thermionic diode. The capacitor value must be significantly larger than that required on the non-regulating converters because of the narrow pulse-widths that must be employed. The capacitor must further have a low AC impedance since the pulse currents are very large.

Typical experimental efficiencies of unregulated low input voltage DC/DC converters are shown in Fig. 10-28. The curves indicate the dependency on input voltage and show that higher efficiencies are more readily obtainable with higher input voltages.

10.2.5 Shunt Load Control

As described earlier, the shunt load control is used to provide a resultant constant current load on the thermionic generator itself regardless of the load of the system. The control for the shunt load device is obtained by measuring the battery charger current and load current and subtracting the sum of the two from the desired constant value selected for the thermionic generator operating current. The measurements and computation can be conveniently accomplished by employing a magnetic type AC operated current detectors.

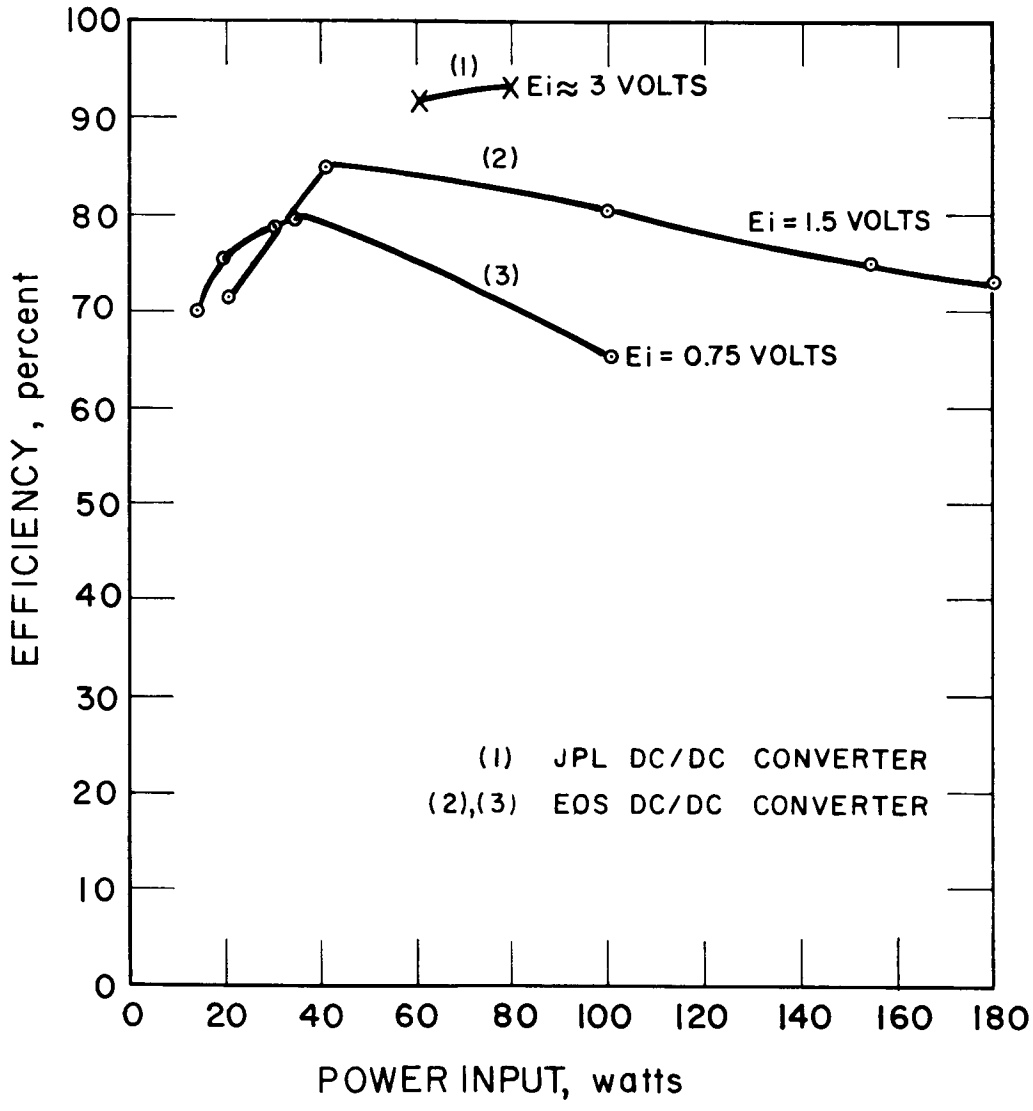

FIG. 10-28 TYPICAL EXPERIMENTAL EFFICIENCY OF UNREGULATED DC/DC CONVERTER

The shunt load consists essentially of a dissipative device whose effective load resistance can be varied. The simplest form of this is a power transistor connected across the bus voltage whose base to emitter voltage is adjusted to provide the appropriate load current. Figure 10-29a shows this simple form of shunt load. For reasons of power handling capability and redundancy, a number of transistors can be connected in a series/parallel arrangement to 1) distribute the power to be dissipated and 2) to provide redundant current paths should a transistor either open circuit or short circuit.

Figure 10-29b is a modification to Fig. 10-29a with a resistor placed in the collector of the transistors. The resistor value is selected to provide the maximum desired loading with a completely saturated transistor. The advantage of this circuit is that a smaller amount of power is dissipated in the transistor thereby reducing the cost, and weight and increasing the reliability.

Figure 10-29c shows a third shunt load device in which all (or nearly all) of the power is dissipated in the collector resistors of the transistors. In this circuit, a fairly large number of transistors and resistors are used with each one providing an incremental load to the system. The transistors are either turned on or off as controlled by a simple analog to digital converter. The input to the A/D converter is the required control input as in the other shunt load devices. One disadvantage of this circuit is that it will provide a step type loading and therefore the system must have a proper amount of "hysteresis" built into it to prevent instabilities. This system does have the advantage that the major power is dissipated in resistors which can operate at higher temperatures than the transistors. This, in turn will reduce the size of the heat radiator that must be provided in the system.

10.2.6 High Voltage DC/DC Converter/Regulator

The initial low input voltage DC/DC converters used in the system do not provide a regulated output voltage for reasons

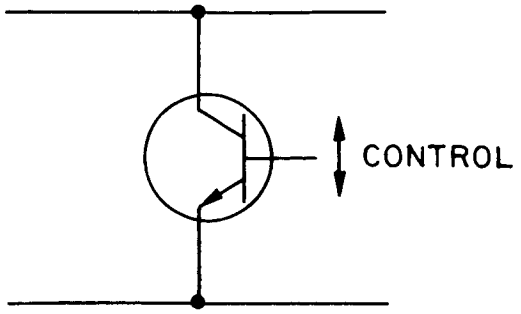

A. TRANSISTOR DISSIPATES POWER

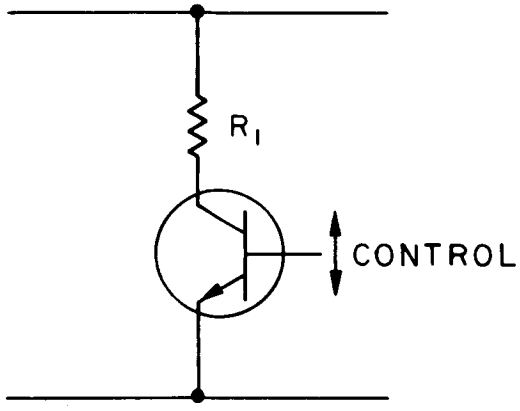

B. TRANSISTOR PLUS RESISTOR DISSIPATES POWER

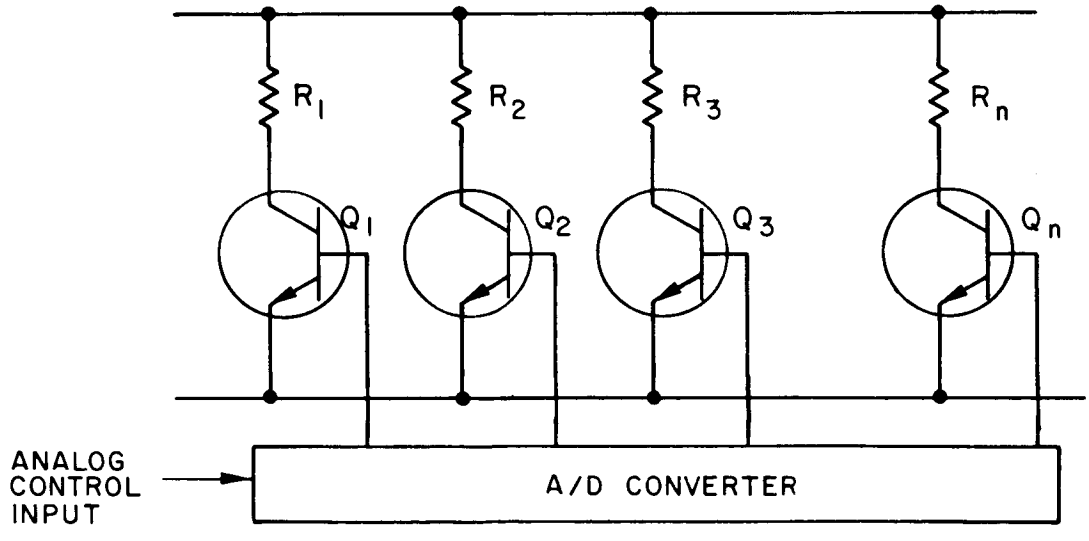

C. RESISTORS DISSIPATE POWER

FIG. 10-29 POSSIBLE SHUNT LOADS

discussed earlier. Therefore, there must be an additional step added to the system to provide the necessary dc voltage regulation. Since high efficiency is required, a switch mode type regulator will be used. A booster regulator type of converter could be employed but for reasons of increased efficiency, reduced weight and reduced complexity, a switch mode down converter/regulator should be used.

Figure 10-30 shows a functional diagram of such a converter/regulator. The input transistor Q1 turns on and off at a prescribed rate and with a prescribed duration to supply an output energy sufficient to provide the desired output voltage. L1 and C2 form an averaging filter for the chopped dc input. The output voltage is sampled and compared to a reference voltage and finally used to control the power transistor Q1. Efficiencies over 90 percent are readily attainable with the device when power drive circuitry is utilized.

10.2.7 Battery Charger

The battery charger will essentially consist of a standard DC/DC pulse-width modulated device with an averaging output filter. The charger will be controlled by various inputs depending on the operating mode, the power available and the battery condition.

The charger will be used as part of the "parasitic" load to provide a constant load current for the thermionic generator. Therefore, the charger must have one control input that limits its input current to a value which will not overload the thermionic generator. (With this input, charging will automatically be discontinued should the load current exceed the thermionic generator output current control point). Battery charging will be constant current but modified by terminal voltage and battery temperature. Therefore, the charger will provide a constant charge current until the terminal voltage reaches a preset value at which time the charge current will be reduced to a low trickle charge value. The preset voltage will be temperature dependent and controlled by a measurement of battery temperature.

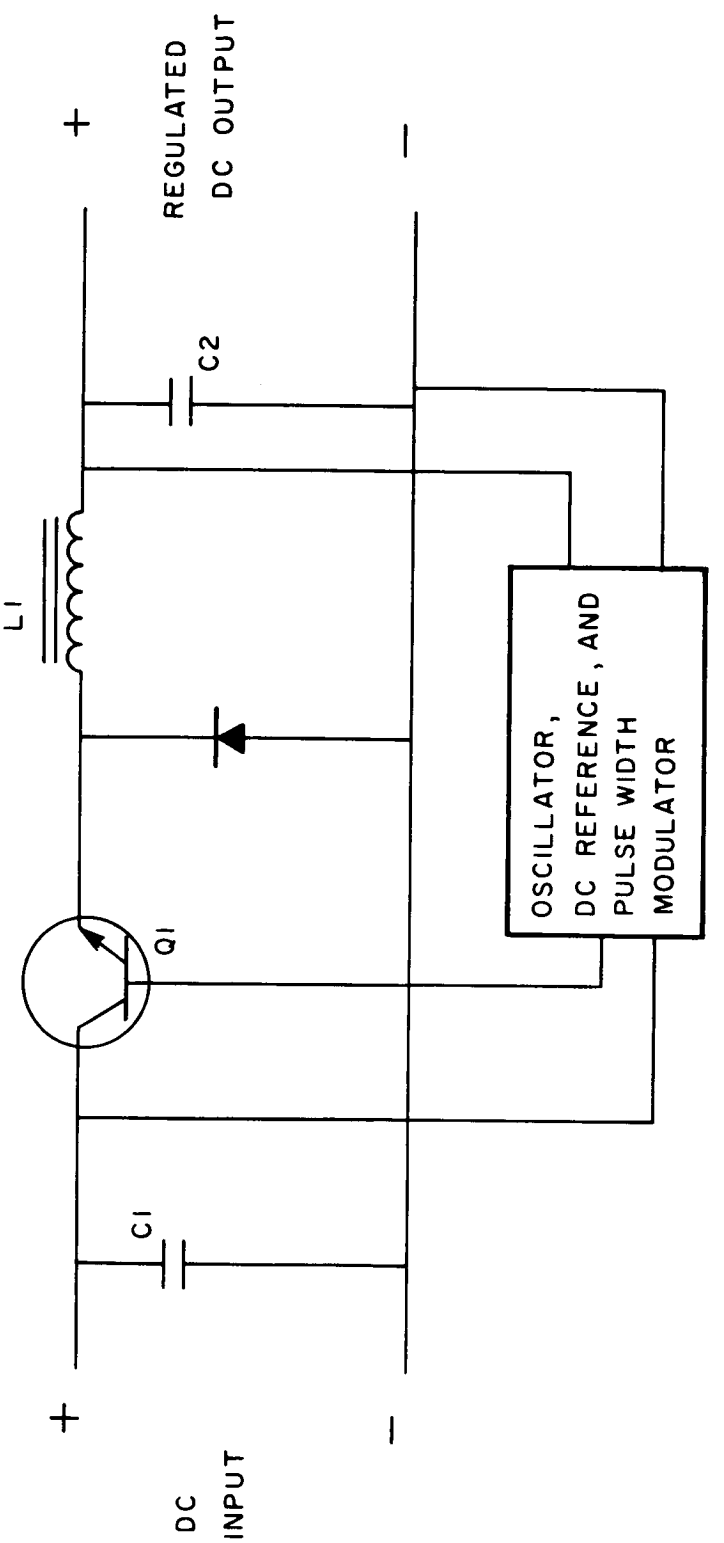

FIG. 10-30 HIGH VOLTAGE SWITCH MODE DOWN CONVERTER/REGULATOR

Fig. 10-31 shows a block diagram of the battery charger with its control inputs.

10.2.8 Battery Converter

Since the battery cannot be connected to the unregulated DC bus by conventional techniques such as are used on Ranger and Mariner vehicles, a DC to DC converter must be connected between the battery and the bus to provide the proper power summation. In order to provide the proper control, a pulse width modulated DC to DC converter must be used which obtains its control input from a measurement of current.

The battery converter is used only when power is required from the battery. This will only occur when the load current exceeds the preset output current capability of the thermionic generator. When this occurs, the battery charger and shunt load are made inoperative and the battery converter activated. The output control for the battery current is obtained by taking the difference between the load current and the thermionic generator preset current such that I_{L2} (battery converter load current) = I_L (load current) - I_{L1} ($I_g = K_1$).

Figure 10-32 shows a block diagram of the battery converter with its control inputs.

Battery

The following electrochemical systems are compared here for potential application to solar thermionic systems.

1. Nickel Cadmium
2. Silver Cadmium
3. Silver Zinc
4. Regenerative hydrogen-oxygen fuel cell

10.2.8.1 Cycle Life, Size, and Weight

The system that has the most extensive cycle life data is the nickel cadmium battery. There is only limited data on silver-zinc rechargeable batteries and a somewhat greater amount

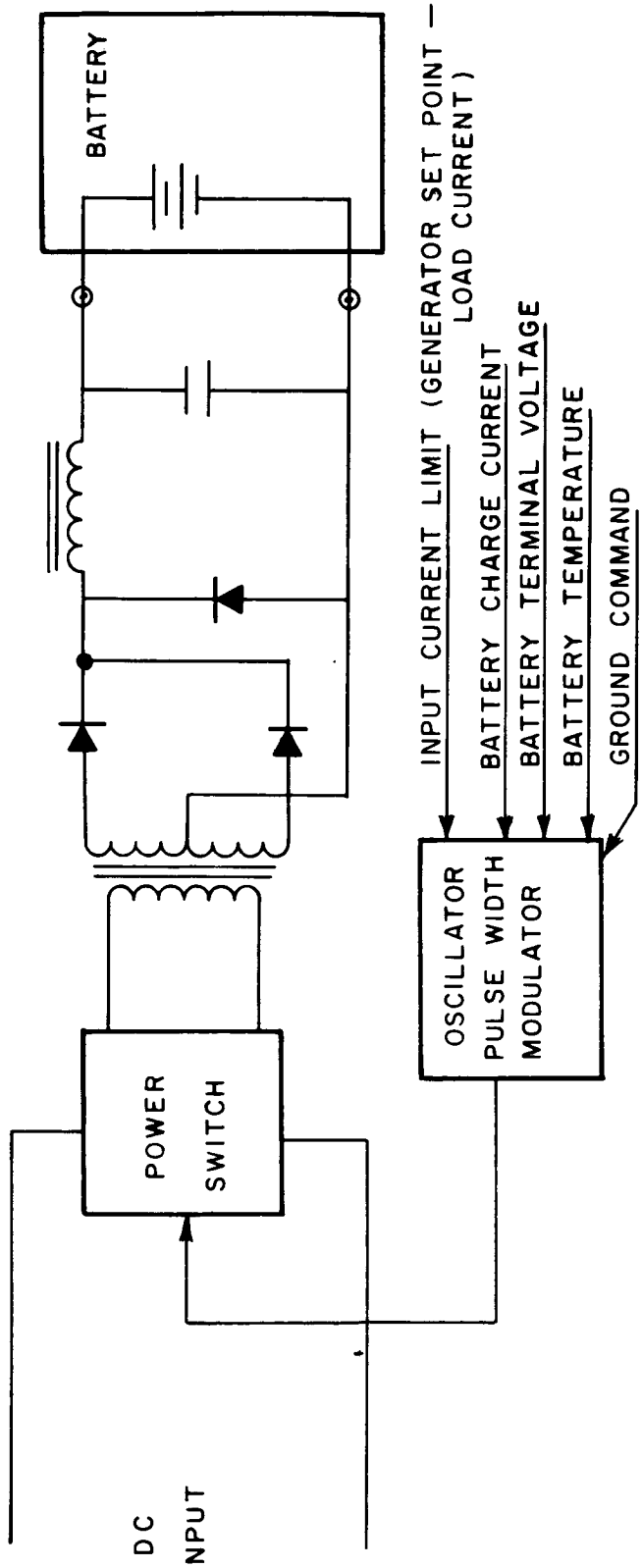

FIG. 10-31 BATTERY CHARGER BLOCK DIAGRAM

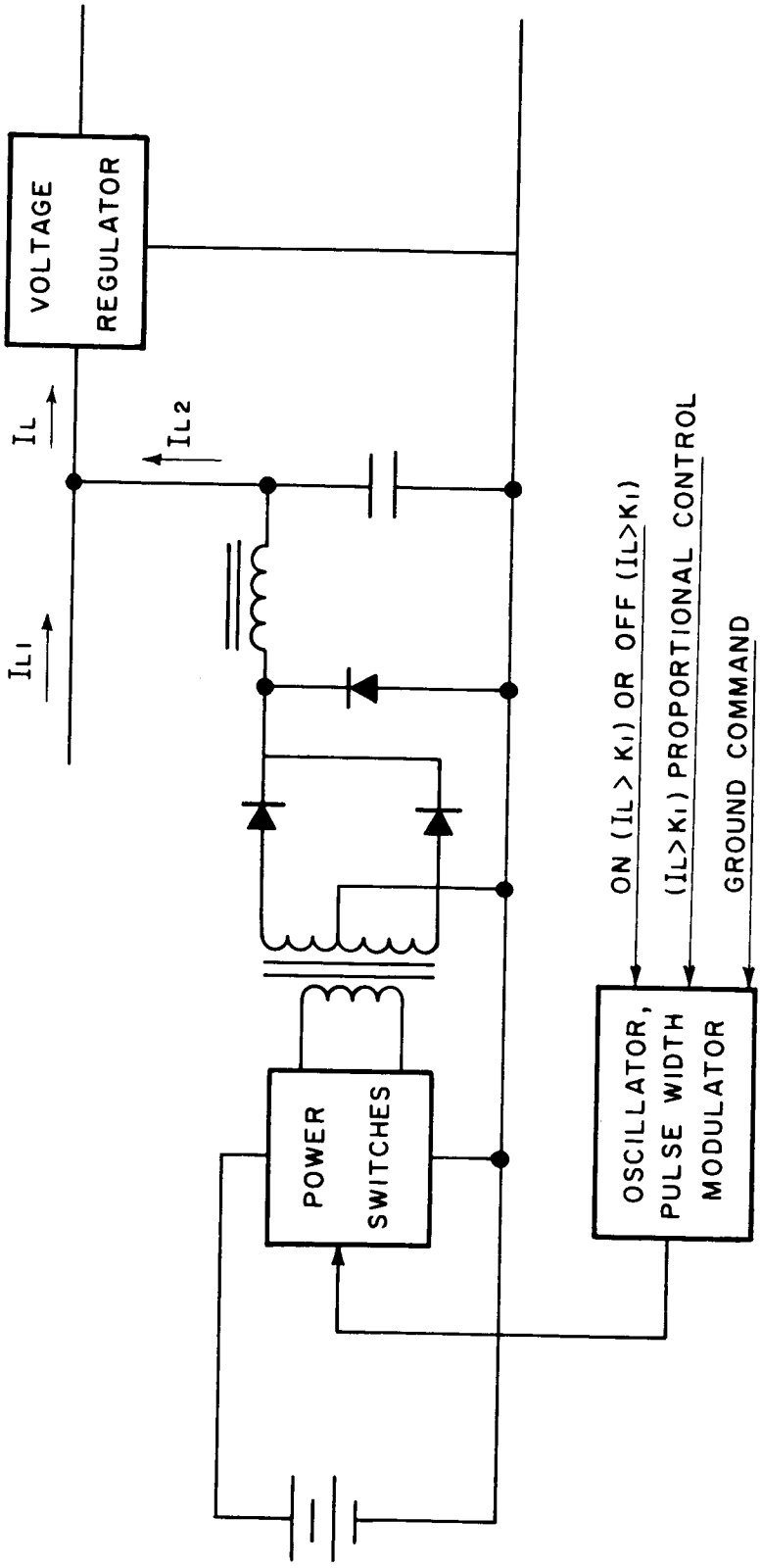

FIG. 10-32 BATTERY CONVERTER BLOCK DIAGRAM

of data on silver-cadmium batteries. The data available is quite scattered, and conducted on different cycles and different test conditions. More recent data shows cycle life improvements over previous data of a year or two ago. It is extremely difficult to obtain absolute values for cycle life capability due to the tremendous scattering of available data. Figure 10-33 is a compilation of various sources of cycle life vs. depth discharge data for the battery systems. Average curves are presented. If ranges were used, the ranges would cover the entire page for each line. It should be pointed out that the standard cycles that are normally used for evaluation of these batteries are the 100 min. cycle, 35 minutes discharge, 65 minutes charge; the two-hour cycle, 35 minutes discharge, 85 minutes charge; and the 24-hour cycle, 1.2 hours discharge, 22.8 hours charge. For slower cycles, such as 50 hour with 3 hours discharge, charging conditions are considerably more relaxed than the other cycles described, since it allows moderate rates of discharge, and long periods for recharging of the battery. This type of cycle would generally improve cycle life performance improvements above what is available in the literature. However, in such a slow cycle, over-all wet life and deterioration come into effect as limiting factors on life, possibly to a greater extent than total cycle life. On the right ordinate of Figure 10-33 is the watt-hour per pound capability of the systems. The values for watt hour per pound at 100 percent of discharge were linearly decreased as a function of depth of discharge on the curve which is not exactly true, but the error is slight. These energy yield capabilities are also subject to variation depending upon details of construction, size of battery, and rate of charge and discharge at which the energy yield is determined. Essentially, lower rates of discharge, as experienced in this application, generally yield higher energy outputs. The levels chosen are realistic values for sealed batteries of the size for this application.

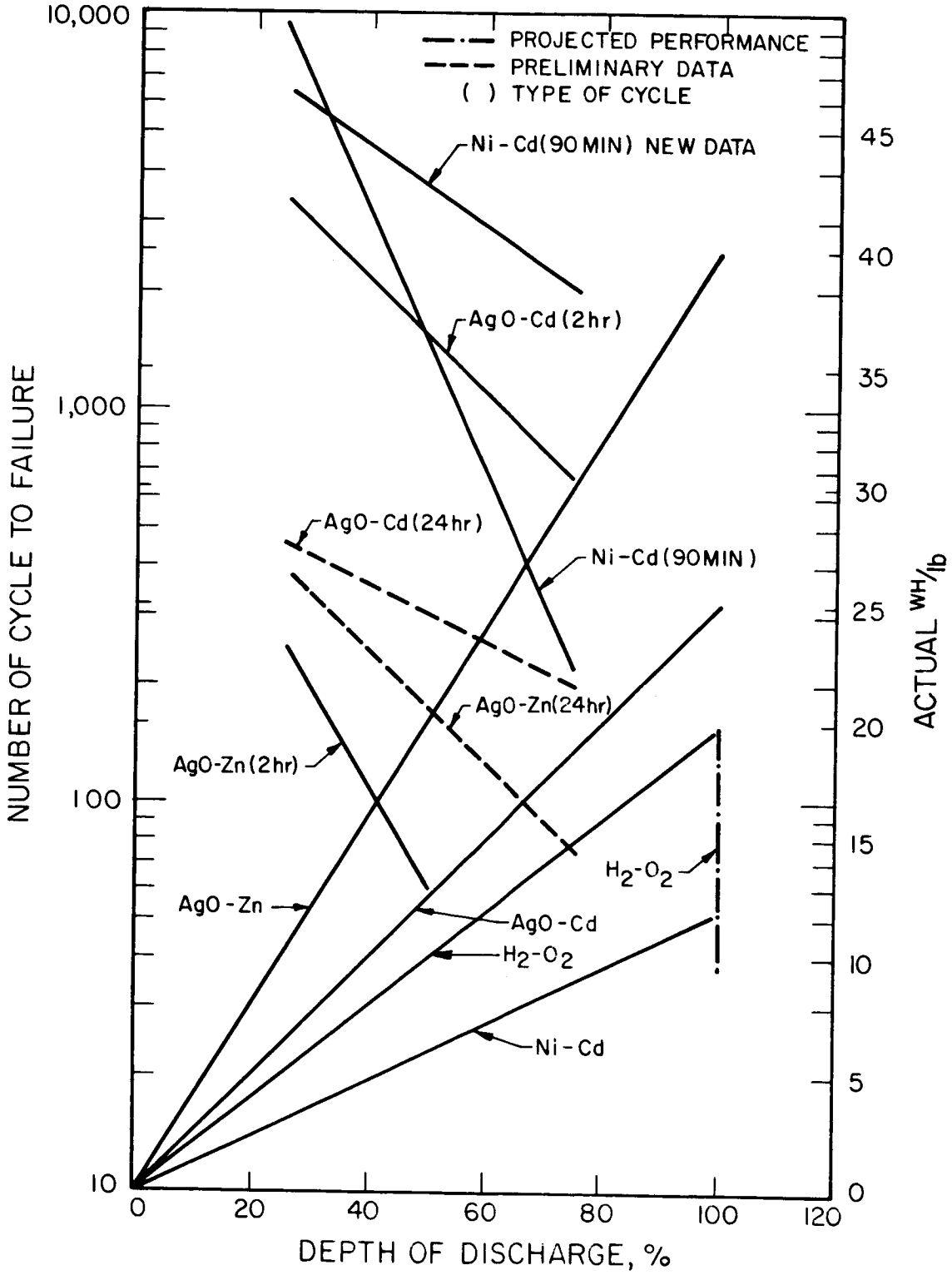

FIG. 10-33 COMPARATIVE PERFORMANCE OF ENERGY STORAGE SYSTEMS

The graph shows cycle life data for both 24-hour and 2-hour cycles for the silver batteries. There is an inconsistency in the order of these curves. The silver zinc system shows better performance at the 24-hour cycle, while the silver cadmium system shows better performance at the 2-hour cycle. However, there is only limited data at the 24-hour cycles, and until more data is available, these curves should not be used as a basis for a choice. The curves are only included to show possible future trends.

The H_2-O_2 system is shown as not being affected by cycle life. The maximum number of cycles yet obtained is 30 cycles on a 90 minute test cycle, but the curve is projected to 200 cycles.

As an example, for a battery delivering something like 75 cycles, it appears that the silver cadmium battery is capable of being discharged at 100 percent of discharge. However, this is not recommended due to the likelihood of series cell imbalance problems. Therefore, a maximum 80 percent depth of discharge should be considered for this system resulting in an energy yield of 20 watt hours per pound. For the silver-zinc system, it appears that a 45 percent depth of discharge could yield 75 cycles, and the energy output at that depth would be 18-watt hours per pound, or very close to the silver-cadmium yield. The nickel cadmium battery even if discharged at 100 percent depth of capacity would only yield 12 watt hours per pound. The regenerative hydrogen-oxygen fuel cell rated at 20 watt hours per pound on the complete package at 100 percent depth of discharge appears to be capable of yielding 20 watt hours per pound also. Therefore, the three systems silver-zinc, silver-cadmium, and hydrogen-oxygen based on just cycle life are almost equivalent in energy output. Table 10-II summarizes this data.

For a three cycle application, any of the systems could be used at an estimated 80 percent depth of discharge. Therefore, the silver-zinc system looks most attractive as shown in Table 10-II.

TABLE 10-II

COMPARISON OF SIZE AND WEIGHT OF RECHARGEABLE SYSTEMS FOR 75 CYCLES

System	% Depth of Discharge	Actual WH/lb/Cycle	Nom. Cell Voltage	No. Cells for 28V	WH/in^3 at 100% Depth	Actual WH/in^3
AgO-Zn	45	18.0	1.48	19	3.3	1.49
AgO-Cd	80	20	1.08	25	2.2	1.75
Ni-Cd	80	9.6	1.22	23	.9	.72
H_2-O_2*	100	20	.88	32	.3	.3
			3 CYCLES			
AgO-Zn	80	36	1.48	19	3.3	2.64
AgO-Cd	80	20	1.08	25	2.2	1.75
Ni-Cl	80	9.6	1.22	23	.9	.72
H_2-O_2*	100	20	.88	32	.3	.3

* Estimate

Table 10-II also shows estimated volumes for all the systems. If advances can be made in the H_2-O_2 system to store gases at higher pressures, its size could be reduced.

10.2.8.2 Total Wet Life

A typical planetary orbiter mission might require a total wet life from launch of up to 450 days. In addition, probably 2-3 months additional wet life would be required for manufacturing of the batteries and delivery to launching facility. This wet life requirement is a problem for the silver-zinc battery. This type of battery deteriorates whether in use or not. The separator materials employed are subject to deterioration by the electrolyte over long periods of time. Typical vented and sealed silver-zinc cells are rated at 1-2 years wet life. The silver-cadmium battery deterioration with age is not as critical. In the case of the nickel-cadmium and the hydrogen-oxygen fuel cell, there seems to be no serious mechanism of deterioration during wet life.

10.2.8.3 Temperature Sensitivity

Of the battery systems, the silver-zinc battery is most sensitive to temperatures. Elevated temperatures, 125°F and above cause increased chemical deterioration, and reduced life. Lower temperatures (30°F and below) on the other hand cause poor electrochemical performance. However, in low rates of charge and discharge application , lower temperatures could probably be tolerated. The silver-cadmium and nickel-cadmium batteries are less affected by temperature variations. However, they do exhibit shorter lives at temperatures above 125°F, and poor performance at temperatures below 30°F. The regenerative hydrogen-oxygen fuel cell requires an operating temperature range of $\sim$ 150°F for operation. This temperature is generally maintained by cell inefficiencies, but if allowed to fall below 120°F performance would drop off considerably.

10.2.8.4 Charge Techniques

In the case of the nickel-cadmium batteries, continuous trickle charging of the cells would be allowable. No elaborate control would be necessary since when the cells became fully charged, the gas recombination mechanism within the cells would take over, and the pressure in the cells would reach an equilibrium level. In the case of the silver-zinc and silver-cadmium cells, the over-charge capability of these cells, at the present state of the art, is behind those of the nickel-cadmium cell. It may be possible to obtain cells of the silver-cadmium type with sufficient over-charge capabilities for this application. If not, it is necessary to provide voltage cut-off and charge control, for end of charge, to prevent over-charging, gasing, and cell bursting. The regenerative hydrogen-oxygen fuel cell can be simply controlled by providing a pressure switch in the cell so that when the cell is charged to a pre-determined gas pressure level, the charging circuit would be disconnected.

10.2.8.5 Sterilization Capabilities

Both silver batteries employ cellulosic type separator materials that are necessary to reduce silver migration, a potential cause of cell failure. These types of materials are not capable of sustaining the sterilization temperatures in the alkaline electrolyte employed within the cells. Therefore, unless new separator systems can be made available, these type batteries could not be sterilized. The nickel cadmium and the regenerative fuel cell batteries use separator materials that are essentially electrode spacers and electrolyte holders. The materials employed in these cells could be made to withstand sterilization requirements.

10.2.8.6 Environmental Capabilities

All of the battery systems have been subjected to ranges of environmental requirements for other application, and it appears that this should not present a problem. The regenerative fuel cell has no test data available, but if the unit is designed

properly, it too should be capable of meeting all types of environmental requirements encountered in space applications.

10.2.8.7 Availability and Experience

The most readily available battery is the nickel cadmium cell. It may be possible that existing cell sizes are available to meet this application. If not, custom cells can be readily designed for the application. The silver-cadmium battery state of the art is similar. Nickel cadmium batteries have been used extensively on essentially all of the satellite systems in use. There have been a few satellite systems employing silver cadmium seal cells in the explorer series, Explorer XII, and others. In the case of the silver-zinc, the only space proven batteries are those that have been used in the Mariner and Ranger applications and these are essentially primary batteries. The Li_2-O_2 system is still in development, and it is estimated that one or two years of work would be required to make such a unit. After that, a considerable amount of testing would be necessary.

10.2.8.8 Performance Characteristics

Figure 10-34 shows typical charge-discharge curves for the various battery systems, and Table 10-III shows typical storage efficiency for the different systems calculated on the basis of the performance as shown in Fig. 10-34. The Ni-Cd system requires considerable overcharge to replace used capacity. At low rates of charge, as encountered in the orbit application, charge input can go up to 200-300 percent. This can be overcome somewhat by reducing the charge period, and increasing the charge current rate.

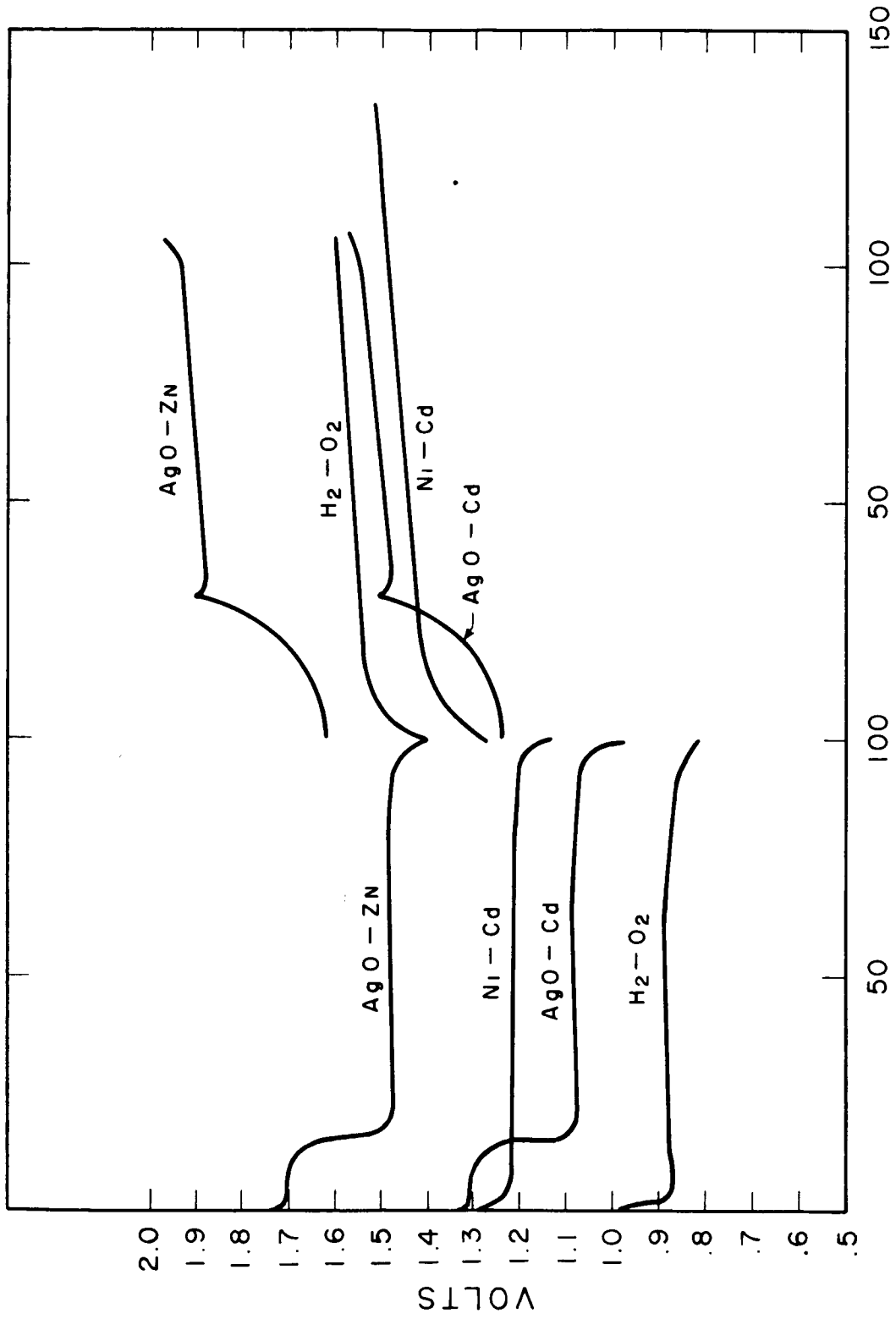

FIG. 10-34 TYPICAL CHARGE-DISCHARGE CURVES PER CELL FOR ENERGY STORAGE SYSTEMS (Medium rate)

TABLE 10-III

TYPICAL STORAGE EFF/PER CELL OF RECHARGEABLE SYSTEMS
(MEDIUM RATE)

System	Nom. Voltage Discharge	Nom. Voltage Charge	Voltage EFF %	Overcharge Required %	Power EFF %
AgO-Zn	1.48	1.9	78	5	74
AgO-Cd	1.08	1.50	73	5	69
Ni-Cd	1.22	1.40	87	35*	64
H_2-O_2	.88	1.50	59	5	56

* This can be much worse for low rate long charge periods.

10.2.8.9 Voltage Regulation

Ranges of output voltages from 20-60 volts do not appear to offer a difficult problem. More cells one used to achieve a higher voltage battery generally results in increased weight, reduced reliability, increased size, and essentially the same percentage regulation. These effects would not, however, be drastic in the range of 20-60 volts.

10.2.8.10 Packaging

Sealed nickel-cadmium batteries are generally packaged in welded deep drawn metal cans with ceramic to metal terminals. These cells are generally connected in a series stack, and contained in an outer metal container. The sealed silver-cadmium and silver-zinc batteries fabricated thus far are generally assembled in plastic cell cases, as conventional vented cells are, then placed in an outer metal container and filled with an epoxy sealing compound to provide the hermetic seal. If desired, it would be possible to locate groups of cells at various locations within the vehicle. The best approach for this would be to connect groups of cells in series since these cells are constructed in a modular concept. However, it probably would be necessary to encase each group of cells with mounting hardware, connectors, etc., thus resulting in increased weight. The H_2-O_2 system would require one cylindrical package or a considerable weight increase would occur.

10.3 Configuration and Performance

Using the information presented in the preceding paragraphs, it is possible to show a final system configuration of the power conditioning equipment for a typical solar-thermionic power system. A block diagram for the system is shown in Fig. 10-35. This diagram does not include certain required controls such as solar flux control, attitude control, cesium reservoir temperature control, and so forth.

As discussed earlier, a thorough tradeoff study should be made to determine the amount of redundancy or diode bypass capability that should be included in the system. For the purposes of showing a completed system, the block diagram assumes the use of several low voltage dc to dc converters connected in an appropriate series-parallel arrangement. Therefore, in this system should one diode fail by opening, power output will be lost for n diodes.

The overall efficiency of the electrical conversion and control equipment can be computed for various operational cases. The first case is the configuration where power is supplied to the load through the power conditioning equipment but not through the battery. In the second case, the power is supplied through the battery. (There are other variations such as the case where part of the power is supplied by the battery while the remainder is supplied by the source.)

Typical efficiences are listed below using individual equipment efficiencies (see Fig. 10-36) but do not consider other system losses such as connecting leads, thermal loss within the generator, etc. Efficiencies listed below are nominal and will vary somewhat depending on the specific application.

Reasonable Efficiencies of Conditioning Equipment

1. Low input voltage DC/DC converter

   η_1 = 90 percent

2. Shunt load

   The shunt load efficiency will include control power loss and will include a factor to compensate for the inability

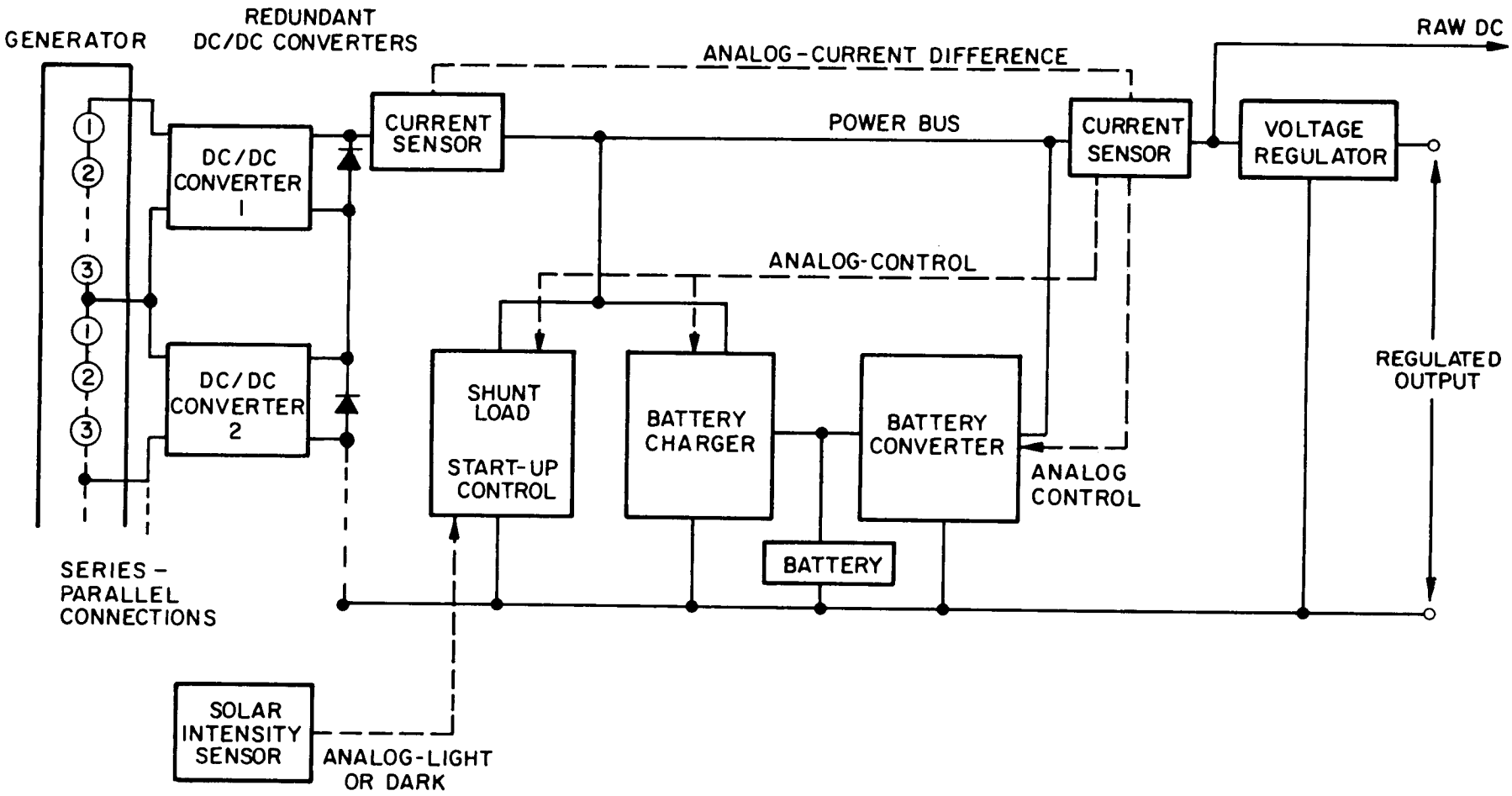

FIG. 10-2 POWER CONDITIONING AND CONTROL BLOCK DIAGRAM

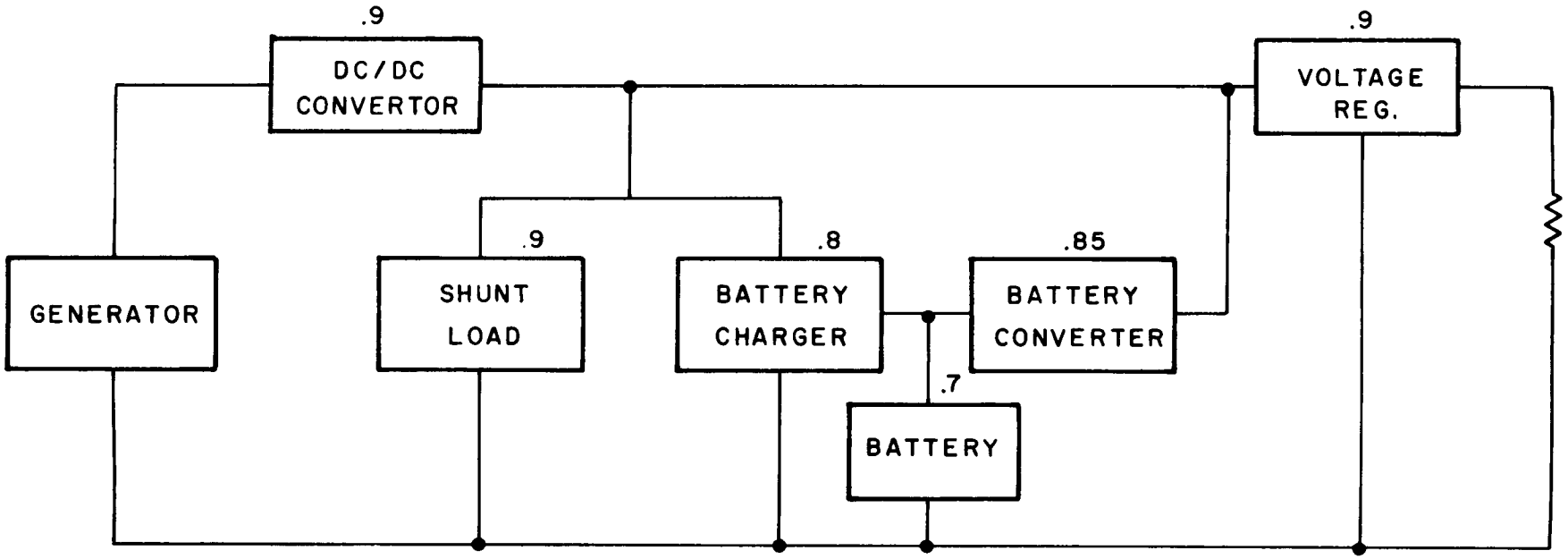

NOMINAL EFFICIENCIES

CASE A, h = 73% (ALL POWER SUPPLIED BY GENERATOR)

CASE B, h = 39% (ALL POWER SUPPLIED BY BATTERY)

CASE C, h = 70% (GENERATOR POWER FOR 90% OF TIME,
BATTERY POWER FOR 10% OF TIME)

FIG. 10-36 BLOCK DIAGRAM SHOWING NOMINAL COMPONENT EFFICIENCIES

to operate exactly at maximum power. The efficiency will be shown for operation at maximum load since this is the case of primary importance.

η_2 = 90 percent

3. Voltage regulator

   η_3 = 90 percent

4. Battery charger

   η_4 = 80 percent

5. Battery DC/DC converter

   η_5 = 85 percent

6. Battery

   The battery power efficiency includes its voltage efficiency plus its overcharge requirement. A silver zinc battery is assumed for this computation

   η_6 = 70 percent

Efficiency - Case A

The first case will exclude the battery. This would be normal sun-powered operation where the load requirement is equal to or less than the source power output (less losses).

$\eta_A = \eta_1 \times \eta_2 \times \eta_3 = 0.9 \times 0.9 \times 0.9 \times 100 = \underline{73}$ percent

Efficiency - Case B

The second case will include the battery. This would be equivalent to operating through the battery charger, battery, and battery DC/DC converter.

$\eta_B = \eta_1 \times \eta_4 \times \eta_6 \times \eta_5 = 0.9 \times 0.8 \times 0.7 \times 0.85 \times 0.9 \times 100 = \underline{39}$ percent

Efficiency - Case C

If we assume a mission that utilizes battery power 10 percent of the time, the resultant conversion efficiency is 73 percent x 0.9 + 39 percent x 0.1 = 70 percent overall to the regulated DC output voltage.

When the output load requirement of the system is less than the output capability of the thermionic generator, the excess power is used to charge the battery or is dissipated in the shunt load. The charger will draw only the amount of excess current available during charging or it will be limited by the charge requirements of the battery. If additional power is available from the generator, it will be absorbed by the shunt load. During peak load requirements, the charger and shunt load are disconnected electrically and the battery converter is activated so that the excess power requirement is obtained from the battery. The output of the battery converter is controlled such that the sum of its output current and the bus output current is equal to the current required by the load.

The weight of the power conditioning and control depends on power level, voltage from the generator, specific load characteristics, the temperature environment, and other related factors.

Figure 10-37 shows typical weight and efficiency characteristics for DC/DC converters in a system situation where the voltage output from the generator varies with power level. Characteristics are shown for 1965 and 1970, the former is based on laboratory development to date at several laboratories and the latter extrapolated from estimates of future capability published by GE, Westinghouse, RCA, and others.

Figure 10-38 shows the specific weight estimated for 1970 DC/DC converters as a function of power level and voltage input.

The low voltage DC/DC converter is the primary contributor to power-conditioning and control of weight. This is illustrated in Table 10-IV which shows a typical weight breakdown for a 300-watt system, where 3 DC/DC converters are used for reliability. As shown, about two-thirds of the weight is occupied by the DC/DC converter. While this ratio will vary according to each system requirement, the application of this ratio and the use of Fig. 10-38 is sufficient for preliminary systems analysis.

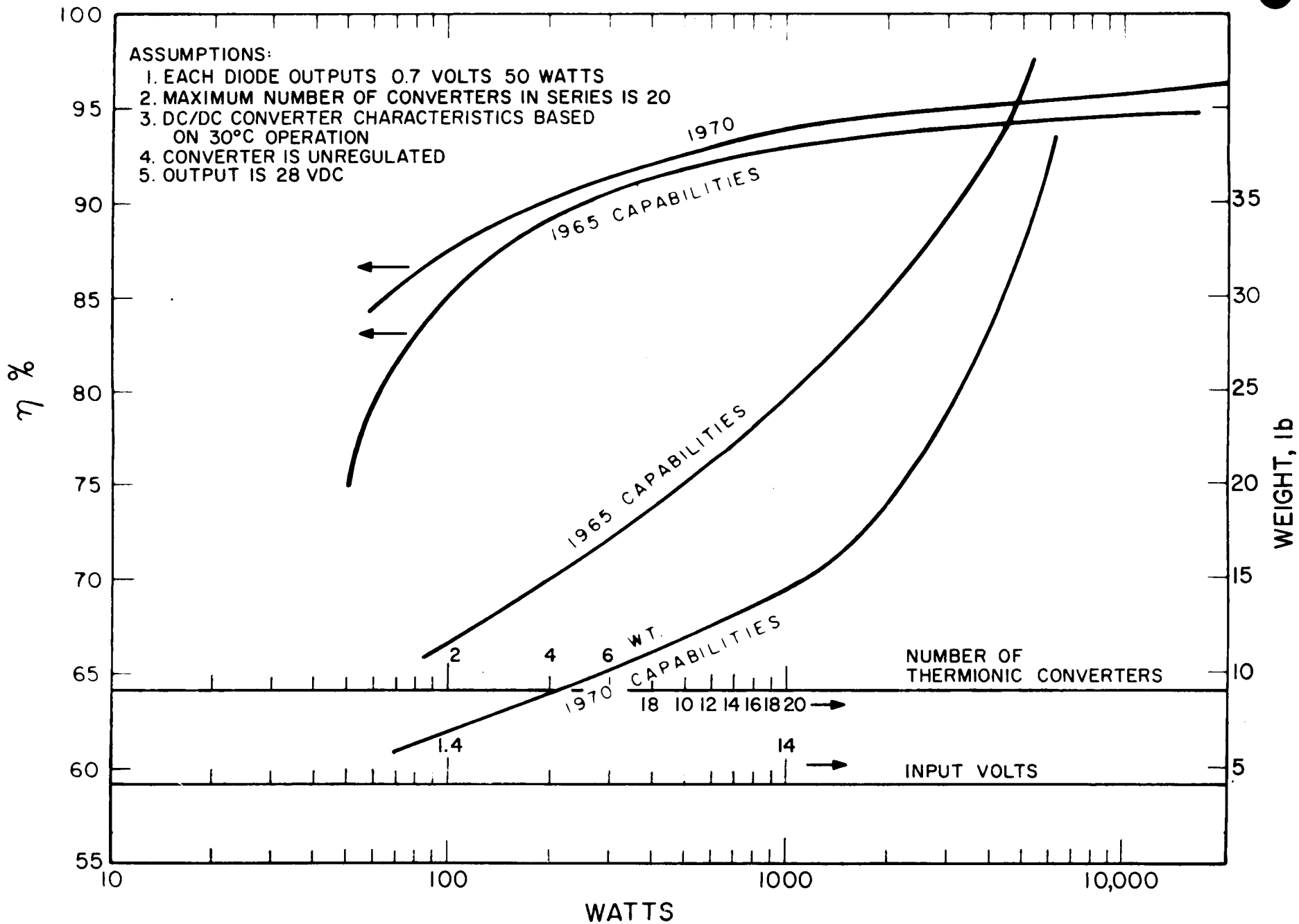

FIG. II-2 WEIGHT EFFICIENCY OF DC DC CONVERTER FOR DIFFERENT INPUTS

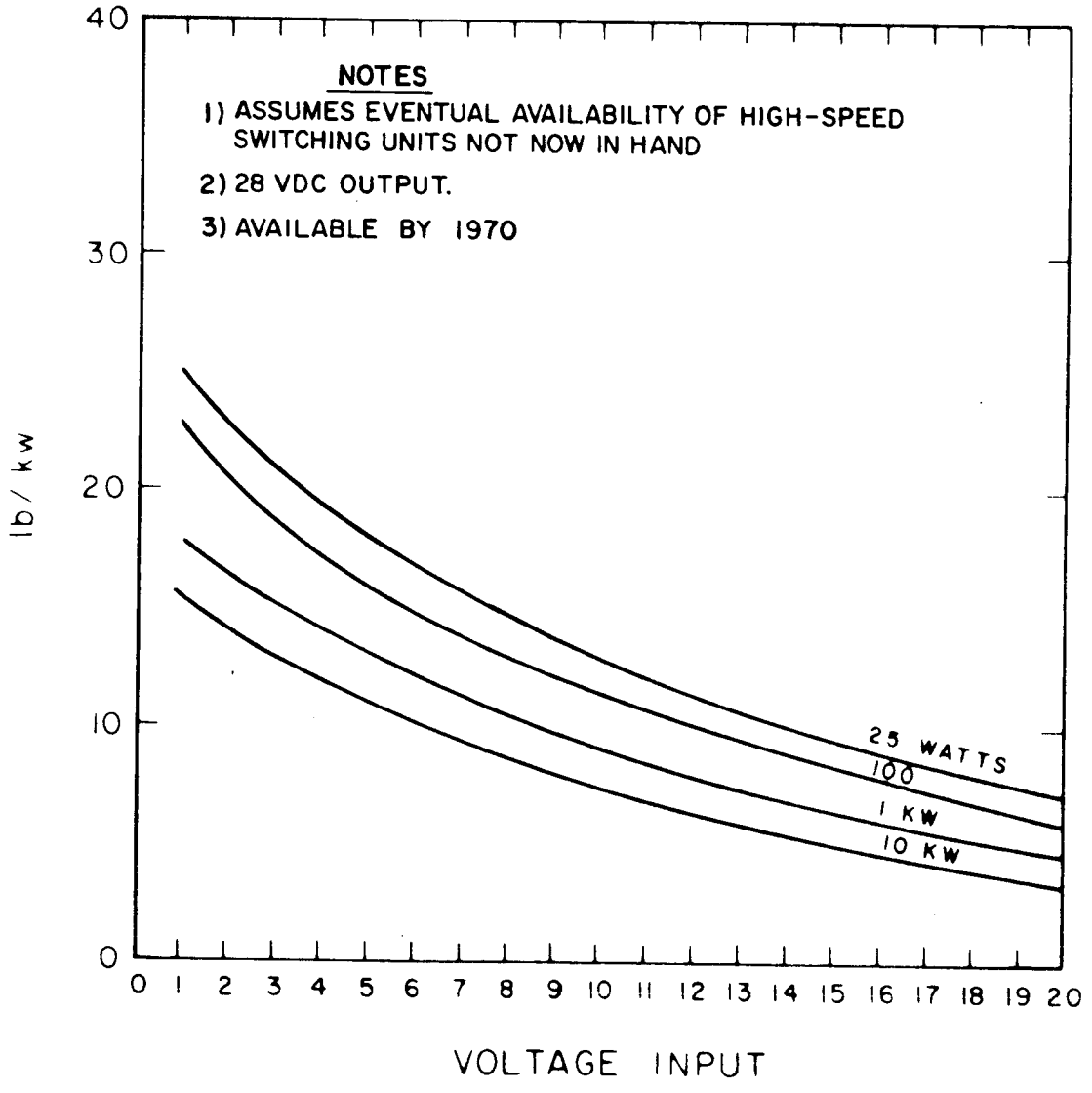

FIG. 10-38 WEIGHT CHARACTERISTICS OF POTENTIAL DC/DC CONVERTERS

TABLE 10-IV

TYPICAL WEIGHT BREAKDOWN - 300-WATT SYSTEM

Item	Quantity	Weight per Unit 1965	Weight per Unit 1970	Total Weight 1965	Total Weight 1970	Efficiency (%) 1965	Efficiency (%) 1970
Low voltage DC to DC converter	3	7	2.5	21	7.5	91	92
Shunt load (less radiator)	1	3	1.0	3	1.0	90	95
Battery Charger	1	2	1.0	2	1.0	80	85
Battery Converter	1	3	1.0	3	1.0	85	90
Voltage Regulator	1	2	0.5	2	0.5	90	92
		Total		31	10.5		

11. RECOMMENDATIONS FOR DEVELOPMENT PROGRAMS

This section contains recommendations for twenty-seven separate programs which represent a logical extension of current technology leading towards flight systems in the near future.

Each program is of importance in the development of high efficiency, reliable solar-thermionic systems. The scope and nature of each program results from analyses and judgments reported elsewhere in this document.

Ideally, solar-thermionic systems problems should be attacked on a broad front with a series of flight systems being prepared which represent progressive increases in system performance, reliability, weight and other features. However, practical considerations place a limit on cost budgets. Consequently, the number of systems which can be developed to flight readiness must be limited.

All of the twenty-seven programs outlined here are important to the development of a 5-foot or 9-1/2-foot system. The flight readiness date for any specific system will depend on the amount of effort which can be reasonably applied in the near future.

Figure 11-1 consists of a PERT-type network which describes major steps leading towards flight readiness for each of five systems. The chart could be converted into a PERT plan with the addition of estimated times of activities and other schedule information. The PERT-type plan in Fig. 11-1 shows only the major milestones and represents a first iteration. Other iterations should be accomplished on a continual basis as part of a system development plan.

The characteristics of each of the five systems in Fig. 11-1 are summarized in Table 11-I. The physical characteristics of the five

TABLE 11-I

SYSTEM CHARACTERISTICS

System	Concentrator	Support	TES	Controls Cs Res	Solar Flux	Nominal Generator Life	Operational Readiness Date
A	5'-Ni	Rigid	No	Yes	No	500 hr	Apr 1966
B	5'-Ni	Unfolding	No	Yes	Yes	2000 hr	Jan 1967
C	5'-New Material	Unfolding	Yes	No	Yes	5000 hr	Jan 1968
D	9-1/2'Ni	Unfolding	No	Yes	Yes	2000 hr	Feb 1967
E	9-1/2'-New Material	Unfolding	Yes	No	Yes	5000 hr	Mar 1968

systems in Table 11-I are based on judgments regarding developmental progress, assuming that serious efforts are taken to achieve systems hardware.

An integrated plan for systems hardware is definitely required with continual updating and shifting of emphasis to insure that flight systems achieve a readiness state. This plan should be continuously reviewed by JPL. In fact, this program is perhaps as important as any of the other programs described in this text.

Milestones illustrated in Fig. 11-1 generally cover the twenty-seven recommended programs; the chart is included as an example of the relationship between programs for any given specific system. Steps leading towards System B are outlined by heavy lines for illustrative purposes.

A list of the recommended programs is shown in Table 11-II. Technical area and program title are listed. The programs were selected on the basis of immediate need and usefulness. Priority establishment should depend on mission selection, systems development schedule, and other related factors.

11.1 Concentrator Programs

11.1.1 Program 1: Evaluation of Mirror Coatings

A major problem area in the development of solar-thermionic systems is the need for confirming the ability of a highly specularly reflective coating to withstand the space environment.

Some experimental evidence has been accumulated which indicates that most types of silver and aluminum coatings will degrade severely in the solar UV and x-ray environment of space. Most success has been obtained with barrier-layer type Al_2O_3/Al coatings. However, to EOS knowledge, the work accomplished to date was performed in a 10^{-5} to 10^{-6} mm. Hg environment. Work accomplished by EOS on gold and copper surfaces at 10^{-9} mm. Hg indicate that experimental data at lower pressures can be misleading.

TABLE 11-II

RECOMMENDED DEVELOPMENT PROGRAMS

Technical Area	Program Title
1. Concentrator	1. Evaluation of Mirror Coating
	2. Establishment Concentrator Coating Techniques
	3. Dynamic Analysis and Test of 5-foot Concentrator Structures
	4. Dynamic Analysis and Test of 9-1/2-foot Concentrator Structures
	5. Development of 9-1/2-foot, 50° to 60° Rim Angle Master
	6. Investigation and Environmental Test of Al, Be and other Mirrors
	7. Rear Surface Coatings for Concentrators
	8. Investigation of Techniques for Stiffening Thin Mirror Skins
	9. Investigation of Torus-Attachment Techniques
2. Generator Support	10. Design and Development of Unfolding Generator Support for 5-foot System
	11. Design and Development of Rigid Generator Support for 5-foot System
	12. Optimization of Generator Support Design
3. Generator	13. High Power Density Diode Advanced Heat Transfer Program
	14. High Power Density Diode Material Development Program
	15. Thermionic Converter and Generator Life Testing Program
	16. Acquisition of Diode Application Data
	17. Prototype Converter and Generator Manufacturing Development Program
	18. Design Study of 1KW Thermionic Generator
	19. Cavity Design and Development
	20. Investigation of Effect of Lower Temperature on Converter Life and Performance
4. Power Conditioning and Control	21. Power Distribution and Control Prototype Assembly and Test
	22. Investigation and Development of High Temperature Low Voltage DC/DC Converters
5. Solar Flux Control	23. Development of Solar Flux Control Mechanisms
	24. Development of Solar Flux Control Electronics
6. Cs Reservoir Control	25. Development of Prototype Cs Reservoir Control System

TABLE 11-II (contd)

7. System Analysis Design and Test	26. Development of Test Plan and Test techniques for Solar-Thermionic Systems 27. Development of Systems Optimization Program

The effects of solar proton and micrometeoroid damage are largely unknown. Simulated solar proton bombardment on reflective aluminum surfaces has resulted in degradation ranging from zero to 10 percent for an equivalent 1000 hr earth-space average sun year exposure. The opinion of many specialists is that solar proton damage is less of a hazard than UV and x-ray damage.

Tests performed by Lewis on reflective samples provided by EOS indicated severe degradation from micrometeoroid bombardment. Considerable question arises, however, as to whether the amount of bombardment simulated 6 months or 60 years in space. Until the statistical variance of micrometeoroids in space is explored further, earth investigations of micrometeoroid bombardment phenomenon are likely to be extremely misleading.

While solar proton and micrometeoroid damage simulation is largely hypothetical, UV degradation is more amenable to accurate simulation if the proper care is taken to provide a space environment. Furthermore, for reflective surfaces, UV degradation is likely to be the most serious factor.

The best way to measure space degradation is to fly samples in space. In lieu of this, EOS recommends that a UV test facility be assembled which can be used for test of reflective samples. Techniques and equipment would be similar to those used sucessfully by EOS on a previous program for AF Cambridge Research Center; this equipment is now in operation at AFCRC.

The vacuum chamber, light source, pumping system and associated fixtures would be JPL equipment. Associated test gear such as a monochromonator and spectrophotometer would be provided by EOS.

Program Tasks

1. Assembly of a laboratory facility to simulate the UV space environment. Equipment can be later incorporated to simulate proton bombardment. Vacuum conditions should be less than 10^{-9} Torr and UV intensity should be capable of ten times the intensity under earth conditions.
2. Perform a series of tests on selected silver and aluminum coatings with a nominal 1000 hr equivalent space exposure to determine the mechanism of degradation and the type of coatings which show least degradation. Samples of coatings would be selected from different vendors with a variety of coatings, interference layers, etc.
3. On the basis of preliminary tests, select several coatings for long life tests under simulated UV environment.
4. Introduce, if possible, the effects of solar proton bombardment.

Program Goals

1. Selection of a coating least susceptible to space degradation.
2. Selection of coating with the following performance goals
   a) 85 percent reflectivity
   b) Greater than 0.15 emissivity
   c) Degradation less than 5 percent for one year at earth conditions

11.1.2 Program 2: Establishment of Concentrator Coating Techniques

At the present time, experience with the coating techniques for 5 to 10-foot concentrators is limited. Coatings used in solar tested mirrors have been vapor deposited aluminum (with and without a silicon monoxide over coat), sprayed silver, and vacuum deposited layers of aluminum and quartz produced by L.O.F.

Several facilities exist for a 5-foot concentrator coating both on the West and East Coast. Only one facility exists for 10-foot concentrators at L.O.F. At present, the techniques for coating are not exact and depend to a considerable extent on the judgment of the particular individual applying the coating.

It is likely that the concentrator surface must be exactly prepared in order to avoid degradation in the space environment. Exact preparation implies the use of known facilities, equipment and techniques which have been proven through test.

It is recommended that a contractor prepare a concentrator coating facility and undertake a program specifically intended to definitize the nature of the coating process. Techniques and rules for the coating process would be derived including pressure, temperature, pump down techniques, filament placement, evaporative source, and others.

Program Tasks

1. Assembly of equipment suitable for vacuum deposition of aluminum, silver, quartz and other suitable coatings on 5 to 10-foot mirrors with a variation in temperatures, pressures, etc.
   Assembly of the facility.
2. Embark on an experimental program to deposit coatings until complete understanding of the interaction of all coating parameters is achieved and the reproducibility of various types of coating is confirmed.

Program Goals

1. Establish a facility which is available on a short-term notice, has the ability to apply coatings which will withstand the space environment and can apply coatings reproducibly.
2. Establish techniques and ground rules for coating which can be used reproducibly.

3. Attain uniformity of reflective coatings over the entire surface of the concentrator and uniformity of degradation to within ±3 percent.

11.1.3 Program 3: Dynamic Analysis and Test of 5-Foot Concentrator Structures

At the present time experimental and analytical data on the ability of concentrator structures to withstand vibration, acoustic and thermal shock environments is inadequate. A comprehensive program is required to establish structural limits on torus attachments, skin thicknesses, materials, and other concentrator features.

This program would help establish analytical background which could be used for future design of concentrators and would help establish safety margins for structural design.

The 5-foot concentrator is selected as being typical of the smaller concentrators that will be used in space. The dynamic analysis would determine the variations in diameter, torus design, rim angle, and other concentrator physical features needed for various mission applications.

Program Tasks

1. Develop fixtures, instrumentation and facility adequate to perform experimental dynamic analysis of 5-foot concentrators for vibration, shock, acoustic.
2. Perform a series of tests which determine vibration characteristics, acoustic characteristics and yield limits of concentrator structures as a function of skin thickness and taper, material, torus and support design, attachments, and generator support design.
3. Using experimental data, derive and confirm theory which will adequately describe concentrator performance.

Program Goals

1. Establish a background of experimental data which can be used for design of concentrators in the 5-foot range.

2. Optimize concentrator/torus weight.
3. Establish the practical advantages and disadvantages of materials and torus attachment techniques.

11.1.4 Program 4: Dynamic Analysis and Test of 9-1/2-Foot Concentrator Structure

This program would be identical in scope to Program 3. However, the dynamic analysis of the 9-1/2-foot concentrator would follow the initial experiments performed with the 5-foot concentrator. This is desirable since the equipment and effort required for test of a 9-1/2-foot concentrator is much greater in scope. Techniques of measurement, equipment design, other factors, can be ironed out on the 5-foot program.

The 9-1/2-foot concentrator was selected as a typical size for larger power solar-thermionic modules in space.

Program Tasks and Goals

This program would be similar or identical to those in Program 3.

11.1.5 Program 5: Development of 9-1/2-Foot 50 to 60° Rim Angle Master

The optimum rim angle for a large mirror is 50° to 60°. It is recommended that a high quality master with a 55° rim angle and 9-1/2-foot diameter be fabricated immediately in order to be able to begin fabrication of large concentrators for the dynamic test program.

In addition, the techniques for making the larger master should be refined to the point where the master can be made with variable rim angles and sizes on a low cost production basis.

Program Tasks

1. Fabricate a high quality 9-1/2-foot master.
2. Establish production techniques which are relatively insensitive to the point where low cost production masters can be made with variable rim angles and diameters according to need.

Program Goals

1. Surface accuracies of less than ± one minute.
2. Surface finish which allows concentrator surfaces to be made with 85 to 95 percent reflectivity.

11.1.6 Program 6: An Investigation and Environmental Test of Al, Be and other Minors

To date, electroformed concentrators have shown most promise in terms of high surface accuracy for minimum weight. However, stretch-formed aluminum concentrators are available which approach the optical performance of electroformed concentrators and exhibit weights on the same order of magnitude.

It is recommended that further investigation into stretch-formed concentrators be initiated to further develop these techniques in competition with the electroformed mirrors. The stretchforming would concentrate on the use of lightweight materials and would employ various support techniques which would, if possible, avoid the use of epoxies or plastic materials. An additional goal would be the use of low permeance material which would avoid magnetic field interaction problems.

Program Tasks

1. Establish the facility and techniques for stretchforming thin skins with minimum distortion employing beryllium, beryllium-aluminum, and other suitable materials.
2. Develop surface coatings which result in a smooth surface without the employment of plastics.
3. Develop skin attachment techniques which eliminate the use of plastic materials.
4. Develop techniques for torus and for support attachments.

Program Goals

1. Establish the limits and weight which can be achieved in stretchformed concentrators in the 5 to 10-foot size with a goal of 3 lbs/KW from the concentrator.

2. Establish coating techniques for the front surface which result in reflectivities of 85 to 95 percent with suitable coatings.
3. Eliminate all plastics from stretchformed concentrators.

11.1.7 Program 7: Rear Surface Coatings for Concentrators

Preliminary analysis indicates the rear surface of the concentrator should be highly emissive in order to maintain low concentrator temperatures. Low temperatures would imply minimum distortion and minimum heat transfer to an adjacent vehicle. However, the techniques for placement of high emissivity coatings on concentrators are not yet well established. Paints of various types are not desirable due to weight and the changes in paint characteristics which will be encountered over a period of time in space. If the variation in paint characteristics over the concentrator surface is great, distortion might be introduced into the concentrator surface. For electroformed structures, dark coatings can be anodized onto the rear surface in fairly simple fashion. However, proper techniques and tooling are necessary for large concentrator structures.

Program Tasks

1. Establish on small samples the feasibility of anodizing the rear of electroformed skins to darken the surface and create high emissivity coatings.
2. Determine the stability of the anodized coatings in a space environment.
3. Perform analysis to determine the best type of coating for the concentrator rear surface under a variety of conditions which include planetary and albedo infrared radiation, the interaction of the rear surface with the vehicle structure, distortion characteristics of the concentrator and other factors.
4. From analysis, establish the need for any type of spectrally selected coating.

Program Goals

1. Determine the need for special coatings on the concentrator rear surface.
2. Establish simple techniques without the use of paints or plastics to create the needed coatings.

11.1.8 Program 8: Investigation of Techniques for Stiffening Thin Mirror Skin

At present, the manufacture and handling of concentrators with very thin skins is limited by:

a) Difficulty in manufacture of very thin skins during removal of the skins from the master and/or other handling

b) The difficulty of testing the concentrator in a one "g" environment due to sag of the mirror skin

In addition, no definitive tradeoffs have yet been made with regard to thinness of the mirror skin vs the weight of stiffening structure required. The major problem in using stiffened skins is the show-through which results from differential thermal expansion effects, shrinkage of epoxy bonds, etc. The program is primarily of an experimental nature, concentrating on minimizing the effects of show-through with various kinds of stiffening structures.

Program Tasks

1. Summarization of the various stiffening approaches which are applicable.
2. Analysis of stiffening approaches and derivation of optimum combined weight, weight vs surface accuracy, and other tradeoffs.
3. Preparation of a number of samples which demonstrate the stiffening of thin skins and the effect on surface accuracy.
4. Assembly of a complete 5-foot concentrator using stiffened skin techniques.
5. Test of the concentrator.

Program Goals

1. Selection of a stiffening technique which allows high mirror efficiency and yet will support a very thin skin in a one "g" environment
2. Establishment of techniques necessary for manufacture

11.1.9 Program 9: Investigation of Torus Attachment Techniques

One area of concentrator fabrication which has not received a great deal of attention is the attachment of the torus to the concentrator skin. Recent acoustic tests resulted in failure of a metal attachment due to overstressed conditions and emphasized the importance of this area.

The attachment material and design can have a significant effect on mirror efficiency, susceptibility to acoustic and vibration environment, and concentrator weight.

Of most concern is the demonstration of attachment techniques that will minimize show-through on the skin and yet maintain a reliable skin support throughout the acoustic and vibration environment expected. Also, thermal shock and cycling effects are of importance.

Program Tasks

1. Summarization of attachment techniques
2. Preparation of samples using two ft diameter concentrators for demonstration of selected techniques
3. Test of samples in a thermal cycle and acoustic environment
4. Based on sample tests, preparation of five ft concentrator with selected attachment
5. Complete environmental test of concentrator

Program Goals

1. Establishment of base line design for attachment technique which is known to withstand thermal cycle, vibration and acoustic environment.

2. Establish bent of manufacturing techniques for forming the attachment.

11.2 Generator Support

11.2.1 Program 10: Design and Development of Unfolding Generator Support for 5-Foot System

The development of a prototype unfolding generator support mechanism must be accomplished in the near future. The three basic steps would be the selection of configuration, the performance of a detailed design, and the assembly and test of a prototype unit.

The generator support mechanism performs the following functions:

a) Support the generator during launch

b) Places the generator in the optimum position for reception of solar energy within closed tolerances

c) Provides an electrical path for current from the generator

d) Provides support for instrumentation leads leading from the generator

e) Operates reliably for the life of the system

Program Tasks

1. Select and design the generator support configuration on the basis of
   a) Arm kinetics
   b) Vibration and shock
   c) Magnetic requirements
   d) Optimization of dimensions and materials
   e) Ability to integrate into practical vehicle configuration
2. Perform engineering design and prototype assembly of deployment mechanisms and support end design
3. Assemble an experimental facility with which the generator support arms can be measured for thermal characteristics during operation

4. Assemble a facility and perform vibration analysis of the generator support structure in the folded and unfolded position.

Program Goals

1. Provide a reliable support for generator which fulfills support functions.
2. Insure reliability and accuracy of unfolding mechanisms and location of generator
3. Establish test techniques which are suitable for further generator support development
4. Assemble a generator support mechanism which exhibits
    a) Minimum temperatures seen by the electronics at the end of the generator support
    b) Minimum weight
    c) Minimum thermal distortion, electrical drop, and concentrator obscuration

11.2.2 Program 11: Design and Development of a Rigid Generator Support for 5-Foot System

A rigid generator support system is another variation of the type of structures which might be applicable to space applications. The design and fabrication of a rigid support structure would confirm many of the design techniques applicable to future generator support design and is a relatively simpler task than the unfolding system.

Program Tasks

1. Detail design of 3-armed support generator
2. Assembly of the prototype system
3. Formation of a test plan
4. Vibration, acoustic, and thermal test program
5. Analysis of the test data

Program Goals

1. Minimization of temperatures seen by the electronics at the end of the generator support

2. Minimization of weight
3. High reliability
4. Minimization of thermal distortion, electrical drops, and obscuration of concentrator

11.2.3 Program 12: Optimization of Generator Support Design

The optimization of generator support design must take into consideration:

a) Obscuration of the concentrator
b) Electrical drops and leads
c) Minimization of thermal conductivity or heat at the support ends
d) Weight

The optimization of the generator support depends intimately on the remainder of the solar-thermionic system. For example, minimum cross section area of the arms would result in lower obscuration numbers and higher electrical losses. The entire optimization process is quite tedious, and can involve many manhours

It is recommended that a computer program be established which can quickly analyze the optimum generator support cross section, material, length, etc. This computer program could become part of a larger overall system analysis recommended in Program 27.

Program Tasks

1. Summarization of applicable data for analysis including minimum cross sections able to withstand vibration, material characteristics, etc.
2. Programming of computer with suitable equations.
3. Performance of sample analysis and checkout of program.

Program Goals

1. Establish the optimum material for the generator support
2. Establish limits on cross sectional area
3. Perform systems analysis which establishes the effects of generator support design on the overall system design.

11.3 Generator

11.3.1 Program 14: High Power Density Diode Advanced Heat Transfer Program

To reach high power densities with a diode of reasonable weight, efficient means of cooling the collector must be derived. It is recommended that boiling heat transfer be investigated.

The heat pipe, or more properly the "vapatron" principle, which was developed approximately 20 years ago to accomplish heat transfer in the anodes of high power transmitting tubes, may be the prime answer to heat transfer problems in two areas in thermionic converters and thermionic converter generators. These two areas are: (1) in the emitter heat transfer path of the converters in a multi-converter generator, such as would be necessary in a 1 kilowatt thermionic generator design, and (2) in the converter collector-radiator heat transfer path.

Presently envisioned configurations for high power thermionic converter generators involving large numbers of converters (15 to 20) are limited in geometrical design by the spacing required to fit the converters around the cavity and by solar flux distributions in the cavity. Radiator design problems also become increasingly difficult where large numbers of converters are integrated into a single generator. Radiator weight reduction by a factor of 2 to 3 could be accomplished in the converter radiator system by the use of the vapatron principle. In addition, the collector heat transfer path could be severely modified to make use of more compact and reliable designs using the retaining ring technique.

Systems which merit investigation are the systems composed of lithium, cesium, turrubidium, sodium, and possibly NaK with tantalum, tungsten, and molybdenum. The latter heat transfer systems would be very useful in the lower temperature regions of the converter, such as the collector and radiator heat transfer

paths. EOS has performed experiments with lithium for cooling arc jet electrodes by the vapatron principle.

Program Tasks

1. Analyze various boiling and condensing systems for the emitter, collector and radiator temperature range of interest to thermionic converters.
2. Perform simple experiments to evaluate the effective boiling-condensing heat transfer coefficient.
3. Design, fabricate, and test a simple collector-radiator heat transfer model for simulated zero gravity operation.
4. Integrate the heat transfer system into several prototype converters to maintain a minimum collector-radiator Δt while operating with heavy heat loads, thereby achieving minimum δ_c and high efficiency.

Program Goals

1. Demonstrate the ability to maintain collector surface temperatures of 600 to 700°C under electrical loads of high power density and thermal loads on the order of 250w/cm^2.
2. Arrive at a practical diode configuration using liquid metal heat transfer on the collector.

11.3.2 Program 15: High Power Density Diode Material Development Program

The realization of maximum thermionic converter performance and reliability can be achieved only by the development of a high bare work function (5 electron volts and higher) emitter material of a uniform and reproducible nature. Such a material would also produce a dramatic increase in performance at emitter temperatures lower than the usual high temperature (2000°K) solar thermionic converter. This one result would do much to decrease the number of stringent requirements placed on any solar concentrator system, as well as open the way to the utilization of other forms of heat sources, such as isotope heat sources. The achievement of such

a high work function material in a form adequate for fabrication of thermionic converters at minimum cost would go a long way toward incre increasing the performance and reliability of present-day converters.

There appear to be four good approaches to the achievement of these high bare work function materials: (1) the utilization of single crystal tungsten or tantalum bar stock with a work function of approximately 4.9 to 5.3 electron volts is utilized, (2) the use of evaporated or sputtered polycrystalline coatings, (3) the use of high packing density alloys, and (4) the controlled growth of single crystal sheet suitable for electrode surfacing.

The integration of single crystal materials into high performance converters will require significant detailed investigations of the etching, the preparation, the slicing and the brazing of these materials to the emitter and collector in an economically feasible fashion. In addition a detailed investigation of the Langmuir-Taylor "S" curves for various cesiated single crystal surfaces should also be undertaken. These particular curves only have meaning in the context that the surface is known by both X-ray diffraction and by electron emission microscope emission patterns. Without the comparative information from both of these analytical methods, one is never sure that the surface of the material being measured is of a true single crystal form. X-ray diffraction data is by nature bulk material data and does not yield information pertaining to the surface. This particular investigation should be delayed for approximately a year.

The use of evaporated and/or sputtered coatings requires studies of the diffusion of substrate materials through the coatings as a function of time and temperature as well as how the work function of the surface is altered by diffusion. Also the actual process of deposition whether by evaporation or sputtering should be investigated, also optimum coating thickness determined from the view point of diffusion.

The utilization of alloys as electrode materials demands knowledge of the effects of time and temperature on work function and composition of alloys. In addition, the determination of the highest packing density alloy should produce the highest bare work function material. Much of the materials technology required for the alloy investigation is at hand.

The controlled growth of single crystal sheet of preferred orientation has already been proven in materials such as iron, wherein single crystal iron sheets on the order of 1 to 2 inches in width by 8 to 10 inches long and 80 mils thick have been grown for utilization in high performance transformer cores. The application of the same principles to materials such as tungsten, tantalum, and rhenium should be investigated for application to cesium vapor thermionic converters. Due to the cost of equipment and the time required for this investigation, it is felt that this approach should be delayed for some future program on advanced thermionic converters.

Program Tasks

1. Investigate substrate diffusion through evaporated and/or sputtered coatings using the electron emission microscope, determining optimum coating thickness and life based on diffusion data.
2. Investigate work function and surface changes in alloys with respect to time at temperature by means of the electron emission microscope.
3. Investigate processing variables such as time and substrate temperature for evaporation and sputtering, the effects of brazing on the surface of materials, and its effect on performance.
4. Integrate the best materials as determined by this program into a test converter structure and evaluate by obtaining Langmuir-Taylor "S" curves.

Program Goals

1. Demonstration of high bare work function surfaces which are stable in a converter environment
2. Integration of the material into a practical diode structure.

11.3.3 Program 15: Thermionic Converter and Generator Life Testing Program

In order to give thermionic converter systems designers and systems users in NASA and other government agencies confidence in the performance of the converters, and to assure them that the converters are of an actual hardware type which could be built in quantity and applied reliably to a system of their choice, a significant number of converters should be operated under controlled conditions for life-times exceeding 5000 hours. The conditions of this life test should be full power under generator conditions, otherwise temperatures in the converter, such as the seal temperature, radiator temperature, etc., will not reach their true application value. Off-maximum operation of the converters on the life tests will result in substantially lower critical element temperatures, a situation which would invalidate the tests for system design purposes.

The value of having meaningful life data on high power converters operating for periods of time in excess of 10,000 hours can not be overstressed. Since these long term tests take between one and two years to complete, it is apparent that unless such tests begin almost immediately, long term failure modes, such as ceramic braze problems, material diffusion, etc., will not be picked up and corrected until a time approaching the late 1960's. The lack of engineering design life test data of this type will jeopardize the application of thermionic converters in space, regardless of achieved converter electrical performance.

The most critical thermionic system design parameters to be specified by NASA and other users are the system life, the percent confidence in this life, and the allowable performance degradation with life. Consider the consequences of alternatively establishing specifications requiring device confidence levels of 90 percent, 95 percent, and 99 percent for 5000 hour operation with a maximum of 10 percent degradation. Examination of Table 11-III shows that, assuming no failures during the life test, 11,500, 15,000, and 23,000 part-hours of test respectively will be required. The situation for 2 failures assumed during the tests is that: 26,600, 31,700, and 42,000 part-hours of test would be required respectively to reach the specified confidence figures. It is obvious that even a small number of failures can drastically increase the required part-hours of test to reach a given confidence figure.

There are two approaches to achieving a given number of part-hours of converter test: (1) test a large number of converters for a moderate period of time (100 converters for 500 hours), and (2) test a smaller sample for a longer period (10 converters for 5000 hours). The second approach is being proposed at this time for two reasons: (1) the test stations are too expensive to consider in large quantities, and (2) it is essential that actual rather than projected 5000-hour life characteristics be obtained. The importance of quality in the initial stages of converter fabrication, the care in rejection of marginal converters at the leak detection stage, and the care in rejection of converters for marginal electrical performance during acceptance testing can not be over stressed. Any marginal converters which reach the life test stage and fail during life test can drastically modify the confidence figures obtained from the life test.

It is recommended to life test ten (10) high performance thermionic converters for a minimum period of 2000 hours each or until failure, whichever comes first. Some of the converters

TABLE 11-III

MTBF* RELIABILITY CHART

Confidence		Required Part-Hours of Test +		
		0 Failure	1 Failure	2 Failures
90 Percent	2000 hours	4,600	7,800	10,640
	5000 hours	11,500	19,500	26,600
95 Percent	2000 hours	6,000	9,500	12,600
	5000 hours	15,000	23,750	31,700
99 Percent	2000 hours	9,200	13,400	16,800
	5000 hours	23,000	33,500	42,000

*Mean time before failure

+Based on 10 diodes being tested simultaneously

should be left on test as long as possible. Also, it is recommended to life test to a minimum of 500 hours a four-converter generater containing high performance converters.

The design philosophy to be used on the life test stations should stress: high vacuum, long life components, and ruggedness so that a minimum of "down-time" and subsequent test interruption will be experienced. Emphasis will be placed on the careful selection of converters to be placed on life test.

Program Tasks

The major tasks of the testing program will be to:

1. Achieve a minimum of 20,000 part-hours of converter life test, to be accomplished nominally on 10 high performance converters each tested 2000 hours.
2. Achieve a minimum of 500 hours laboratory test, utilizing electron beam heating, on a four-converter generator containing high performance converters.
3. Demonstrate a device MTBF (mean time before failure) of 5000 hours with a given confidence level such as 95 percent. Referring to Table 11-III, this is equivalent to saying that 95 percent of the devices will be able to operate continuously for a period of time just under 7 months without failure or performance degradation that would render the device useless in its intended application. It will, of course, be necessary to carefully define that point of minimum acceptable reliability, i.e., end-of-life point, so that there will be a definitive goal and hence, a realistic yardstick for measurement.
4. Design and assemble ion-pumped life-test stations and associated measuring apparatus to be used on the life-test program.

Program Goals

1. Establish adequate life testing techniques
2. Acquire initial converter and generator reliability data

The cost of performing a large number of life tests on individual diodes can be significantly reduced with the introduction of automatic checkout and monitoring equipment. With moderate data monitoring techniques it is possible to continuously monitor a large number of variables in many different selected modes, and as rapidly as necessary. It is also possible to store data for future printout and to provide a visual display of information.

Described below is a typical set of equipment which is recommended as being part of the life test program. This equipment will be compatible with a large variety of life test stations and a wide variety of inputs.

Figure 11-2 illustrates in block diagram form the automatic checkout and monitoring equipment which is recommended by EOS as a basic unit applicable to the life test stations.

The equipment is in five main sections:

1. Input provisions
2. Load system (dynamic and static)
3. Safety system
4. Data storage
5. Printout and display

The input will consist of a patch board with several varieties of input jacks suitable for monitoring up to 300 inputs. The inputs can be heater currents, heater voltages, electrode and reservoir temperatures, output voltages, and output currents. The input can range from millivolts to 10 volts.

The parameters of the converters to be monitored will be fed directly to the data system which utilizes the following major equipment:

1. A cross-bar scanner with a programming capability to enable all 300 inputs, or various combinations of these inputs, to be scanned and subsequently printed out.

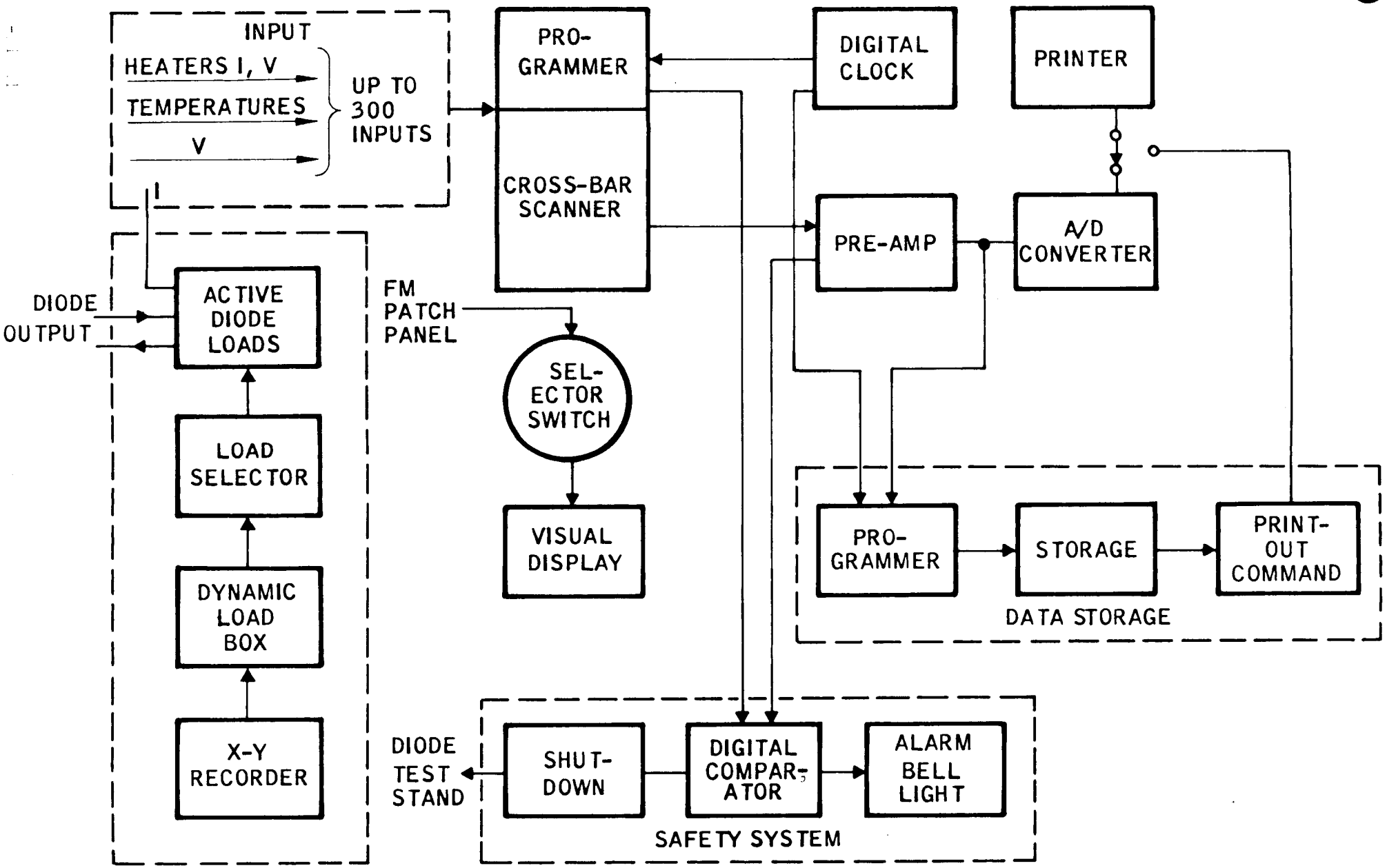

FIG. II-2 AUTOMATIC CUTOUT AND MONITORING EQUIPMENT FOR LIFE TESTS

2. A digital clock which can be adjusted to provide any given rate of printout ranging from seconds to hours; also, printout can be arranged to complete a scan in seconds with dwell-times ranging up to hours. The digital clock also provides a means to establish the time data was acquired.
3. A selector switch with any given input can be visually displayed on a strip chart recorder, oscilloscope, etc.
4. Preamps and analog to digital converters for converting the input into the printout format.
5. A digital printer is utilized for providing a permanent record of the test.

The load system will contain active transistor controlled loads which can maintain diode output at any preselected value of current or voltage. In addition, a dynamic load box will be provided along with an X-Y recorder with which instantaneous sweep data can be obtained for any diode. In addition, the load box will be designed to enable a point by point trace of steady-state data to be obtained by automatically adjusting the load to preset levels and maintaining this level until stabilization is achieved at which time the data will be recorded.

The system will include data storage such that data can be accumulated and read out in any desired time. For example, the storage system to be programmed to store a complete set of data once every hour. It could then be commanded at some future date to print out the current output from a selected diode for any entire weeks' period.

The inclusion of a storage printout system creates an extremely versatile automatic-like test station which will save considerable time in reduction of data. Costs include a paper type storage unit which has been selected because of its unlimited capacity to store data gathered over a relatively long period of time. A tape recorder is also included so that the information can be printed out upon command.

11.3.4 Program 16: Acquisition of Diode Application Data

At the present time, data accumulated in laboratory tests concerns the performance of a thermionic converter at constant emitter temperatures with variations of power into the converter and optimized cesium reservoir and radiator temperatures.

This condition does not exist in operational systems. Instead, the generator will most likely experience a constant power input. The emitter, reservoir, radiator and collector temperatures will vary depending on the load which the converter experiences. It is imperative that application data be acquired on diodes which can give the system designer ground rules for matching the converter performance with electrical load and solar power input and can establish reliability limits.

Program Tasks

1. Establish a test program which will establish the variations in converter temperature as a function of load variation with constant power input.
2. Perform a series of cyclical tests to determine the effects of these temperature variations on the life and degradation of the converter.
3. Establish criteria for converter design.

Program Goals

1. Establishment of a handbook of design data.
2. Provide practical guidelines of the system designer.

11.3.5 Program 17: Prototype Converter and Generator Manufacturing and Development Program

The tasks described here are primarily concerned with the improvement of techniques currently employed on prototype "Production" diodes to reduce cost, increase reliability, and eliminate potential long life problems.

Statement of Problem

There are generally many features of an developmental (or prototype) device design which can be improved when application of the device reaches the production phase. When sophisticated devices, such as the thermionic converter, are fabricated in small quantities (less than 50 to 100) and with numerous design changes, low-cost and "foolproof" manufacturing techniques are not used due to their cost on a per unit basis in "one of a kind" or small sample programs. For example, with regard to prototype converter fabrication, automatic milling and machining techniques are not, at present, applied to fabricating the molybdenum radiator-collector subassembly due to the high machine setup charge in relationship to the small number of units desired for a particular design modification. The paradox is, that in general, it is only through the use of such automatic processes that device reliability can be increased while simultaneously the per unit cost is being reduced.

In the initial stages of hardware programs, such as the thermionic converter prototype fabrication program now exemplifies, a fine balance must be achieved between the cost of a process and its general utility for increasing the reliability of the device. If converters were to be fabricated in lots of several hundred to a thousand, the initial setup costs of a process would no longer be a major factor.

Many of the fabrication procedures, such as cesium loading, which are used in present-day converters are not optimum from a cost, reliability, or manufacturing standpoint. These procedures, at present, are a trade-off between the cost to develop new processes and the cost to continue using old processes. In many cases, the processes used simply represent a direct carry-over from the research and development phases.

In the past, most thermionic converter development programs have stressed performance on a one-of-a-kind basis and seldom

have recognized or stressed a trade-off between reliability and performance, such as is necessary on all hardware programs.

Program Tasks

1. Eliminate known weak points in the prototype converter design as it now exists and prepare the design for manufacturing.
2. Evaluate those converter processes and subassemblies which realistically may be problem areas for long-term life.
3. Eliminate weaknesses in the converter processing and design which become apparent from the results of the life-test program and are not now known or anticipated.
4. Introduce new manufacturing processes into the converter (and generator) fabrication which will increase device reliability and reduce cost.
5. Utilize a manufacturing approach throughout this phase of the program.

Program Goals

The major goals of this program are to:

1. Establish the institute those design changes in the converter prototype necessary to achieve the converter life and reliability required for first generation system application (95 percent confidence, 5000 hour).
2. Establish those manufacturing procedures which can lead to a cost reduction in the converters.
3. Improve the manufacturing design of the thermionic generator.
4. Investigate the applicability of advanced assembly techniques to converter and generator fabrication.

11.3.6 Program 18: Design Study of 1kw Thermionic Generator

The practical realization of a 1 kilowatt thermionic generator in conjunction with a 1-1/2-foot mirror (roughly) must await

the development of better methods for transferring heat from the absorber cavity to the emitters, and better mechanical designs of the general generator heat transfer and heat rejection paths. Since it appears possible to develop a high temperature boiling and condensing heat transfer system, it is worthwhile to start on an analytical and mechanical design for a 1 kilowatt and larger generator utilizing these principles. Such a generator would have a wide latitude of design possibilities in comparison with the present generator concepts wherein the heat transfer occurs primarily by direct radiation to the individual converter emitters. The present generator designs, in general, do not allow for non-uniformities in the mirror nor changes in the mirror due to meteoroid impact. Utilizing the heat pipe principle, one can envision generator designs which are essentially insensitive to changes in the solar image within the generator cavity. The advancement of a carefully thought out 1 kilowatt generator design based on sound engineering foundations would go a long way toward developing the confidence of the ultimate system user in the general merit of the thermionic generator for space application. This is particularly true for the power ranges at several kilowatts, since no proven space generator now exists for this range. This particular program would ideally consist of a simple design analysis of the heat transfer paths, shielding problems, and mechanical layout, with some supporting experiments involving cavity heat transfer in order to arrive at a generator and generator mockup which would essentially prove the principles involved in design. Converters would not necessarily have to be used in this mock-up proof of the design principles.

Program Goals

1. Perform a design analysis of a 1 KW thermionic generator utilizing a high temperature boiling and condensing liquid metal heat transfer system.

2. Prepare a detailed heat transfer analysis and temperature distribution for several typical generator configurations after developing a general analytical model.
3. Prepare assembly drawings for a 1KW generator showing all constructional features and mechanical and electrical layout. A mechanical mockup will be prepared to check assembly details.

11.3.7 Program 19: Cavity Design and Development

A serious source of system loss is the reflection and reradiation losses from the cavity. Another serious problem is the equalization of temperatures throughout the cavity for best matching of the converters at high efficiency.

To date, cavity test and analysis programs are inadequate to accurately predict cavity performance. It is known that the cubicle cavities used to date have not resulted in uniform temperature distribution.

The cavity design strongly interacts with the concentrator rim angle, surface accuracy, and reflectivity. Cavity entrance diameter is a parameter highly dependent on concentrator characteristics and cavity characteristics.

It is recommended that a test and analysis program be established to investigate in detail the design of the cavity for the generator. The test program would include the test of sample cavities with simulated converters. The analysis program would include the effects of:

1. Cavity shape
2. Entrance diameter
3. Interior emissivity
4. Internal surface area

A test cavity would be designed and assembled to simulate to a reasonable extent the expected temperature distribution in a real cavity. The test cavity would have the following features:

1. The ability to simulate in a scaled manner the heat transfer from the cavity which would occur in a generator design
2. The ability to be tested with a 5 ft mirror used on a 60 mw/cm^2 day in Pasadena
3. The ability to change cavity shape and emissivity characteristics
4. Ability to open cavity entrance diameter when desired
5. Ability to open rear of cavity when desired
6. Ability to integrate actuators and flux control mechanisms

Program Tasks

1. Design and assembly of test cavity
2. Design of test facility
3. Assembly of test facility
4. Establishment of analytical background for cavity analysis
5. Programming of computer for cavity analysis
6. Through analysis and test, establishment of ground rules for cavity design which depend on power level, converter, etc.

Program Goals

1. Design of cavity for different power levels which will equalize temperature distribution and minimize losses

11.3.8 Program 20: Investigation of Effect of Lower Temperatures on Converter Life and Performance

This program would be conducted in conjunction with Programs Nos. 15 and 16 in order to acquire further data on the performance, efficiency, life and reliability of converters which are operated at lower temperatures than 1700°C.

At the present time, not enough information exists regarding the tradeoff between lower temperatures, performance and life. Long term life tests are required to establish further data

points on the rate of converter deterioration, life vs. power density, the effect of load variations on the operating temperatures throughout the converter, and other parameters.

The program tasks would be similar to those summarized in Programs 15 and 16. Life and diode application data would be acquired.

The program goals would be to derive sufficient information for definitive analytical tradeoffs between cavity temperature, power output from the system, and converter life.

11.4 Converters

11.4.1 Program 21: Power Distribution and Control Breadboard Assembly and Test

To date, information regarding the operation of systems electronics and the resultant effect on generator and diode performance is limited. To EOS knowledge, no experiments have as yet been performed to determine the interaction of the generator source and a complete power system.

The operation of electronics is fairly well understood. However, the optimization of the control of the generator output, and the resultant maximizing of the efficiency and lbs/kilowatt figure for the system will not be well understood until definitive experiments are performed. It is recommended that an experimental prototype system be assembled and tested.

The program would consist of the assembly and test of the breadboard for a power distribution and control system applicable to a 5-foot solar-thermionic system. The test would use simulated generator and battery power sources.

The design, assembly and use of the generator simulator is a major item in the program. To date, tests of solar-thermionic systems electronics depend upon the operation of actual

thermionic diodes or generators. For extensive tests on systems electronics, the need for operating laboratory generators is a handicap which can be overcome by the use of a simulated power supply. This simulator will be designed to simulate the steady-state characteristics of generators with a variety of voltage and current outputs.

The program will result in definitive information concerning the difficulties and problem areas in control and distribution of power from the solar-thermionic generator (or generators), and an indication of the maximum efficiency that can be achieved from such a system.

A block diagram of the proposed power distribution and control system is illustrated in Fig. 11-3. This schematic results from studies accomplished during this program.

Three generator simulators would be assembled, capable of 0 to 200 watts output. The simulators can be placed in series (as shown) or used individually. Part of the test program will involve different series and parallel arrangements to determine operational problems.

The output from the generator simulator is fed to an unregulated dc to dc converter. In Fig. 11-3 the converters are shown in an arrangement such that if a single generator or dc/dc converter should fail, two-thirds of the power output can still be obtained from the system.

The shunt load control is used to provide a resultant constant current load to a thermionic generator, regardless of the system load. The control for the shunt load device is obtained by measuring the battery charger current and load current and subtracting the sum of the two from the desired constant value selected for the thermionic generator operating current.

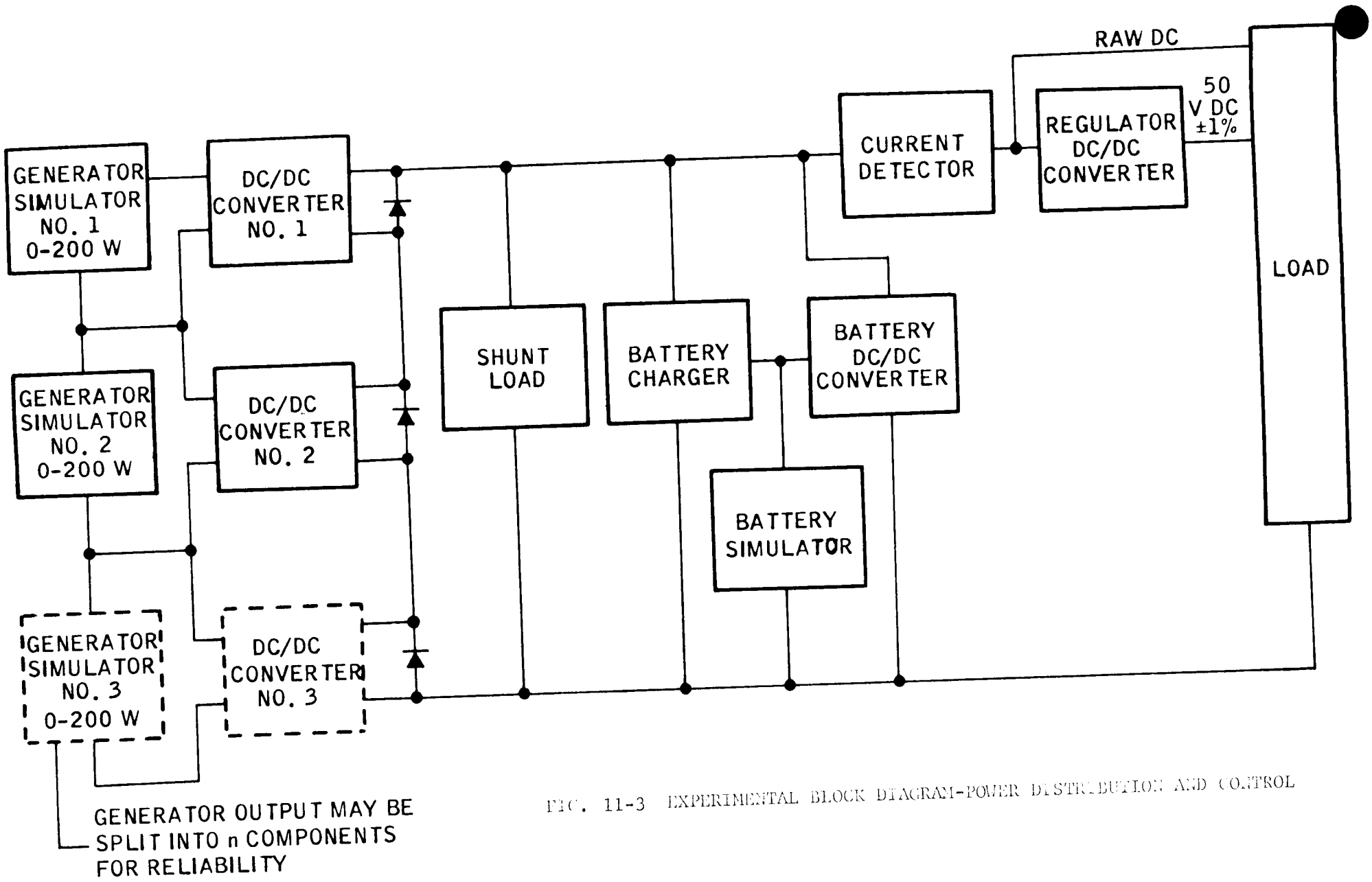

FIG. 11-3 EXPERIMENTAL BLOCK DIAGRAM-POWER DISTRIBUTION AND CONTROL

The battery charger will essentially consist of a standard dc/dc pulse-width modulated device with an averaging output filter. The charger will be controlled by various inputs depending on the operating mode, power available, and the battery condition. The charger will be used as part of the "parasitic" load to provide a constant load current to the thermionic generator. Therefore, the charger must have one control input that limits its input current to a value which will not overload the thermionic generator. Battery charging will be constant current, but modified by terminal voltage and battery temperature. Therefore, the charger will provide a constant charge current until the terminal voltage reaches a preset value at which time the charge current will be reduced to a low trickle charge value. The preset voltage will be temperature dependent and controlled by a measurement of battery temperature.

The battery will be simulated by a dc power supply. During test, characteristics of a silver-zinc, silver-cadmium, and nickel-cadmium batteries will be simulated.

Since the battery cannot be connected to the unregulated dc bus by conventional techniques such as are used on Ranger and Mariner vehicles, a dc/dc converter must be connected between the battery and the bus to provide the proper power summation. In order to provide the proper control, a pulse-width modulated dc/dc converter must be used to obtain this control input from a measurement of current. The battery current is used only when power is required from the battery. This will only occur when the load current exceeds the preset output current capability of the thermionic generator. When this occurs, the battery charger and shunt load are made inoperative and the battery converter activated. The output control for the battery current is obtained by taking a difference between the load current and the thermionic generator preset.

The necessary dc voltage regulation will be provided by a voltage regulator. For reasons of increased efficiency and reduced weight and reduced complexity, a switch-mode-down converter/regulator is recommended.

The selection of the number of low voltage dc/dc converters which accept the output from the generator will depend on a more detailed study of the reliability and weight tradeoffs. One of the objectives of the proposed systems test is to provide applications data regarding the problems of placing generators and dc/dc converters in series-parallel combinations. If the failure of one or more generators is anticipated, the use of two or more dc/dc converters seems reasonable. However, an optimum number of dc/dc converters does exist depending on the desired unregulated bus voltage and its effect on the efficiency of the system.

The generator simulator design would provide I-V characteristics of the generator for power ranges of 0 to 200 watts at voltage levels from 0.5 to 1.2 volts. The I-V curve would be "steady-state", i.e., will simulate the case where a constant amount of power is available to the generator. The slope and shape of the I-V curve will be variable within limits determined by the detailed design.

It should be noted that the proposed generator simulator is the first of a series of simulators which should advance in sophistication as more is learned about the system. The second iteration would include a simulator which accounts for the transient characteristics of the generator and/or could provide higher power outputs.

The load, for purposes of systems test, would be, first, a passive series resistance and then an active circuit which simulates constant power load lines. As indicated, for certain modes of operation the load would split between raw dc and regulated output to determine the effects on system performance.

Program Goals

Program goals are summarized as follows:

1. Attain a complete understanding of the functioning and interaction of the generator and power distribution and control systems.
2. Attain a breadboard efficiency of 75 percent for a power distribution and control system and obtain an understanding of the losses in the system for various modes of operation.
3. With a background of experimental performance, design a system for minimum weight.
4. Attain an understanding of the tradeoffs in redundant components, weight, reliability, and other factors to increase overall systems reliability.

11.4.2 Program 22: Investigation of High Temperature Low Voltage dc to dc Converters

One of the major problems in the utilization of thermionic generators in space involves a power conditioning device which will convert the low voltage, high current converter output to a level capable of being used on the spacecraft. The low voltage dc to dc converters, which to date have been investigated and applied to low voltage conversion devices, consist primarily of configurations of germanium semiconductors. Germanium type semiconductors deteriorate in performance very rapidly at ambient temperatures greater than $50^{\circ}C$. It will be difficult to locate these power conversion devices far enough from the hot thermionic converter generator so that their temperatures could be maintained at a value lower than $50^{\circ}C$. Although these power conditioning devices work remarkably well under laboratory conditions, they are completely inadequate for any practical thermionic space power system. The problem must be faced soon, otherwise a major link in the thermionic generator system will be missing, when the time comes to apply such a system. A backup program relating to the development of high temperature switching devices should be

undertaken immediately in order to achieve a dc to dc converter which is capable of operating at temperatures on the order of 500°C to 700°C.

One such device is a cesium vapor thyratron which, under the proper design conditions, conceivably could operate with zero forward volt drop at currents of 100 to 500 amperes. Such a cesium vapor switch could be made an integral part of the cavity absorber utilizing cavity thermal power. The power actually transmitted to the spacecraft under these conditions would be high voltage, low current power. This power is easy to transmit reasonably long distances without heavy bus bars or weight problems. This approach may bear more immediate fruit than the high temperature semiconductor approach, which has not been successful over the last ten years.

Program Goals

1. Perform a comparative analysis of silicon, germanium, and other advanced semiconductor devices to determine the tradeoffs between performance (efficiency, lifetime, weight) and operating temperature for present and near future components.
2. Perform a design analysis of a high temperature, low voltage dc to dc cesium vapor thyratron operating with cavity thermal power. Determine the relationship between efficiency, voltage, weight, and operating temperatures.
3. Fabricate and test several experimental models of the cesium vapor thyratron to demonstrate feasibility and evaluate performance characteristics.

11.5 Solar Flux Control

11.5.1 Program 23: Development of Solar Flux Control Mechanisms

It is recommended that an investigation of a solar flux control subsystem and its interaction with cavity temperature distribution be initiated immediately.

The basic components of the solar flux control prototype system are illustrated in Fig. 11-4 and consist of the:

1. Test concentrator (mounted in a tracker)
2. Flux control mechanisms
3. Test cavity with instrumentation
4. Actuator mechanisms
5. Heat sink for the cavity
6. Flux control electronics

The flux control mechanisms and actuators can take a variety of forms. Three mechanisms are recommended for more detailed investigation. They may include the clam shell, iris, flat, or expanding cavity types. The actuators will probably be bourdon tubes as these actuators, through previous study, were found to be most suitable for this application.

The flux control electronics will control the actuating mechanisms by command or automatic feedback. The electronics will be assembled in prototype form (see program 24).

The test cavity would be assembled under program 19.

Program Tasks

1. Assembly of a flux control test facility including a test cavity.
2. Design and assembly of flux control mechanisms.
3. Design and assembly of flux control electrodes.
4. Tests using solar radiation of several solar flux control prototypes.

Program Goals

1. Demonstration of the ability of a solar flux control to regulate solar flux input to the cavity while maintaining uniform temperatures within the cavity and with adequate sensitivity.
2. Demonstration of the actuation mechanisms.
3. Demonstration of compatibility with the electronics.

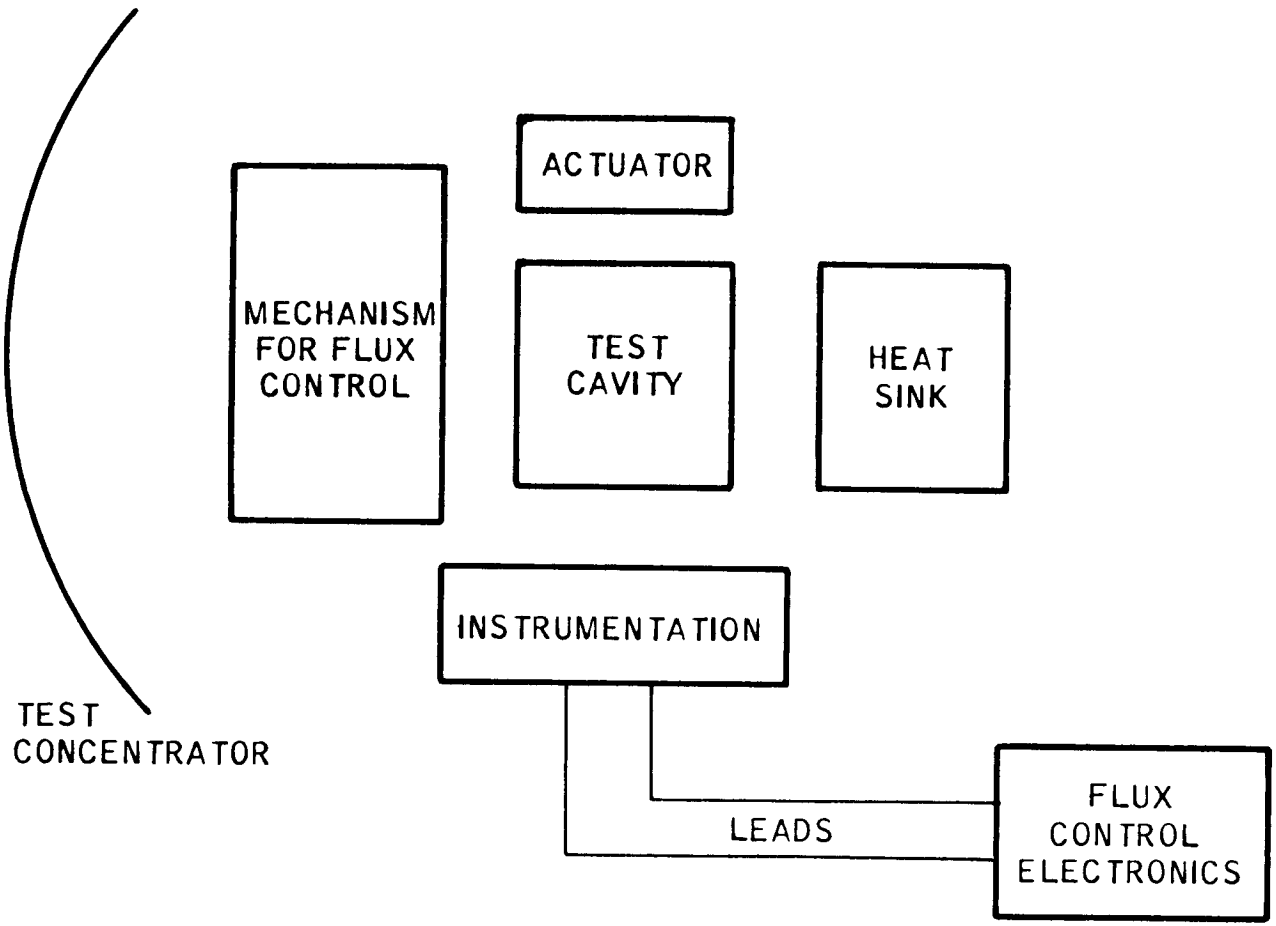

FIG. II-1 BASIC COMPONENTS OF A FLUX CONTROL

11.5.2 Program 24: Development of Solar Flux Control Electronics

The object of this program would be the design and assembly of a lightweight, low power electronic unit which would control the solar flux control mechanisms by sensing solar intensity, ground commands, and/or other sensors. This program would run in parallel with the assembly and test of the flux control mechanisms and would result in a complete solar flux control system.

The electronic system includes the sensor, signal conditioning, power leads, and actuator devices for the mechanisms. Actuator devices include bourdon tube and bimetallic elements.

Program Tasks

1. Design of electronics.
2. Assembly and test of prototype electronics with flux control mechanism.

Program Goals

1. Minimization of weight and watt-hour erequirement of a practical solar flux control electronic system.

11.6 Cesium Reservoir Control System

11.6.1 Program 25: Development of Prototype Cesium Reservoir Control System

At present, it appears that an active cesium reservoir control system can be useful to minimize startup time for the generator, to provide vernier control for converter operation, and compensate for changing solar flux input.

The circuits required for cesium reservoir control are already known. It remains, however, to integrate these circuits into actual cesium reservoir operation in a practical manner. Only by attempting the prototype development program can the complete range of problems be explored.

Program Tasks

1. Perform detailed design of the active control system, instrumentation requirements, and sensor requirements.
2. Integrate the temperature sensor into a practical converter configuration.
3. Assemble the active cesium reservoir control.
4. Perform laboratory tests determining effectiveness of the control.

Program Goals

1. Minimize weight and watt hour requirement of the cesium reservoir control system.
2. Minimize startup time of the generator by quickly heating the cesium reservoir.

11.7 Systems Analysis and Test

11.7.1 Program 26: Development of Test Plan and Test Techniques for Solar-Thermionic Systems

This task concerns the establishment of a test plan for a solar-thermionic system which would qualify the system for flight use.

At the present time, it is impossible to simulate an exact space environment with an artificial source of adequate collimation to simulate the solar radiation environment.

Even if the entire system is enclosed in a vacuum chamber and pointed towards the sun through a window, the intensity is not adequate to power the system at full level.

A complete systems test should include physical integration as well as electronic test. Typical test steps would include:

1. Unfolding of the support mechanisms.
2. Mechanical integration of the vehicle.
3. Full power test of the power source.
4. Full power test of the electronics.

Program Tasks

1. Establish a test flow plan for a complete flight system.
2. Define the equipment needed for each step.
3. Summarize the techniques possible for simulating the solar power input to the generator and perform laboratory tests that confirm the predicted result.
4. Establish the validity of solar tests for the generator in a vacuum chamber.
5. Determine the time and cost requirements for each step of the test process.

Program Goals

1. Establish a plan for solar-thermionics systems test which insures reliable operation in space.
2. Minimize the cost and time required for solar-thermionic systems test.

11.7.2 Program 27: Development of System Optimization Program

At the present time, a complete systems analysis involves considerable reiteration and optimization. It is entirely feasible to set up a systems optimization program on a computer which, using a variety of assumptions, can result in an optimized system for any given power level, solar intensity, concentrator characteristics, generator efficiencies, electronic characteristics, etc.

It is recommended that such a program should be established in the near future. The components of this program would include subroutines for concentrator and cavity analysis, generator support analysis, optimum loading for the generator, optimum voltage output of dc converter and related items. The subroutines could be combined to result in an optimum system.

Program Tasks

1. Derivation of the analytical expressions for the optimization routine.

2. Summarization of assumptions in tabular form for input to the computer.
3. Test runs of the analysis program and checkout.

Program Goals

1. Establish a program by which changes in system design can be quickly verified with regards to their effect on overall effect on system performance.
2. Establishment of a program which can quickly determine optimum systems in any given mission environment.

APPENDIX I

SPACE ENVIRONMENTAL EFFECTS ON REFLECTIVE SURFACES

APPENDIX I

SPACE ENVIRONMENTAL EFFECTS ON REFLECTIVE SURFACES

1. SPACE ENVIRONMENT DEFINITION

Engineering assessment and evaluation of the behavior of materials in space requires complete knowledge of the space environment in the regions to be encountered by these materials. A survey of the current state of knowledge of space physics reveals many wide gaps in the data and many variations in models set forth to explain and correlate scattered data collected in space explorations with terrestrial and astronomical observations. It is, therefore, difficult to conclude with precision the environments a particular earth satellite or planetary probe will encounter during a planned mission. This section attempts to summarize the current knowledge of the space environment in order to provide guidelines for analysis and engineering of solar-concentrators. The material provided in this section is quantitative wherever possible, but in many instances where data are inconclusive, questionable, or lacking, the best estimates of recognized experts have been provided.

Environments to which materials in space will be exposed have been classified into the following headings:

1. Atmospheric particles
2. Meteoroids
3. Electromagnetic radiations
4. Geomagnetic fields
5. Charged particles

In the present study program we are primarily concerned with effects of the environment on solar-concentrator reflective surfaces.

Since reflection is primarily a surface characteristic we are particularly sensitive to aspects of the environment that might not ordinarily pose much of a hazard to materials or structures in which mechanical strength, chemical or electrical characteristics alone are the prime considerations. An example is the damaging effect to surfaces resulting from exposure to low energy charged particles as opposed to the more penetrating charged particle and electromagnetic radiations. Unfortunately, it is the low energy charged particle of space of which the least is known. Most of the early space exploratory satellites and probes have contained simple detectors that were selective for high energy radiations to the exclusion of the low energy particles. Recent data, from Explorers 12 and 14 with more sophisticated equipment, indicate that high levels of the lower energy particles exist in the Van Allen belt regions. Another region of which little is known is the area immediately in the vicinity of the magnetopause and the regions of interplanetary space. Another cause for uncertainty arises from temporal variations due to solar storms of varying intensities that distort the geomagnetic trapping areas causing unpredictable and wide fluctuations in intensity, energy, and spatial distribution of the charged particles. Certainly the space "weather" is very difficult if not impossible to predict with a high degree of accuracy.

The region of space considered, for purposes of this study, is bounded by 300 nautical miles out to the outer limits of the magnetopause, i.e., to 10 to 12 earth radii, or about 40,000 to 48,000 miles altitude. Of principal concern then, are the trapped radiations occurring within the magnetosphere; the changes in these belts resulting from solar flares; and the cosmic and solar emissions in the form of electromagnetic and charged particle radiations penetrating this region.

Treatment of cosmic radiation has been limited to basic data sufficient to indicate the relative effectiveness, or ineffectiveness, of damage from this source of radiation. More complete treatises are

readily available in the literature and standard reference books. For the purposes of this study, cosmic rays are a negligible factor in materials degradations.

The subject of temperature and pressure as a function of altitude has been included to be complete. However, at the altitudes under consideration, we are primarily concerned with the atomic density or the number of particles per unit volume found in space and the speed of these particles (their kinetic temperature). These data may be of importance when considering the relative speed of a satellite and slowly, or swiftly, moving uncharged atomic particles on collision with the surfaces of the satellite.

In the case of micrometeoroids, the potential physical damage possible to surfaces of the satellite from these bits of matter can be easily appreciated. In some cases, there can be actual penetration of the surface by swift, dense meteoroids. These cases are somewhat a matter of chance and the degree of risk can be inferred.

The extremely high levels of electromagnetic radiant energy in the ultraviolet region of the spectrum originating with the sun combined with the earth's albedo, cause a good deal of attention to be focused on this subject. In particular, the existing intensities and spectral distributions of these electromagnetic radiations are of concern when studying materials effects because of the possible selective absorption or sensitivity of the material to particular wavelengths. Degradation of spectral reflectance with excess absorptivity of the reflecting surface following prolonged exposure is of concern to the optical engineer. The damaging effect of the combined environment or reflecting surfaces exposed in space missions is certain to be more apparent than for other satellite structures.

1.1 Temperature

From a practical point of view the conditions of temperature in space are somewhat paradoxical. Temperature, being defined in terms of the average random kinetic energy of the molecules or translational motion, is determined from the following equation:

$$\frac{mv^2}{2} = \frac{3kT}{2}$$

where v = average molecular velocity

k = Boltzmann constant

m = particle mass

T = temperature

From this it can be seen that temperature is proportional to the mass and the square of the velocity of the molecule or particle. As can be noted from Fig. 1 (Ref. 1) the kinetic temperature rises rapidly at altitudes above 100 km, which means that the particle is moving at very high speeds. At altitudes of 400 km and greater, the kinetic temperature is approximately 1,000°K but here the atomic density is only about 10^7 atoms/cm^3. This low density of high temperature molecules or atoms will not greatly affect the temperature of the satellite. At these and higher altitudes the vehicle achieves a thermal balance between the sun (6000°K), earth (288°K blackbody), moon (123-400°K blackbody), its own internal heat sources, and space (4°K blackbody). Even at a pressure of 10^{-3} mm Hg (~ 100 km) and an assumed vehicle temperature of 300°K, the ratio of heat transfer by conductive means is about 10^{-3} of the radiative process. Heat transfer effects may usually be adequately simulated by testing pressures of 10^{-5} mm Hg.

1.2 Pressure-Density

Atmospheric pressure decreases from 760 mm Hg at sea level to a figure of less than 10^{-12} mm Hg beyond 4000 miles altitude (approximately one earth radius). (Refs. 1, 2, and 3). Figure 2 (Ref. 1) charts pressure as a function of altitude. As the pressure changes with altitude, there is also a change in the relative concentrations or densities of the constituent molecules or atoms, Fig. 3 (Ref. 4). At lower altitudes the N_2 molecule is predominant. At about 200 km altitude O_2 molecules dissociate into single neutral atoms and predominate. At altitudes above 1000 km He atoms begin to predominate.

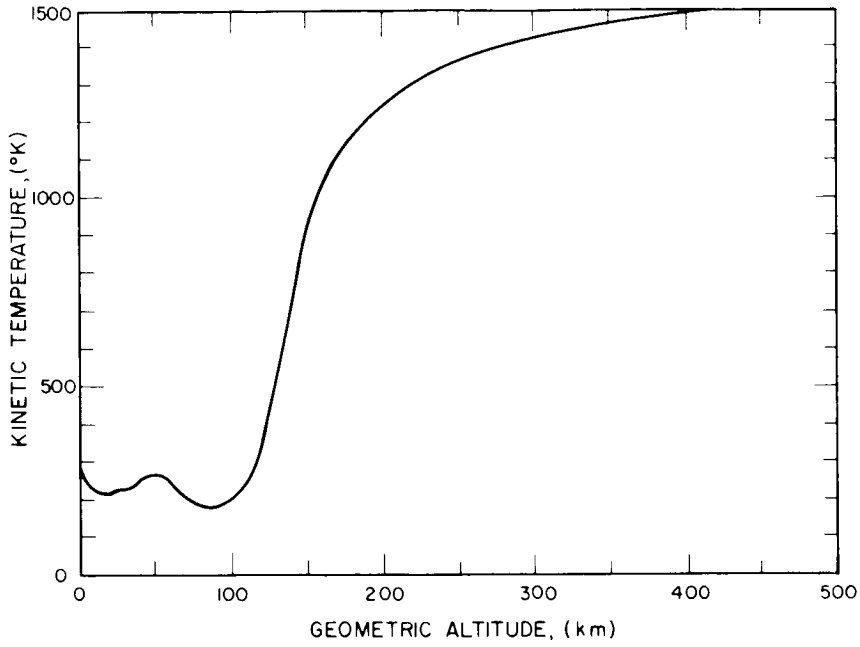

FIG. 1

KINETIC TEMPERATURE AS A FUNCTION OF ALTITUDE (Ref. 1)

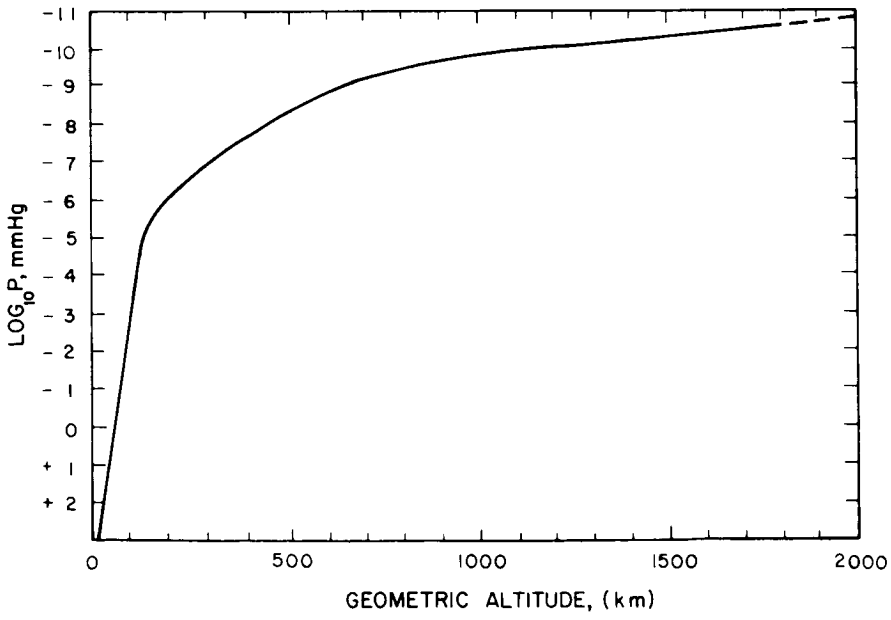

FIG. 2

ATMOSPHERIC PRESSURE AS A FUNCTION OF ALTITUDE (Ref. 1)

Above about 2500 km, H atoms predominate as noted from Fig. 4 (Ref. 5), which gives atmospheric and constituent particle density as a function of altitude. Table I (Ref. 2) tabulates atmospheric pressure, temperature, particle density, concentration, and ionic composition at selected altitudes.

Singer (Ref. 6) defines the base of the exosphere as the level above which one half of the escaping atoms will undergo a collision. From this base at the top of the atmosphere, molecules may escape into space. At lower altitudes molecules are prevented from escaping by collisions with other molecules in the overlying atmosphere. The exosphere is, therefore, the fringe of the atmosphere that extends into space. This altitude is calculated to be 530 km which is equivalent to a geocentric radius of 6900 km. In the absence of collisions above the base of the exosphere, there will be no thermodynamic equilibrium and, in general, no Maxwellian distribution of velocities of the particles. Therefore, the concept of temperature cannot be used above this altitude.

1.3 Electromagnetic Radiations

Infrared, Visible, Near Ultraviolet (λ>3000Å)

The total flux of solar electromagnetic radiation per unit area at 1 AU (astronomical unit) from the sun is known as the solar constant. The solar constant is given as follows:

$$2\ 0\ (\pm 0.04)\ \text{calories/cm}^2\text{/min}$$

or

$$1.4\ (\pm 0.028)\ \times 10^6\ \text{erg/cm}^2\text{/sec}$$

The greatest bulk, or approximately 98.7 percent of electromagnetic energy existing within our solar system emanates from the sun in the spectral range above 3000Å in the region between 0.3 and 7 microns

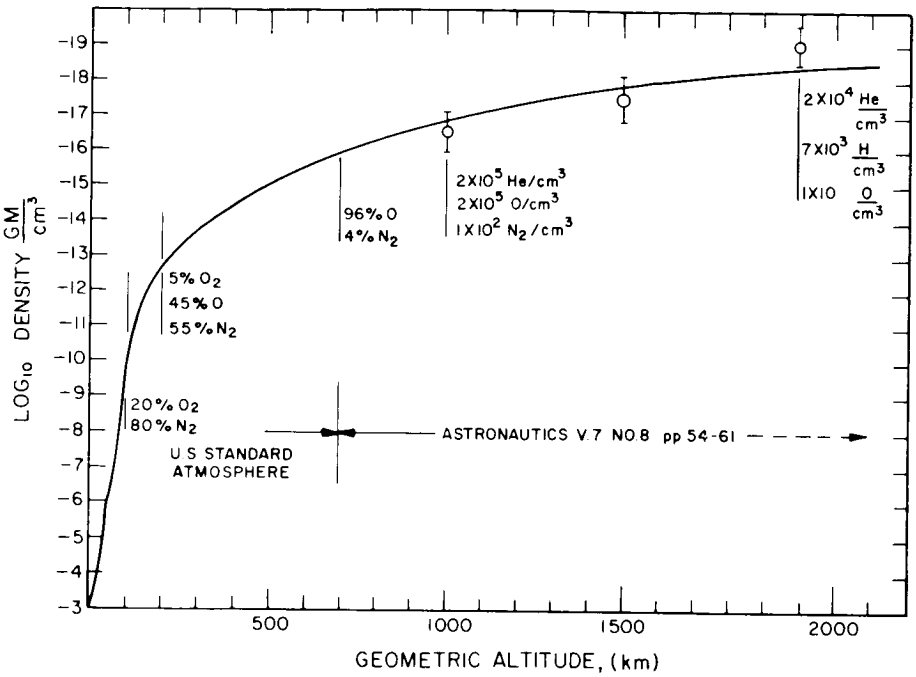

FIG.

ATMOSPHERIC DENSITY AS A FUNCTION OF ALTITUDE (Ref. 4)

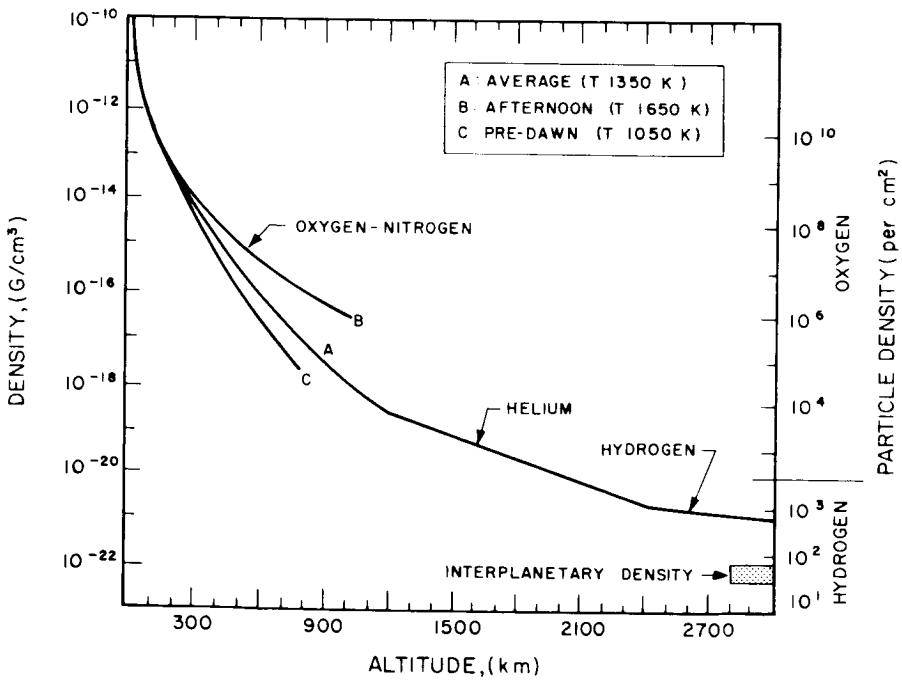

FIG.

DENSITY OF THE UPPER ATMOSPHERE (Ref. 5)

TABLE I ATMOSPHERIC PRESSURE, TEMPERATURE, PARTICLE DENSITY AND COMPOSITION AT SELECTED ALTITUDES (Ref. 2)

Altitude	Pressure, mm Hg	Temperature		Concentration molecules, atoms, or ions/cm^3	Composition
		°C	°F		
Sea level	$760 \simeq 10^{3}$	-40 to +40	-40 to +105	2.5×10^{19}	78% N_2, 21% O_2, 1% A
30 km (100,000 ft)	$50 \simeq 10^{2}$	-40	-40	4×10^{17}	N_2, O_2, A
200 km (125 mile)	10^{-6}	10^{3}	10^{3}	10^{10}	N_2, O, O_2, O^+
800 km (500 mile)	10^{-9}	10^{3}	10^{3}	10^{6}	O, O^+, H
6500 km (4000 mile)	10^{-13}	10^{3}	10^{3}	10^{3}	H^+, H
Above 22,000 km (14,000 mile)	$< 10^{-12}$	10^{3} to 10^{5}	10^{3} to 10^{5}	10^{1} to 10^{2}	85% H^+, 15% He^{++}

The sun's energy spectrum is given in Fig. 5 for altitudes greater than 100 km (Ref. 2). The spectrum closely approximates the emission of a theoretical blackbody solar disk at a temperature of 6000°K, a commonly accepted figure used in calculations involving solar energy. At distances large with respect to the sun's diameter, the irradiance may be considered to vary in accordance with the inverse square of the distance to the sun.

The sun's energy output remains very constant. Variations caused by sun spots and solar flares cause less than 0.4 percent change in output. Most of this change occurs at the short wavelengths. This is further discussed in Subsection I.7. Table II (Ref. 2) gives a breakdown of the fraction of total energy and the total energy on a cumulative basis with increasing wavelength values.

Important to satellites is the effect of the atmosphere's reflectance and scattering properties, or albedo radiation, which causes an increase in the radiant energy to which the vehicle surfaces are exposed. The earth's hemispherical reflectance (albedo) averages 0.36 to 0.39 at visible wavelengths, with seasonal changes from about 0.3 to 0.4. Estimates for the near infrared are about 0.3; for the near ultraviolet about 0.5 (Ref. 2). For a 100-mile earth orbit and an assumed albedo of 0.3, the maximum radiant energy per unit area on a spherical vehicle is 400 watts/meter^2. Figure 6 shows the energy per unit area of spherical and flat surfaces as a function of altitude resulting from the earth's albedo and the earth's thermal radiant energy (Ref. 3).

Besides reflected sunlight, there will also be thermal emission from planets at far-infrared wavelengths. Close to the earth, this amounts to about 2×10^5 erg/cm^2/sec, peaking at 120,000Å (12 microns). Much less than 0.1 percent of this radiation is at visible and ultraviolet wavelengths. The same is true of the radiation from the other planets. These radiations, as well as the zodiacal light

TABLE II CUMULATIVE ENERGY DISTRIBUTION IN SUNLIGHT, AT EARTH'S DISTANCE FROM THE SUN (Ref. 2)

Up to wavelength, Å	Fraction of total energy	Energy, at sunspot maximum (including flares) erg/cm^2-yr
0.1	10^{-11}	10^2 - 10^*
1	10^{-11}	10^2 - 10^3
10	10^{-8}	10^5 - 10^6
100	10^{-6}	10^7 - 10^8
500	10^{-6}	10^8
1,000	10^{-5}	10^8
1,500	10^{-5}	10^9
2,000	10^{-4}	4×10^9
2,500	1.3×10^{-3}	6×10^{10}
3,000	1.2×10^{-2}	5×10^{11}
4,000	9×10^{-2}	4.0×10^{12}
5,000	0.24	1.1×10^{13}
6,000	0.37	1.6×10^{13}
7,000	0.49	2.2×10^{13}
8,000	0.58	2.6×10^{13}
9,000	0.65	2.9×10^{13}
10,000	0.71	3.2×10^{13}
15,000	0.88	3.9×10^{13}
20,000	0.94	4.2×10^{13}
30,000	0.98	4.3×10^{13}
70,000	0.999	4.4×10^{13}

*10^9 to 1.10^{10} photons/cm^2-yr shorter than 0.1 Å.

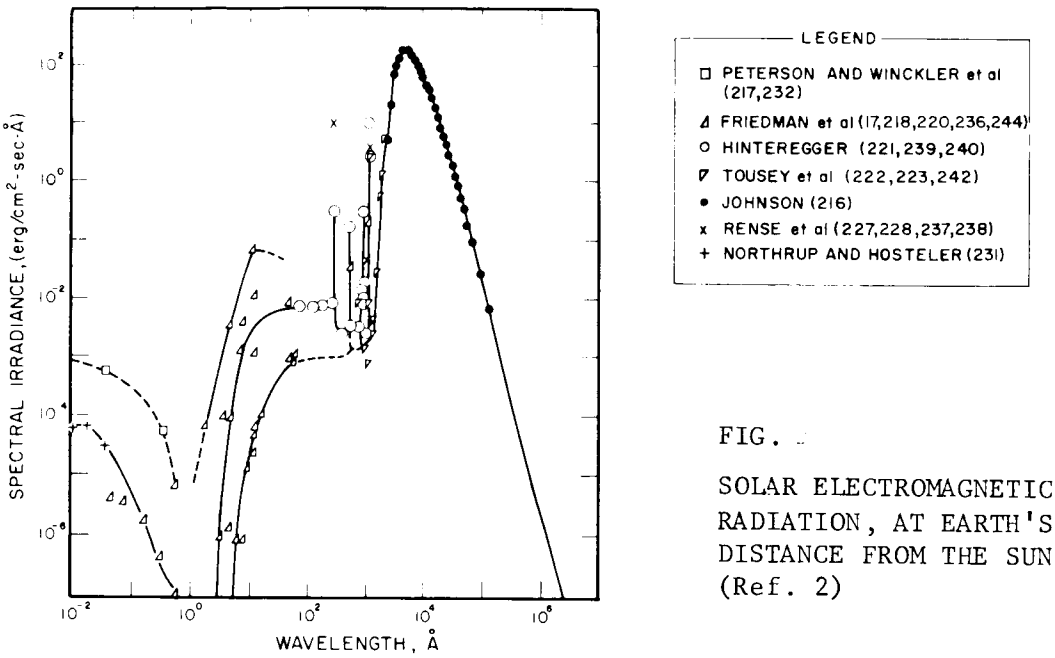

FIG.

SOLAR ELECTROMAGNETIC RADIATION, AT EARTH'S DISTANCE FROM THE SUN (Ref. 2)

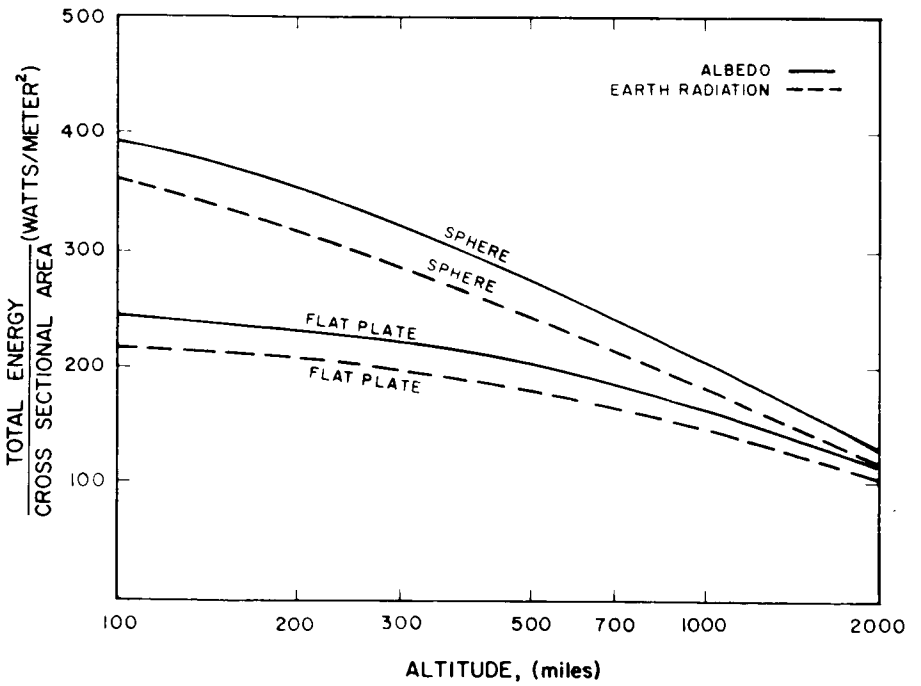

FIG.

ALBEDO AND EARTH RADIATION VARIATION WITH ALTITUDE (Ref. 3)

caused by scattering of solar radiation by interplanetary dust particles of the order of 10^{-3} cm in size distributed throughout interplanetary space, are of negligible energy when compared to the direct solar radiation.

Meteoroids

Damage to materials can result from meteoroids by erosion, perforation, spallation, and pressure shocks. The extent of damage is related to the flux rate, particle size and density, and impact speed. As is generally true of other elements of the space environment these data are not yet too accurately defined with respect to spatial distribution and are variable with time. Meteoroids may be classified as meteorites, meteors, and micrometeoroids or dust. These differ as to mass, density, orbit, and origin.

Meteorites

Masses of stone or metal reaching the earth from outer space, are believed to be of asteroidal origin and orbit the sun not far from the ecliptic. Their masses are often above 1 gram with densities of 3 to 3.5 gm/cm^3; about 10 percent are iron-nickel fragments with densities of 7 to 8 gm/cm^3. Their velocities are usually about 20 km/sec though they may have velocities of a maximum of 72 km/sec. They do not concentrate around the earth so that their flux in the vicinity of the earth is so low that collision with an earth satellite is highly improbable.

Meteors

Visual flashes are caused by the entrance of meteoric particles into the earth's atmosphere. The majority of these particles, detectable visually or by radio, radar, or photography, are presumed to come from comet debris. They are mostly porous dust balls with a very low overall density, probably near 0.1 gm/cm^2 with a mass generally less than 1 gm down to the limit of detectability of 10^{-5} gm. Orbits are elliptic, mostly with high eccentricities, and occur at all angles

to the plane of the ecliptic. These meteoric particles do not concentrate around the earth. Their velocities relative to the earth or a satellite range from a few km/sec outside the earth's gravitational field up to about 72 km/sec and average about 30 km/sec. Close to the earth the minimum velocity is increased by the earth's gravitational field to 11 km/sec. Closer to the sun, velocities increase. Some of the meteors are associated in showers moving together in elliptic orbits which the earth may intersect once or twice a year. Figure 7 gives the distribution of velocities for sporadic and shower meteors (Ref. 7). Figure 8 charts the number of particles as a function of ecliptic latitude, (Ref. 7).

Micrometeoroids

The fine dust particles are believed by some to be of the same cometary origin as the visible meteors. Density of the particles, or porous aggregates of dust, range from 0.05 to 3.5 g/cm^3. Minimum masses vary from about 4×10^{-10} g, at a density of 0.05 g/cm^3, to about 7×10^{-14} g, at a density of 3.5 g/cm^3. The maximum size approaches 10^{-5} g. Dust orbits around the sun are, in general, nearly circular and are near the plane of the ecliptic. Relative velocities are mostly under 20 km/sec. Predictions of increased dust concentration around the earth are confirmed by examination of the altitude dependence of micrometeoroid flux as measured by sounding rockets, satellites, and space probes. Attempts to quantitate the data indicate flux variation with a power of R_e of between R_e^{-1} and R_e^{-2} where R_e is the geocentric radius. The dust cloud around the earth extends out about 10^6 km. The particles composing it are either spiralling in toward the earth or orbiting around it. Velocities relative to the earth probably average 7 to 15 km/sec at low altitudes, and 3 to 10 km/sec at higher altitudes. The dust cloud is held by gravitation. Atmospheric drag, including electrostatic drag, and interactions with solar radiation pressure may play a part in the earth's capture of this dust from the heliocentric orbits. In interplanetary space, the dust concentration increases toward the sun at about the 3/2 power of solar distance.

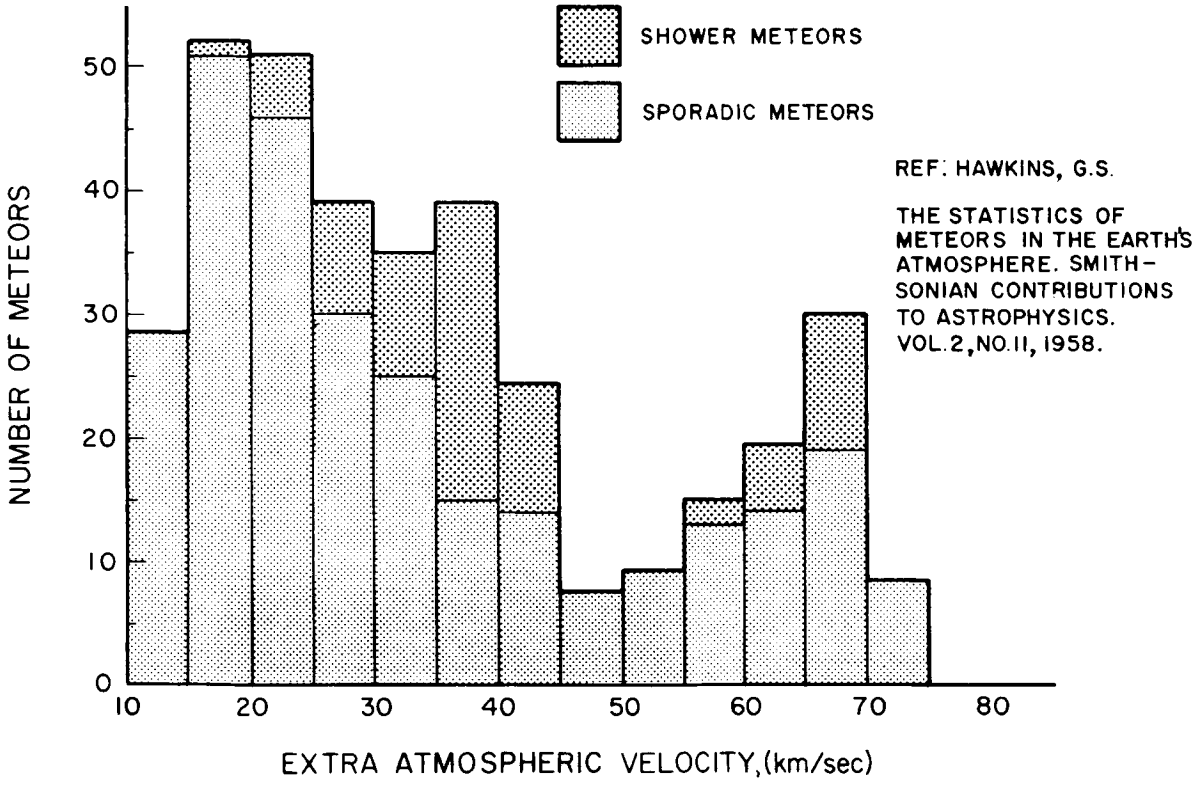

FIG. 7 DISTRIBUTION OF CORRECTED VELOCITIES FOR 285 SPORADIC AND 74 SHOWER METEORS (Refs. 7, 29)

The chart given in Fig. 9 (Ref. 8) gives a comparison of data on cumulative meteoroid impact rates near the earth estimated by various workers. Whipple's curve, labeled 1963A, Fig. 9 represents the most recent estimation of influx rate by an expert in this field of study. This curve and the curve labeled "B" in the figure have been calculated for an average particle density, ρ, of 0.44 g/cm^3.

1.4 Degradation of Reflecting Surfaces by Micrometeoroids

In this section equations are developed to predict the effect of micrometeoroid bombardment on reflecting surfaces in earth orbit. Numerical results, which are given for several sets of assumptions, indicate degradation of reflectivity from this source is not too severe. However, since detailed data on the micrometeoroid flux are not yet available and since the theory of hypervelocity impact is not fully developed, these numerical results must be considered as only a first approximation.

1.4.1 General Approach

A micrometeoroid striking the reflecting surface of a thick target is assumed to create a hemispherical pit in the surface, as is indicated by hypervelocity projectile experiments (Ref. 9). It is further assumed that the circular area defining the top of the pit has zero reflectivity, which is the worst case. In the following treatment normal incidence is assumed for the entire micrometeoroid flux, although it is realized that this in general will not be the case. When further inputs on orbits and orientations of the reflection experiment are available the following equations can be corrected for proper angle of incidence distributions.

It has been shown (Refs. 9 and 10) that the volume of material displaced to form the pit is directly proportional to the kinetic energy of the impinging particle. The constant of proportionality, K_T, involves only physical properties of the target material.

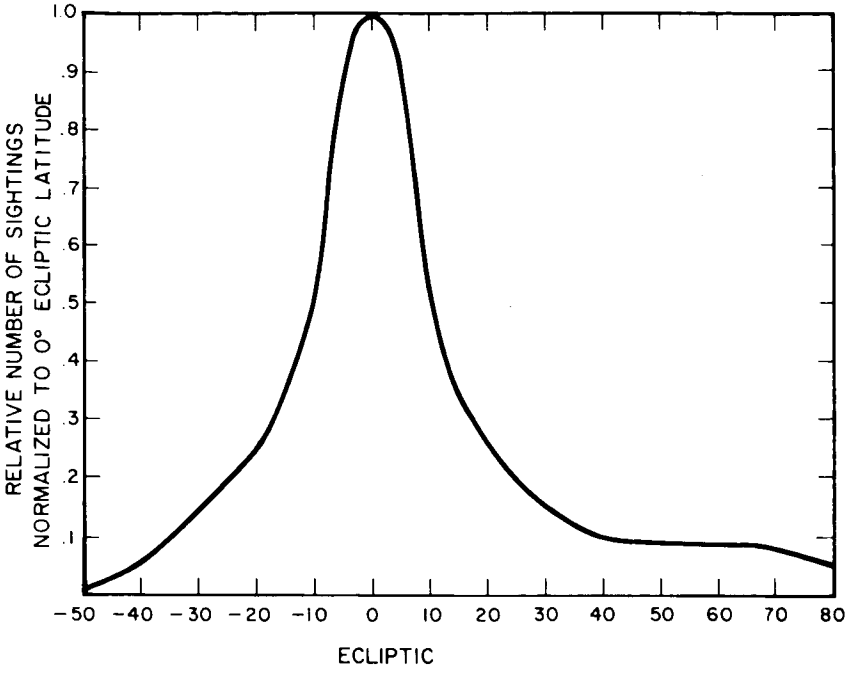

FIG.

DISTRIBUTION OF VISUAL SPORADIC METEOR-RADIANTS IN ECLIPTIC LATITUDE (Ref. 7)

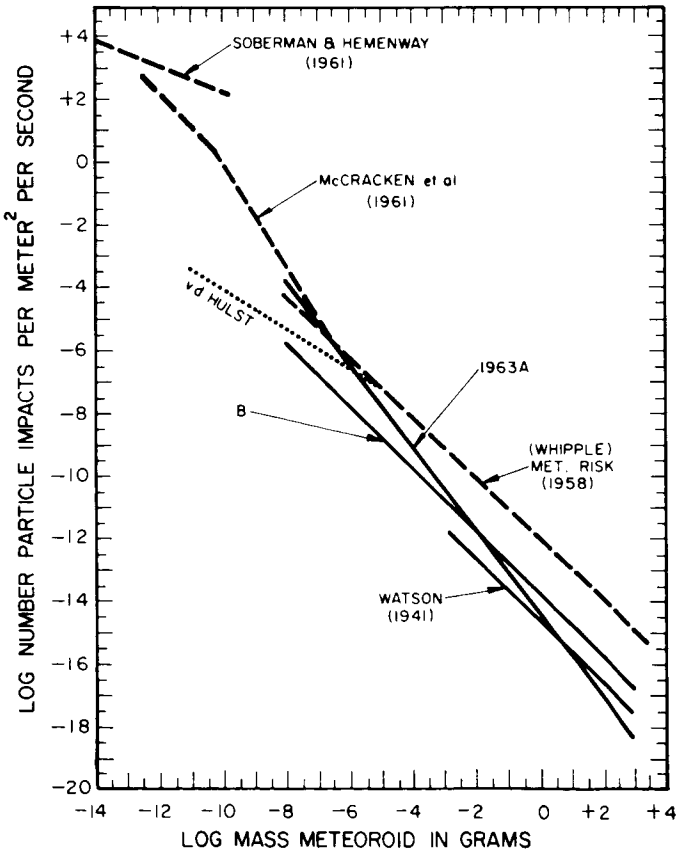

FIG.

CUMULATIVE METEOROID IMPACT RATES NEAR THE EARTH (Ref. 8)

Since there are at least three different theories (Refs. 11, 12, and 13) on the calculation of this constant (as discussed later), we will leave K_T as unknown for the moment, and formulate the above statement as:

$$V = 1/2\ mv^2/K_T \tag{1}$$

where V = volume of hemispherical pit (cm^3)

m = mass of micrometeoroid (grams)

v = velocity of micrometeoroid (cm/sec)

K_T = target constant ($ergs/cm^3$)

The area removed from the reflecting surface (i.e., target) is calculated from the formulas for the volume of a hemisphere and the area of a circle to be:

$$A = \left(\frac{3\pi^{1/2} V}{2} \right)^{2/3} \tag{2}$$

where A = area removed from surface (cm^2).

Combining Eqs. 1 and 2 yields:

$$A = \left(\frac{3\pi^{1/2}\ mv^2}{4K_T} \right)^{2/3} \tag{3}$$

This expression gives the area of reflecting surface removed for any micrometeoroid of mass m and velocity v.

In order to calculate the integrated effect of the micrometeoroid flux we need a distribution function relating the number and mass of these particles. This function is provided by the work of Whipple (Ref. 11) as:

$$N = K_W/m \tag{4}$$

where N = number of particles per unit area per unit time ($cm^{-2}\ sec^{-1}$)

K_W = Whipple's constant = 5.3×10^{-16} $g/cm^2/sec$

The differential form of Eq. 4,

$$dN = -K_W \, dm/m^2 \tag{5}$$

may be combined with Eq. 3 to yield:

$$AdN = -\left(\frac{3\pi^{1/2} v^2}{4 K_T} \right)^{2/3} \cdot K_W \cdot m^{-4/3} \, dm \tag{6}$$

If we assume a constant velocity for all particles, as is generally accepted (Ref. 9 and 11), Eq. 6 may be integrated to give:

$$\int AdN = 1/3 \left(\frac{3\pi^{1/2} v^2}{4 K_T} \right)^{2/3} \cdot K_W \cdot m^{-1/3} \Big|_{m^*}^{\infty} \tag{7}$$

The desired quantity, $\int AdN$, which is the fractional area loss per unit time due to the entire flux, can now be found, given the required constants and the lower limit of mass, m^*, are known. This lower limit of mass can be calculated based on Whipple's consideration (Ref. 11) that when the solar radiation pressure on a particle exceeds the solar gravitational force, the particle will be forced out of the solar system. The governing equation is:

$$m^* = \frac{5.76 \times 10^{-11}}{\rho_m^2} \tag{8}$$

where ρ_m = assumed micrometeoroid density (g/cm^3).

We now return to consideration of the target constant, K_T, which is the energy required per unit volume in the formation of the pits. As mentioned above, at least three approaches have been proposed for calculating K_T. The first, suggested by Whipple, (Ref. 11), involves the thermal energy required to melt the target material. This is formulated as:

$$K_{T1} = \rho_T \, (C\Delta T + \Delta H) \tag{9}$$

where ρ_T = density of target material (g/cm^3)

C = specific heat of target material (ergs/g, ^oC)

ΔT = difference between target temperature and melting point of target material (^oC)

ΔH = latent heat of fusion of target material (ergs/g)

The second approach, proposed by Barnes (Ref. 12), is based on an empirical fit of data from hypervelocity impact experiments. Barnes' equation is:

$$K_{T2} = 3.94 \times 10^{-2} \rho_T v_s^2 \qquad (10)$$

where v_s = velocity of sound in the target material (cm/sec).

The third approach, put forth by Eichelberger and Gehring (Ref. 13) is also based on hypervelocity impact experiments. Their form of the equation is:

$$K_{T3} = 2.5 \times 10^8 B \qquad (11)$$

where B = Brinell hardness number of the target material.

Considering the wide variety of material properties used in these three approaches the calculated results for area loss agree remarkably well, as is shown in the following section.

1.4.2 Calculated Results

Three of the five materials of interest as mirror substrates are aluminum, copper and nickel. In the case of copper or nickel a thin film of silver or aluminum would typically be deposited on the surface to enhance reflectivity; however, these films are so thin (200 to 1000Å) that we will assume the substrate properties control the pit formation. Physical properties of these substrate materials used in calculating the targets constants (K_{T1}, K_{T2}, and K_{T3}) are given in Table III.

TABLE III

PHYSICAL PROPERTIES OF MIRROR SUBSTRATE MATERIALS

Material	ρ(g/cm^3)	C(erg/g/°C)	ΔH(erg/g)	M.P.(°C)	v_s(cm/sec)	B
Al	2.7	10.4×10^6 (300°C)	3.2×10^9	660.	5.10×10^5	76
Cu	8.93	4.4×10^6 (550°C)	2.0×10^9	1083.	3.56×10^5	140
Ni	8.90	5.4×10^6 (700°C)	3.0×10^9	1453.	4.97×10^5	200

The quantities in Table III are used to calculate the three different K_T's shown in Table IV. For ΔT in the K_{T1} equation (Eq. 9) the melting point is used, i.e., the substrate temperature is assumed to be 0°C. It is seen, however, that even if a temperature several hundred degrees above or below 0°C were used K_{T1} would change very little.

TABLE IV

TARGET CONSTANTS FOR MIRROR SUBSTRATE MATERIALS

Material	K_{T1} (Eq. 9)	K_{T2} (Eq. 10)	K_{T3} (Eq. 11)
Al	2.70×10^{10}	2.68×10^{10}	0.4×10^{10}
Cu	6.07×10^{10}	4.72×10^{10}	3.5×10^{10}
Ni	9.70×10^{10}	7.87×10^{10}	5.0×10^{10}

The other two quantities which must be specified in order to make use of Eq. 7 are the average micrometeoroid velocity, v, and the density, ρ_m, of these particles (from which is calculated the lower mass limit, m*, by Eq. 8. For velocity we have chosen two cases: 4×10^6 cm/sec, which is believed to be typical (Refs. 9, 14, and 15), and 7.2×10^6 cm/sec, which is believed to be the maximum possible

velocity (Ref. 14). For density we have also chosen two cases: 8.9 g/cm^3, which represents a pure nickel micrometeoroid, and 1.0 g/cm^3, which is believed to be more typical of micrometeoroids (Ref. 16). The lower mass limits, m*, calculated from these densities using Eq. 9 are, respectively, 7.35×10^{-13} g and 5.76×10^{-11} g.

The fractional surface area loss per year for all combinations of the three materials, the three target constants, the two assumed velocities and the two assumed densities, calculated from Eq. 7, are given in Table V. It is seen from Table V that even with the most pessimistic set of assumptions the surface area losses per year are relatively small: 3.3% for Al, 0.97% for Cu, and 0.76% for Ni.

1.4.3 Results Based on Whipple's 1963 Estimate of Micrometeoroid Environment

Very recently a new estimate by Whipple of the micrometeoroid environment has become available (Ref. 1). Using this new estimate, the predicted effects on the metal-substrate mirrors are somewhat smaller than those given above.

Based on recent experimental data, Whipple estimates that the micrometeoroids have a mean velocity of 2.2×10^9 cm/sec, a mean density of 0.44 g/cm^3, and a distribution given by:

$$N = 3.31 \times 10^{-19} \, m^{-1.34} \tag{12}$$

where N = number per cm^2 per second

m = mass in grams

The new density estimate yields a lower limit of mass, $m^* = 2.9 \times 10^{-10}$ g. (See Eq. 8)

The revised form of Eq. 7, resulting from the above changes is:

$$\int AdN = 2.98 \times 10^{-19} \left(\frac{3^{-1/2} \, v^2}{4K_t} \right)^{2/3} m^{-0.67} \Big|_{m^*}^{\infty} \tag{13}$$

Using Eq. 13 the calculated values of the fractional area loss per year for the three materials and three target constants discussed above are given in Table VI.

TABLE VI

FRACTIONAL SURFACE AREA LOSS PER YEAR FOR MIRROR SUBSTRATE MATERIALS BASED ON NEW WHIPPLE ESTIMATE

Material	Using K_{T1}	Using K_{T2}	Using K_{T3}	Other Assumptions
Al	8.8×10^{-4}	8.8×10^{-4}	3.1×10^{-3}	$V = 2.2 \times 10^{6}$; $\rho = 0.44$
Cu	5.1×10^{-4}	6.0×10^{-4}	7.4×10^{-4}	$V = 2.2 \times 10^{6}$; $\rho = 0.44$
Si	3.7×10^{-4}	4.3×10^{-4}	5.8×10^{-4}	$V = 2.2 \times 10^{6}$; $\rho = 0.44$

1.5 Solar Wind

The solar wind consists of more or less steady streams of plasma flowing from the corona approximately radially outward from the sun. The study of plasmas in space is closely connected with the study of interplanetary magnetic fields. In fact, it is preferable to think of a plasma measurement and magnetic field measurement as two aspects of a single experiment. The high electrical conductivity of the plasma causes the magnetic flux lines to be effectively frozen into the plasma. In the normal case in interplanetary space, the kinetic energy density of the plasma is greater than the magnetic energy density, so that the magnetic field is carried along by the plasma motion. Near the earth the situation is reversed, and the solar plasma is excluded from regions where the geomagnetic energy density is greater than the energy density in the plasma, so that a cavity (the magnetosphere) is formed.

This plasma consists primarily of protons; heavier ions are expected to be present in about the ratios found in the solar atmosphere: about 15 percent atomic He, and less than 1 percent heavier elements (Ref. 2). Densities and energies of the quiet sun emissions

TABLE V

FRACTIONAL SURFACE AREA LOSS PER YEAR FOR MIRROR SUBSTRATE MATERIALS

Material	Using K_{I_1}	Using K_{I_2}	Using K_{I_3}	Other Assumptions
Al	1.2×10^{-3}	1.2×10^{-3}	4.4×10^{-3}	$v = 4.0 \times 10^6$; $\rho = 1.0$
Cu	7.2×10^{-4}	8.5×10^{-4}	1.0×10^{-3}	$v = 4.0 \times 10^6$; $\rho = 1.0$
Ni	5.3×10^{-4}	6.0×10^{-4}	8.2×10^{-4}	$v = 4.0 \times 10^6$; $\rho = 1.0$
Al	5.3×10^{-3}	5.3×10^{-3}	1.9×10^{-2}	$v = 4.0 \times 10^6$; $\rho = 8.9$
Cu	3.1×10^{-3}	3.6×10^{-3}	4.4×10^{-3}	$v = 4.0 \times 10^6$; $\rho = 8.9$
Ni	2.3×10^{-3}	2.6×10^{-3}	3.5×10^{-3}	$v = 4.0 \times 10^6$; $\rho = 8.9$
Al	2.7×10^{-3}	2.7×10^{-3}	1.5×10^{-2}	$v = 7.2 \times 10^6$; $\rho = 1.0$
Cu	1.6×10^{-3}	1.8×10^{-3}	2.3×10^{-3}	$v = 7.2 \times 10^6$; $\rho = 1.0$
Ni	1.2×10^{-3}	1.3×10^{-3}	1.8×10^{-3}	$v = 7.2 \times 10^6$; $\rho = 1.0$
Al	1.2×10^{-2}	1.2×10^{-2}	3.5×10^{-2}	$v = 7.2 \times 10^6$; $\rho = 8.9$
Cu	6.7×10^{-3}	7.9×10^{-3}	9.7×10^{-3}	$v = 7.2 \times 10^6$; $\rho = 8.9$
Ni	4.9×10^{-3}	5.6×10^{-3}	7.6×10^{-3}	$v = 7.2 \times 10^6$; $\rho = 8.9$

or solar wind are variously given as falling between 10 and 100 particles/cm^3 at energies of from 5 to 0.5 kev (Refs. 2, 3, 18, and 19). In terms of flux rate, the range varies from 4 x 10^8/cm^2/sec at 500 ev (Ref. 18) to 5 x 10^9/cm^2/sec at about 1 kev (Ref. 20). Direction is presumed to be generally radial from the sun (Ref. 2) but could be random. The necessary electrons to neutralize the positive particles may be present in a flux as high as a few times 10^{10} e/cm^2/sec at E < 2 ev (Ref. 2).

Solar flare radiations occur about once a month at the maximum of the 11-year solar period and perhaps 1 or 2 per year at the solar minimum. The proton flux near the earth associated with a major flare is typically 10^4 proton/cm^2/sec at energies above 20 Mev, extending up to 10^2 p /cm^2/sec above 100 Mev and 10^0 p/cm^2/sec above 500 Mev.

Record flares, occurring perhaps twice each solar maximum have had proton fluxes 10 times as great. The proton flux accompanying a solar storm usually lasts about a day. One measurement after a flare of moderate size showed 10^6 to 10^7 electron/cm^2/sec at roughly 50 kev (Refs. 2, 3 and 20). There are also low-energy flare protons at 0.5 to 20 kev; the flux of these is not well known. It may be lower than 10^8 proton/cm^2/sec (Ref. 2), or as high as 10^{12} proton/cm^2/sec (Refs. 2 and 20). Low-energy electrons at 0.25 to 10 ev presumably accompany the low-energy protons; their flux may be 1 to 40 times the proton flux. These low-energy particles are effectively shielded by the geomagnetic field and exist primarily in regions outside the magnetosphere.

1.6 Effect of Charged Particles on Reflective Surfaces

Although preliminary estimates, made earlier during this study program, indicated charged particles would have a relatively small effect on a reflective surface, recent experimental evidence shows these particles, especially low to medium energy protons, may cause significant reflectivity degradation and an undesirable increase in the thermal control parameter, α/ε. The damage mechanism is nonuniform sputtering of the metal surface, which, in the case of aluminum, results in a high density of irregular pits on the surface in size range of 1 to 5 microns.

The evidence of this type of damage was developed in recent experiments by D. L. Anderson (Ref. 21) and D. L. Anderson and G. J. Nothwang (Ref. 22) in which space proton bombardment of polished metal surfaces was simulated with 1 kev hydrogen ions. Their results for polished pure aluminum, which is most generally used for reflective surfaces, are of particular interest. Bombardment with an integrated flux of 10^{21} hydrogen ions per cm^2 increased the solar absorptivity (α) of the surface to 0.23, compared with its initial value of 0.09. Therefore, total solar reflectivity was degraded from 0.91 to 0.77. However, the degradation of specular reflectivity, which is the measure of a solar concentrator's performance, is even more severe. Study of the photomicrographs of the Al surface before and after this treatment (Ref. 21) leads one to a conservative estimate that after sputtering at least 30 percent of the remaining total reflectivity is diffuse; thus the specular reflectivity is estimated as 0.54. It should be noted that even at an integrated flux of 10^{20} hydrogen ion an increase in α from 0.09 to 0.13 was measured by Anderson.

In order to assess the significance of the above results one must relate the laboratory experiment with 1 kev protons (hydrogen ions) to the space environment. With the present sparse and often conflicting data on the charged particle space environment this is quite difficult.

1.7 Ultraviolet X-Rays (λ less than 3000 Å)

The fraction of total radiant energy below 3000 Å is about 1.2% of the sun's energy amounting to about 1.7×10^2 $erg/cm^2/sec$. Principal lines are given in Table VII. A chart of the solar ultraviolet spectrum is given in Fig. 10 (Ref. 23). During periods of solar flares the levels can be increased by several orders of magnitude for periods of a few hours. (Ref. 24).

The main reason for interest in these uv and x-ray emissions is because the photon energies are sufficiently high to initiate chemical reactions and ionization of materials. Such reactions can begin at wavelengths below 3000 Å in the near ultraviolet. Again, because

TABLE VII INTENSITY AT 1 ASTRONOMICAL UNIT PRODUCED BY THE STRONGEST SOLAR EMISSION LINES (Ref. 9)

λ(Å)	Identification	Erg/cm²/sec
1892.03	Si III (1)	0.10
1817.42 *	Si II (1)	0.45
1808.01		0.15
1670.81	Al II (2)	0.08
1657.00 *	C I (2)	0.16
1640.47	He II (12)	0.07
1561.40 *	C I (3)	0.09
1550.77	C IV (1)	0.06
1548.19	C IV (1)	0.11
1533.44	Si II (2)	0.041
1526.70	Si II (2)	0.038
1402.73	Si IV (1)	0.013
1393.73	Si IV (1)	0.030
1335.08	C II (1)	0.050
1334.53	C II (1)	0.050
1306.02	O I (2)	0.025
1304.86	O I (2)	0.020
1302.17	O I (2)	0.013
1265.04	Si II (4)	0.020
1260.66 *	Si II (4)	0.010
1242.78 *	N V	0.003
1238.80	N V	0.004
1215.67	H Ly-α	5.1
1206.52	Si III (2)	0.030
1175.70 *	C III (4)	0.010
1139.89 *	C I (20-23)	0.003
1085.70 *	N II (1)	0.006
1037.61 *	O VI (1)	0.025
1031.91	O VI (1)	0.020
1025.72	H Ly-β	0.060
991.58 *	N III (1)	0.010
989.79 *	N III (1)	0.006
977.03	C III (1)	0.050
949.74	H Ly	0.010
937.80	H Ly	0.005
835 *	O II III	0.010

The value for Lyman-α applies to the intensity within the 1-Å wide central part of the line based on an ion-chamber reading of 6.0 erg/cm²/sec).

* Indicated that the line is a blend of lines of other elements or is an unresolved multiplet.

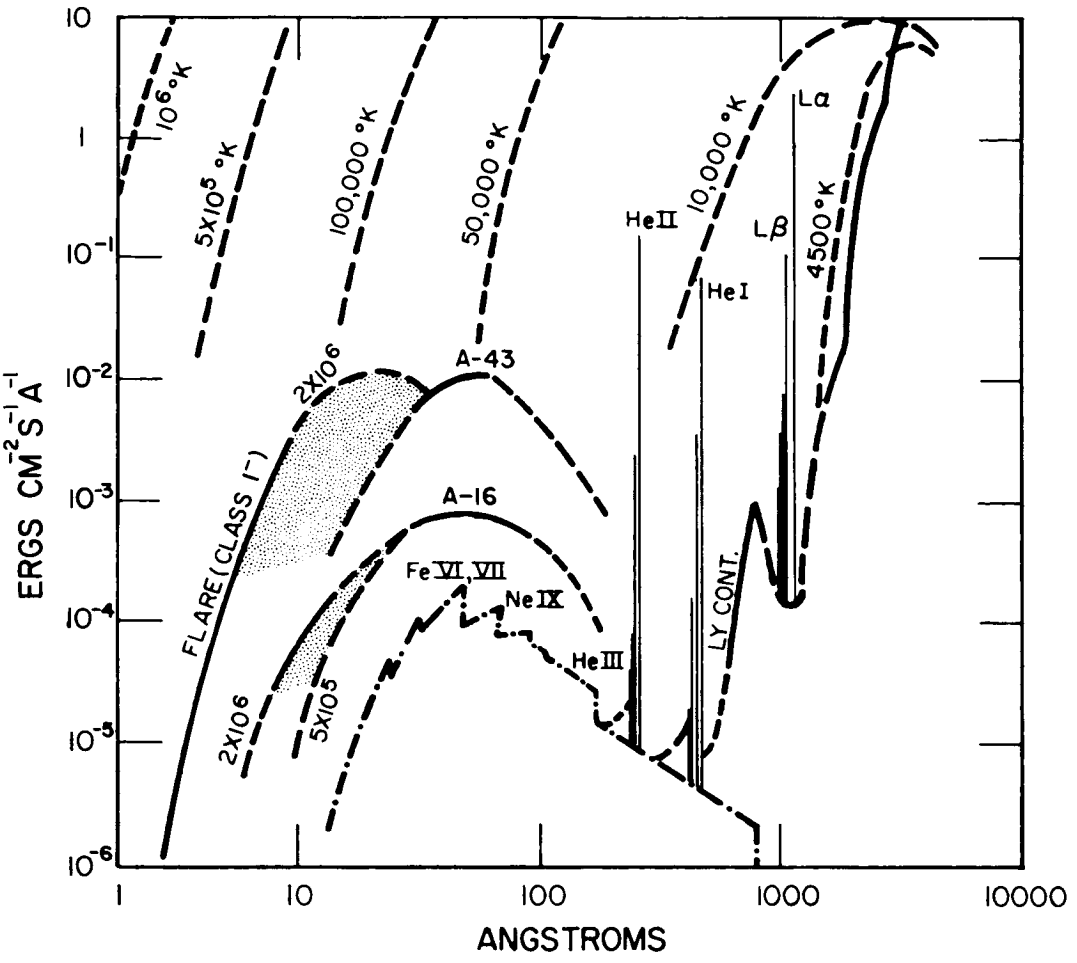

FIG. 10 SOLAR SPECTRAL ENERGY DISTRIBUTION FROM 2000 Å TO X-RAYS (Ref. 21)

of concern with surface effects these radiations are of more than usual interest even though their intensity levels are low. In view of transient nature of sunspots and solar flares the most practical presentation of data is in terms of yearly averages.

Figure 10 (Ref. 23) summarizes results of rocket measurements of solar spectral energy distribution above the atmosphere. This chart gives data obtained during sunspot minimum in 1953 and 1954, marked A-16, and during sunspot maximum in 1956, marked A-43. They represent the minimum and maximum fluxes observed during a sunspot cycle. The shaded region added to the A-16 curve is the increment of flux measured below 20Å and attributed to localized hot spots at 2 million degrees K. Near sunspot minimum in 1953 and 1954 the rocket measurements indicated a marked reduction in x-ray emission below 20Å. In some experiments no emission at all was detected below 10Å. With the approach to solar maximum, the overall x-ray flux increased, especially at the shorter wavelengths. In the 2 to 8 Å band the minimum to maximum variation was a factor of several hundred; from 8 to 20 Å, at least a factor of 45; in the 44 to 60 Å band, the variation was approximately sevenfold. Assuming that the x-ray spectrum had a gray-body distribution it was not possible to fit the measurements in these three wavelength intervals by a single temperature. The longer wavelength emission could be adequately described by a temperature between 0.5 to 1.0 x 10^6 degrees K, but the shorter wavelength range, below 20 Å required a temperature closer to 2 x 10^6 degrees K.

Rocket measurements have shown that the entire night sky as seen from 100 km is aglow with a diffuse Lyman α radiation which produces an illumination of 10^{-2} ergs/cm^2/sec for the entire hemisphere. The intensity drops to a minimum in the direction opposite to the sun and it is concluded that most of the radiation is solar radiation scattered by neutral hydrogen. While much of this hydrogen is probably associated with the earth, part of the scattered radiation may originate from neutral atoms in inter-planetary space.

Many reflective surfaces being considered for solar concentrator use have dielectric coatings over the metallic reflective materials. These coatings are used both to provide mechanical and chemical protection for the metal layer, and to lower the ratio of solar absorptivity to infrared emissivity in order to limit the temperature extremes experienced by the mirror structure in orbit. However, the dielectric coatings may be subject to degradation in the space environment, resulting in the lowering of reflectivity.

A specific example of this type of degradation was reported recently (Ref. 25). A large number of reflective aluminum samples coated with various types and thicknesses of anodic oxide, and a few samples coated with evaporated dielectric such as SiO, MgF_2 and TiO_2 were irradiated with a good approximation to the solar ultraviolet spectrum while being held under vacuum of 10^{-5} torr. Although a wide variety of results was obtained, most samples showed a significant decrease in reflectivity (typically 3 percent to 10 percent) after an ultraviolet irradiation equivalent to solar irradiation from 300 to 1200 hours. Evidence was developed to show that the reflectivity degradation was due to increased absorption in the coating, probably caused bypphoton-created vacancies.

Although it was not investigated in Ref. 25, it seems most probable that the radiation constants of interest for thermal control, i.e., solar absorptivity and infrared emissivity, were also changed to a significant degree.

Recent findings of Hass on the effects of ultraviolet irradiation on the ultraviolet reflectance of slowly deposited SiO aluminum mirror overcoatings indicate that much is still to be learned on radiation material interactions in this spectral region. Metals are not exempt from possible optically degrading effects. An example of findings of interest is the work of Ivanova (et al) who measured reflectance degradation of aluminum and rhodium mirrors for irradiation in the Schumann region of the spectrum (1,100Å to 1,800Å) under the action of ultraviolet

light in a vacuum. Some ultraviolet of longer wavelength was undoubtedly present in their test. As mentioned previously, Earth albedo supplies a portion of the ultraviolet. Much of the damage to nonmetals has been attributed to this radiation.

Electromagnetic radiation within the approximate spectral range of 2,000Å to 50Å may be referred to as the vacuum ultraviolet. Shorter wavelengths can be considered to lie in the soft x-ray region. Vacuum ultraviolet radiation is emitted when matter is excited into energy states between which transitions can occur and whose energy differences correspond to the frequencies involved.

Thus, using an electron volt-angstrom conversion factor of 12,390, the energy equivalent of the 1,500Å to 50Å wavelength range is 8 electron volts to 240 electron volts. The creation of excited states of matter with such high energies is equivalent to producing temperatures of the order 10^6 ^oK.

Because of the high level of absorption of most materials (including SiO) in the vacuum ultraviolet, the mass absorptive rate in ergs/g-yr is potentially important. Solar radiation of the wavelength range 500Å to 1,000Å provides 10^8 ergs/cm^2-yr of ionizing radiation. Penetration ranges at 100Å to 1,000Å are not well known but probably lie between 10^{-4} and 10^{-7} g/cm^2. The resulting ionization dose of 10^{12} to 10^{15} erg/g-yr will damage the thin layer reached by radiation and will very probably affect optical absorption. Electronic excitation, which is of concern from the vacuum ultraviolet up to 3,000Å, can also affect optical reflectivity. The mechanism for the ionization and excitation damage is roughly one of releasing electrons from their equilibrium positions in the crystal lattice resulting for some cases in trapped electrons and holes or color centers. The amount of radiation absorbed in a color center may be anywhere from 1/10 to 100 times that required to produce the center. Therefore, radiation below 3,000Å can effect the absorption of radiation at longer wavelengths.

Organic materials will also receive 10^{12} to 10^{15} erg/g-yr from sunlight of 100Å to 1,000Å. Such doses will cause severe degradation to the properties of thin exposed layers of all known polymers. No experimental work has been conducted on polymers in the 100Å to 1,000Å range and only limited work has been done in the 1,000Å to 3,000Å range.

Material degradation experiments conducted by Moore in the vacuum ultraviolet indicated the somewhat anomolous fact that for copper and gold reflecting surfaces overcoated with SiO less degradation in 2,500Å reflectance occurred for samples irradiated by vacuum ultraviolet radiation in a vacuum of 10^{-9} mm Hg than when the sample was exposed to vacuum alone. The previously mentioned recent findings of Hass support these results at least partially by demonstrating that the reflectivity of SiO overcoated aluminum mirrors can be increased by depositing the film in the presence of ultraviolet radiation.

Some Russian investigaters irradiated aluminum and rhodium mirrors with no overcoatings and found that irradiation in the 1,700Å to 1,000Å region caused a drop in reflectivity. Decrease in reflectivity was attributed to oxidation by residual oxygen in the apparatus where the measurements were made. Such a result might also indicate the need for a high vacuum as an environmental condition.

1.8 Trapped Radiations - Magnetosphere

The earth's geomagnetic field is effective in shielding the earth from solar cosmic rays and, to some extent, galactic cosmic rays, by bending or deflecting these primary, charged particle radiations away from the earth. The higher energy cosmic particles can penetrate the field even at the geomagnetic equator where the field strength is a maximum. However, the lower energy solar particles are much more readily deflected. The geomagnetic field also has the property of trapping and holding, for long periods of time, charged particles that are generated within the magnetosphere or penetrate it from without. This trapping ability comes about as the result of the Lorentz force acting on a charged particle moving in a magnetic field. The effect of this motion

in the earth's dipole field is to cause the particle to mirror between the poles and remain trapped within the force lines. Particles originating too low in altitude will not mirror before encountering the earth's atmosphere where they are absorbed. Close to the earth the field strength is higher than at greater atitudes. This causes longitudinal drift of the protons westward and the electrons eastward.

Various models of the trapping region have been proposed. These models and the intensity levels and spatial distributions are changing almost daily as new data become available from orbiting satellites and space probes. To this date the intensity of the trapped radiation, its composition, and the energy spectrum of each component as a function of position in space, direction, and time have not been established conclusively. Until recently, most space radiation measurements have been made with detectors that excluded the softer, lower energy components of the trapped radiations. The resultant effect was to find favored regions within the magnetosphere for high-energy protons and electrons which constitute the better known inner and outer Van Allen belts.

The spatial distribution of the trapped radiations of the magnetosphere may be visualized as a toroidal configuration encircling the earth about the geomagnetic equator. The Van Allen belt radiation is often described in terms of two main belts; an inner zone centering at about 1.5 R_e (earth radii), or 9500 km geocentric radius, distinguished primarily by the existence of high-energy protons of $E_e \geq 30$ Mev; and an outer, more diffuse, belt of electrons with $E_e \geq 1.6$ Mev centering at about 3.5 R_e. The distribution of these energetic particles is given in Fig. 11 (Refs. 26 and 27).

Later articles cite new evidence of high-flux levels of low energy protons and electrons existing broadly within the magnetosphere (Refs. 28, 29, 30, 31, and 32). An approximation by Van Allen (Ref. 28) of the structure of these low-energy radiations is given in Fig. 12. More quantitative data on these electron and proton intensities are

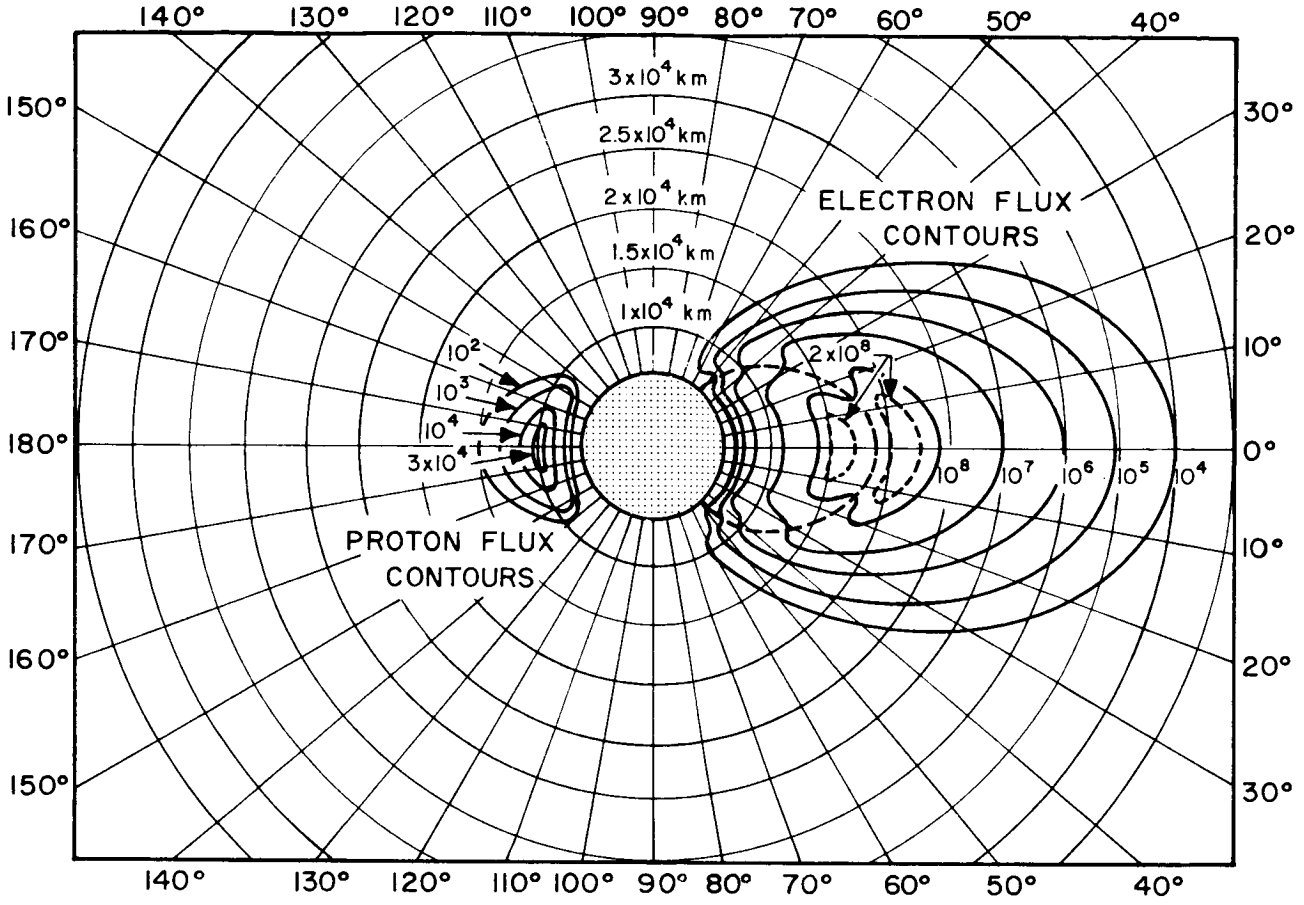

FIG. 11 QUIET DAY FLUX (electrons/cm^2/sec) CONTOURS OF ELECTRONS WITH ENERGIES GREATER THAN 20 kev WHICH FORM THE ELECTRON BELT OF THE VAN ALLEN RADIATION BELT. THE HIGH ENERGY PROTON FLUX CONTOURS OF E ≥ 30 Mev ARE ALSO SHOWN FOR REFERENCE (Refs. 16,17)

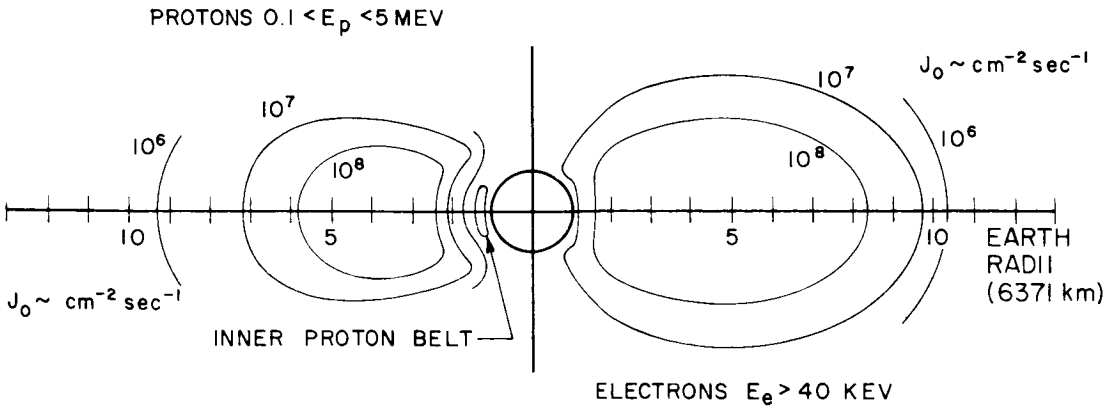

FIG. 12 QUIET DAY LOW ENERGY ELECTRON AND PROTON FLUX CONTOURS AS APPROXIMATED BY VAN ALLEN (Ref. 18)

given in Table VIII (Ref. 32). This appeared in the literature in March 1963 authored by Frank, Van Allen, Whelpley, and Craven. In May 1962, Davis and Williamson reported (Ref. 33) on the low-energy trapped protons measured by Explorer 12. In May 1962, Freeman reported the presence of an intense flux of low energy protons or ions trapped in the inner radiation zone (Ref. 34). Gringauz, et al. (Ref. 35) reported measurements of very low energy, E_e from 200 ev to 20 kev, electrons existing in the outer regions of the magnetosphere. Electrons trapped in the inner zone following as a result of Star Fish fission electrons form an artificial belt of a fairly durable type below the lower level of the inner radiation zone. The combined results of these various data are summarized in Fig. 13 for electrons and Fig. 14 for protons. The energy distributions of electrons and protons vary with altitude and latitude. There is also a time variation introduced by magnetic storms. The electron and proton energy distributions for the steady state or quiet sun are given in Fig. 15 for the geomagnetic equator and at selected altitudes. From Fig. 14 there is a broad peak of intensity occurring at between 3 and 4 R_e. At this same geocentric radius on the geomagnetic equator the electron flux is below the peak level noted at about 6.5 R_e, but only about a factor of three lower. In the inner regions the flux levels are less susceptible to magnetic storms and disturbances which cause temporal variations in radiation intensities within the magnetosphere and cause major changes in the magnetosphere boundary, as noted in Fig. 16 (Ref. 36). In the region of the 1.5 to 20 R_e reliable data are lacking to certain of the electron and proton intensities. For these reasons it is concluded that the intensities given for the trapped radiation levels in the region of 3 to 4 R_e are the most reliable and also most stable as to time variations. For maximum exposure of a surface in the radiation zone a circular orbit in the equatorial plane with a radius of 3 R_e would be ideal. Eccentric orbits of between 3 and 4 R_e between latitudes of $\pm 20^o$ would still expose the surface to a substantial fraction of the total possible exposure.

TABLE VIII

ELECTRON AND PROTON FLUXES MEASURED BY EXPLORER 14
NEAR THE EQUATORIAL PLANE (REF. 22)

R_e, (Radial) Geocentric Dist.		Energy Range	J_o, Particles/cm^2/sec
39,000 km	electrons	≥ 40 kev	1.5×10^8
39,000 km	electrons	≥ 230 kev	1.5×10^6
39,000 km	electrons	≥ 1.6 Mev	2×10^5
20,000 km	protons	≥ 500 kev	$4 (\pm 2) \times 10^6$
20,000 km	electrons	≥ 230 kev	4×10^4
20,000 km	protons	≥ 4.5 Mev	1.5×10^4
31,000 km	electrons	≥ 40 kev	1×10^8
31,000	electrons	≥ 230 kev	5×10^6
31,000	electrons	≥ 1.6 Mev	1×10^6
55,000	electrons	≥ 40 kev	2×10^7
55,000	protons	≥ 500 kev	5×10^4
55,000	electrons	≥ 230 kev	3×10^4
55,000	electrons	≥ 1.6 Mev	1.5×10^3
65,000	electrons	≥ 40 kev	1×10^6
65,000	protons	≥ 500 kev	1.5×10^4
65,000	electrons	≥ 230 kev	6×10^3
65,000	electrons	≥ 1.6 Mev	2×10^2
75,000 to 103,000	protons	≥ 500 kev	500
"	electrons	≥ 40 kev	500

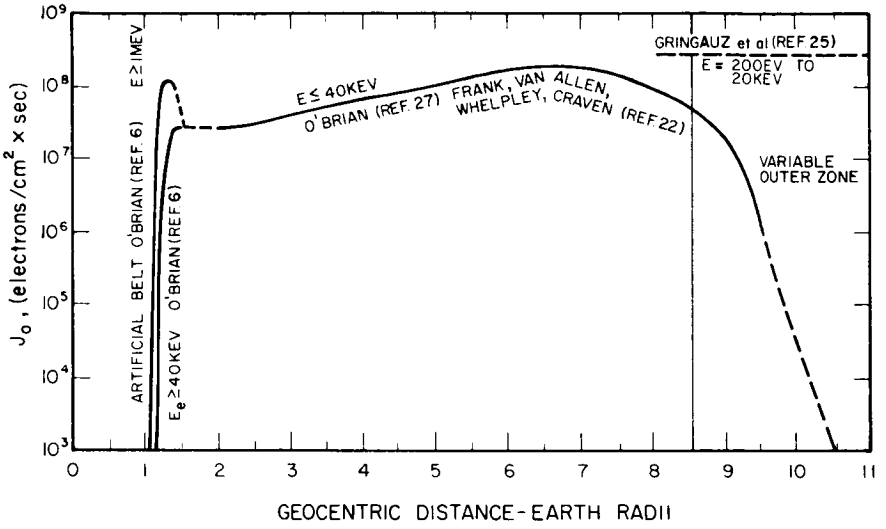

FIG. 13

ELECTRON FLUX DISTRIBUTION OF THE MAGNETOSPHERE AS A FUNCTION OF GEOCENTRIC RADIAL DISTANCE ON THE GEOMAGNETIC EQUATOR

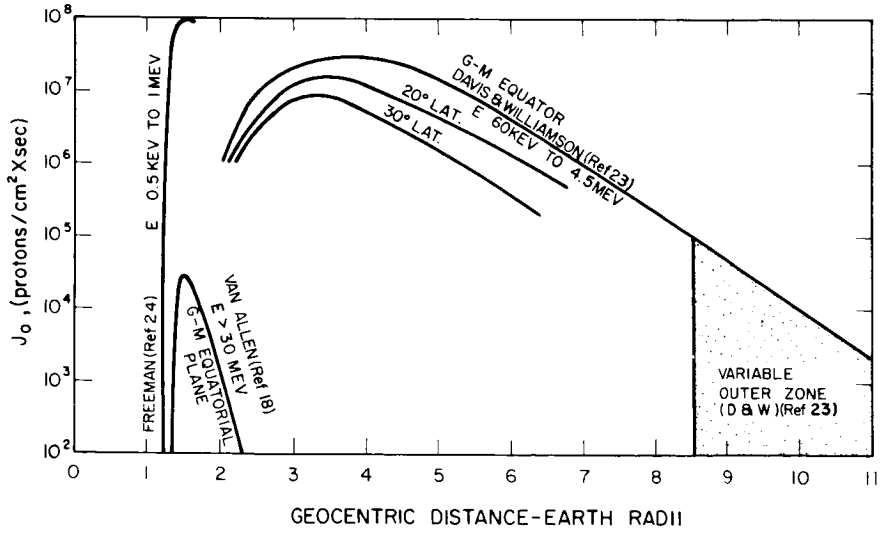

FIG. 14

PROTON FLUX DISTRIBUTION OF THE MAGNETOSPHERE AS A FUNCTION OF GEOCENTRIC RADIAL DISTANCE

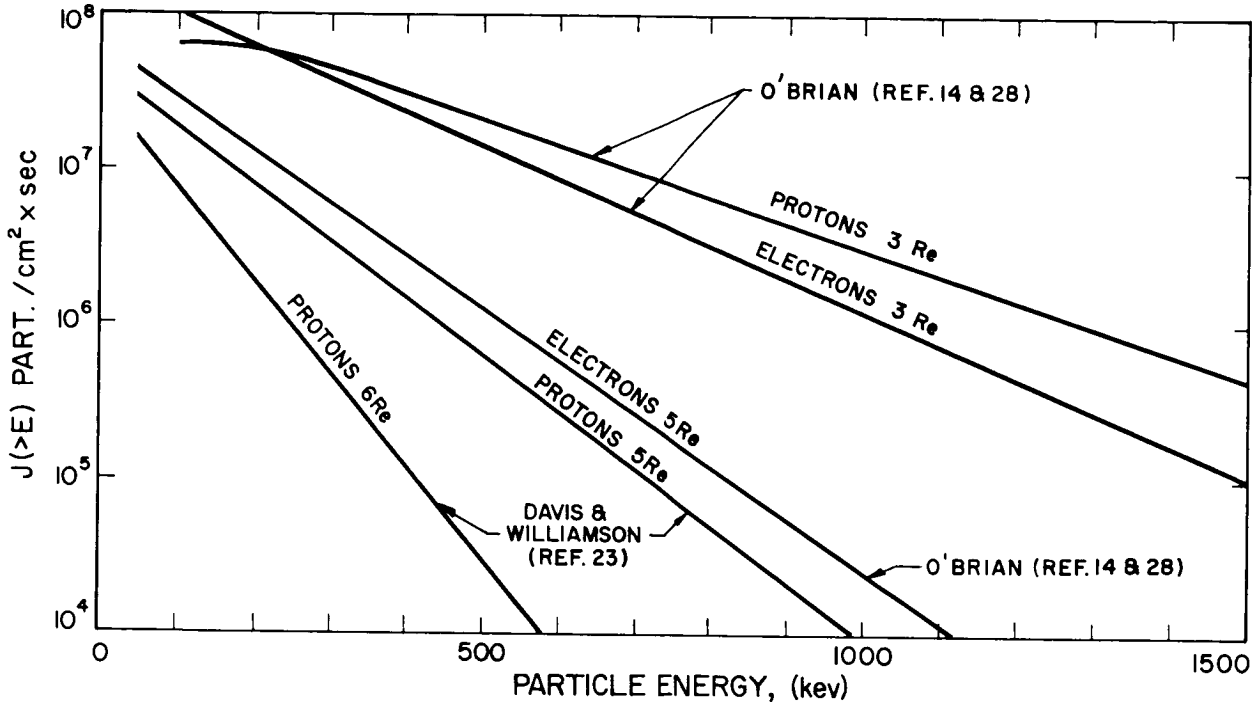

FIG. 13 INTEGRAL ELECTRON AND PROTON SPECTRA ON THE GEOMAGNETIC EQUATOR AT VARIOUS GEOCENTRIC RADIAL DISTANCES

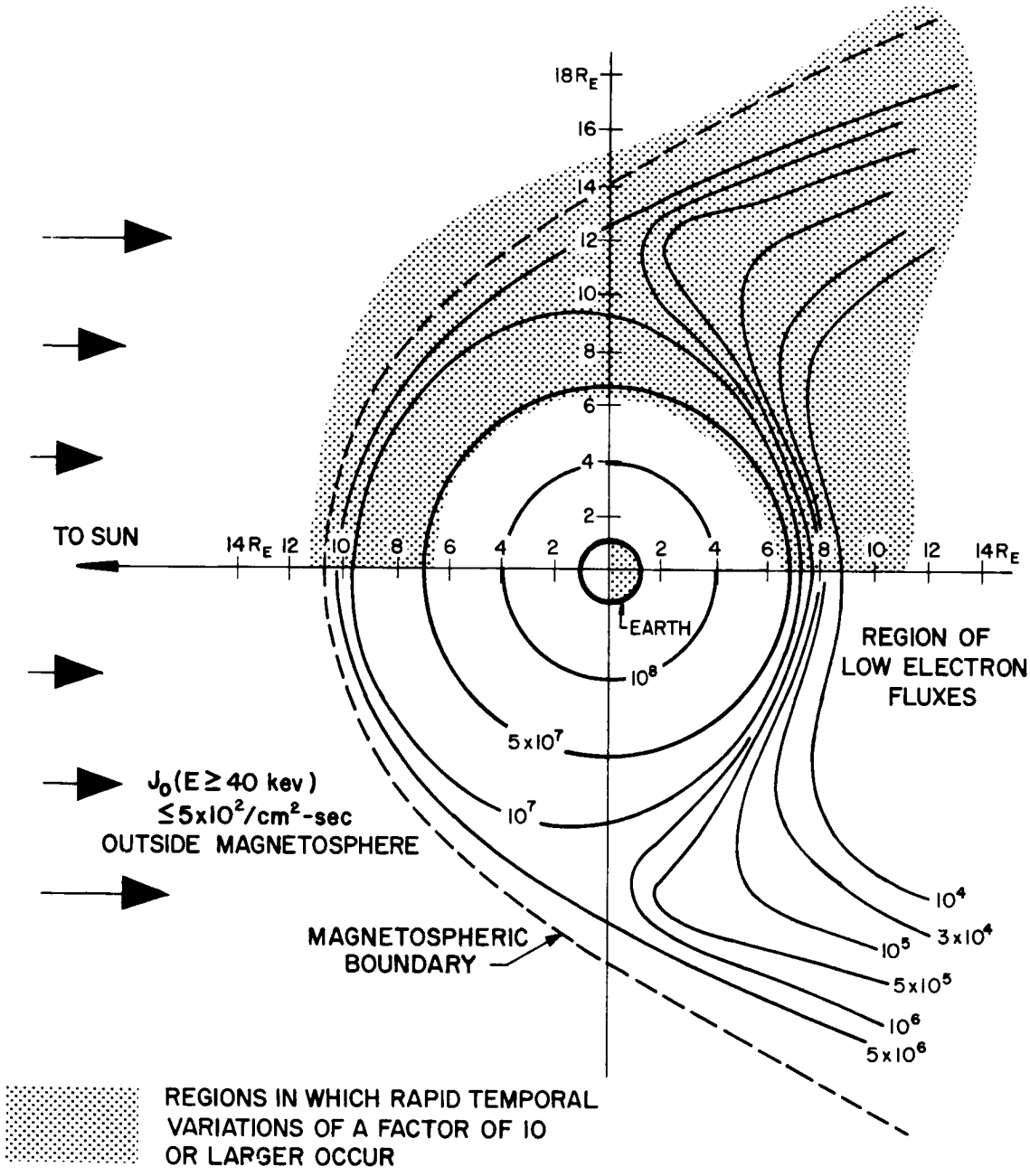

FIG. — SUMMARY OF OBSERVED OMNIDIRECTIONAL INTENSITIES OF ELECTRONS (E ≥ 40 kev) IN THE MAGNETIC EQUATORIAL PLANE OBTAINED FROM APPROXIMATELY TWENTY COMPLETE ORBITS OF EXPLORER 14 DURING OCTOBER-DECEMBER 1962 AND FROM EXPLORER 12 DURING AUGUST-DECEMBER 1961 (Ref. 26)

APPENDIX I

REFERENCES

1 U. S. Standard Atmosphere, 1962

2 L. D. Jaffe and J. B. Rittenhouse, Behavior of Materials in Space Environments, TR 32-150, Nov 1961

3 D. D. Carlson, Space Environments and Simulation Requirements, AEDC TDR 62-209, Nov 1962

4 Astronautics, Vol. 7, No. 8, 1962, pp. 54-61

5 R. Jastrow, Inter-Planetary Environment / Lectures in Aerospace Medicine, Jan 1962 (B.A.F.B. School of Aerospace Medicine)

6 B. J. O'Brian, "Review of Studies of Trapped Radiation with Satellite-Borne Apparatus," Space Science Reviews, 1962-1963, pp. 415-484

7 A. C. B. Lovell, Meteor Astronomy, Oxford University Press, 1954

8 F. L. Whipple, J. of Geophys. Res., Vol. 68, No. 17, Sep 1963, pp. 4929-4939

9 E. H. Davison and P. C. Winslow, "Space Debris Hazard Evaluation," NASA Tech. Note, D-1105, 1961

10 R. D. Collins and W. H. Kinard, "The Dependency of Penetration on the Momentum per Unit Area of the Impacting Projectile and the Resistance of Materials to Penetration," NASA Tech. Note, D-238, 1960

11 F. L. Whipple, "The Meteoric Risk to Space Vehicles," Vista in Astronaut., Vol. 1, Pergamon Press, New York, 1958, pp. 115-124

12 R. S. Barnes, "The Effect of the Radiations Encountered by Materials in Space," J. Brit. Interplanetary Soc., Vol. 18, 1962, pp. 377-381

13 R. J. Eichelberger and J. W. Gehring, "Effects of Meteoroid Impacts on Space Vehicles," J. ARS, No. 32, 1962, pp. 1583-1591

14 A. B. Thompson and C. F. Gell, "Meteoroids as a Hazard in Space Flight," (presented at ARS Space Flight Report to the Nation, New York, Oct 1961)

15 J. E. Duberg, "The Meteoric Hazard in the Environment of a Satellite," NASA Tech. Note, D-1248, 1962

16 M. Dubin and C. W. McCracken, "Measurements of Distributions of Interplanetary Dust," Astron. J., Vol. 67, 1962, pp. 248-256

17 F. L. Whipple, "On Meteoroids and Penetration," Adv. in Astron. Sci., Vol. 13, 1963, pp. 590-598

18 State University of Iowa, Publication No. 1079, Jun and Aug 1962

19 B. J. O'Brian, "Radiation Belts," Scientific American, Vol. 208, No. 5, May 1963, pp. 84-96

20 W. P. Saylor, et al., Space Radiation Guide, AMRL-TDR-62-86, 1962

21 D. L. Anderson, "Ion Bombardment and Its Effects on the Optical Properties of Metals," (paper presented at the American Vacuum Society Meeting, Boston, Mass., Oct 16-18, 1963)

22 D. L. Anderson and G. J. Nothwang, "Effects of Sputtering with Hydrogen Ions on Total Hemispherical Emittance of Several Metallic Surfaces," NASA Tech. Note, D-1646, Jan 1963

23 Herbert Friedman, "Rocket Spectroscopy," Space Science, John Wiley, 1963, pp. 549-627

24 J. H. Shaw, "Results of Scientific Research in Space," J. Applied Optics, Mar 1962, pp. 87-95 (paper presented at NASA)

25 The Boeing Company, Photovoltaic Concentrator Development, Interim Report No. 1, Jul 1962, JPL Contract 950270 (Sub-contract under NASA, Contract NAS7-100)

26 D. P. Le Galley, Space Science, John Wiley, 1963

27 C. G. S. Goetzel, Lockheed Missiles and Space Company, Space Materials Handbook, Contract AF 04(647)-673, Jan 1962

28 J. A. Van Allen, "Brief Note on the Radiation Belts of the Earth," T.I.D. 7652, Book 1, Nov 1962 (given at a symposium on Protection Against Radiation Hazards in Space)

29 Cain, Chapman, J. of Geophys. Res., Vol. 67, No. 7, Jul 1962

30 J. A. Van Allen, Space Science, John Wiley, 1963, p. 226

31 Alan Rosen, Space Science, John Wiley, 1963, p. 275

32 L. A. Frank, J. Van Allen, W. Whelpley, J. D. Craven, J. of Geophys. Res., Vol. 68, No. 6, pp. 1573, Mar 1963

REFERENCES (contd)

33 L. R. Davis and J. M. Williams, "Low Energy Trapped Protons," Space Research III, 1962, pp. 365-375

34 J. W. Freeman, "Detection of Low Energy Protons or Ions Trapped in the Inner Radiation Zone," J. of Geophys, Res., Vol. 67, No. 3, Mar 1962, p. 921

35 L. J. Gringauz, and S. M. Balinda, "On Results of Experiments with Charged Particle Traps in the Second Radiation Belt - Space Research," 1962, pp. 432-437

36 J. Van Allen and Frank Macagno, J. of Geophys, Res., Vol. 68, No. 6, Mar 1963

APPENDIX II

REFLECTANCE MEASUREMENTS AND SIMULATED MICROMETEORITE TESTS

APPENDIX II

REFLECTANCE MEASUREMENTS AND SIMULATED MICROMETEORITE TESTS

In 1963, tests were performed at NASA/Lewis to determine the effects of simulated micrometeorite fluxes on selected reflective surfaces provided by EOS. Silicon carbide particles, accelerated by a shock tube, were impinged on the test surfaces. Resulting degradation in total reflectance was then measured and was found to be high when compared to analytical predictions based on available data.

To better understand and document the effects indicated by these initial experiments, another series of reflectance samples was tested. These samples, which were submitted to NASA/Lewis for testing, were made from electroformed nickel substrates 15/16 inch in diameter and about 0.060 inch thick. Surfaces to be tested were prepared in the following categories:

1. Chemically deposited silver, 600 to 1,000Å
2. Bare electroformed nickel
3. Vacuum deposited: chromium 100Å, aluminum 1,000Å
4. Vacuum deposited: chromium 100Å, silicon monoxide 2,500Å aluminum 1,000Å
5. Vacuum deposited: chromium 100Å, silicon monoxide 2,500Å aluminum 1,000Å
6. Vacuum deposited: chromium 100Å, silicon monoxide 2,500Å aluminum 1,000Å, silicon monoxide, 20,000Å

The reflectance measurements of the samples before and after micrometeorite testing, as well as measurements of control samples retained by EOS, are listed in Table I. Figure 1 shows samples 1 and 3 from the six groups. At EOS the samples were measured at 0.625, 0.7, and 1.0 micron with a Beckman DU spectrophotometer. Each sample was measured at least three times. The measurement given in an average of

TABLE I

REFLECTANCE MEASUREMENTS

0.625μ TEST WAVELENGTH

Group	Sample	Reflectance		Loss	Net Reflectance
		Before Test %	After Test %		
1	1	98.1	33.5	64.6	48.7
	2	96.8	81.6	15.2	
	3	97.2	—	—	
2	1	66.9	27.8	39.1	31.4
	2	66.8	63.0	3.8	
	3	66.7	63.3	3.4	
3	1	92.3	21.8	70.5	26.5
	2	91.6	86.6	5.0	
	3	91.9	87.5	4.4	
4	1	92.3	41.6	50.7	47.2
	2	93.1	—	—	
	3	92.1	86.5	5.6	
5	1	81.5	36.0	45.5	40.3
	2	92.0	86.9	5.1	
	3	92.0	87.2	5.2	
	4	79.9	77.4	2.5	
6	1	84.9	43.3	41.6	42.0
	2	69.2	70.0	(0.8)	
	3	61.2	65.0	(3.8)	
	4	84.1	83.5	0.6	

Samples:
Sample 1 was tested at NASA/Lewis. Samples 2, 3 and 4 were control samples.

TABLE I
(continued)

1.0μ TEST WAVELENGTH

Group	Sample	Reflectance		Loss	Net Reflectance
		Before Test %	After Test %		
1	1	98.5	54.5	44.0	65.6
	2	98.3	-	-	
	3	98.6	87.5	11.1	
2	1	74.6	29.6	45.0	32.2
	2	74.7	71.9	2.8	
	3	73.9	71.5	2.4	
3	1	94.6	23.0	71.6	26.4
	2	94.3	90.6	3.7	
	3	94.0	90.9	3.1	
4	1	94.2	44.1	50.1	45.8
	2	94.3	-	-	
	3	93.2	91.5	1.7	
5	1	93.1	41.8	51.3	43.0
	2	91.7	88.9	2.8	
	3	91.5	90.6	0.9	
	4	92.5	92.6	(0.1)	
6	1	92.6	50.8	41.8	52.4
	2	83.9	83.1	0.8	
	3	92.1	90.0	2.1	
	4	85.0	83.0	2.0	

TABLE I
(continued)

0.700 μ TEST WAVELENGTH

Group	Sample	Reflectance Before Test %	Reflectance After Test %	Loss	Net Reflectance
1	1	99.3	40.5	48.8	53.3
	2	99.8	86.5	13.3	
	3	100.1*	—	—	
2	1	69.9	29.2	40.7	34.3
	2	69.9	64.3	5.6	
	3	69.5	65.0	4.5	
3	1	91.1	22.2	68.9	26.4
	2	91.1	86.0	5.1	
	3	90.2	86.8	3.4	
4	1	89.0	42.5	46.5	44.8
	2	89.7	—	—	
	3	88.8	86.5	2.3	
5	1	79.5	33.4	46.1	36.0
	2	89.2	84.2	5.0	
	3	82.4	83.8	(1.4)	
	4	81.6	76.3	4.3	
6	1	83.0	46.2	36.8	40.1
	2	72.6	81.4	(8.8)	
	3	65.5	79.4	(13.9)	
	4	82.9	78.6	4.3	

*The 100.1 percent silver reflectance measurement, compared with published values, indicates that the experimental error was in the order of ± 0.6 percent.

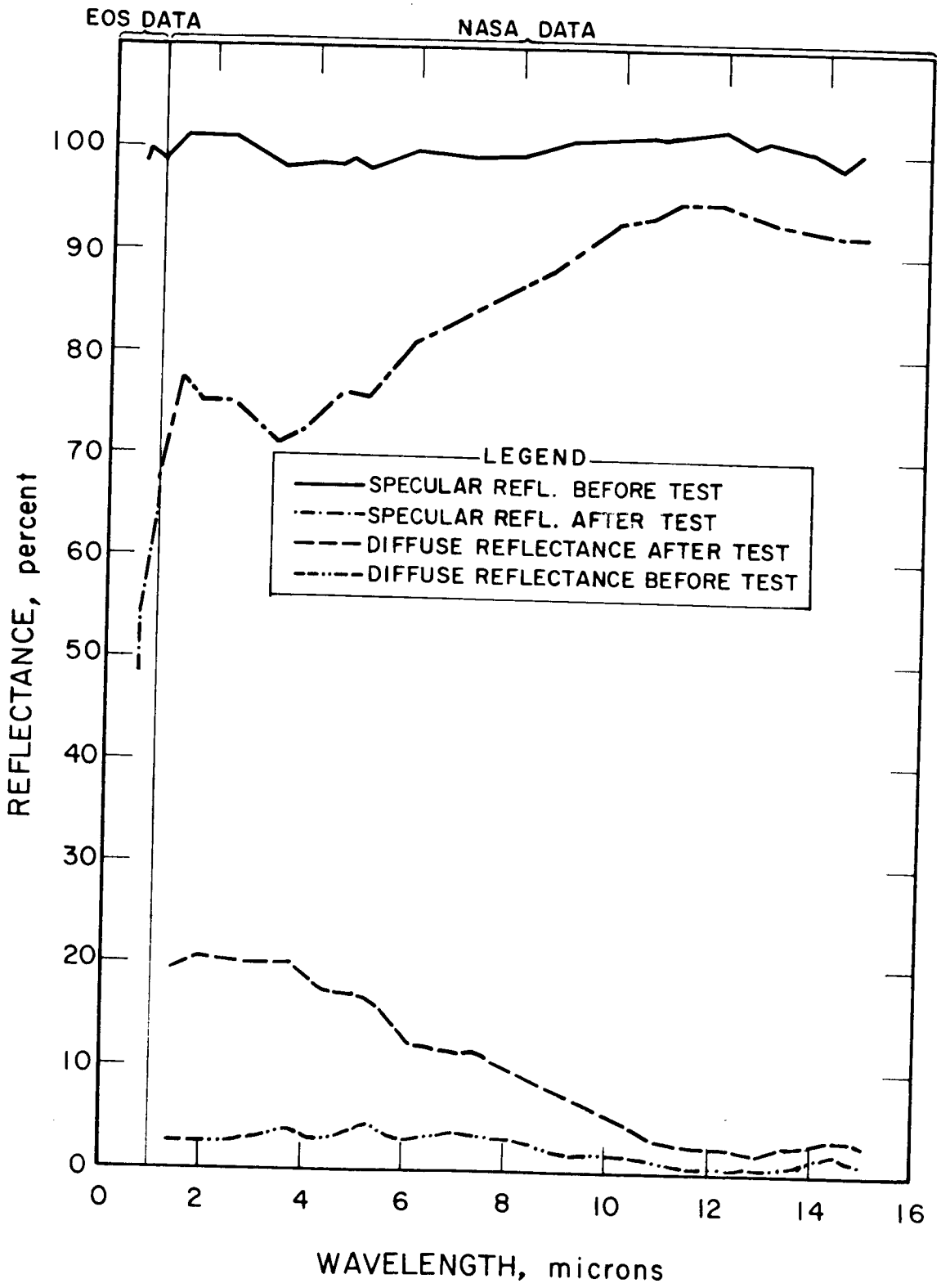

FIG. 1 REFLECTANCE OF SAMPLE I-1 BEFORE AND AFTER MICROMETEORITE TESTING

three readings. Reflectance measurements were made by the goniometer method. The 100 percent reflectance level was measured by placing the photocell in line with the spectrophotometer beam. An aluminum standard was then referenced. This standard was referred to after testing each sample. The spectrophotometer beam made an angle of incidence of 7½° with the reflective surface and the aluminum standard.

The initial reflectance measurements of Samples 1 to 3, Groups 1 through 4, correlated closely with each other and with published reflectance data. The maximum variation between samples within a group was 1.3 percent, which indicates the reproducibility between measurements and coating samples.

The initial reflectance variations among samples within Groups 5 and 6 were caused by differences in thickness of the silicon monoxide overcoating. The silicon monoxide overcoating acted as a selective spectral filter. Visual observation of these samples indicated a range of colors; i.e., the samples within a group did not have maximum absorption of the same wavelength. This observation correlated with the reflectance measurements.

The first and second samples of each coating group were sent to NASA Lewis for testing. The first samples were exposed to a hypervelocity cloud of silicon carbide particles between 2 and 14 microns in diameter which were accelerated in a 3-inch shock tube to a velocity of 8,500 ft/sec. These articles were then impacted against the test samples at the following levels of kinetic energy:

Sample	Kinetic Energy $\Sigma_i \frac{1}{2} m_i v_i^2$
1-1	0.70 joule
2-1	1.21 joules
3-1	1.42 joules
4-1	0.66 joule
5-1	1.09 joules
6-1	1.22 joules

The test procedure used was similar to that discussed in the NASA/ Lewis TP 8-63, "Alteration of Surface Optical Properties by High Speed Micron Size Particles". For these tests, the average silicon carbide particle size was 6.35 microns. Using kinetic energy as the appropriate independent variable for scaling damage, a test kinetic energy of 1 joule on a 15/16-inch disc diamter is equivalent to a near-earth space of about 8 months.

The second and third samples of each group were used as control samples to eliminate the effects of corr[illegible]on on the results of the experiment. Figures 1 through 6 summarize the diffuse and specular measurements made by both EOS and NASA/Lewis between the wavelength of 0.625 and 15 microns.

The 1 to 15-micron specular reflectance data were derived by subtracting the diffuse from the total reflectance. The NASA data covered this wavelength range.

Reflectance between the wavelengths of 0.02 to 1 micron is particularly important since about 75 percent of the total solar intensity is represented by this wavelength region.

Low specular and high diffuse reflectance in the 0 to 1-micron region are due to surface roughness caused by the simulated micrometeorite test. Small pits act as a diffuser of low wavelengths and a reflector to higher wavelengths.

Some of the differences between the reflectance values above and below 1 micron are also due to the differences in measurement techniques. Several readings above 1 micron indicate specular reflectances greater than 100 percent.

Electro-Optical Systems reflectance measurements taken on the control samples for Groups 1 through 4 indicate a consistent loss in reflectivity due to corrosion and aging effects. Control samples from Groups 5 and 6 do not show a similar pattern. This can probably be explained by a fact that, initially, the silicon monoxide coatings on these samples were absorbing at

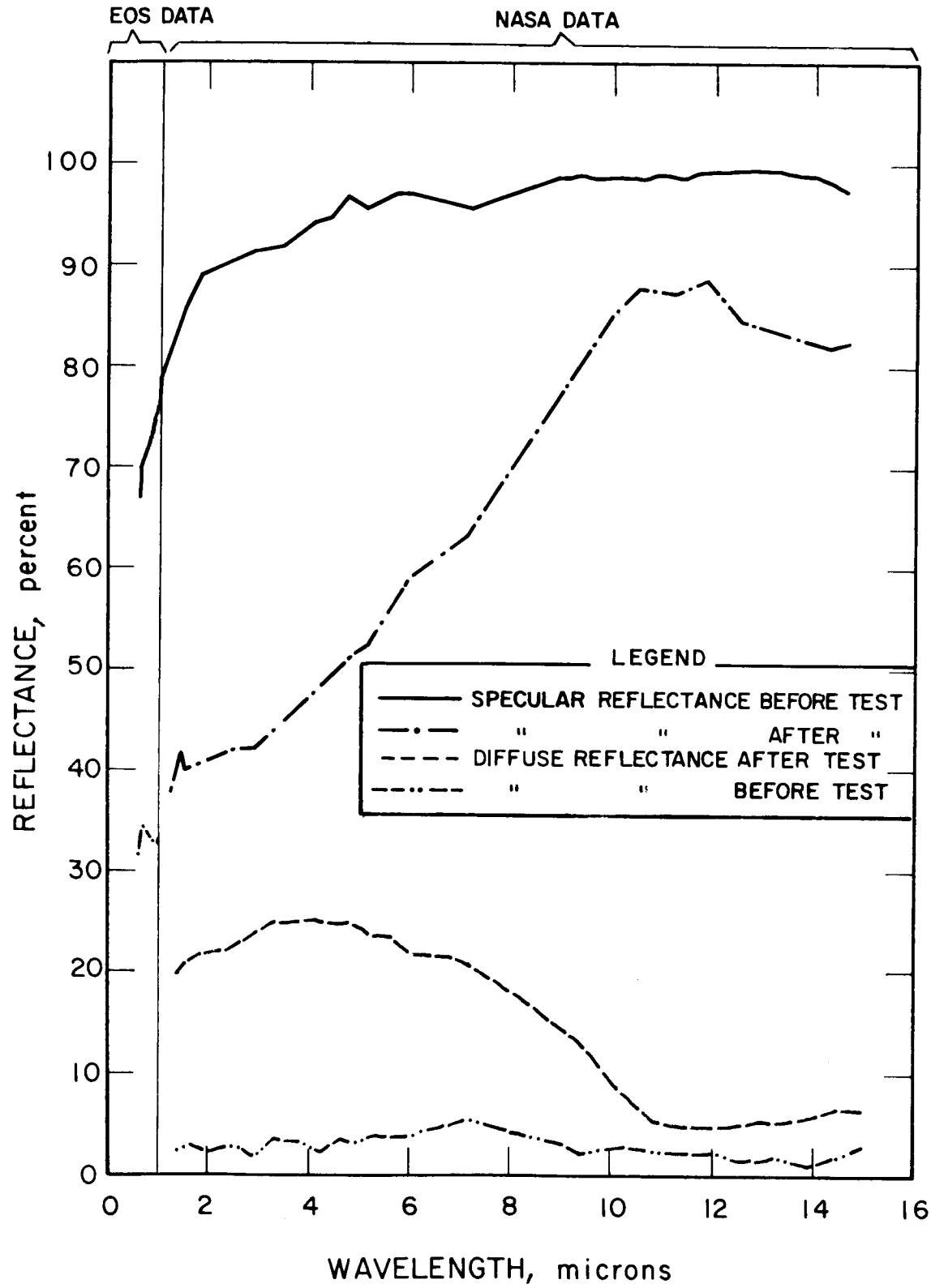

FIG. 2 REFLECTANCE OF SAMPLE 2-1 BEFORE AND AFTER MICROMETEORITE TESTING

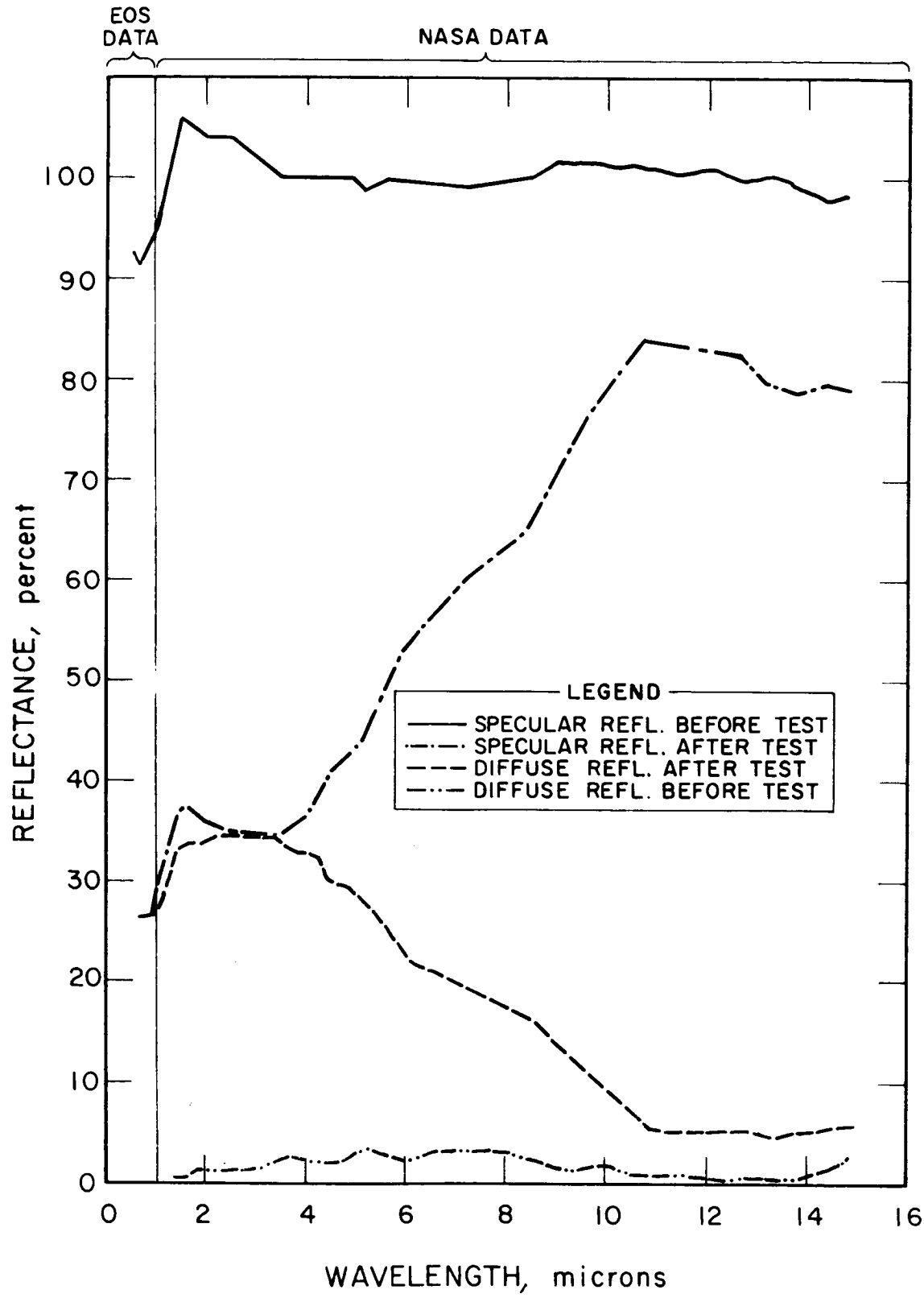

FIG. REFLECTANCE OF SAMPLE -1 BEFORE AND AFTER M' ROMETEORITE TESTING

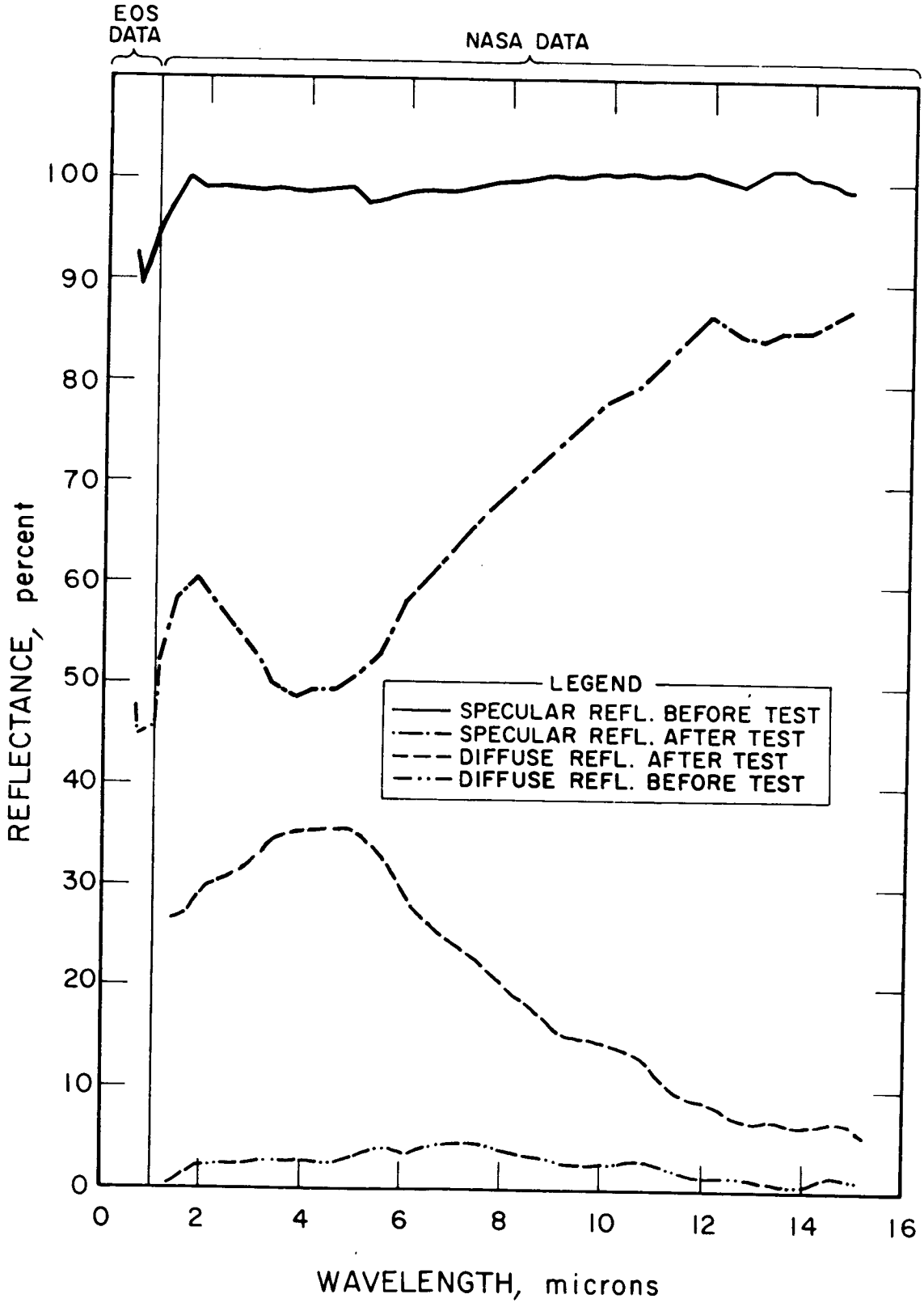

FIG. - REFLECTANCE OF SAMPLE -1 BEFORE AND AFTER MICROMETEORITE TESTING

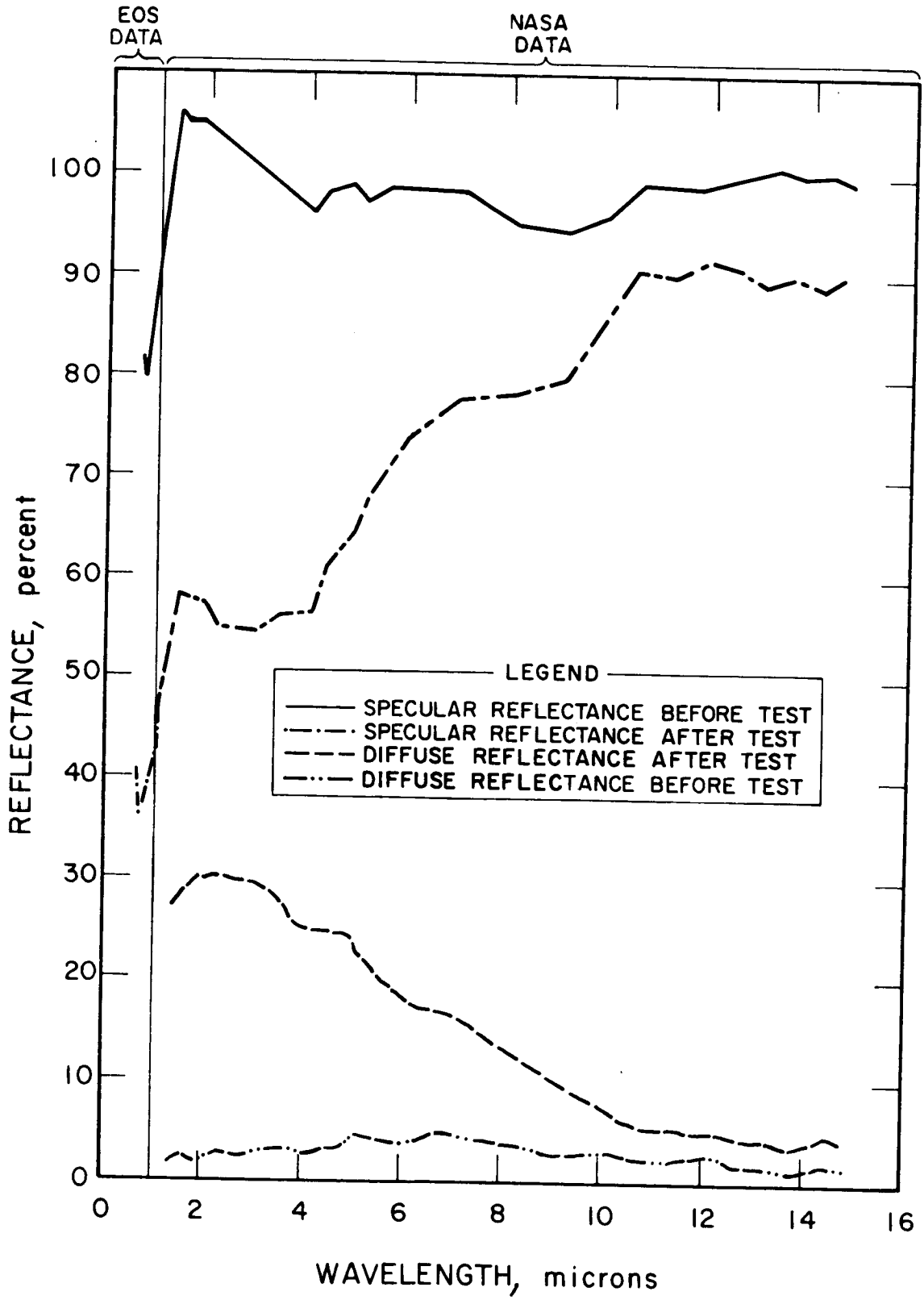

FIG. 5 REFLECTANCE OF SAMPLE 5-1 BEFORE AND AFTER MICROMETEORITE TESTING

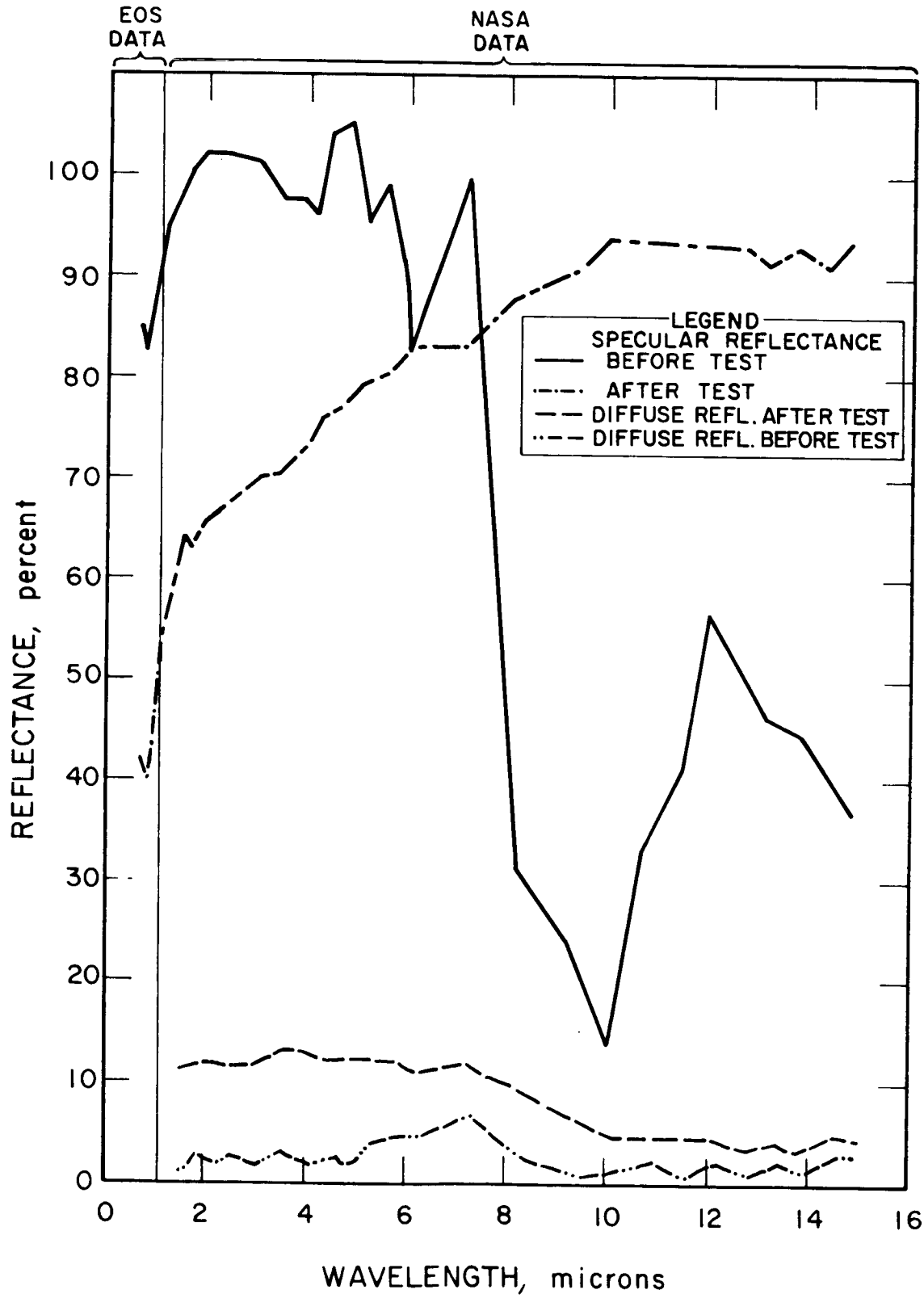

FIG. 9 REFLECTANCE OF SAMPLE 6-1 BEFORE AND AFTER MICROMETEORITE TESTING

different wavelengths. Oxidation and water absorption then may have further altered the absorption characteristics of the silicon monoxide protective films.

Electro-Optical Systems reflectance measurements on the tested samples were corrected for corrosion degradation as measured on the control samples, to yield the net reflectance values.

Comparison of the micrometeorite resistance between coating groups is difficult because the kinetic energy of each test varied considerably. However, the following preliminary conclusions can be drawn from the limited sampling:

1. The reflectance of chemically deposited silver is superior (both before and after simulated micrometeorite impingement) to all other coatings, provided the silver is protected from chemical corrosion.
2. The reflectance of silicon monoxide-protected aluminum coatings (as in Group 6) is superior to that of bare electroformed nickel, both before and after micrometeorite testing. The Group 6 coating had a higher net reflectance after testing than the Group 5 coating. The relative reflectances were reversed before testing. This may indicate that the thick silicon monoxide coating has some advantage in protecting the collector surface, providing the thickness can be controlled to yield maximum collector reflectance throughout the mission.
3. It is difficult to compare the relative merits of various aluminum undercoatings as listed in Groups 3 and 4, since the test kinetic energy of each varied, by a factor of two. The control samples, however, indicate that the chromium-silicon monoxide-aluminum coating sandwich has better corrosion resistance than the chromium-chromium-aluminum sandwich. The possibility of galvanic coupling between the chromium-aluminum sandwich in Group 3 may explain this. In Group 4, these metals are separated by the silicon monoxide dielectric coating. In calculating the net reflectance, it has

been assumed that the corrosion for the tested samples was the same as that incurred by the control samples. However, the tested samples probably corroded faster than the control samples. This may account for some of the large reflectance losses in the 0.625 to 1.0 micron range measured at EOS relative to those measured at NASA/Lewis at slightly higher wavelengths and immediately after the micrometeorite testing.

Up to wavelengths of 1 micron, the thermal properties of the coating materials do not appear to affect sample area degradation as one might expect if a comparison were made between solid target discs made from the coating materials. The thin-film mechanical and thermal properties of the coating materials are probably more dominant than the bulk thermal properties.

The results described above assume that the total kinetic energy is the appropriate independent variable.

Whatever the independent variable should be, these micrometeorite tests indicate the importance of testing reflectance degradation in space at the earliest possible date to accurately predict the life of reflective solar power systems.